Patient Specific JAK2 V617F iPS Cells for Modelling Bone Marrow Fibrosis

Von der Fakultät für Mathematik, Informatik und Naturwissenschaften der RWTH Aachen University zur Erlangung des akademischen Grades eines Doktors der Naturwissenschaften genehmigte Dissertation

vorgelegt von

Janik Böhnke M.Sc.

aus Einbeck

Berichter: Univ.-Prof. Dr. Martin Zenke
Univ.-Prof. Dr. Dr. Wolfgang Wagner
Univ.-Prof. Dr. Gabriele Pradel

Tag der mündlichen Prüfung: 13.05.2022

Table of contents

Zusammenfassung

Bei der Myelofibrose wird blutproduzierendes Knochenmark durch die Einlagerung von extrazellulären Matrixproteinen (ECM) durch fibrotisches Gewebe ersetzt. Der Auslöser ist die maligne Proliferation hämatopoetischer Stammzellen (HSC), welche durch veränderte Zytokinexpression die Aktivierung, Proliferation und Differenzierung von mesenchymalen und stromalen Stammzellen (MSC) in Myofibroblasten bewirken. Die Myelofibrose entsteht als primäre Myelofibrose (PMF) oder als Sekundärerkrankung aus myeloproliferativen Neoplasien (MPN) wie der Polycythaemia Vera (PV). In mehr als 95% der PV Patienten ist die JAK2 V617F Mutation der Auslöser. Die *Gain-of-Function* Mutation führt zu einer Phosphorylierung der Tyrosinkinase JAK2 ohne die Bindung eines Liganden (wie Thrombopoietin (TPO) oder Erythropoietin (EPO)). Hierdurch wird die Blutproliferation dauerhaft stimuliert, was insbesondere Megakaryozyten und Thrombozyten betrifft.

In dieser Arbeit wurden reprogrammierte JAK2 V617F mutierte induzierte pluripotente Stammzellen (iPS Zellen) von drei PV Patienten verwendet. Die JAK2 V617F^{hom} Mutation wurde in den iPS Zellen eines Patienten mit CRISPR/Cas9 repariert. Zudem wurde CRISPR/Cas9 für den funktionalen Knockout des Chemokins CXC motif ligand 4 (*CXCL4*, auch *platelet factor 4, PF4*) genutzt, welches als möglicher Effektor bei der Ausbildung von Myelofibrose gilt.

Weiterhin haben wir in unserem Labor ein Differenzierungsprotokoll zur Generierung von HSC und Megakaryozyten aus iPS Zellen etabliert und verbessert. Die JAK2 V617F differenzierten HSC und Megakaryozyten zeigten im Vergleich zu unmutierten Zellen eine beschleunigte Differenzierungskinetik, eine schnellere Maturierung, die vermehrte Bildung von Erythrozyten aus HSC und die TPO unabhängige Differenzierung von HSC in Megakaryozyten. RNA Sequenzierung zeigte deutliche Unterschiede in der Genexpression von JAK2 V617F Megakaryozyten im Vergleich zu JAK2 unmutierten Klonen, wie beispielsweise eine geringere Expression von Genen der ECM.

Die JAK2 V617F Megakaryozyten wurden zusammen mit BM-MSC (*bone marrow*-MSC, Knochenmark-MSC) für ein 2D Kokulturmodell genutzt, um die Interaktionen von Megakaryozyten und MSC genauer zu untersuchen. Hierbei wurde keine vermehrte Myelofibrose in der Kokultur mit JAK2 V617F^{hom} Megakaryozyten im Vergleich zu unmutierten Zellen festgestellt werden.

Insgesamt wurde in dieser Arbeit eine große Bandbreite an klonalen iPS Zellen aus drei verschiedenen PV Patienten generiert, die Differenzierung dieser Zellen zu HSC und Megakaryozyten etabliert und mit Expressionsanalysen sowie ersten Kokulturversuchen die Basis für weitere funktionale Studien zur Erforschung von Myelofibrose geschaffen.

Abstract

Bone marrow fibrosis is the central pathologic feature in myelofibrosis. The malignant proliferation of hematopoietic clones with abnormal cytokine expression causes an increased production of extracellular matrix (ECM) proteins from mesenchymal stem/stromal cells (MSC), leading to fibrotic tissue. Myelofibrosis develops as a primary disease (primary myelofibrosis, PMF) or a secondary disease from myeloproliferative neoplasms (MPN) such as polycythemia vera (PV). Here, the Janus kinase JAK2 is mutated in over 95% of cases. The gain-of-function mutation JAK2 V617F leads to phosphorylation of the tyrosine kinase without ligand binding (such as thrombopoietin (TPO) or erythropoietin (EPO)). This results in permanent activation of blood cell proliferation, especially of megakaryocytes and platelets.

In this work, induced pluripotent stem cell (iPS cell) clones from three PV patients with JAK2 V617F mutation were used. JAK2 V617F was repaired in one iPS cell clone using CRISPR/Cas9 technology. In addition, a functional knockout of the chemokine CXC motif ligand 4 (*CXCL4,* also known as *platelet factor 4*, *PF4*), which is suspected of playing an essential role in establishing bone marrow fibrosis, was performed in two iPS cell clones. Next, a protocol to differentiate iPS cells into hematopoietic stem cells (HSC) and megakaryocytes was established and further developed in our laboratory. The generated megakaryocytes had significant differences caused by the JAK2 genotype. JAK2 V617F megakaryocytes showed a strong differentiation bias towards erythrocytes, accelerated differentiation kinetics with faster maturation, and TPO-independent development of megakaryocytes. Furthermore, transcriptome analysis revealed differences in gene expression, such as downregulation of ECM genes in JAK2 V617F megakaryocytes.

The generated megakaryocytes were used together with BM-MSC (bone marrow MSC) for a 2D co-culture model to investigate the interactions between these two cell types. Here, no increased fibrosis was detected in JAK2 V617F clones compared to the controls. Altogether, a broad set of MPN patient-specific iPS cell clones was established, which were successfully differentiated to HSC and their progeny megakaryocytes with a protocol established in our lab. Combined with BM-MSC, preliminary experiments of co-culture models demonstrate a fundamental basis for further functional studies on myelofibrosis.

1 Introduction

1.1 Stem cells

The term stem cell was used for the first time in 1868 by Ernst Haeckel, describing an unicellular organism as the ancestor of multicellular organisms (Haeckel, 1868). Today, we know today that all cells of the human body develop from stem cells, starting with the fertilized ovum dividing and differentiating into all cells of the adult organism. Stem cells are defined as cells with an unlimited self-renewal potential, giving rise to differentiated cell types by symmetric and asymmetric cell division (Yamashita et al., 2010).

In general, stem cells are characterized as totipotent, pluripotent, multipotent, and unipotent by their potential to differentiate into different cell types (Figure 1A, Kelly, 1977). Totipotent stem cells can develop a fully formed organism from one cell (embryonic stem cells until morula's 8-cell stadium). Pluripotent cells can differentiate into the three germ layers named ectoderm, endoderm, and mesoderm (embryonic stem cells after morula's 8-cell stadium, Figure 1B). Multipotent cells are restricted to tissue-specific cells, like hematopoietic stem cells (HSC), while unipotent cells can only form one particular cell type (Mahla, 2016).

In adults, these different stem cells remain in specific anatomic locations, so-called stem cell niches. Here, they control homeostasis by replacing dead cells and renewing tissues and organs. For example, HSC reside in the bone marrow producing white and red blood cells (D. L. Jones & Wagers, 2008).

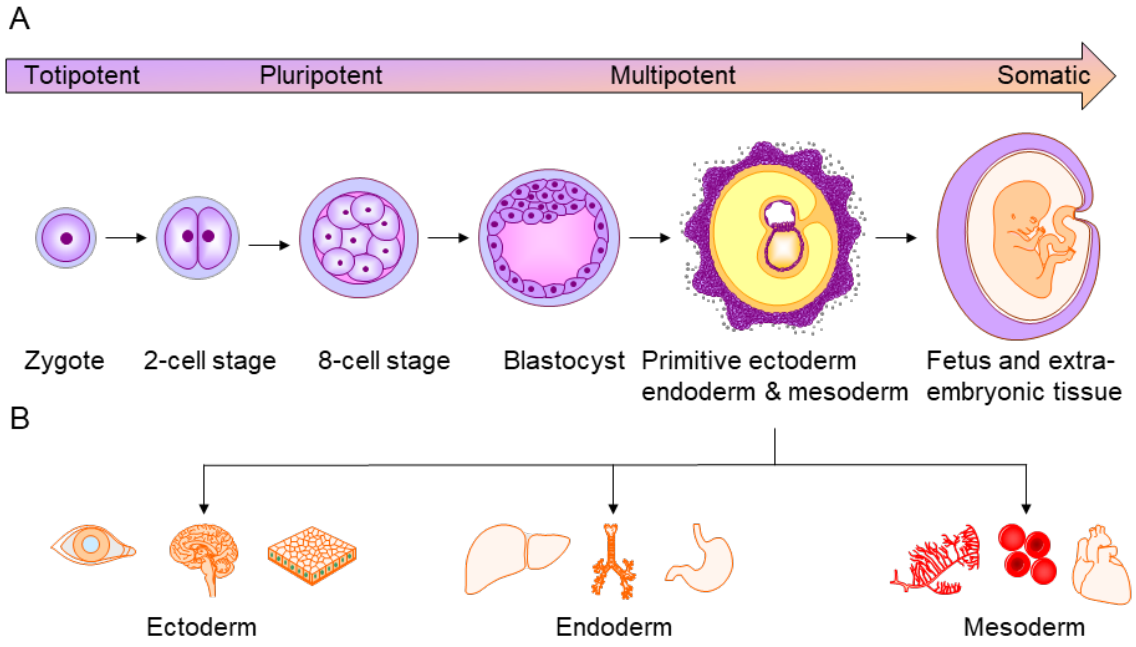

Figure 1: Human embryonic development.
(A) Cells divide in the zygote and lose their totipotent capacity in the 8-cell stage. Following differentiation steps develop the pluripotent blastocyst and subsequently, the bilaminar disc formation leads to primitive multipotent ectoderm, endoderm, and mesodermal tissue. In the further development, the embryo is formed. **(B)** Organs and tissues derived from ectoderm, endoderm, and mesoderm. Ectoderm forms neurons and the sensory nervous system, including skin, endoderm builds most of the gastrointestinal and respiratory tract and mesoderm generates muscles and the blood system, including vessels. Adapted from Surani & Tischler, 2012.

Stem cells from different origins are used to model tissues and diseases, such as pluripotent human embryonic stem (hES) cells from the inner cell mass of the blastocyst, embryonic carcinoma cells, or multipotent stem cells from different tissues. Especially for the usage of hES cells, there are ethical concerns as these cells are derived from a fertilized fetus used in test-tube fertilization. Nevertheless, hES cells are still used, e.g., in a recent study by Yu et al., where blastocytes were produced from hES cells for the first time (L. Yu et al., 2021).
Therefore, over many decades researchers tried to create stem cells from somatic cells. Takahashi and Yamanaka overcame this problem in 2006 with the reprogramming of mouse fibroblasts to so-called induced pluripotent stem cells (iPS cells) through the retroviral transduction of octamer-binding transcription factor 4 (OCT4), sex-determining region Y-box 2 (SOX2), krüppel-like factor 4 (KLF4) and c-Myc (Takahashi and Yamanaka, 2006).

1.1.1 iPS cells

One year after the first generation of mouse iPS cells, the first human iPS cell lines were generated by reprogramming human fibroblasts (Takahashi et al., 2007; J. Yu et al., 2007). Multiple methods emerged in the following years to reprogram different cell-types without the permanent insertion of DNA into the genome: reprogramming by transfection of plasmids (Yu et al., 2009), adenoviral reprogramming, transfection with messenger RNA (mRNA, Warren et al., 2010), chemical reprogramming (Hou et al., 2013) and the reprogramming by introducing proteins into the cells (Gump & Dowdy, 2007).
The first generated human iPS cells were cultured on mouse embryonic fibroblasts (MEF) in a serum-free medium containing basic fibroblast growth factor (bFGF). Regarding the clinical application of iPS cells, e.g., the use of iPS cell-derived platelets in transfusion medicine, biologically defined matrixes like laminin, vitronectin, or ECM extract from mouse sarcoma (Matrigel) combined with defined medium serum-free medium instead of MEF are utilized for the growth of iPS cells.
iPS cells grow as tight flat colonies with defined borders, high nuclei to cytoplasm ratio and an unlimited self-renewal capacity (Maherali & Hochedlinger, 2008). There are

several pluripotency markers to characterize iPS cells, such as the tumor related antigen 1-60 and 1-81 (Tra-1-60 and Tra-1-81), the stage specific antigen 3 and 4 (SSEA3, SSEA4) as surface markers, and OCT3 and OCT4, the homeobox protein NANOG, or SOX2 as intracellular marker. Moreover, iPS cells can differentiate into all cell types of the human body, proven by teratoma assays in mice (Maherali & Hochedlinger, 2008). The field of iPS cell understanding is still growing and research on methods like the characterization based on DNA methylation, embryonic body (EB) differentiation assay or directed differentiation into the ectodermal, endodermal and mesodermal lineage are gaining more importance (Asprer & Lakshmipathy, 2015).

1.1.2 iPS cells for disease modeling and clinical application

Before the era of iPS cells, mostly cell lines or model organisms were used for clinical research and disease modeling due to the ethical concerns of using hES cells. However, these techniques only partially reflect the human *in vivo* situation. Model organisms lack properties of the human system and cell lines are adapted to their artificial environments, like genetic modifications and characteristics similar to the behavior of cancer cells, such as increased proliferation without senescence (van Staveren et al., 2009).

iPS cells are an inexhaustible source of cells that can differentiate into all cells of the body. Therefore, they are of great interest for basic clinical research and direct application in humans, e.g., through the controlled differentiation of iPS cells into specialized cells and tissues. Since 2007, when the first human iPS cells were generated, many different protocols were established to differentiate iPS cells into neurons, heart cells, hematopoietic stem cells, or even whole organs, among many others (Figure 2).

iPS cells are used to understand early embryonic development, diseases such as viral infections, or the role of different genes during development. For example, Bilz et al. showed that the rubella virus infection in iPS cells alters the gene expression and differentiation capacity towards the three lineages ectoderm, endoderm, and mesoderm, reflecting the situation of virus infections during pregnancy causing congenital defects (Bilz et al., 2019). iPS cells are also used for genetic disease modeling like down syndrome or hereditary heart diseases (Brigida & Siniscalco, 2016; Buikema & Wu, 2017). Furthermore, iPS cells provide an essential tool for dissecting the molecular mechanisms causing the disease acquired during a lifetime. Moreover, iPS cells helped significantly to understand neurogenerative diseases like Parkinson's or Alzheimer's by

differentiating patient-derived iPS cells into neurons and other affected cells (Galet et al., 2020).

The emerging tool of iPS cell-derived organoids extends the possibilities to model diseases and personalize drugs. Protocols for organoids have already been described for many organs, like heart, liver, prostate, stomach, and kidney (Schutgens & Clevers, 2020). Techniques for differentiating iPS cells into hematopoietic cells have been established for a long time, but as the bone marrow is not a solid organ, organoid modeling for a better understanding is challenging.

Although there are many excellent and exciting approaches using iPS cells in clinical therapy, no method has yet made it beyond clinical test phase II. A study by Deinsberger et al. (2020) analyzing all iPS cells used in clinical trials showed that only 131 clinical studies involving iPS cells worldwide are registered (Deinsberger et al., 2020). Only 23% of these cases iPS cell-derived products were transplanted into patients. Overall, iPS cells are a tool to study congenital diseases and disease mechanisms. They are used for drug screening, regenerative medicine, and toxicology screens. For example, in our laboratory, patient-specific iPS cells with KIT D816V mutation were used for drug screening and identified nintedanib as a novel treatment option of mastocytosis and mast cell leukemia (Dorrance, 2021; Toledo et al., 2021).

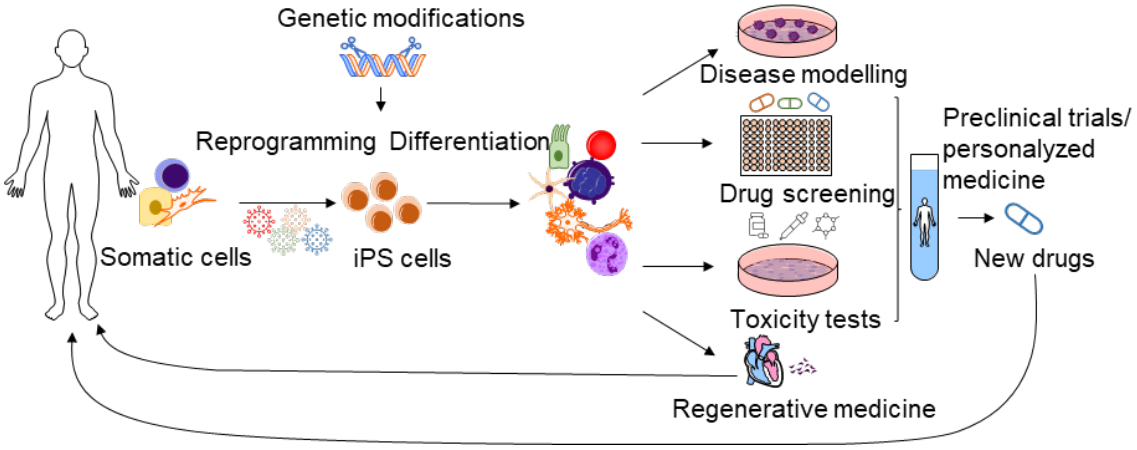

Figure 2: Clinical application of iPS technology.
Somatic cells (e.g., fibroblasts, mononucleated blood cells) are reprogrammed into iPS cells, modified, and differentiated into specialized cells for disease modeling, high throughput drug screening, and toxicity tests. They are also used in regenerative or personalized medicine. (Adapted from Bellin et al., 2012).

1.2 Hematopoiesis

The hematopoietic (Greek for blood-making) system interacts and penetrates all parts of the body, transports nutrients, oxygen, hormones, and cytokines, has an essential role in the immune defense, and stabilizes the temperature and pH (C. C. Zhang & Sadek, 2014). Hematopoiesis comprises the differentiation of rarely dividing long-term

hematopoietic stem cells (LT-HSC) into highly proliferative primed progenitors, which give rise to every cell type in the hematopoietic system. Hematopoiesis is localized in a defined compartment of the bone marrow and the spleen and is not restricted to a single solid organ. As a consequence, it is challenging to study hematopoietic processes in the human system (Brand & Morrissey, 2020).

Thus, most of our knowledge was gained from studying animal models (e.g., mouse, rat, and zebrafish), *in vitro* culture of primary human material, and the differentiation of iPS cells or ES cells into the hematopoietic lineages. However, each system has drawbacks and cannot perfectly represent the human body, firstly because many factors are missing or, in animal models, are different than in the human system. Secondly, they cannot mimic the hematopoietic niche completely as *in vitro* cultures only focus on selected cell types (Ditadi et al., 2016; Slukvin, 2016). Combining different models to circumvent the drawbacks is essential to extent our knowledge of the hematopoietic niche.

In addition, there are two different types of hematopoiesis: primitive embryonic hematopoiesis and definitive adult hematopoiesis. This complicates the understanding of hematopoiesis and diseases in this system. A complete understanding of the hematopoietic niche with different models is crucial for regenerative medicine and curing hematopoietic diseases or cancer.

1.2.1 Waves of hematopoiesis

Due to ethical concerns, studying primitive hematopoiesis in humans is particularly difficult, and most of our knowledge derives from studies in mice. In the 20th century, two hypotheses of embryonic hematopoiesis were developed: (i) Jordan postulated in 1916 the ventral endothelium of the aorta as the source of embryonic HSC, the so-called hemogenic endothelium (Jordan, 1916), whereas (ii) Murray postulated in 1932 a common progenitor of endothelium and hematopoietic cells, the so-called hemangioblast (Murray, 1932). For decades, these theories were thought to be contradictory, but new evidence shows that they go hand in hand, as illustrated in Figure 3.

Kennedy et al. showed 2007 in hES cell *in vitro* experiments the existence of hemangioblasts: FLK1^{+} (fetal liver kinase 1, or vascular endothelial growth factor receptor VEGFR 2) mesodermal cells give rise to hematopoietic and endothelial cells (Kennedy et al., 2007). Furthermore, it was shown in an *ex vivo* culture that mice FLK1^{+} cells could build hematopoietic, endothelial and smooth muscle cells (Huber et al., 2004). These findings still have to be validated *in vivo*. The existence of hemogenic endothelium and its essential role in hematopoietic processes has been proven in many studies. In

2008 Zovein et al. showed by lineage fate tracing experiments in mice that hematopoietic cells had their origin in endothelial cells (Zovein et al., 2008).

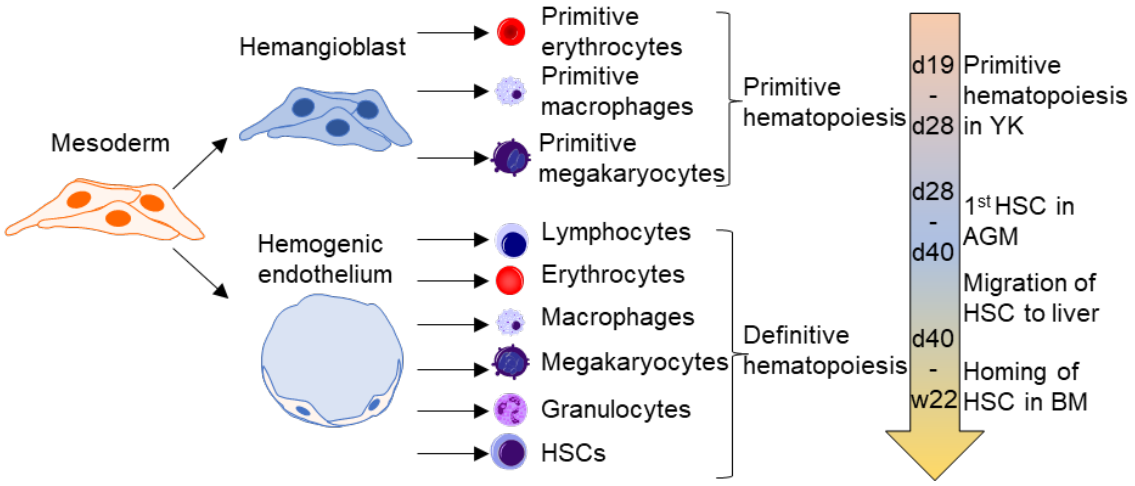

Figure 3: Simplified model of primitive and definitive hematopoiesis in the human embryo.
In early embryonic development from day 19 to 28 of gestation, mesodermal cells differentiate into the hemangioblast located in the yolk sac (YK). The production of primitive erythrocytes, macrophages, and megakaryocytes starts. Around day 28 of gestation, mesodermal cells form the hemogenic endothelium, producing definitive hematopoietic cells first in the aorta-gonad-mesonephros. These cells migrate around day 40 to the liver and around week 22 of gestation to the bone marrow (adapted from Lacaud & Kouskoff, 2017; Yoder, 2014 and Lange et al., 2021).

According to the current understanding, hematopoiesis takes place in waves. In the first wave, the hemangioblast is generated in the yolk sac, an area outside the embryo (day 19 to 28). Here, primitive erythrocytes (larger compared to definitive erythrocytes and containing a nucleus), macrophages (developing without a monocyte stage) and megakaryocytes (reduced ploidy and lower platelet production) are generated. Later, erythro-myeloid progenitors (EMPs) start to form in the yolk sac in the second wave. Here, erythrocytes and most of the cells of the myeloid linage are produced. The first definitive HSC are formed inside the embryo in the aorta-gonad-mesonephros (AGM) region starting at day 28. These HSC can self-renew and differentiate into all lineages of the adult system. They migrate with the start of blood circulation together with the second wave yolk sac cells into the liver and approximately in week 22, cells migrate to their final place in the bone marrow (Lange et al., 2021, Figure 3).

Proper understanding of the different stages of hematopoiesis during embryonic development is crucial for the *in vitro* differentiation of iPS cells into HSC, where embryonic development steps are recapitulated.

1.2.2 Hierarchical and continuous model of hematopoiesis

Several models have been established and redefined over the last decades for adult hematopoiesis. All have in common that LT-HSC are the source of all hematopoietic cells

in the adult organism. They are a quiescent and only rarely dividing population, generating the pool of actively dividing short-term HSC (ST-HSC).

In the hierarchical model, ST-HSC subsequently differentiate in a stringent hierarchical manner: Common myeloid progenitors (CMP) differentiate into megakaryocyte erythrocyte progenitors (MEP) and granulocyte monocyte progenitors (GMP), whereas the common lymphoid progenitor (CLP) differentiates directly into B-/T- and natural killer cells. This model defines a one-way street to the final differentiated mature cells. Intermediate cell populations are classified by distinct surface protein expression (Chotinantakul & Leeanansaksiri, 2012).

The use of modern single-cell RNA sequencing (RNA-Seq) methods has revolutionized the hierarchical model. It is now possible to examine individual stages of maturation in unprecedented depth. This led to new theories in which models of continuity replaced the hierarchical model. Brand & Morrissey suggest a large pool of LT-HSC (c-kit^{high} (type III receptor tyrosine kinase), Sca-1^{high} (stem cells antigen-1), CD34^{+} (cluster of differentiation 34), FLT3^{-} (fms like tyrosine kinase 3)) and ST-HSC (c-kit^{+}, Sca-1^{+}, CD34$^{+,}$ and FLT3^{+}) with features of intermediate states that are already, to some extent, primed in their path of differentiation (Brand & Morrissey, 2020). This means that fate decision is already decided partially. These cells form the pool of HSC and differentiate along a continuum to finally differentiated blood cells.

A more committed progenitor pool of MEP-like cells with c-kit^{+}, Sca-1^{-}, CD34^{low}, CD16/32^{-}, IL7R^{-} (interleukin 7 receptor) builds erythrocytes, megakaryocytes, and platelets. Another pool of lymphoid-primed multipotent progenitors (LMPP) like cells build pools of cells with c-kit^{+}, Sca-1$^{+,}$ and IL7R^{+} differentiating into monocytes, eosinophils, and dendritic cells (DC) and another pool with c-kit^{+}, Sca-1^{-}, CD34^{+}, CD16/32^{+} and IL7R^{-} cells differentiating into B-/T-cells and natural killer cells (Figure 4, Laurenti & Göttgens, 2018).

In these models, fate decisions are not a classical one-way road but more a fate probability. MEP-like cells still have low probabilities of differentiating into LMPP lineage cells and the other way around (Brand & Morrissey, 2020). Recent studies showed different pathways for the differentiation of DC and shortcuts from HSC to megakaryocytic progenitors (Haas et al., 2018; Notta, 2016; Velten, 2017; Figure 4).

Further studies are needed to fully illuminate the mechanisms of hematopoiesis with all effectors. Still, the role of DNA methylation, regulation of transcription factors, and effects of stem cell niche composition are poorly understood. Quantitative analysis of single cell secretomes and transcriptomes will elucidate these factors.

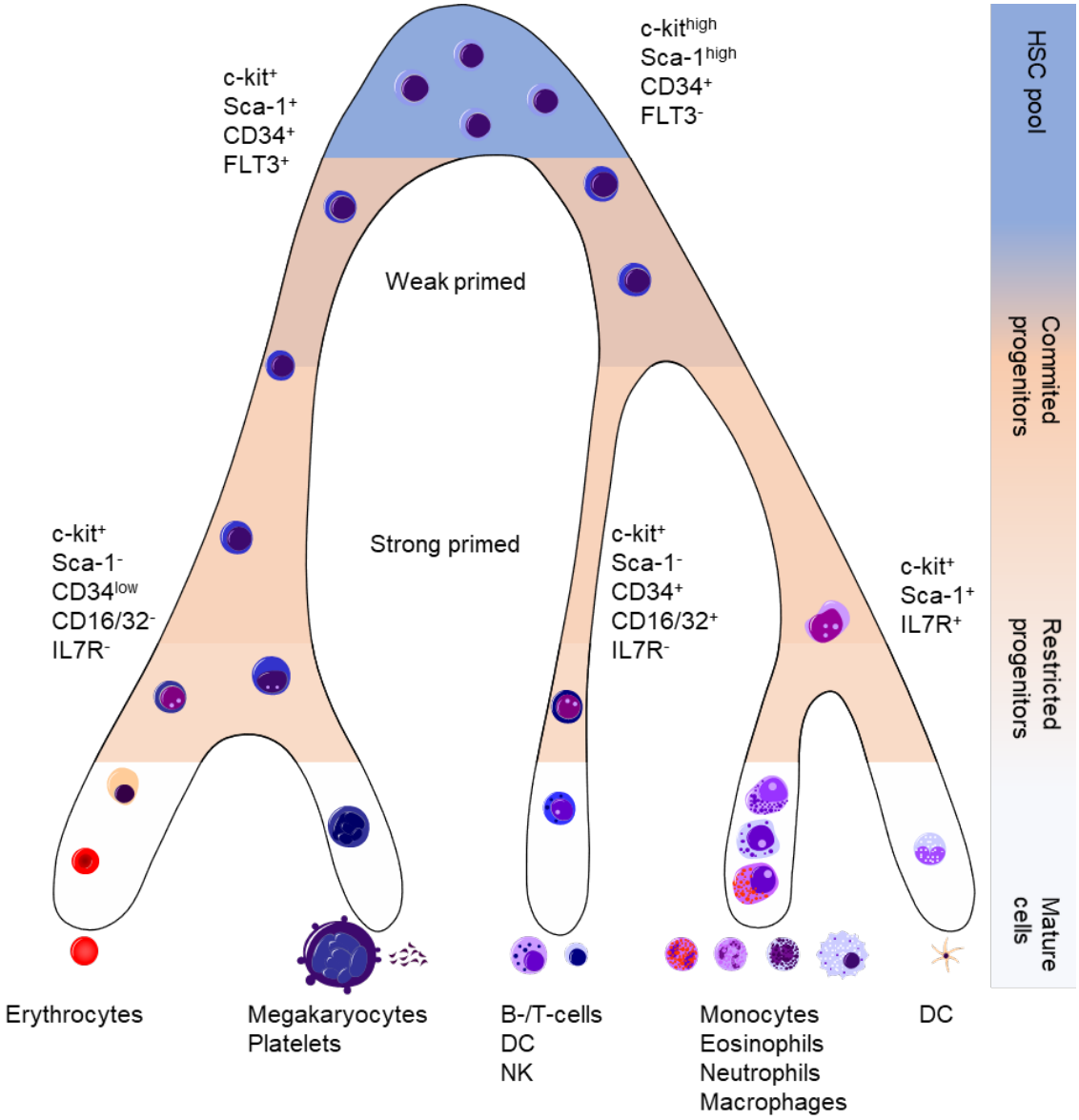

Figure 4: Visualization of the continuous hematopoiesis model.
Based on new single-cell RNA seq data, new models of hematopoiesis show a continuum of differentiation. A pool of LT- and ST-HSC with features of intermediate states differentiate first into committed progenitors to more restricted progenitors and finally matured cells. All fate decisions are defined by probabilities differentiating to a distinct mature cell rather than a definitive decision. Marker expression indicated at different stages does not reflect distinct stages of varying maturation stages but helps to make broad classifications. DC: dendritic cells, NK: natural killer cells. (Adapted from Laurenti & Göttgens, 2018)

1.2.3 Megakaryopoiesis

Megakaryocytes (Greek for large-nucleus cells) are the largest cells in the hematopoietic system, with a size up to 0.15 mm. In adults, they are primarily located in the bone marrow. They can be easily characterized by phase-contrast microscopy due to their size and the scattered polyploid nucleus, making them look like multinucleated cells. The primary biological function of megakaryocytes is the production of platelets. Platelets are small non-nucleated, disc-shaped fragments of the megakaryocytes' outer cell

membranes circulating in the blood system with a critical role in homeostasis, blood clotting, and inflammation (Behrens & Alexander, 2018).

Together with erythrocytes and macrophages, megakaryocytes are the first cells produced during embryonic development in humans, already starting in the fifth week of gestation (Fukuda, 1974, Figure 3). The fetal megakaryocytes differ in the way of differentiation, morphology, and function. They have a higher proliferative potential, are significantly smaller, show a lower ploidy and produce fewer platelets than their adult counterparts (De Alarcon & Graeve, 1996). Analysis of the cytoplasm showed that all components, like multiple α-granules and demarcation systems, are similar to adult megakaryocytes, including the expression of all surface markers (Ma et al., 1996). Fuchs et al. showed in a study from 2012 that in man of the age of two years more adult megakaryocytes are generated next to fetal ones. From four years onwards, the transition to adult megakaryopoiesis is completed (Fuchs et al., 2012).

Megakaryocytes emerge from HSC of the HSC pool, which differentiate subsequentially into MEPs, megakaryoblasts, pro-megakaryoblasts, and megakaryocytes, forming the proplatelets. During maturation, the ploidy and cell size increase due to an endomitosis called process, whereafter the proliferation potential is lost (Nimmo et al., 2015). Mature megakaryocytes develop a demarcation system for platelet production and migrate to the sinusoids in the bone marrow. Here, they release the proplatelets into the bloodstream, where they get separated into platelets by shear forces in the bloodstream (Junt et al., 2007, Figure 5).

In recent studies, this stringent model has been revised. In 2013 Sanjuan-Pla et al. identified platelet-biased LT-HSC and Notta et al. showed in 2016 that these primed megakaryocyte progenitor cells in the LT-HSC department could differentiate into megakaryocytes without the MEP step induced by inflammatory stress (Notta, 2016; Sanjuan-Pla, 2013).

Several cytokines and transcription factors regulate the process of differentiation of MEPs into fully matured megakaryocytes. Transcription factors are DNA binding proteins, activating, or repressing promotors and therefore regulating the gene expression. Many transcription factors have been identified during HSC differentiation into mature megakaryocytes, guiding the differentiation and maturation. The time- and dose-dependent expression of the transcription factors NF-E2 (transcription factor, nuclear factor, erythroid 2), EGF (epidermal growth factor), GATA1, GATA2, RUNX1 (runt-related transcription factor 1), TAL1/SCL (T-cell acute lymphocytic leukemia protein 1/ stem cell leukemia gene), and FLI1 (Friend leukemia integration 1 transcription factor),

to name a few of them, is critical for the differentiation of HSC into megakaryocytes (Noetzli et al., 2019). GATA1 marks the initial priming of HSC into the myeloid lineage (Arinobu et al., 2007) but is driving the erythroid commitment in later stages, whereas GATA2 is driving megakaryocyte commitment (Ikonomi et al., 2000). RUNX1 represses the erythrocyte transcription factor KLF1, the antagonist of megakaryocyte-specific transcription factor FLI1 (Kuvardina et al., 2015). SCL (also known as TAL1) regulates the NF-E2 expression essential for maturation and platelet production of megakaryocytes (McCormack et al., 2006).

Cytokines are proteins that regulate the growth and differentiation of cells. Thrombopoietin (TPO) is the primary regulator in megakaryopoiesis and essential for differentiation and maturation. The liver produces TPO, which binds to the myeloproliferative leukemia protein receptor MPL on megakaryocytes, stimulating the JAK-STAT pathway (janus kinase signal transducers and activators of transcription; Decker et al., 2018, Figure 8). Due to the internalization of TPO after binding to MPL, there is an inverse correlation between the platelet and megakaryocyte mass and the TPO plasma concentration. A high TPO concentration causes an increased stimulation of thrombopoiesis and, therefore, high clearance of TPO.

Other cytokines involved in megakaryopoiesis are the interleukins 3, 6, and 11 (IL-3, IL-6, and IL-11, respectively), leukemia inhibitory factor (LIF), the c-kit receptor binding stem cell factor SCF, and FLT3L. When combined, these cytokines enhance megakaryopoiesis and thrombopoiesis, but ablation experiments have shown that only TPO is essential for megakaryocytic differentiation (Behrens & Alexander, 2018).

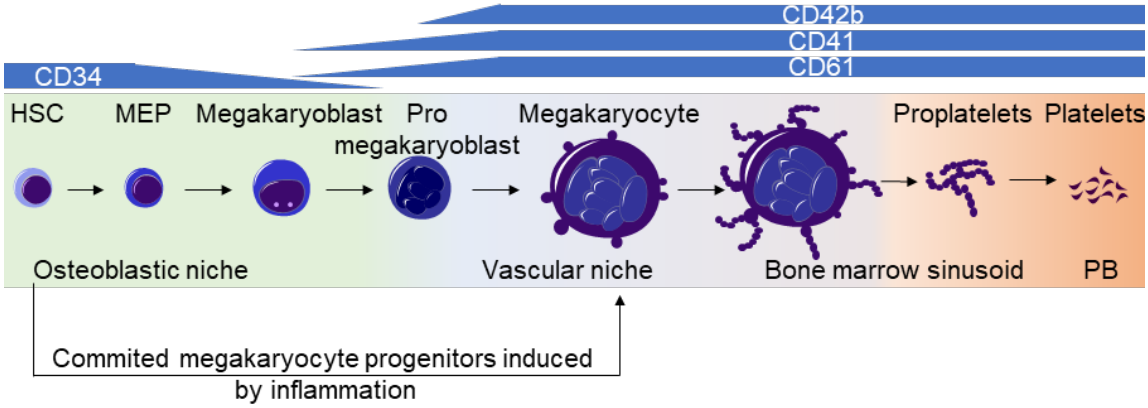

Figure 5: Schematic overview of megakaryopoiesis.
$CD34^+$ HSC differentiate in their osteoblastic niche subsequently into megakaryocyte erythrocyte progenitors (MEP), megakaryoblasts, pro megakaryoblasts, and megakaryocytes. This process resides in the vascular niche. With the onset of increasing ploidy, megakaryocytes become $CD41^+$, $CD42b^+$, and $CD61^+$ positive and lose the expression of CD34. Mature megakaryocytes start to form the demarcation system for the production of proplatelets. They migrate to the bone marrow sinusoid and release proplatelets into the peripheral blood (PB) stream. Here proplatelets separate into platelets due to shear forces. Committed megakaryocyte progenitors in the HSC pool can differentiate directly into megakaryocytes without the MEP step in stress situations like inflammation (adapted from Behrens & Alexander, 2018; Szalai et al., 2006).

1.2.4 The HSC niche and the role of MSC

The majority of blood cells are produced in the red bone marrow in bones of the spine, hip, shoulder, ribs, and skull. The hematopoietic stem cell niche concept was already conceived in 1978 but defining the exact localization took several years (Schofield, 1978). HSC are located in the perivascular niche, mainly adjacent to the sinusoidal blood vessel and arterioles and to the transition zone vessels (Crane et al., 2017; Kiel, 2005). The stem cell niche is composed of HSC surrounded by other cells with hematopoietic and non-hematopoietic origin maintaining the balance of quiescent, self-renewing, and differentiating cells by expressing several cytokines and chemokines and by direct cell-cell interactions. The cytokines identified as essential for maintaining the niche are SCF, CXCL12 (CXC-motif-chemokine 12), TPO, angiopoietin (ANGPT1), bFGF, and TGF-β (transforming growth factor β). A combination of different hematopoietic cells expresses these factors. Endothelial cells, perivascular cells, and especially mesenchymal stem/stromal cells (MSC) play a significant role in maintaining the hematopoietic stem cell niche (Crane et al., 2017; Kfoury & Scadden, 2015).

MSC are a heterogeneous group of multipotent progenitor cells with the potential to differentiate into osteoblasts, chondrocytes, myocytes, and adipocytes. They are located in different organs and tissues of the human body. MSC express the surface markers CD29, CD73, CD90, and CD105 (Dominici et al., 2006). Many studies have been conducted to separate and describe different MSC subpopulations in the HSC niche in recent years. Nestin positive MSC (Nes^+-MSC), GLI1 positive MSC ($GLI1^+$-MSC), Leptin receptor-positive MSC ($LepR^+$-MSC), and CXCL12 abundant reticular MSC (CAR-MSC) are just some of the characterized populations found in the stem cell niche (H. Gleitz et al., 2018). The exact function of these different subpopulations is still unclear and overlaps between these groups.

MSC do not only play a role in maintaining the stem cell niche. It was shown in several studies that in hematopoietic diseases and especially in bone marrow fibrosis, MSC lose their capacity to support the niche by differentiating, proliferating, and changing their cytokine expression (El Agha et al., 2017; H. Gleitz et al., 2020; Schneider et al., 2017). Altogether, understanding the HSC niche and blood homeostasis is complex. The knowledge of all components is critical for developing therapies and drugs for the treatment of hematopoietic diseases.

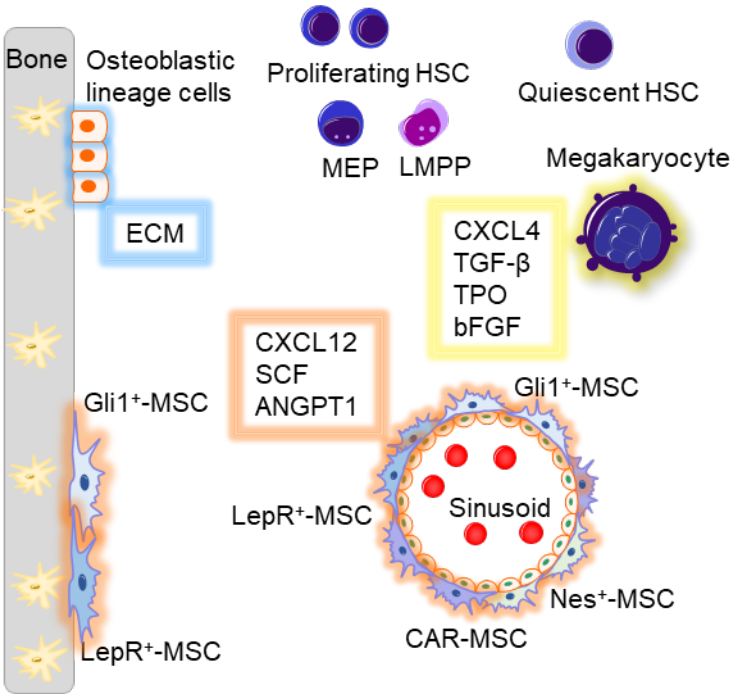

Figure 6: Schematic overview of the hematopoietic stem cell niche in the adult human bone marrow.
Simplified overview of the hematopoietic stem cell niche with a focus on different MSC subpopulations. MSC and osteoblastic lineage cells express cytokines and chemokines, maintaining the equilibrium of quiescent and proliferation of HSC, MEP, LMPP, and megakaryocytes (Adapted from Crane et al., 2017; H. Gleitz et al., 2020 and Kramann & Schneider, 2018).

1.2.5 Hematopoiesis in a dish

Since the early 2000s, several groups published protocols for the differentiation of hES cells (Eto et al., 2002; Kaufman et al., 2001) and applied them to iPS cells after their establishment in 2007 (Takayama et al., 2008; Ye et al., 2009). In general, two different approaches can be distinguished: (1) directed differentiation through the culture of iPS cells in a medium with specific cytokines (Liu et al., 2015) and (2) forced differentiation through the overexpression of transcription factors (Moreau et al., 2018). Also, the way how the cells are cultured and differentiated differs fundamentally in different protocols. Some protocols rely on an initial mesodermal differentiation with the help of EB, which form in ultra-low attachment plates, hanging droplets, or round-bottom 96-well plates (Zeevaert et al., 2020). Others differentiate cells as monolayers (Börger et al., 2016). Also, various protocols use co-cultures for the specific differentiation of HSC.

A common drawback of all protocols is that the differentiated hematopoietic cells often resemble cells from the primitive hematopoiesis, such as low nucleated megakaryocytes with less platelet production or erythrocytes with embryonic hemoglobin expression (Demirci & Tisdale, 2018). In addition, the efficiency of many differentiation protocols is still unsatisfying, especially for rare cell types like DC (Sontag et al., 2017). The lineage bias towards the myeloid and especially the erythroid lineage of some differentiation protocol also lowers the production of other cell types (Tursky et al., 2020).

To overcome problems in quantity, several groups established HSC differentiation protocols in bioreactors (Eicke et al., 2018; Thon et al., 2014). These could be an efficient way to produce platelets or erythrocytes for clinical purposes, but progress in effectivity must be made. The problems of differentiation efficiency towards specific cell types and the differentiation bias can be solved using forced forward reprogramming, helping to increase the production of the desired cell type (Moreau et al., 2018). However, it is questionable to what extent the overexpression of transcription factors reflects the *in vivo* situation. In addition, foreign DNA is inserted into the genome, which causes problems for a later possible clinical use.

1.3 Myeloproliferative neoplasms (MPN)

The term MPN covers several malignant chronic blood diseases of the myeloid lineage. In 2001 The World Health Organization (WHO) defined this term for the first time. Updates of the classification were published in 2008, 2014, and 2016. MPN can be divided based on the phenotype into classical MPN and non-classical MPN. The classical MPN include BCR-ABL positive chronic myeloid leukemia (CML) and BCR-ABL negative polycythemia vera (PV), essential thrombocythemia (ET), and primary myelofibrosis (PMF). The non-classical MPN consist of chronic neutrophilic leukemia (CNL), chronic eosinophilic leukemia (CEL), and unclassifiable MPN (Arber et al., 2016). The common characteristic for MPN is a driver mutation that activates proliferation pathways without an external stimulus by cytokines. These driver mutations result in increased counts of erythrocytes, megakaryocytes, granulocytes, and their progenitors. The first known mutation causing classical MPN was the BCR-ABL mutation (Nowell, 1962). A chromosome translocation between chromosomes 9 and 22 leads to a fusion protein of the ABL gene (or ABL1; for Abelson Murine Leukemia Viral Oncogene Homolog 1) and BCR gene (breakpoint cluster region gene) activating MAPK (mitogen-activated protein kinase) and STAT pathways. This causes a higher production of granulocytes (Melo & Barnes, 2007).

With the discovery of the JAK2 V617F mutation in 2005 (James et al., 2005), MPL mutation in 2006 (A. D. Pardanani, 2006), and CALR (calreticulin) mutation in 2013 (Klampfl et al., 2013; Nangalia et al., 2013), the drivers of the BCR-ABL negative MPN were identified. The three mutations have the same mechanism: the activation of JAK2 bound receptors without an external stimulus by cytokine binding and phosphorylation in downstream pathways.

In most cases, MPN are not induced by one single but by several earlier mutations. Frequently, DNA sequencing is performed when MPN patients already show symptoms

and this makes it difficult to identify and study these side mutations. Williams et al. showed in a whole-genome sequencing study from 2020 that first mutations can already occur in the uterus (Williams et al., 2020). Mutations in the DNA (cytosine-5)-methyltransferase 3A (DNMT3A) were acquired in the first weeks of gestation. Other typical driver mutations are located in additional sex combs-like 1 (ASXL1) or Tet methylcytosine dioxygenase 2 (TET2). Models show that a single mutation in a gene like DNMT3A takes 30 years to generate a clonal fraction of 1%. A combination of DNMT3A, TET2, and JAK2 mutated HSC causes doubling times of 200% per year instead (Williams et al., 2020). Furthermore, the combination of different mutations is crucial for choosing the correct therapy. A case report from Kiladjian et al. in 2010 showed that IFNα (interferon α) treatment of a JAK2 V617F TET2 mutated patient reduced numbers of JAK2 V617F mutated clones but did not affect the biclonal cells (Kiladjian et al., 2010).

1.3.1 JAK2 V617F

JAK proteins are nonreceptor tyrosine kinases associated with the cytoplasmic part of homodimeric cytokine receptors. In humans, there are four JAK proteins. JAK1-3 and tyrosine kinase 2 (TYK2) are ubiquitously expressed and involved in several crucial processes of embryogenesis, immune response, angiogenesis, and proliferation (Kisseleva et al., 2002).

The JAK proteins are composed of four functional domains illustrated in Figure 7: (1) The N-terminal FERM domain is involved in the linkage of the protein in the plasma membrane. (2) The SH2 domain allows the docking of other proteins. (3) The pseudokinase domain (JH2) is negatively regulating the kinase domain JH1 and regulates cytokine pathways due to ATP binding and autophosphorylation, and (4) the JH1 domain phosphorylates other proteins (E. Chen & Mullally, 2014).

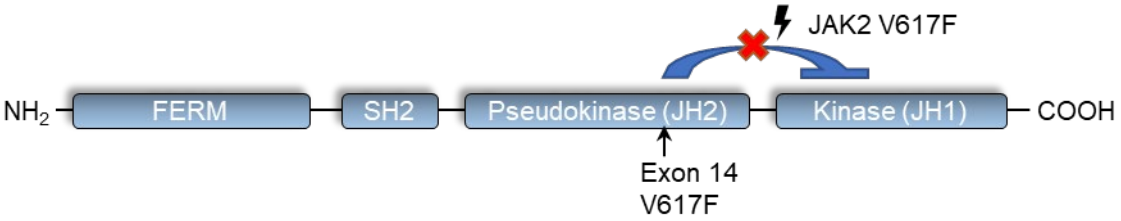

Figure 7: Structure of the JAK2 protein.
The JAK2 protein comprises 4 functional domains: the N-terminal FERM domain, the SH2 domain, the pseudokinase domain (JH2), and the kinase JH1 domain. The JAK2 V617F mutation can be found on exon 14 in the JH2 domain. Adapted from Chen & Mullally, 2014.

In 2005 James et al. discovered the JAK2 V617F point mutation (James et al., 2005). The somatic substitution of G to T in the hematopoietic lineage causes the replacement of valine (V) with phenylalanine (F) at the amino acid position 633. JAK2 V617F is a gain-

of-function mutation in the JH2 domain, which results in the constitutive phosphorylation of the protein, leading to activated downstream signaling (Gnanasambandan & Sayeski, 2011). The JAK2 V617F mutations is found in over 95% of PV patients and more than 50% of ET and PMF patients (Levine et al., 2007). The broad spectrum of different disorders caused by the JAK2 V617F mutation can be explained by the allelic burden and the function of JAK2 in various receptors of the hematopoietic pathway. PV is associated with the homozygote mutation of JAK2, whereas in ET, JAK2 is mutated heterozygous (Godfrey et al., 2012).

JAK2 is attached to the cytoplasmic part of the TPO receptor MPL, the erythropoietin receptor (EPOR), and the granulocyte-colony stimulating factor receptor (G-CSF-R). All these receptors play a role in myeloproliferation. MPL can also activate TYK2 (Shimoda et al., 1997) and G-CSFR JAK1 (Royer et al., 2005). Downstream, JAK2 is activating STAT1, STAT3, and STAT5, and the MAPK and PI3K/Akt (phosphoinositide-3-kinase/ RAC-alpha serine/threonine-protein kinase) pathway, leading to differentiation, proliferation, and angiogenesis. Due to the JAK2 mutation, these pathways stay activated even without the binding of cytokines and cell proliferation is enhanced. Malignant hematopoietic clones can cause myelofibrosis in later stages (E. Chen & Mullally, 2014, Figure 8).

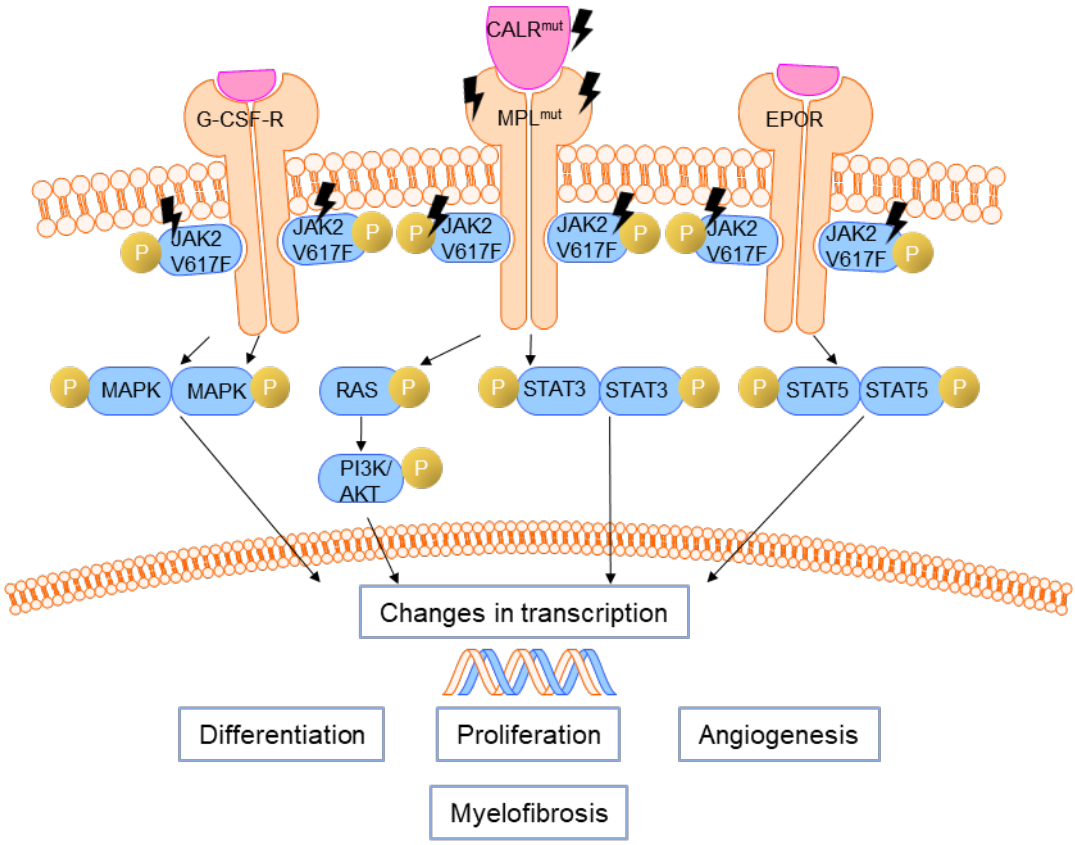

Figure 8: Alteration in the JAK2 signaling caused by mutations in JAK2, MPL, and CALR.

The JAK2 coupled receptors G-CSF-R, MPL, and EPOR get activated by mutations in CALR, MPL, and JAK2 even without stimulus by a binding cytokine. Due to the mutation, MAPK, PI3/AKT, and STAT pathways get activated, changing the transcription, and causing differentiation, proliferation, and angiogenesis. This can also cause myelofibrosis in later stages. The flashes indicate the mutated proteins. (Adapted from Levine et al., 2007 and Vainchenker & Kralovics, 2017)

1.3.2 Polycythemia vera (PV)

PV is one of the BCR-ABL$^-$ classical MPN characterized by a high erythrocyte production without physiological stimulus. In over 98% of PV, a mutation of the JAK2 tyrosine kinase is the main trigger. Besides the higher erythrocyte level in the blood, increased blood viscosity, increased hematocrit and hemoglobin levels, lower EPO concentrations in blood serum, and higher leukocyte and thrombocyte counts are common clinical symptoms in early disease stages. In later stages, thrombosis, strokes, myocardial infarctions, and an enlarged spleen can be observed additionally in PV patients (Levine et al., 2007).

PV itself causes only a modest reduction of life span, mostly connected to thrombosis events. A small number of PV cases can develop into acute myeloid leukemia (AML) or myelofibrosis. The reason and mechanism are still not understood completely.

Although there is no cure for PV, some therapies have been developed that expand the life span of patients. Phlebotomy to reduce the hematocrit level and blood viscosity and a low dosage of acetylsalicylic acid to reduce the thrombosis risk are first therapies. In progressive PV, hydroxyurea, IFNα, and the JAK2 inhibitor ruxolitinib are applied. The application of imatinib and other JAK2 inhibitors is also discussed. (Shallis & Podoltsev, 2021).

1.3.3 Myelofibrosis in MPN

Myelofibrosis is characterized by the deposition of fibers in the bone marrow replacing hematopoietic tissue. It is a clonal malignant disease of dysregulated HSC caused by mutations in the JAK2 pathway resulting in abnormal proliferation and cytokine expression. Myelofibrosis can develop either as PMF or secondarily from PV or ET, also referred to as secondary myelofibrosis. Changes in the bone marrow go hand in hand with splenomegaly because blood production is outsourced to the spleen (Tefferi, 2021). Apart from an allogenic stem cell transplantation, no cure is available so far. JAK2 inhibitors like ruxolitinib show promising results, but they only comb the symptoms and slow down disease progression. Clinical studies searching for effective drugs are ongoing. Treatment with IFNα was shown to reduce anemia in over 50% of patients (Ianotto et al., 2018) and Imide, like thalidomide, are especially effective in patients with

TET2 mutation (Schlenk et al., 2017). Furthermore, clinical studies are performed targeting the mTOR (mammalian target of rapamycin) pathway. Telomerase inhibitors are currently under investigation, and new JAK2 inhibitor studies are conducted (Guglielmelli et al., 2011; A. Pardanani et al., 2015; Mesa et al., 2017). Crucial for therapy response is not only the JAK2, CALR, or MPL mutation but also further driver mutations like ASXL1 or TET2 influencing the efficacy of treatment.

Extensive research is needed to understand mechanisms developing fibrosis to find new therapeutic targets. It is still unknown which factors drive the progression from ET or PV to MF. Also, for PMF, early disease progression remains unclear as symptoms are occurring when disease progression is already advanced.

Recent studies using mouse bone marrow fibrosis models gave mechanistic insights into the effectors of myelofibrosis. A murine model of MPN showed that dysregulated malignant HSC differentiate into malignant megakaryocytes and cause inflammatory processes in the bone marrow niche, which dysregulates and damages Nes^+-MSC accelerating the MPN phenotype (Arranz et al., 2014). In consequence, Nes^+-MSC are not driving fibrosis but contribute to disease progression. In 2017 two studies were published using fate trace experiments in mouse MPN models to identify the fibrosis-driving cells. They identified $GLI1^+$-MSC and $LepR^+$-MSC as critical players in fibrosis progression (Decker et al., 2018; Schneider et al., 2017). MSC get stimulated and activated by malignant HSC, which show an upregulation in cytokines and chemokines like CXC motif ligand 4 (CXCL4, also known as platelet factor 4 (PF4)), TGF-β, TPO, bFGF, and inflammatory cytokines like IL-6. These lead to proliferation and differentiation of the $GLI1^+$-MSC and $LepR^+$-MSC, which lose their supportive function of the niche and differentiate into ECM producing myofibroblasts (Figure 9). They also change their cytokine profile, upregulate CXCL4, produce reactive oxygen species (ROS), and downregulate CXCL12, SCF, and ANGPT1. Those processes accelerate fibrotic transformation (Decker et al., 2018; Schneider et al., 2017).

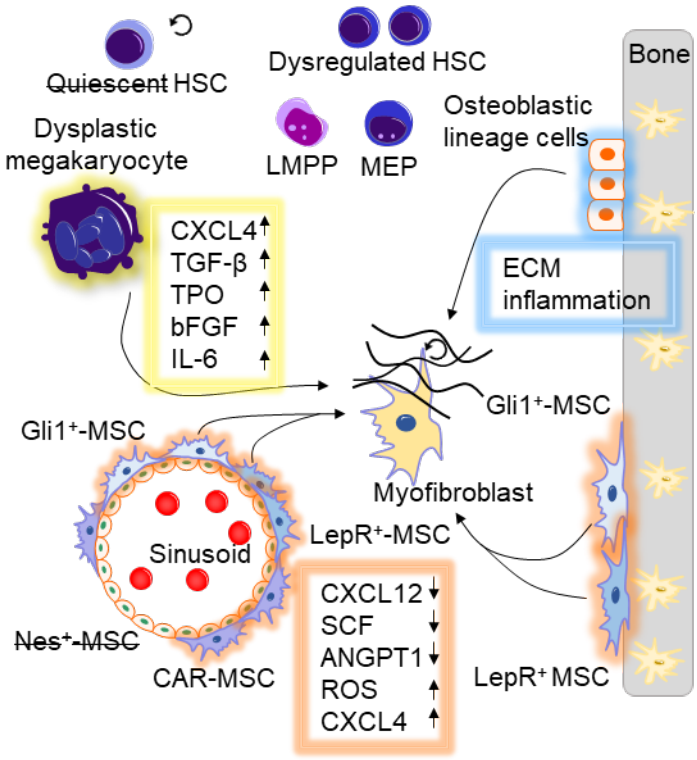

Figure 9: HSC niche in fibrotic state.
Due to MPN driver mutations like JAK2, CALR, or MPL, HSC are dysregulated and differentiate into malignant megakaryocytes with changes in their expression profile. Upregulation of CXCL4, TGF-β, TPO, bFGF, and inflammatory cytokines like IL-6 causes the loss of Nes$^+$-MSC and activation of GLI1$^+$- and LepR$^+$-MSC. CXCL12, SCF, and ANGPT1 are downregulated, CXCL4 is upregulated, and more ROS are produced. The different cytokine expression in the niche also activates quiescent HSC and MSC differentiating into myofibroblasts, producing ECM proteins. (Adapted from Crane et al., 2017; H. Gleitz et al., 2020 and Kramann & Schneider, 2018).

1.4 Characteristics and function of CXCL4 and CXCL4L1

CXCL4 and CXCL4 like 1 (CXCL4L1), both located in chromosome 4 in a genomic section harboring several other CXCL proteins (Figure 10A/B), are proteins from the CXC motif chemokine group characterized by four cysteines. The first two cysteines are separated by any amino acid "X", followed by 24 amino acids until the third cysteine and 15 amino acids between the third and fourth cysteine. CXCL4 and CXCL4L1 have three exons: a non-coding regulating region, a signaling domain, and the mature protein domain. CXCL4 is encoded on the reverse strand, CXCL4L1 on the forward strand (Figure 10C, Van et al., 2014).

CXCL4 is mainly produced by megakaryocytes. It is stored as homotetramers bound to chondroitin sulfate during maturation in α-granules of the shedding platelets. After platelet activation (e.g., by thrombin), CXCL4 is released in response to protein kinase C. It promotes blood coagulation and accumulates at the site of inflammation. Moreover, it locally enhances the immune response and plays a role in several inflammatory diseases such as atherosclerosis or rheumatoid arthritis (Vrij et al., 2000).

CXCL4 acts by binding to the chemokine receptor CXCR3A and CXCR3B (CXC-motif-chemokine receptor 3 A/B) and interacts with chondroitin sulfate and glycosaminoglycans. Also, the binding to several chemokines like CXCL12, bFGF, and VEGF is described (Carlson et al., 2013). Besides megakaryocytes, CXCL4 is produced by monocytes, activated T-cells, and microglia (Schaffner et al., 2005). CXCL4 inhibits

the proliferation of T-cells (Fleischer et al., 2002), promotes monocyte survival and macrophage activation (Scheuerer et al., 2000), and induces the differentiation of monocytes to more mature DC with increase responsiveness (Ran et al., 2013).

In murine experiments, it was shown that CXCL4 is the main effector in myelofibrosis and that ablation of CXCL4 reduces fibrosis. Moreover, it was demonstrated that the expression of CXCL4 directly correlates with the severity of the disease and can be used as an early myelofibrosis marker (Gleitz et al., 2020; Schneider et al., 2017). If these observations reflect the human situation is still not clear.

A variant of CXCL4 in humans, the nonallelic variant CXCL4L1 (also PF4var1; PF4V1), was first described in 1989 (Green et al., 1989). CXCL4 and CXCL4L1 differ only in three amino acid residues of the mature protein. These changes reside in the C-terminus of the protein: Pro58 → Leu, Lys66 → Glu, Leu67 → His (Ruytinx et al., 2018, Figure 10D). Similar to CXCL4, CXCL4L1 can interact with the CXCR3A and CXCR3B and affects monocytes and T-cells. In contrast to CXCL4, CXCL4L1 is synthesized and secreted constitutively by platelets but also smooth muscle cells, T-cells, and others (Lasagni et al., 2007). The angiostatic effect of CXCL4L1 is higher than in CXCL4 (Kuo et al., 2013) and the interaction with VEGF and bFGF is less pronounced (Carlson et al., 2013). In 2019 Zhang et al. hypothesized that CXCL4L1 also plays a role in cancer, as the downregulation of CXCL4L1 serum level was correlated with poor prognosis in prostate cancer (Zhang et al., 2019). The role of CXCL4L1 in myelofibrosis remains unclear, since most of the studies were performed in mouse models, where the variant does not exist. Also, the blood level of CXCL4L1 in myelofibrosis patients was not included in studies so far.

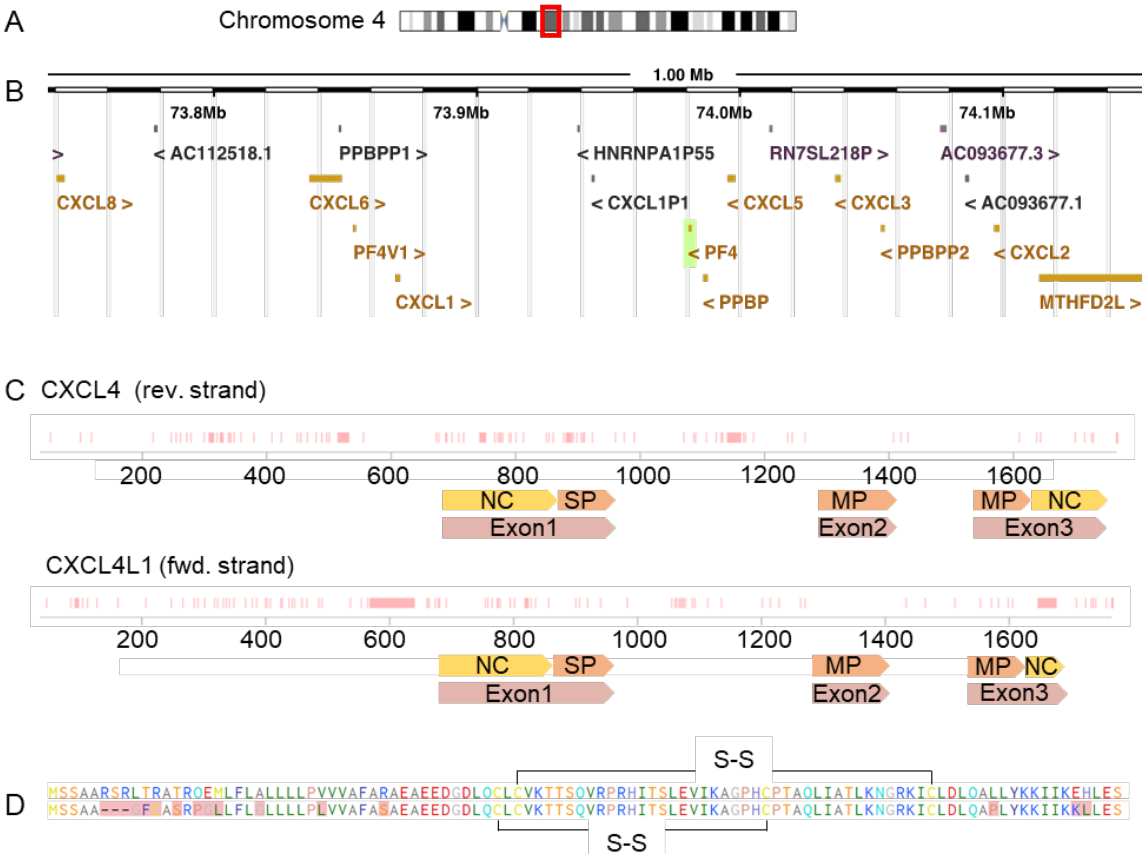

Figure 10: Gene locus of CXCL4 and CXCL4L1.
(A) Schematic representation of the CXCL4 and CXCL4L1 locus on human chromosome 4. **(B)** Schematic representation of the CXC gene cluster on chromosome 4q. **(C)** Schematic representation ot the CXCL4 and CXCL4L1 gene structure. Red bars show differences in base pairs between CXCL4 and CXCL4L1. NC: noncoding, SP: signal protein, MP: mature protein. **(D)** Aminoacid sequence of CXCL4 (top) and CXCL4L1 (bottom). Red marked amino acids are different in CXCL4 and CXCL4L1.

1.5 CRISPR/Cas9

Genome editing and genomic engineering hold enormous potential for applications in basic science, biomedicine, and biotechnology. Meganucleases, Zink finger, and TALE proteins have been widely used in science for genome editing in the past decades. However, these systems present drawbacks in applicability, costs, efficiency, and duration that hampers its broad application. In 2012, Emmanuelle Charpentier and Jennifer Doudna published one of the first papers on the CRISPR (Clustered Regularly Interspaced Short Palindromic Repeats)/Cas9 system for efficient genome editing, which revolutionized the field (Jinek et al., 2012). The CRISPR system derives from the prokaryote adaptive immune system to protect bacteria from foreign nucleic acids, such as viruses and bacteriophages (Horvath & Barrangou, 2010)

In 1987, Ishino et al. identified in the bacterial strain Escherichia coli K12 a repetitive sequence of 29 nucleotides interrupted by variable regions of 32 nucleotides (Ishino et

al., 1987). In the following decades, others described these repeating regions in different prokaryotes, like bacteria and archaea. In 2007 Barrangou and colleagues showed that bacteria infected with phages can integrate parts of foreign DNA as spacers into the CRISPR regions of their genome and develop immunity against the phages (Barrangou et al., 2007). It took five more years to describe a method to use CRISPR for gene editing as we know it today.

The defense mechanism against foreign nucleic acids in prokaryotes proceeds as followed: in the first contact with a pathogen, foreign DNA is cleaved by the Cas protein in short 20 bp sequences, which are inserted into a CRISPR array sequence, the protospacer. This locus is transcribed into a pre-CRISPR RNA (pre-crRNA). The Cas9 protein processes the pre-crRNA into mature crRNA containing the spacer sequence, which is derived from the foreign DNA and is flanked by adjacent repeat motifs for the binding of the Cas protein. In a second contact with the same DNA, the crRNA can bind specifically to the foreign DNA and guide the Cas9 endonuclease to inactivate the invading genetic material by cleaving it (Horvath & Barrangou, 2010, Figure 11A).

For this recognition, the targeted sequence must be followed by the Protospacer Adjacent Motif (PAM) sequence, where the Cas9 protein binds. This PAM sequence consists of two to six bases specific for different prokaryotic species. As these PAM sequences do not occur in the prokaryotic genome, it is an essential targeting component that discriminates own DNA from invading DNA. The most used PAM sequence is the NGG sequence from *Streptococcus pyogenes,* where N is any nucleotide and G stands for guanine (Horvath & Barrangou, 2010).

The Alt-R® CRISPR-Cas9 system was developed by Integrated DNA Technologies (IDT, Coralville, IA, USA) based on the *S. pyogenes* CRISPR-Cas9 to optimize genome editing for producing on-target double-stranded DNA breaks (Vakulskas et al., 2018). The 2-part system combines the optimized shortened target-specific CRISPR RNA (crRNA, with 36 nt: 20 nt target-specific protospacer region, along with the 16 nt tracrRNA fusion domain) and the oligonucleotide with an optimized shortened trans-activating crRNA (tracrRNA) oligonucleotide (67 nt, Figure 11). The gRNA complex formation and the ribonucleoprotein complex (RNP) formation are performed manually in the lab and then delivered into cells (Figure 11B).

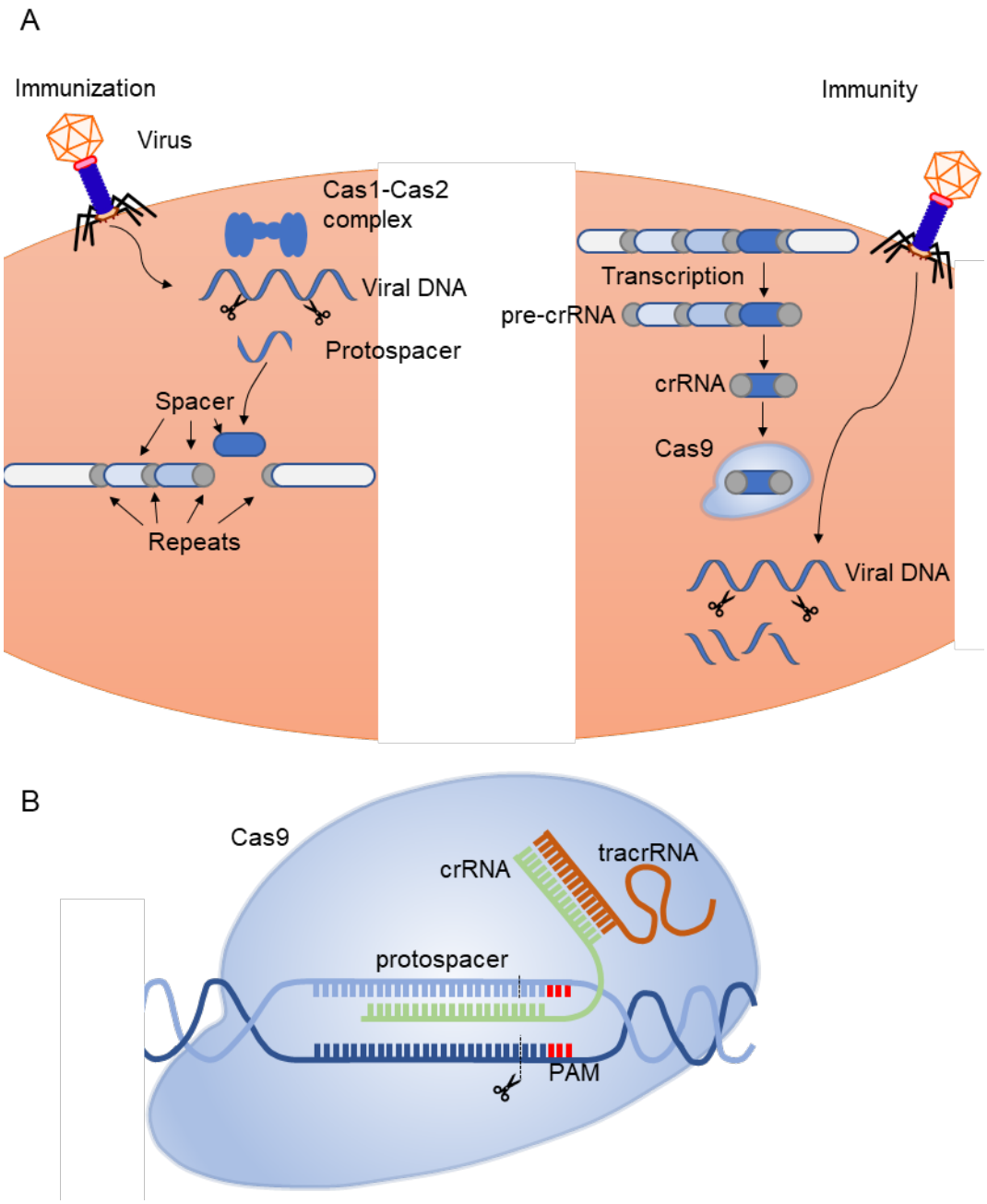

Figure 11: The CRISPR/Cas9 system in bacteria and clinical application.
(A) Mechanism of the CRISPR immune response in bacteria: foreign DNA is recognized by the Cas1/Cas2 complex, cleaved, and the protospacer is integrated into the CRISPR sequence. By the second contact, the preRNA is transcribed. The mature crRNA complexes with the Cas9 protein and cleaves the invading DNA. (Adapted from Horvath & Barrangou, 2010). **(B)** ALT-R system from IDT. The complexed crRNA:tracrRNA complexes with the Cas9 protein cleaving the genomic DNA. (Adapted from IDT).

1.6 Aims and objectives

This thesis aims by (i) using the CRISPR/Cas9 technology to repair the JAK2 V617F mutation in iPS cells and to generate a functional CXCL4 knockout, (ii) establishing a protocol for the efficient generation of iPS cell-derived megakaryocytes, (iii) dissecting the effect of the JAK2 V617F mutation on megakaryocytic development, and (iv) using MSC and megakaryocytes for the establishment of a co-culture model to dissect the role of the megakaryocyte MSC crosstalk in myelofibrosis development and fibrosis progression.

Myelofibrosis can arise as PMF or as a secondary disease developed from other MPN such as PV. The switch from PV to myelofibrosis is poorly understood and has been studied mainly in murine models. To investigate the underlying mechanisms of PV transformation into myelofibrosis, we use a patient-specific iPS cell model derived from PV patients with a JAK2 V617F mutation. We use the CRISPR/Cas9 technology to extend our clone set by generating: (i) the missing JAK2 V617F genotypes to obtain JAK2 unmutated, JAK2 V617F^{het,} and JAK2 V617F^{hom} clones from the same patient and (ii) a functional knockout of CXCL4, a putative effector of myelofibrosis.

These iPS cells are used for the differentiation into megakaryocytes and MSC to establish a co-culture model. As a control, BM-MSC from healthy donors will also be used in the co-culture. Furthermore, we dissect the role of the JAK2 mutation in megakaryocytes with different assays like kinetics studies, flow cytometry analysis, CFU-assays, and RNA-Seq analysis.

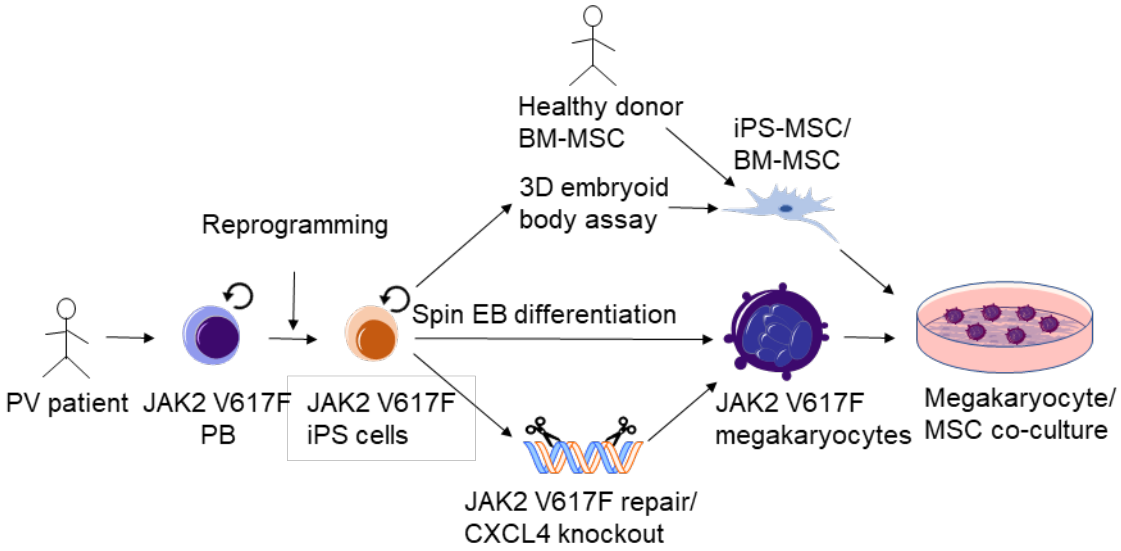

Figure 12: Schematic representation of the aims and objectives.
iPS cells bearing the JAK2 V617F mutation are generated from PV patients and used to differentiate into megakaryocytes and MSC. CRISPR/Cas9 is used to repair the JAK2 V617F mutation and to generate a functional CXCL4 knockout. The generated megakaryocytes and MSC are then used for the establishment of a co-culture model. PB: peripheral blood, BM: bone marrow.

2 Materials and methods

2.1 Cell culture

If not described otherwise, cell culture work was performed under sterile conditions in a laminar flow hood. Cells were cultured in a Heracell incubator in a humidified atmosphere with 5% CO_2 at 37ºC (both Heraeus, Hanau, Germany). Cells were grown on tissue plastic dishes (TPP, Trasadingen, Switzerland) and disposable plasticware like falcon tubes and pipettes were from Becton Dickinson (Franklin Lake, NJ, USA). The Heraeus Megafuge 16 (Thermo Fisher Scientific, Waltham, MA, USA) was used for centrifugation steps with falcon tubes, 96-well plates, and flow cytometry tubes were centrifuged with the Heraeus Multifuge 3L (Heraeus).

Cells were daily monitored on the Leica DM IL microscope (Leica Microsystems, Wetzlar, Germany), phase contrast pictures, and colony picking was performed with the digital inverted EVOS® FL microscope (Thermo Fisher Scientific). Cells were counted with a Neubauer chamber and trypan blue for dead cell exclusion (Sigma Aldrich, St. Louis, MO, USA).

All cells were cryopreserved in 90% FCS (Thermo Fisher Scientific) and 10% dimethyl sulfoxide (DMSO, Sigma Aldrich), stored one day at -80ºC, and then transferred to liquid nitrogen for long-term storage. For thawing, cells were incubated for a few minutes in the water bath at 37ºC and washed with 9 ml KnockOut™-DMEM (KO-DMEM, Thermo Fisher Scientific). After centrifugation at 350 g for 4 min, the supernatant was discarded, and the cells were seeded in the respective medium and conditions.

2.1.1 Reprogramming of monocytes into iPS cells

All iPS cell lines described in this thesis were reprogrammed from peripheral blood mononucleated cells (PBMNC) isolated by Ficoll (2.1.10). The cells were cultured for 2-3 days in StemSpan™ SFEM medium (Stemcell Technologies, Vancouver, Canada) supplemented with SCF (supernatant of SCF secreting stable transfected CHO KLS C6 cells), TPO (Miltenyi Biotech, Bergisch Gladbach, Germany), FLT3L (Peprotech, Rocky Hill, NJ, USA) and hyper-IL6 (IL-6/soluble IL-6 receptor fusion, kindly provided by Dr. Stefan Rose-John, Institute of Biochemistry, Christian-Albrechts University, Kiel, Germany (Fischer et al., 1997)), further referred to as HSC medium. The Cyto-Tune™-iPS Sendai Reprogramming Kit (Thermo Fisher Scientific) was used according to the manufacturer's protocol to reprogram the cells. The virus particles containing OCT4,

KLF4, c-Myc, and SOX2 were mixed 1:1. $5x10^5$ cells were incubated in 270 µl HSC medium with 40 µl of the Sendai virus mix for 48 h.

Four days later, the cells' formed grape-like structures were transferred on a MEF layer in HSC medium. During the following medium changes, the HSC medium was replaced stepwise by iPS medium (Table 2) and the cells were cultured for two weeks with daily medium change. When the colonies reached the right size, colonies were picked, and the remaining colonies were harvested in bulk and cryopreserved. The iPS cell generation was achieved in collaboration with S. Sontag; Ph.D., C. Küstermann; Ph.D., and M. A. S. de Toledo, Ph.D., Institute for Biomedical Engineering, Department of Cell Biology, RWTH Aachen University, Medical School, Aachen, Germany.

2.1.2 Generation and irradiation of MEF

MEF are used as feeder-layer for the culture of iPS cells. MEF were generated by sacrificing CD1 mice embryos on embryonic day 13.5. The uterus was opened, and embryos were extracted from the fetal bag. The placenta, head, limbs, and inner organs were removed, the carcasses were collected and cut into tiny pieces. The hashed corpses were incubated five times with 0.05% Trypsin/EDTA (Thermo Fisher Scientific) for 4 min at 37ºC to generate a single-cell suspension. Finally, the cell suspension was centrifuged (350 g, 4 min) and the supernatant was discarded. The MEF were resuspended in MEF medium (Table 1) and seeded on 15 cm dishes coated with gelatin (2.5 embryos per plate). The medium was exchanged every second day and the cells were split and expanded twice before inactivation by γ-Irradiation with 30 Gy (30 grey, performed by Transfusion Medicine, RWTH Aachen University Hospital, Aachen, Germany). The cells were cryopreserved at a concentration of $4x10^6$ cells per cryovial.

Table 1: MEF medium composition.

Reagent	Volume		Company
High glucose DMEM	440	ml	Thermo Fisher Scientific
FCS	50	ml	Thermo Fisher Scientific
Penicillin/streptomycin (5,000 U/ml)	5	ml	Thermo Fisher Scientific
L-glutamine (200 mM)	5	ml	Thermo Fisher Scientific

2.1.3 Culture of iPS cells

The iPS cell culture on inactivated MEF monolayer was performed with iPS medium (Table 2). The medium was exchanged daily, and cells were passaged every 5-6 days. The day before passaging, MEF were seeded on gelatin-coated 6-well plates at a cell

density of 300,000 cells/cm^2. For passaging the iPS cells, the old medium was discarded, cells were washed once with PBS and collagenase type IV (both Thermo Fisher Scientific) was added to each well. Cells were incubated for 45-60 min at 37°C until the colonies' rim started to detach. Cells were rinsed twice with 2 ml KO-DMEM, and cell clumps were collected in a 15 ml falcon. The supernatant was discarded after sedimentation and cell clumps were resuspended in 1 ml iPS medium. Medium on the MEF coated plates was aspirated, and MEF were washed once with PBS. 2 ml of iPS medium per well was added and the iPS cell clumps were equally distributed in a ratio of 1:6.

Table 2: Composition of iPS medium for iPS cell culture on MEF-feeder.

Reagent	Volume		Company
KO-DMEM	384	ml	Thermo Fisher Scientific
KnockOut™ serum replacement (KO-SR)	50	ml	Thermo Fisher Scientific
Penicillin/streptomycin (5,000 U/ml)	5	ml	Thermo Fisher Scientific
L-glutamine (200 mM)	5	ml	Thermo Fisher Scientific
Non-essential amino acids solution (100x)	5	ml	Thermo Fisher Scientific
β-mercaptoethanol (stock 50 mM)	1	ml	Thermo Fisher Scientific
bFGF (stock 100 µg/ml)	50	µl	Peprotech

For feeder-free culture, iPS cells were cultured on Matrigel™ (Corning, New York, NY, USA) coated plates in StemMACS™ iPS Brew XF (iPS Brew, Miltenyi Biotech). Matrigel was diluted in KO-DMEM according to the batch-dependent manufacturer protocol. 1 ml KO-DMEM Matrigel mix was used to coat one well on a 6-well plate. For passaging, cells were washed once with PBS and incubated with 0.5 mM EDTA (Thermo Fisher Scientific) for splitting in colonies. After 3 min incubation at RT, EDTA was discarded, and cells were washed twice with PBS. Cells were detached by pipetting carefully with 1 ml iPS Brew per well and seeded 1:6 in freshly coated Matrigel plates.

For single-cell splitting, Accutase (PAN-Biotech, Aidenbach, Germany) was incubated for 4 min at 37ºC. Cells were detached with 2 ml KO-DMEM and centrifuged for 4 min at 350 g. The supernatant was discarded, the cells were resuspended in 1 ml iPS Brew and counted with a Neubauer counting chamber. Cells were seeded in a density of 100,000 per well on a 6-well plate with 1:1000 Y-27632 (Abcam, Cambridge, UK) on a freshly coated Matrigel plate.

2.1.4 EB assay

iPS cells were cultured for 2-3 passages on a MEF layer until confluency of over 70%. Cells were incubated for 10-15 min with 1 U/ml dispase (Stemcell Technologies) and washed twice with KO-DMEM. Cells were detached and sedimented as big clumps in a falcon tube, transferred to suspension culture plates in EB medium, and cultured for 6 days, changing medium and detaching the forming EB every second day. On day 6, cells were seeded on gelatin-coated dishes and cultured for 8 more days with EB medium, generating a heterogeneous layer. On day 14, cells were washed once with KO-DMEM and incubated for 4 min with 0.05% Trypsin/EDTA and detached, rinsing them with KO-DMEM. Cells were centrifuged and replated von gelatin-coated glass coverslips (Thermo Fisher Scientific) for 3 days. Afterward, immunostaining for germ layer-specific markers was performed (2.7.1).

Table 3: Composition of EB medium.

Reagent	Volume		Company
IMDM (Iscove's Modified Dulbecco's Media)	19	ml	Thermo Fisher Scientific
FCS	3.75	ml	Lonza (Basel, Switzerland)
Protein-free hybrodoma medium	1.25	ml	Thermo Fisher Scientific
Penicillin/streptomycin (5,000 U/ml)	250	µl	Thermo Fisher Scientific
L-glutamine (200 mM)	250	µl	Thermo Fisher Scientific
β-mercaptoethanol (stock 50 mM)	50	µl	Thermo Fisher Scientific
L-ascorbic acid (10 mM)	25	µl	Sigma Aldrich

2.1.5 Differentiation of iPS cells into iPS-MSC

For differentiation of iPS cells into iPS-MSC, the EB assay (2.1.4) was performed until day 6. After transferring the cells to gelatin-coated plates by detaching them with 0.05% trypsin/EDTA, MSC medium was used (Table 4). The medium was changed every third day and cells were passaged every seventh day by washing the cells once with PBS and incubating them for 4 min with 0.05% Trypsin/EDTA at 37ºC. Cells were washed with MSC medium, centrifuged, and seeded on a fresh gelatin-coated 6-well plate with 300,000 cells/well. Cells were finally differentiated after 35 days and flow cytometry measurements were performed with CD29, CD73, CD90, CD105 as positive MSC markers and CD45, CD34, CD31 as negative MSC markers (2.4).

Table 4: MSC medium composition.

Reagent	Volume		Company
Low glucose DMEM	480	ml	Thermo Fisher Scientific
FCS	10	ml	Lonza
Penicillin/streptomycin (5,000 U/ml)	5	ml	Thermo Fisher Scientific
L-glutamine (200 mM)	5	ml	Thermo Fisher Scientific

2.1.6 Isolation of BM-MSC

BM-MSC were isolated from human hip bone from endoprosthesis operations under sterile conditions under a flow hood. The bone was vortexed in PBS for 1 min at maximum speed in a urine beaker, the liquid was collected with a perfusion syringe and used for flushing the spongiosa of the bone multiple times. The liquid was collected in a 50 ml falcon and the flushing was repeated with fresh PBS five times. Cells were collected by centrifugation at 500 g for 10 min. The supernatant was discarded, cell sediment was washed with 10 ml PBS and centrifuged again. The supernatant was discarded, and the cells were resuspended in 30 ml MSC medium and divided into 3xT75 flasks. The next day, medium was changed, and the attached cells were washed twice gently with PBS. Medium change was performed twice a week until cells were reaching confluency. Splitting of the cells was performed, washing the cells once with PBS and incubating them with 0.05% Trypsin/EDTA for 4 min at 37ºC. After washing and centrifugation, cells were seeded at 5,000 cells/cm^2. After two passages, BM-MSC were cryopreserved.

2.1.7 Differentiation of MSC into adipogenic and osteogenic lineage

For the osteogenic and adipogenic differentiation, 10,000 iPS-MSC per well were seeded in MSC medium on a 12-well tissue culture plate. After reaching confluency of 60-70%, the medium was switched to osteogenic or adipogenic differentiation medium, respectively (Table 5 and Table 6) and cells were cultured for three more weeks changing the medium twice a week. The staining was performed according to 2.7.4.

Table 5: Osteogenic differentiation medium composition.

Reagent	Volume		Company
Low glucose DMEM	212.5	ml	Thermo Fisher Scientific
FCS	25	ml	Lonza
Penicillin/streptomycin (5,000 U/ml)	2.5	ml	Thermo Fisher Scientific
L-glutamine (200 mM)	2.5	ml	Thermo Fisher Scientific
Dexamethasone (100 µM)	0.25	ml	Sigma Aldrich
L-ascorbic acid-2-PO_4 (10 mM)	5	ml	Sigma Aldrich
β-glycerophosphate (1 M)	2.5	ml	Sigma Aldrich

Table 6: Adipogenic differentiation medium composition.

Reagent	Volume		Company
High glucose DMEM	43.4	ml	Thermo Fisher Scientific
FCS	5	ml	Lonza (Basel, Schweiz)
Penicillin/streptomycin (5,000 U/ml)	0.5	ml	Thermo Fisher Scientific
L-glutamine (200 mM)	0.5	ml	Thermo Fisher Scientific
Dexamethasone (100 µM)	0.5	ml	Sigma Aldrich
3-isobutyl-1-methylxantine (0.5 M)	0.05	ml	Enzo Life Science (Lörrach, Germany)
Insulin (10 mg/ml)	0.05	ml	Sigma Aldrich
Indometacin (50 mM)	0.1	ml	Sigma Aldrich

2.1.8 Differentiation of iPS cells into megakaryocytes and HSC

For differentiation of iPS cells into megakaryocytes and HSC, a modified spin EB based protocol from a publication by Liu et al. was used (Figure 13, Liu et al., 2015). On day 0, 80% confluent iPS cells on Matrigel were incubated and detached for 4 min with 37°C prewarmed Accutase and washed twice with 3 ml prewarmed KO-DMEM. Cells were counted with the Neubauer chamber and seeded in a 96-well round-bottom plate at a density of 3,000 cells/well in serum-free medium (SFM, Table 7) with Y-27632 (10 µM), bFGF (10 ng/ml), BMP4 (10 ng/ml, Miltenyi Biotech), Transferrin (6 µg/ml, Sigma Aldrich), and L-ascorbic acid (50 µg/ml). The plate was centrifuged for 5 min at 350 g.

Table 7: Serum-free medium (SFM).

Reagent	Volume		Company
IMDM	38	ml	Thermo Fisher Scientific
Ham's F-12	38	ml	Thermo Fisher Scientific
BSA (for cell seeding)	2	ml	House made
Human albumin (starting on day 2)	2	ml	Grifols, Barcelona, Spain
Chemical defined lipid concentrate	0.8	ml	Thermo Fisher Scientific
GlutaMAX	0.8	ml	Thermo Fisher Scientific
1-thioglycerol	0.32	ml	Sigma Aldrich

On day 2, 50 µl of the SFM, supplemented with bFGF, BMP4, SCF (1:200), Transferrin, L-ascorbic acid, and VEGF (10 ng/ml, Peprotech) was added. From day 3 to day 7, 50 µl medium per well was replaced with fresh medium every day. Starting with day 8, no BMP4 and VEGF were added and from day 11 on, TPO (20 ng/ml) was added.

Cells were harvested on day 14 with 1000 µl pipette tips and filtered through a 100 µm cell strainer. Cells are centrifuged for 5 min at 300 g in 15 ml falcon tubes, resuspended in 1 ml SFM medium, and counted. For the isolation of megakaryocytes for RNA isolation, $CD61^+$ cells were separated by magnetic beads activated cell sorting (MACS, Miltenyi Biotech). For the further maturation without MACS, cells were seeded in 24-well plates at a density of $1x10^6$ cells/ml in SFM containing SCF (1:800), Transferrin, L-ascorbic acid, TPO, and IL-11 (100ng/ml, Miltenyi Biotech).

For the culture of $CD61^+$ cells after MACS purification, cells were cultured in $1x10^6$ cells/ml in SFM containing SCF (1:800), Transferrin, L-ascorbic acid, TPO, and IL-11 (100 ng/ml, Miltenyi Biotech) with the caspase inhibitor Q-VD-OPH (50 µM, Selleckchem, Houston, TX, US) for 2 days.

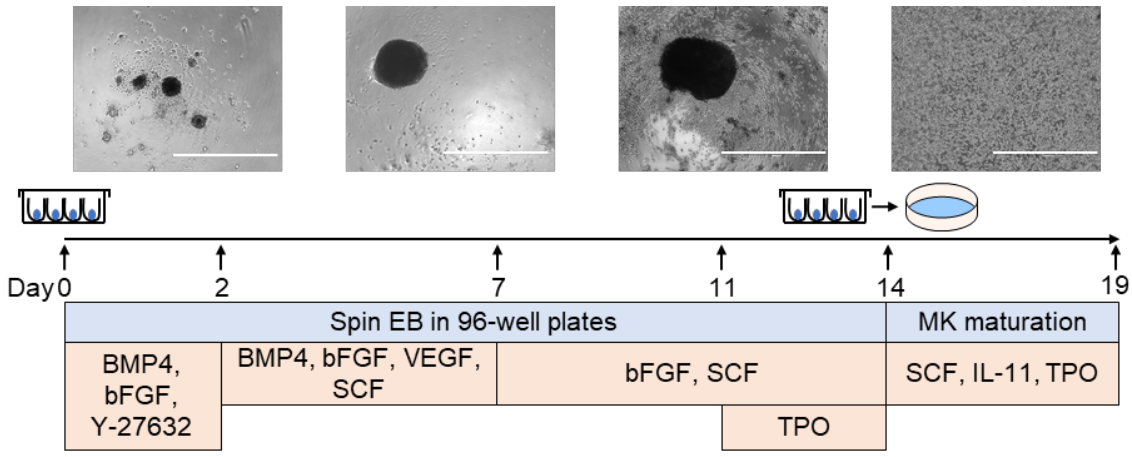

Figure 13: Hematopoietic differentiation of iPS cells into megakaryocytes.

Three thousand cells per well were seeded into a 96-well plate, formed embryonic bodies, and differentiated into hematopoietic progenitors and megakaryocytes. Cells were harvested and maturated in 24-well plates. Scale: 1000 µm.

2.1.9 Other tested protocols for megakaryocyte differentiation

2.1.9.1 StemSpan™ megakaryocyte expansion supplement

$CD34^+$ cells were generated from iPS cells. To this end, iPS cells were cultured on MEF layer until reaching a confluency of 80%. Colonies were detached with dispase and cultured on suspension culture plates in EB medium. After 5 days, EB were seeded on gelatin-coated plates and cultured for 14 more days in progenitor medium (Table 8). Subsequently, cells in the supernatant were harvested and $CD34^+$ cells were separated by MACS and cultured for 14 days in StemSpan™ medium supplemented with StemSpan™ MES (Megakaryocyte Expansion Supplement) following the manufacturer's instruction. Furthermore, StemPro™-34 SFM (Stemcell Technologies) and EB medium supplemented either with MES or with TPO only as the central cytokine of megakaryocyte differentiation were tested in addition to StemSpan™ (Figure 14).

Table 8: Progenitor medium composition.

Reagent	Volume		Company
StemPro™-34 SFM	48.5	ml	Stemcell Technologies
Penicillin/streptomycin (5,000 U/ml)	500	µl	Thermo Fisher Scientific
L-glutamine (200 mM)	500	µl	Thermo Fisher Scientific
Non-essential amino acids (100x)	500	µl	Thermo Fisher Scientific
SCF (1:200)	250	µl	CHO KLS C6 cell supernatant
FLT3L (25 µg/ml)	50	µl	Peprotech
Hyper IL-6 (1000x)	25	µl	Fischer et al., 1997, kindly provided by S. Rose-John
IL-3 (150 µg/ml)	10	µl	Miltenyi Biotech

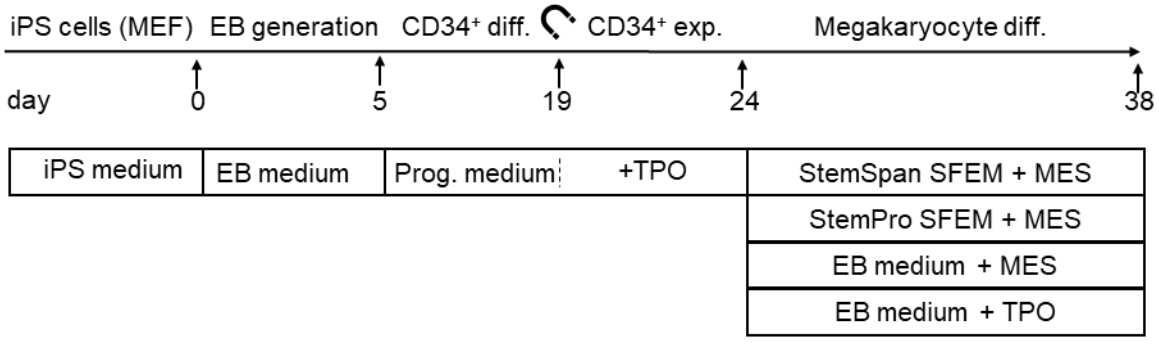

Figure 14: Schematic overview of testing StemSpan™ megakaryocyte expansion supplement. On MEF layer cultured iPS colonies were detached and seeded on ultra-low attachment plates to form EB. After culture in EB medium, supernatant cells were harvested and $CD34^+$ HSC were purified by MACS. After further expansion, megakaryocyte differentiation was initiated using different medium conditions.

2.1.9.2 2D differentiation of iPS cells into megakaryocytes

The slightly modified method published by Börger et al. in 2016 was used to test the generation of megakaryocytes from iPS cells in a 2D culture model. iPS cells were plated as single cells on Matrigel-coated plates and differentiated within 24 days into megakaryocytes. STEMdiff™ APEL™ 2 medium (Stemcell Technologies) was used for differentiation, supplemented with VEGF and BMP4 until day 4, TPO, SCF and IL-3 from day 4 until day 12 and with TPO and SCF from day 12 until day 24 (Figure 15).

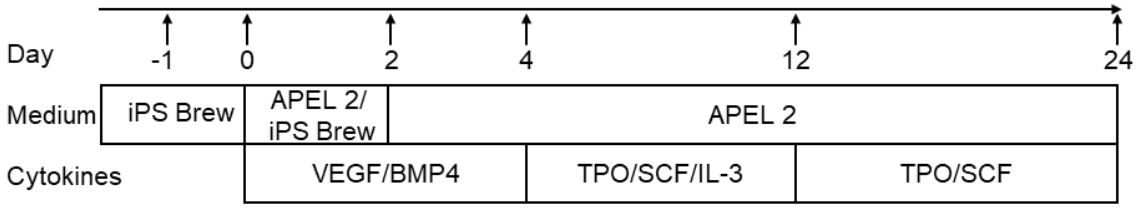

Figure 15: Schematic overview 2D differentiation of iPS cells into megakaryocytes.
Experimental scheme of the 2D iPS differentiation into megakaryocytes published by Börger et al. in 2016. iPS cells cultured on Matrigel are grown for 24 days in APEL 2 medium supplemented with VEGF and BMP4 in the first 4 days, TPO, SCF, and IL3 until day 12 and TPO and SCF until day 24.

2.1.10 Ficoll

Ficoll density gradient solution is a neutral, highly branched, hydrophilic polysaccharide (Saccharose-Epichlorohydrin-Copolymer) that can separate PBMNC and platelets by density gradient centrifugation. The blood was passed through a 100 µm cell strainer and diluted 1:2 with cold PBS containing 2 mM EDTA. 15 ml of the Ficoll (GE Healthcare, Little Chalfont, UK) was transferred to a 50 ml falcon tube and the sample was carefully added on top without mixing of the two phases. Cells were centrifuged for 20 min at 500 g without brake. Afterwards, the milky interface contained the PBMNC and the top transparent layer the platelets. The PBMNC were washed twice with PBS containing 2 mM EDTA and used for reprogramming (2.1.1). The platelets were washed once, centrifugated at 750 g for 10 min, and subjected to the platelet activation assay (2.1.11).

2.1.11 Platelet activation assay

Platelets isolated from cord blood (CB) using Ficoll or iPS cell-derived platelets from spin EB differentiation were used. To isolate the platelets from the other cells in spin EB, a first centrifugation step for 4 min at 100 g was performed, followed by another centrifugation step with 750 g for 10 min. All further centrifugation steps are performed with 750 g for 10 min. Both, iPS cell-derived and CB-derived platelets, were resuspended in flow cytometry buffer (Table 9) and divided into two parts: non-activated resting platelets and activated platelets.

The resting platelets were fixed with 4% PFA for 20 min and washed twice. They were stored at 4°C for staining together with the activated platelets. The activated platelets were incubated with 0.2 U/ml thrombin (Peprotech) for 10 min at RT, fixed with 4% PFA for 20 min. Both conditions were stained for CD41, CD42b, CD61, and CD62p.

2.1.12 Co-culture of BM-MSC and megakaryocytes

To establish the co-culture of BM-MSC and megakaryocytes, different approaches were established as summarized in Figure 16. Conditioned medium or the megakaryocyte lysate (Figure 16A), MACS purified megakaryocytes (Figure 16B), and early unpurified megakaryocytes and hematopoietic cells from spin EB day 11 were used for the co-culture. All experiments for performed twice. After co-culture, the fibrotic transformation was validated by α-SMA immunostaining 2.7.1), the quantitative analysis of α-SMA by flow cytometry (2.4), or collagen staining (2.7.2).

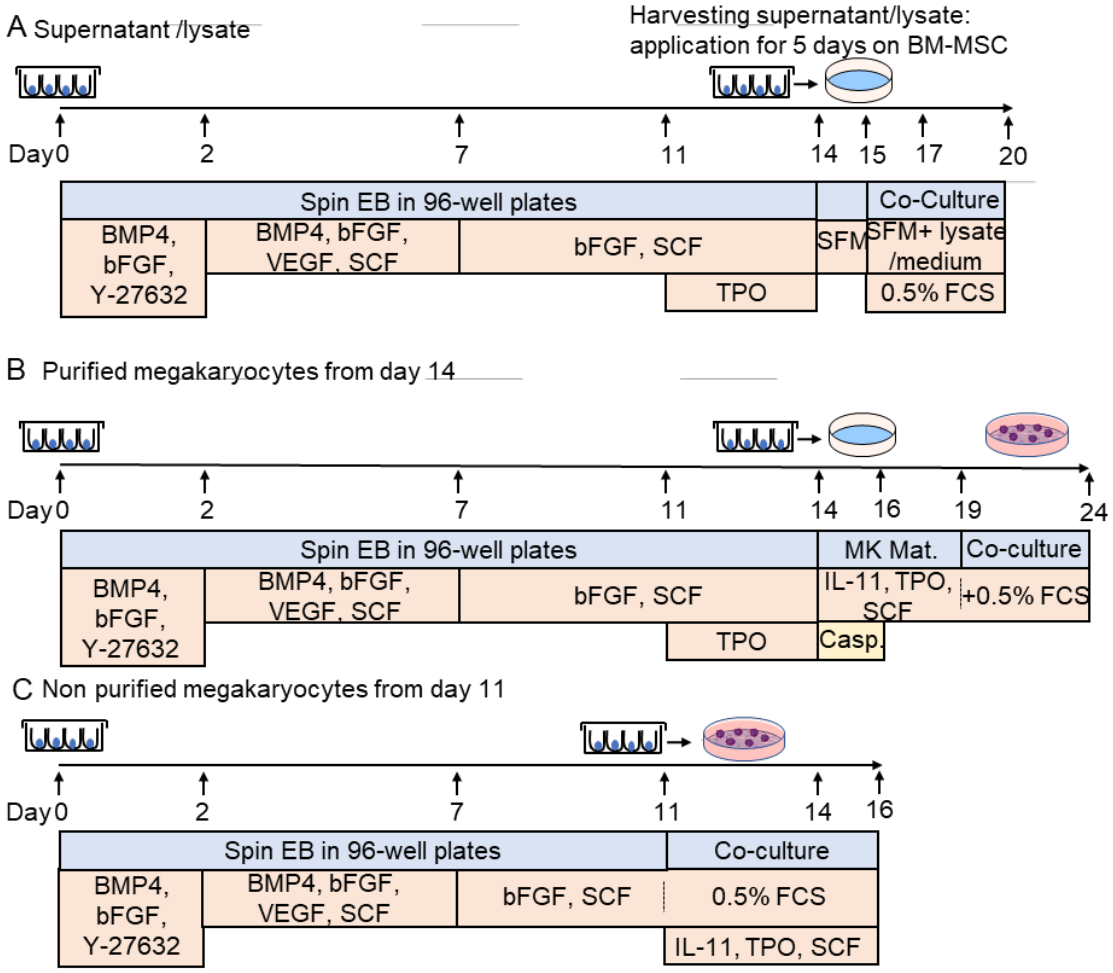

Figure 16: Summary scheme of co-culture experiments.
Schematic overview of different approaches for the co-culture of BM-MSC and megakaryocytes. **(A)** Megakaryocytes were differentiated for 14 days with the spin EB protocol, $CD61^+$ cells were MACS purified and cultured for 1 day in SFM without cytokines. The megakaryocyte cell lysate was generated by snap freezing in liquid N_2. Additionally, the supernatant was collected. Both were applied for 5 days on BM-MSC

in SFM containing 0.5% FCS. **(B)** Megakaryocytes were differentiated for 14 days with the spin EB protocol, $CD61^+$ cells were MACS purified cultured for 5 days in SFM containing IL-11, TPO, and SCF, and the first 2 days Q-VD-OPH caspase inhibitor (casp.). Cells were then co-cultures for 5 days with BM-MSC in SFM with 0.5% FCS. **(C)** Megakaryocytes and other hematopoietic cells were differentiated for 11 days with the spin EB protocol and used without purification for a 5-day co-culture with BM-MSC in SFM containing 0.5% FCS, IL-11, TPO, and SCF.

2.2 Magnetic activated cell sorting (MACS)

Cells were harvested at day 14 of megakaryocyte differentiation and counted with the Neubauer counting chamber. For the isolation of $CD34^+$ and $CD61^+$, cells were positively selected by MACS using CD34 and CD61 MACS MicroBeads (Miltenyi Biotech) following the manufacturer's instruction. As MACS buffer, PBS with 2% FCS and 2 mM EDTA was used.

2.3 Colony-forming unit (CFU) assay

For evaluation of the differentiation capacity of $CD34^+$ HSC, CFU assays were performed. Cells were harvested on day 14 of megakaryocyte differentiation (2.1.8), passed through a 40 µm cell strainer, and MACS for $CD34^+$ cells was performed. $CD34^+$ cells were seeded at a density of 10,000 cells/ml in StemMACS™ HSC-CFU light with EPO, human (Miltenyi Biotech) according to the manufacture's protocol and incubated for 10 days at 37°C. The different colonies were evaluated by microscopy and individual colonies were picked and analyzed by cytospin and Diff-Quick staining (2.7.3). Colonies with >200 densely packed red/ brownish cells were classified as burst forming unit erythrocyte (BFU-E), smaller red/brownish colonies with <200 cells as colony-forming unit erythrocyte (CFU-E). Colony-forming unit granulocytes were consisting of translucent compact colonies. Sparsely growing big translucent colonies with >20 cells were characterized as colony-forming unit macrophages (CFU-M). Colonies with bigger and larger translucent cells were considered as colony-forming unit granulocytes macrophages (CFU-GM) and colonies with bigger and larger translucent cells and red/ brownish cells as colony-forming unit granulocytes, macrophages, erythrocytes megakaryocytes (CFU-GEMM).

2.4 Flow cytometry

Flow cytometry was used to characterize and quantify surface and intracellular protein expression of HSC, megakaryocytes, platelets, and MSC. Therefore, cells were harvested as described before and collected in flow cytometry tubes (Sarstedt, Nürmbrecht, Germany). For intracellular markers, cells were fixed with 4% PFA and permeabilized with 0.3% Triton X-100 (Merck) in flow cytometry buffer (Table 9), followed by blocking with normal goat serum for 30 min.

Cells were incubated in the following steps, with the antibody in specific dilution (Table 10) for 30 min at 4°C, washed once with flow cytometry buffer, and resuspended in 200 µl flow cytometry buffer. The cells were measured using flow cytometry with a Canto II instrument (Beckton Dickinson (BD), Franklin Lakes, NJ, USA). Data were analyzed with the FlowJo software (Tree Star, Inc., Ashland, OR, USA). IgG isotype control-stained cells were used as control. All flow cytometry experiments were performed in collaboration with the Flow Cytometry Core Facility, Interdisciplinary Center for Clinical Research, Medical Faculty, RWTH Aachen University, Aachen, Germany.

Table 9: Flow cytometry buffer composition.

Reagent	Volume		Company
PBS	500	ml	Thermo Fisher Scientific
EDTA (0.5 M)	2	µl	Thermo Fisher Scientific
BSA	2.5	g	PAN Biotech

Table 10: Fluorochrome labeled antibodies for flow cytometry measurements.

Marker	Fluorochrome	Clone	Dilution	Company
CD31	PE	WM59	1:200	BD
CD34	APC	581	1:100	BD
CD43	FITC	1G10	1:100	BD
CD45	APC-Vio770	5B1	1:200	Miltenyi Biotech
CD117	PE-Cy7	104D2	1:100	Thermo Fisher Scientific
CD41	PE-Cy7	H1P8	1:1000	Biolegend (San Diego, CA, USA)
CD42b	APC	H1P1	1:100	Biolegend
CD61	FITC	VI-PL2	1:500	Biolegend
CD62b	PE	AK4	1:200	Biolegend
CD90	APC	5E10	1:100	Immunotools (Friesoythe, Germany)
CD105	FITC	REA794	1:300	Miltenyi Biotech
α-SMA	Alexa Flour 594	1A4	1:200	R&D Systems (Minneapolis, MN, USA)
CD73	PE	AD2	1:100	Immunotools
CD29	PE-Vio 770	TS2/16	1:100	Miltenyi Biotech
CD235a	PE	HIR1	1:2000	Thermo Fisher Scientific

2.5 PCR and NGS

DNA concentrations were measured with the Nanodrop spectrophotometer ND-1000 (Thermo Fisher Scientific), and PCR was performed with the Epgradient thermocycler (Eppendorf, Hamburg, Germany). The PCR products were run with 6x loading dye (Thermo Fisher Scientific) on ethidium-bromide containing 1% agarose gels in 1x Tris-borate-EDTA (TBE) buffer.

Table 11: Program used for PCR.

Step	Cycles	Temperature	Time
Initial denaturation	1x	94°C	5 min
Denaturation	35x	94°C	30 sec
Annealing		xx°C	30 sec
Elongation		70°C	1 min
Final elongation	1x		5 min
End	1x	10°C	∞

2.5.1 DNA isolation

According to the manufacturer's instructions, DNA was isolated using the NucleoSpin® Tissue Kit (Macherey Nagel, Düren, Germany). Suspension cells were collected, washed once with PBS, and DNA isolation was performed. For adherent cells like MSC, cells were detached for 4 min with 0.05% Trypsin/EDTA and washed once with PBS.

2.5.2 PCR for detection of CXCL4^{KO} and CXCL4/L1^{dKO}

For the detection of the CXCL4^{KO} and CXCL4/L1^{dKO} after CRISPR, six primer pairs were designed, depicted in Figure 18, with blue arrows for CXCL4^{KO} and black arrows for CXCL4/L1^{dKO,} respectively (Table 12). The unmodified CXCL4 fragment has a length of 641 bp for the CXCL4^{KO} and 1189 bp for the CXCL4/L1^{dKO}. For CXCL4L1 in the CXCL4/L1^{dKO}, the unmodified size is 1157 bp. The PCR was performed with the master mix displayed in Table 13 and the program in Table 11. For Sanger sequencing, samples were sent to Eurofins Genomics (Luxembourg, Luxembourg).

Table 12: Primer for the detection of CXCL4^{KO} and CXCL4L1^{dKO}.

Primer	Sequence 5' to 3'
CXCL4^{KO} fwd	TAA TCT TGG CTG GCC AGA ACC
CXCL4^{KO} rev	TCC CCA TCT TCA GCT TCAG
CXCL4^{dKO} fwd	CAC CCT GTC ACT AGC ACT GGC TGAA
CXCL4^{dKO} rev	CCT CCC CCA GAC AGA AGT TGT TCT AAC
CXCL4L1^{dKO} fwd	CAC CCT GTC ACT GGC AGT GAC TGA G
CXCL4L1^{dKO} rev	CCT CTC TCA GAC AGA GGT TGT GCT GAT

Table 13: PCR conditions for CXLC4 PCR.

Reagent	Volume		Company
10x Taq buffer	2	µl	Thermo Fisher Scientific
dNTP (10 mM)	0.2	µl	Thermo Fisher Scientific
Primer fwd (100 pmol)	1	µl	Eurofins Genomics
Primer rev (100 pmol)	1	µl	Eurofins Genomics
$MgCl_2$	1	µl	Merck
Taq polymerase	0.2	µl	produced in house in E. coli
Template DNA	100	ng	
ddH_2O	fill up to 25	µl	

2.5.3 Allele-specific PCR for JAK2

To detect the JAK2 V617F mutation in patient-derived iPS cells, the approach from Jones et al. (2005) was used. Three PCR reactions specific for detecting JAK2 and JAK2 V617F and sequencing/control were used (Figure 17 and Table 14). The master mix described in Table 15 and the PCR program in Table 11 were used. For Sanger sequencing, samples from the sequencing PCR were sent to Eurofins Genomics.

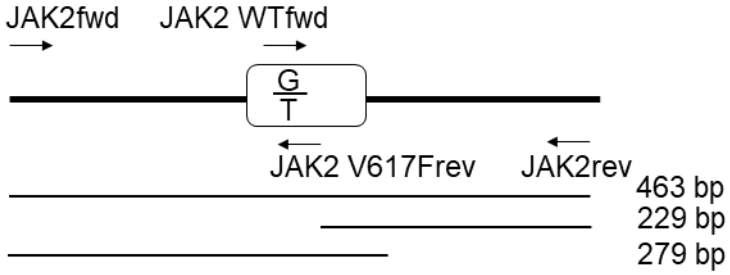

Figure 17: Position of allele-specific primer for JAK2 and JAK2 V617F.

Table 14: Primer for allele-specific JAK2 and JAK2 V617F PCR.

Primer	Sequence 5' to 3'
JAK2fwd	TCC TCA GAA CGT TGA TGG CAG
JAK2rev	ATT GCT TTC CTT TTT CAC AAG AT
JAK2 WTfwd	GCA TTT GGT TTT AAA TTA TGG AGT ATA TG
JAK2 V617Frev	GTT TTA CTT ACT CTC GTC TCC ACA AAA

Table 15: Standard conditions for allele specific JAK2 and JAK2 V617F PCR.

Reagent	JAK2 WT		JAK2 V617F		Sanger		Company
10x Taq buffer	2.5	µl	2.5	µl	2.5	µl	Thermo Fisher Scientific
dNTP (10 mM)	0.5	µl	0.5	µl	0.5	µl	Thermo Fisher Scientific
DMSO	1	µl	1	µl	1	µl	Sigma Aldrich
$MgCl_2$ (25 mM)	2.5	µl	2.5	µl	2.5	µl	Merck
Taq polymerase	1	µl	1	µl	1	µl	produced in E. coli
JAK2 fwd	-	µl	5	µl	5	µl	Eurofins Genomics
JAK2 rev	5	µl	-	µl	5	µl	Eurofins Genomics
JAK2 WT fwd	2.5	µl	-	µl	-		Eurofins Genomics
JAK2 V617F rev	-	µl	2.5	µl	-		Eurofins Genomics
Template DNA	200	ng	200	ng	200	ng	

2.5.4 NGS analysis

DNA was isolated according to 2.5.1 and NGS of MPN associated genes was performed in collaboration with Angela Maurer, Medical Clinic IV, RWTH Aachen University Hospital, Aachen, Germany. Thirty-one genes associated with MPN were analyzed (ABL1, ASXL1, BARD1, CALR, CBL, CHEK2, CSF3R, DNMT3A, ETNK1, ETV6, EZH2, IDH1, IDH2, JAK2, KIT, KRAS, MPL, NF-E2, NRAS, PDGFRA, PTPN11, RUNX1, SETBP1, SF3A1, SF3B1, SH2B2, SRSF2, TCF12, TET2, TP53, U2AF1; Kirschner et al., 2018). 250 ng isolated gDNA was used for library preparation and sequencing was performed on a MiSeq® sequencing (Illumina, San Diego, CA, USA). The MiSeq onboard software was used for demultiplexing and FastQ file generation (MiSeq Control Software v2.6 and real-time analysis software v1.18.54, Illumina). SeqNEXT software (v4.4.0 build 509, JSI medical systems, New York, NY, USA) was used for alignment and variant calling. Non-synonymous variants with a bidirectional frequency of ≥ 5% were classified. 5: Pathogenic, 4: likely pathogenic, 3: uncertain, 2: likely not pathogenic of little clinical significance, and 1: not pathogenic of no clinical significance. NGS was

performed in Genomics Core Facility, Interdisciplinary Center for Clinical Research, Medical Faculty, RWTH Aachen University, Aachen, Germany.

2.6 RNA

2.6.1 RNA isolation and RT-qPCR

RNA was isolated with the NucleoSpin RNA II Kit (Machery Nagel) following the manufacturer's instructions. RNA concentration was measured using a Nanodrop spectrophotometer ND-1000. According to the manufacturer protocol, cDNA synthesis was performed using a High-Capacity cDNA Reverse Transcription Kit (Thermo Fisher Scientific). 1 µg RNA was diluted into 13.7 µl RNAse-free water and used as a template for the reverse transcription PCR (RT-qPCR) with random primer (Table 16). The RT-qPCR was performed with the following steps: 25°C for 10 min, 37°C for 2 h, and 94°C for 4 min.

Table 16: RT-qPCR reaction set up.

Reagent (Stock concentration)	Volume		Company
RT-qPCR buffer (10x)	2.0	µl	Thermo Fisher Scientific
RT-qPCR random primer (10x)	2.0	µl	Thermo Fisher Scientific
RiboLock RNase inhibitor (40 U/µl)	0.5	µl	Thermo Fisher Scientific
dNTP (100 nM)	0.8	µl	Thermo Fisher Scientific
Multiscribe® reverse transcriptase (50 U/µl)	1.0	µl	Thermo Fisher Scientific
RNA (1 µg)	13.7	µl	

After cDNA synthesis, the cDNA was diluted 1:5 with distilled water and used for RT-qPCR (Table 17). The samples were measured in duplicates and the housekeeping gene glyceraldehyde-3-phosphate dehydrogenase (GAPDH) was used for normalization. The RT-qPCR was performed using the standard program (Table 18) of a StepOnePlus Real-Time PCR System and the data were analyzed with the StepOne™ Software v2.1 (both Thermo Fisher Scientific), Microsoft Excel (Redmond, WA, USA), and GraphPad Prism (GraphPad Software Inc. v.6.0, La Jolla, CA, USA).

Table 17: Quantitative PCR reaction set up.

Reagent	Volume		Company
ddH_2O	2.5	µl	
Primer mix (10 µM)	0.5	µl	Eurofins Genomics
Fast SYBR® green	5	µl	Thermo Fisher Scientific
cDNA	2	µl	

Table 18: Standard program for RT-qPCR.

Step	Cycles	Temperature	Time
Initial denaturation	1x	95°C	20 sec
Denaturation	40x	95°C	3 sec
Annealing and elongation		60°C	30 sec
Melt curve	1x	95°C	15 sec
	1x	60°C	60 sec
		+0.3°C to 95°C	
	1x	95°C	15 sec
End	1x	RT	∞

2.6.2 RNA sequencing (RNA-Seq)

RNA-Seq was performed in the Genomics Core Facility, Interdisciplinary Center for Clinical Research, Medical Faculty, RWTH Aachen University, Aachen, Germany. The quality of the RNA of purified $CD61^+$ megakaryocytes was quality checked by TapeStation 4200 (Agilent, Santa Clara, CA, USA) and RNA integrity number (RIN) was measured. RNA concentration was determined with the Fluorometer Quantus™ (Promega, Fitchburg, MA, USA). Ribosomal RNA depletion was performed using the NeBNext® rRNA Depletion Kit according to manufacturer's instructions and the library preparation was performed with the NeBNext®Ultra™II Directional RNA Library Prep Kit for Illumina (both New England BioLabs, Ipswich, MA, USA). For the analysis, 100 ng RNA was used. Samples were sequenced in paired end reads (2x76 bp, dual indexed) on two NextSeq High Output Kits v2.5 (150 cycles) on a NextSeq 500 instrument (both Illumina). Data was analyzed in collaboration with Martin Graßhoff, M.Sc. and Ivan Costa, Ph.D., Institute for Computational Genomics, Medical Faculty, RWTH Aachen University, Aachen, Germany.

2.7 Staining

2.7.1 Immunostaining

For immunofluorescent staining, cells were cultured on gelatin- or Matrigel-coated glass coverslips. Cells were washed once with PBS and fixed for 20 min with 4% PFA at RT. After washing thrice, cells were permeabilized and incubated in 0.3% Triton X-100 in PBS for 30 min. Blocking was performed with normal goat serum. The primary antibody was incubated overnight at 4°C. The next day, cells were washed thrice and incubated with the secondary antibody 1 h at RT. For multiple staining, this procedure was repeated. Cells were incubated with 1:1000 Hoechst (Hoechst Frankfurt, Germany) diluted in 0.3% Triton X-100 for 10 min at RT. After washing twice, all liquid was discarded, the coverslips were dried, and mounted with mounting solution (Dako, Hamburg, Germany) on a glass slide. Fluorescence was observed with the Axiovert 200 microscope (Carl Zeiss, Oberkochen, Germany). Images were processed with Image J (National Institute of Health, Bethesda, MD, USA).

Table 19: List of antibodies used for immunostainings.

Antigen	Clone	Species	Subtype	Dilution	Company
Primary					
OCT4	Sc-9081	Rabbit	IgG	1:200	Santa Cruz (Santa Cruz, CA, USA)
TRA 1-60	TRA 1-60	Mouse	IgM	1:200	Merck Millipore
SSEA-4	MC-813-70	Mouse	IgG	1:20	Merck Millipore
Albumin	188835	Mouse	IgG	1:100	R&D Systems
AFP	189502	Mouse	IgG	1:100	R&D Systems
cTNT	200805	Mouse	IgG	1:100	R&D Systems
Nestin	10C2	Mouse	IgG	1:100	Merck Millipore
β-III-tubulin	TuJ-1	Mouse	IgG	1:100	R&D Systems
α-SMA	1A4	Mouse	IgG	1:500	R&D Systems
GLI1	Polyclonal	Rabbit	IgG	1:200	Novus Biologicals (Littleton, CO, USA)
Secondary	Fluorochrome				
Anti-mouse	Alexa Fluor 488	Goat	Anti IgG	1:200	Thermo Fisher Scientific
Ani-mouse	Alexa Fluor 594	Goat	Anti IgG	1:200	Thermo Fisher Scientific
Anti-mouse	Alexa Fluor 647	Goat	Anti IgG	1:200	Thermo Fisher Scientific
Anti-mouse	Alexa Fluor 594	Goat	Anti IgM	1:200	Thermo Fisher Scientific

Anti-rabbit	Alexa Fluor 488	Goat	Anti IgG	1:200	Thermo Fisher Scientific
Anti-rabbit	Alexa Fluor 594	Goat	Anti IgG	1:200	Thermo Fisher Scientific

2.7.2 Collagen staining

Collagen staining was performed with Sirius Red solution (Chondrex, Woodinville, WA, USA) after 5 days of stimulation of BM-MSC following manufacturers' instruction. Cells were fixed with 4% PFA for 20 min and incubated with the solution for 30 min. Afterward, cells were washed until no red color was visible in the water, dried, and mounted with Dako on glass slides. Pictures were taken with the Leica DMRX microscope and the Leica Application Software suite v3.1.0.

2.7.3 Cytospin and Diff-Quick staining

Diff-Quick (also Wright's stain) is a hematologic stain with a mixture of eosin and methylene blue to distinguish blood cell types. The solutions stain the cell's compartments based on the ionic charge producing varying blue, red, and violet shades. Combined with the neutral benzidine staining for erythrocytes, this staining can distinguish between erythrocytes, granulocytes, leukocytes, macrophages, megakaryocytes, and more. A cytospin chamber was assembled with a filter card and glass slide and prepared by adding 200 µl ddH_2O per spot and spinning at 400 rpm for 4 min in a CytospinTM 4 cytocentrifuge (Thermo Fisher Scientific). 50,000 to 100,000 cells were applied to each spot and centrifuged at 400 rpm for 4 min. The glass slides were air-dried, and cells were fixed with methanol for 4 min followed by incubation in 1% benzidine solution (Sigma Aldrich) for 2 min and 30% H_2O_2 solution for 90 sec. The slides were washed 30 sec with ddH_2O and air-dried. For the Diff-Quick staining, slides were incubated five times for 5 sec in Diff-Quick solution I and 30 sec in Diff-Quick solution II (both Merck Millipore, Burlington, MA, USA) and afterward washed twice for 30 sec in ddH_2O. Glass slides were air-dried and mounted with Entallan (Merck). Pictures were taken with the Leica DMRX microscope and the Leica Application Software suite v3.1.0.

2.7.4 Staining of adipogenic and osteogenic differentiation

Cells of the osteogenic differentiation were washed with PBS, incubated with 4% paraformaldehyde (PFA) for 15 min, and stained for 20 min with Alizarin Red S solution (Sigma Aldrich) at 37°C. The cells were washed until no red color in the PBS was visible. After the staining, pictures were taken with the EVOS® FL microscope.

Cells of the adipogenic differentiation were also fixed with PFA, washed, and then permeabilized for 5 min with 0.2% Triton X-100 (Merck, Darmstadt, Germany) in PBS. After washing twice, cells were incubated for 5 min with 1:1000 Hoechst in PBS. After discarding the Hoechst solution, staining with BODYPI was performed, diluting BODYPI™ (Thermo Fisher Scientific) 1:10,000 in water and incubating the cells for 15 min. After discarding the BODYPI solution and washing the cells thrice with water, pictures were taken with the EVOS® FL microscope using the Hoechst and GFP channel.

2.8 Protein extraction, SDS Page, and Western blot

For protein extraction JAK2:CXCL4^{KO} and JAK2 V617F:CXCL4^{KO} iPS cell-derived hematopoietic cells were harvested on day 14 of spin EB differentiation. The cell suspension was collected in a 15 ml tube. Cells were counted and centrifuged for 4 min at 300 g at 4°C. Cells were washed once with PBS followed by resuspension in lysis solution: 50 mM Tris-HCl pH 7.4, 1% NP-40, 0.1% sodium dodecyl sulfate (SDS), 0.25% sodium deoxycholate, 150 mM NaCl, 5 mM EGTA, 50 mM NaF, 1 mM Na3VO4 (all Sigma Aldrich) and 1x protease inhibitor mix (Roche, Basel, Switzerland). The cells were incubated 1 h on ice, vortexing the solution every 10 min. Samples were centrifuged at 13,000 g and 4°C for 4 min. The concentration was determined by the Bradford protein assay (BioRad, Berkeley, CA, USA) using BSA (Sigma Aldrich) for a standard curve. The absorption was measured at 595 nm with a Tecan photometer (Männedorf, Switzerland).

For the SDS-Page, 40 µg protein lysate was used. The samples were heated for 5 min with 4x loading buffer at 95°C, chilled on ice, and then applied on an 8% SDS gel. After 2 h at 60 mA, the separated proteins were plotted for 2 h with 160 mA on methanol activated polyvinylidene difluoride (PVDF) membrane (Thermo Fisher Scientific) using a semi-dry blotting device from BioRad. The membrane was blocked afterward for 30 min with 4% milk powder washed thrice with Tris-buffered saline (TBS) containing 0.5% Tween20 (T-TBS Buffer, Merck) and incubated overnight at 4°C with the first antibody: CXCL4 (clone 170138 mouse anti-human, 1:1,000, Thermo Fisher Scientific). CXCL4L1 (polyclonal rabbit anti-human, 1:1,000, Thermo Fisher Scientific) and β-actin (clone AC-74, mouse anti-human 1:5,000, Sigma Aldrich) in T-TBS. The next day, the membrane was washed thrice and incubated with the secondary antibody at RT for 1 h: CXCL4 and β-actin with horseradish peroxidase (HRP) conjugated sheep anti-mouse antibody and for CXCL4L1 with HRP conjugated donkey anti-rabbit antibody (all 3 at 1:10,000, GE Healthcare). The membrane was washed, and proteins were detected with SuperSignal

West Pico chemiluminescence substrate (Thermo Fisher Scientific). Blots were exposed and pictures were taken with a Gel-Doc system (BioRad)

2.9 CRISPR/Cas9 mediated genome editing

2.9.1 Design of CRISPR/Cas9 mediated CXCL4^{KO} and CXCL4L1^{KO}

The CRISPR guide RNA (gRNA) sequences were selected with the CRISPR.MIT.EDU website by the Zhang Lab (https://zlab.bio/guide-design-resources, Cambridge, MA, USA) and double-checked with the IDT DNA website. CXCL4 and CXCL4L1 have three exons, including noncoding sequences, the signal protein, and the protein-coding part (Figure 18A). For the CXCL4 knockout, two pairs of gRNAs were designed for the Cas9 nickase system to generate double-strand breaks spanning the first exon to achieve the complete deletion of the first exon, to render the protein dysfunctional or not being generated. Guides were designed with a maximum offset of eight base pairs and the Cas9 cleavage site at the 5' overhang of the guides. The first pair targets the start of exon one and the second pair intron one so that a possible INDEL will not occur in the coding sequence of the gene (Figure 18B). Furthermore, sequences were analyzed with the Basic Local Alignment Search Tool (BLAST) from the National Center for Biotechnology Information (NCBI, Bethesda, MD, USA) for possible off-target effects. Only guides with at least two mismatches in the seed region between nucleotide 5 and11 were used (Ran et al., 2013).

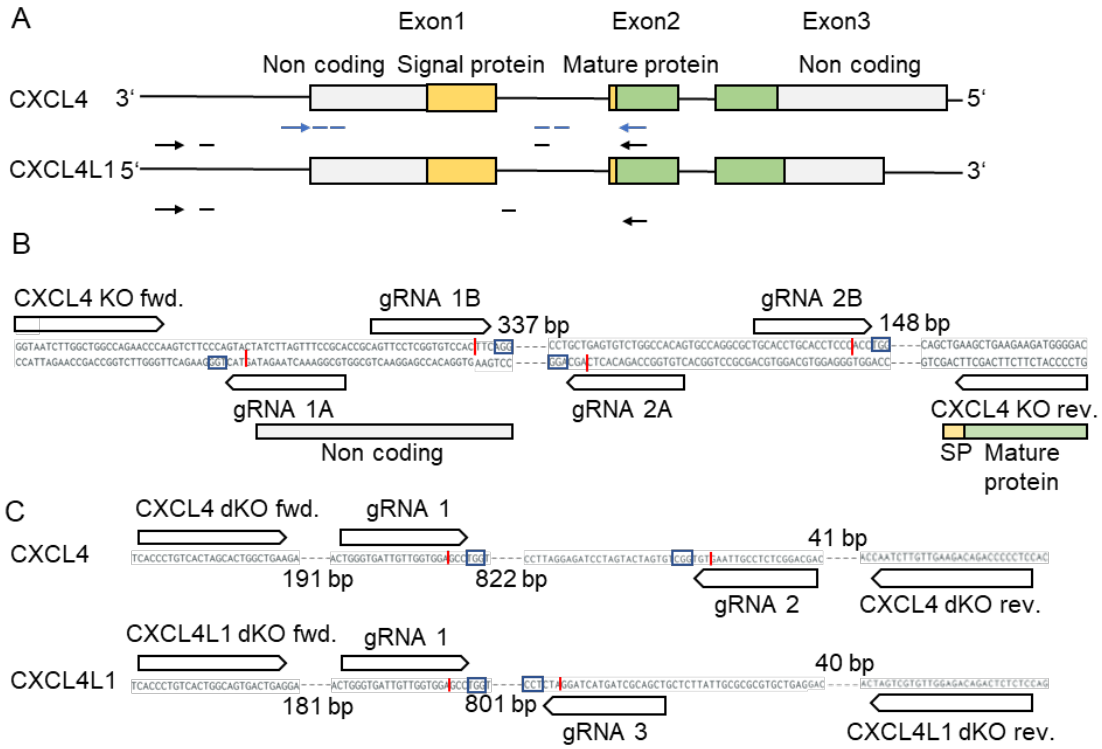

Figure 18: Design and position of guides for CXCL4^{KO} and CXCL4/L1^{dKO}.
(A) CXCL4 and CXCL4L1 exon structure with annotation of sequencing primer (arrows) and sgRNA guides (lines). CXCL4^{KO} annotation in blue, CXCL4/L1^{dKO} in black. **(B)** CXCL4^{KO} sequencing primer and sgRNA position in detail. **(C)** CXCL4^{KO} and CXCL4/L1^{dKO} sequencing primer and gRNA position in detail. Adapted from Boehnke et al., 2021.

For the double CXCL4 and CXCL4L1 knockout, the Cas9 nuclease was used because it was impossible to design four different guides matching both genes. One guide was placed in front of the first exon cutting in both genes CXCL4 and CXCL4L1. The other two guides were designed in the first Intron. These will cause the complete knockout of the whole first exon of CXCL4 and CXCL4L1 and therefore cause a dysfunctional or absent protein.

Table 20: List of used gRNA for CRISPR

gRNA	Sequence
gRNA 1A	GTACTATCTTAGTTTCCGCA
gRNA 1B	AGTTCCTCGGTGTCCACTTC
gRNA 2A	GCTGAGTGTCTGGCCACAGT
gRNA 2B	CTGCACCTGCACCTCCCACC
gRNA 1	TGGGTGATTGTTGGTGGAGCC
gRNA 2	AGCAGGCTCTCCGTTAAGTG
gRNA 3	AGCTGCGATCATGATCCTAG
JAK2 gRNA	GTAAAACTACAGGCTTTCTAA
JAK2 donor template	TTCTCACAAGCATTTGGTTTTAAATTATG GAGTATGTGTCTGTGGAGACGAGAGTAA

2.9.2 Design of CRISPR/Cas9 mediated repair of JAK2 V617F

The gRNA for targeting the JAK2 V617F locus was designed like the CXCL4 targeting gRNAs. The goal was a repair of the mutation and not a knockout. Therefore, a fluorescence-labeled guide was designed additionally containing the repair for the G to T mutation and additional a silent mutation in the following glycine codon (Figure 18B). This additional mutation should prevent the Cas9 protein from modifying the same position multiple times and therefore enhance the repair efficacy. As the targeted region has limited PAM sequences necessary for the Cas9 targeting, the nuclease system was used.

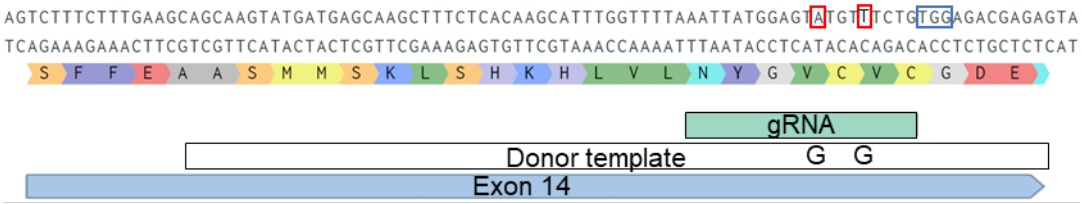

Figure 19: Design and position of the guide targeting the JAK2 V617F mutation.
Schematic overview of the DNA sequence in JAK2 exon 14 with amino acid sequence. Red boxes indicate the changed base pairs and the blue box the PAM sequence.

2.9.3 CRISPR/Cas9 editing

For the knockout of CXCL4 and CXCL4L1 protein and repair of the JAK2 V617F mutation, the ALT-R system of IDT DNA was used based on the *S. pyogenes* CRISPRCas9 system for an optimized genome editing for producing on-target double-stranded DNA breaks (Vakulskas et al., 2018). The two-part system combines the optimized, shortened, target-specific CRISPR RNA (crRNA, with 36 nt: 20 nt target-specific protospacer region, along with the 16 nt tracrRNA fusion domain) oligonucleotide with an optimized, shortened tracrRNA oligonucleotide (67 nt, Figure 11B). The gRNA complex formation and the RNP complex formation were performed manually and then delivered into the cells by the AMAXA nucleofector system. For annealing of crRNA and tracrRNA, both were incubated 1:1 for 5 min at 95°C in a thermocycler (Eppendorf) and chilled at RT for 30 min. For the crRNA:tracrRNA:Cas9 RNP complex formation, 1.7 µl of the crRNA:tracrRNA complex was incubated with 2.5 µl of the Cas9 protein at RT. The RNP was delivered into the cells with the Neon™ transfection system (Thermo Fisher Scientific) following the manufacturer's instructions with 1350 volt.

2.10 Statistical analysis

Graphical display and statistical analysis were performed with GraphPad Prism 6 and represented with the mean ± standard deviation (SD). Statistical significance was analyzed using two-tailed, unpaired Student t-test. P values <0.05 were considered statistically significant (*p<0.05, significant; **p<0.01, very significant; ***p<0.001, extremely significant; ****p≤0.0001, extremely significant).

3 Results

3.1 Generation and characterization of iPS cells

iPS cells with JAK2 V617F mutation were generated from patients with PV by previous Ph.D. students (Küstermann, 2019; Sontag, 2017). Single-cell iPS cell clones were generated and characterized by allele-specific PCR for the JAK2 genotype.

From patient 1 (female, allele burden 37%), the JAK2 unmutated clone number 007 and JAK2 V617F^{het} clone number 009 were used (referred to as PV1 JAK2 and PV1 JAK2 V617F^{het}, Table 21). JAK2 V617F^{hom} clone number 021 was used from patient 2 (male, allele burden 96%, referred to as PV2 JAK2 V617F^{hom}), and from patient 3 (male, allele burden 25%), the unmutated clone JAK2 number 026 and the heterozygous clone JAK2 V617F^{het} number 006 (referred to as PV3 JAK2 and PV3 JAK2 V617F^{het}) was used in this thesis and verified by allele-specific PCR (Table 21, Figure 20). The unmutated JAK2 clones showed a band for JAK2 at 229 bp and the control band at 463 bp. The homozygous clones had two bands, the 279 bp JAK2 V617F band and the control band, and the heterozygous clones had all three bands. More genotypes were generated with the CRISPR/Cas9 technology (3.2.1).

Table 21: Reprogramed iPS cell clones used in this thesis.

Patient	Age	Gender	Disease type	Allele burden	Sample type	Clone number	JAK2 mutation
Patient 1	45	f	PV	37%	PB	007	JAK2
						009	JAK2 V617F^{het}
Patient 2	47	m	PV	96%	PB	021	JAK2 V617F^{hom}
Patient 3	38	m	PV	25%	PB	026	JAK2
						006	JAK2 V617F^{het}

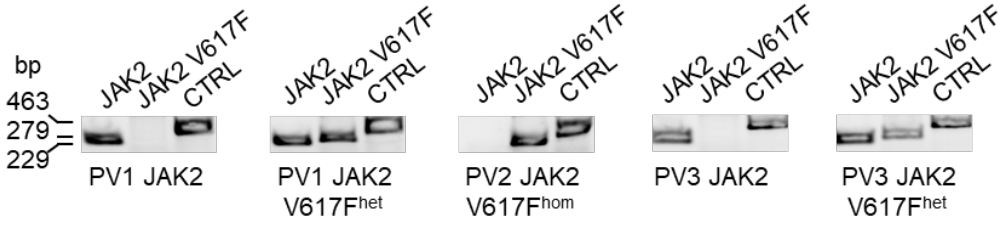

Figure 20: Allele-specific PCR for iPS cell clones.
Representative agarose gel after allele-specific PCR for PV1 JAK2, PV1 JAK2 V617F^{het}, PV2 JAK2 V617F^{hom}, PV3 JAK2, and PV3 JAK2 V617F^{het}. For each tested clone: left JAK2 (fragment size 229 bp), JAK2 V617F (fragment size 279 bp), and control (fragment size 463 bp). Reprogramming was performed by pervious Ph.D. students (Küstermann, 2019; Sontag, 2017).

3.1.1 iPS cell clones had further mutations and polymorphisms

Besides mutations in the JAK2 locus, patient-derived iPS cells gained other disease-specific MPN-related modifications during disease progression. Clones were screened

for these additional mutations by NGS. A panel with 31 genes related to MPN was used to analyze all iPS cell clones (Kirschner et al., 2018; Toledo et al., 2021).

Both clones of PV1 had mutations in CBL and the JAK2 V617F^{het} clone in TET2 (Table 22). No further mutations were found in PV2 JAK2 V617F^{hom}, but clinically not relevant polymorphisms in ASXL1, EZH2, and the tumor protein TP53. PV3 had no further mutations but polymorphisms in ASXL1, TP53, TET2, and SETBP1 in all clones.

Furthermore, clones from all three patients were analyzed for chromosomal abnormalities to exclude their influence on the phenotypes observed in experiments (Figure 21). The heterochromatin block of the long (q-) arm of chromosome 9 was shifted in both PV1 clones to the short (p-) arm by two fracture events and a 180° rotation (inv(9)(p12q13)). This reorganization occurs with a frequency of 1.5 % in the European population and is not considered as a chromosomal aberration. Clones from PV2 and PV3 had no chromosomal abnormalities.

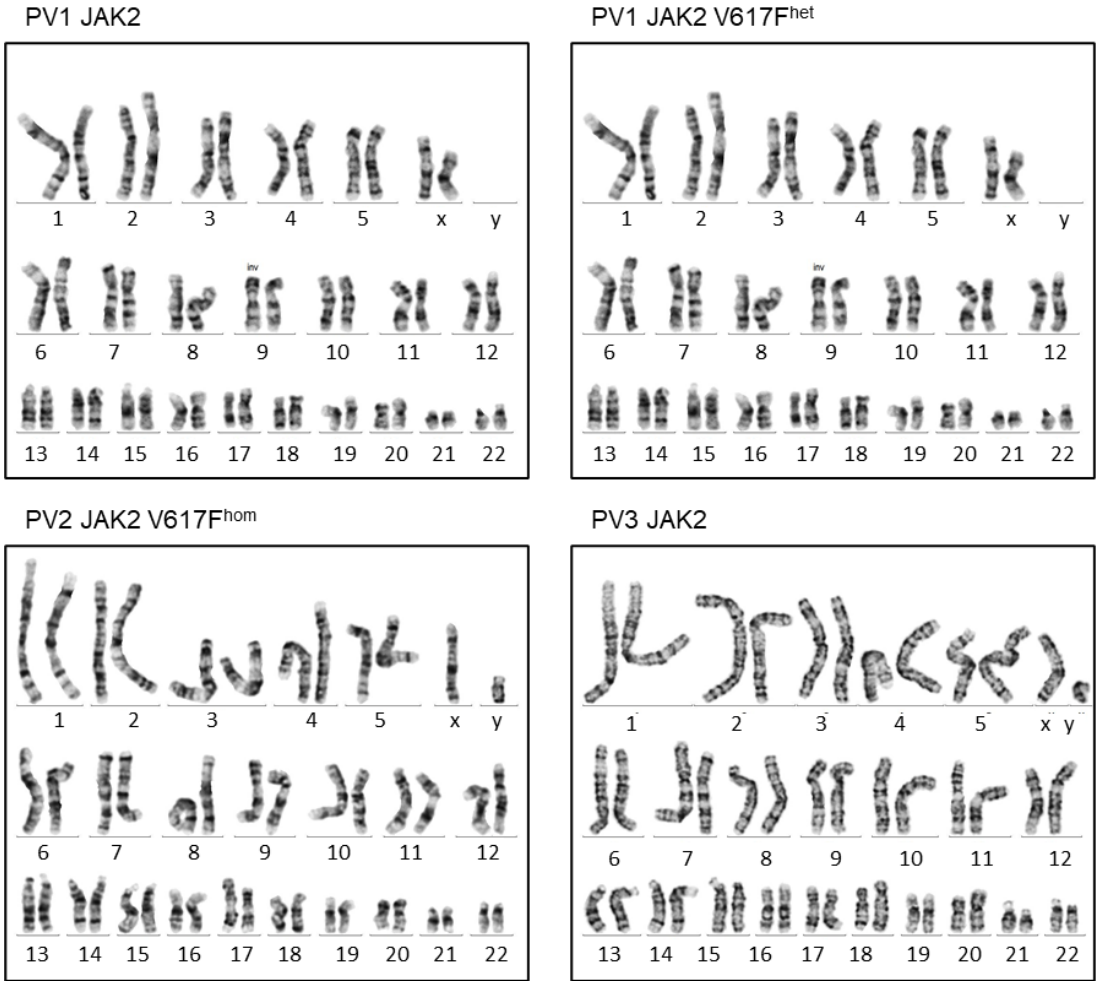

Figure 21: Karyotyping of iPS cell clones shows no aberrations.
Karyogram of PV1 JAK2, PV1 JAK2 V617F^{het}, PV2 JAK2 V617F^{hom}, and PV3 JAK2. PV1 has an inversion (inv) in chromosome 9, PV2 and PV3 have a normal karyotype. In collaboration with the Institute for Human Genetics, Uniklinik RWTH Aachen, Germany.

Table 22: NGS analysis of MPN-associated genes.
NGS analysis of MPN-associated genes of PV1 JAK2 and JAK2 V617F^{het}, PV2 JAK2 V617F^{hom} and PV3 JAK2 and JAK2 V617F^{het} iPS cell clones (in collaboration with the Medical Clinic IV, RWTH Aachen University Hospital, Aachen, Germany). c. HGVS, Human Genome Variation Society notation at the transcript level; p. HGVS, Human Genome Variation Society notation at the protein level; -, mutation not detected. Mutation classification: 1, not pathogenic or of no clinical significance; 2, likely not pathogenic or of little clinical significance; 3, variant of uncertain significance; 4, likely pathogenic or of clinical significance; 5, definitely pathogenic or of clinical significance. CBL, JAK2, and TET2 are classified as mutations, ASXL1, EZH2, TP53, TET2, and SETB1 as polymorphisms. *clones were analyzed by Caroline Küstermann (Küstermann, 2019).

Gene	Transcript	Loc.	c. HGVS	p. HGVS	Mutation class.	PV1 JAK2*	PV1 JAK2 V617F^{het}*	PV2 JAK2 V617F^{hom}	PV3 JAK2	PV3 JAK2 V617F^{het}
CBL	NM_005188	E9	c.T1364del	p.Y455del	1	39%	25%	-	-	-
JAK2	NM_001322194	E4	c.1849G>T	p.V617F	5	-	29%	99%	-	39%
TET2	NM_001127208	E3	c.35A>G	p.N12S	1	-	27%	-	-	-
ASXL1	NM_015338	E12	c.2444T>C	p.L815P	1	-	-	100%	100%	100%
EZH2	NM_004456	E6	c.553G>C	p.D185H	2	-	-	51%	-	-
TP53	NM_000546	E4	c.215c>G	p.P72R	2	-	-	99%	52%	52%
TET2	NM_001127208	E11	c.5284a>G	p.I1762V	2	-	-	-	50%	50%
SETPB1	NM_015559	E4	c.3301G>A	p.V1101I	1-2	-	-	-	51%	51%

3.1.2 iPS cell clones

For quality assessment of the iPS cell clones, morphology was evaluated, staining for pluripotency markers was performed, and differentiation potential into the three lineages ectoderm, endoderm, and mesoderm was evaluated. For PV1 derived clones, the quality assessment was already performed by Caroline Küstermann (Küstermann, 2019).

All clones grew as tightly packed colonies with sharp edges and a high nucleus to cell plasma ratio. Immunostainings for the pluripotency marker TRA-1-60, SSEA-40, and OCT4, combined with the nucleus staining (Asprer & Lakshmipathy, 2015), showed a uniform expression pattern in PV2 JAK2 V617F^{hom} and PV3 JAK2 (Figure 22A). The surface proteins TRA-1-60 and SSEA-40 are localized at the outer cell membrane, the transcription factor OCT4 is localized in the nucleus.

The neuroectoderm markers nestin and β-III-tubulin, the endoderm markers albumin (ALB) and α-fetoprotein (AFP), and the mesoderm markers cardiac troponin T (cTNT) and α-smooth muscle actin (α-SMA) are commonly used to validate three lineage differentiation potential (Zeevaert et al., 2020). Immunostainings of these markers verified the differentiation potential PV2 JAK2 V617F^{hom} and PV3 JAK2 (Figure 22B and supplemental Figure 42).

In summary, generated iPS cells had no other clinically relevant mutations than JAK2 V617F, show normal karyotypes, typical morphology with uniform pluripotency marker expression, and three lineage differentiation potential, which makes them suitable for further applications.

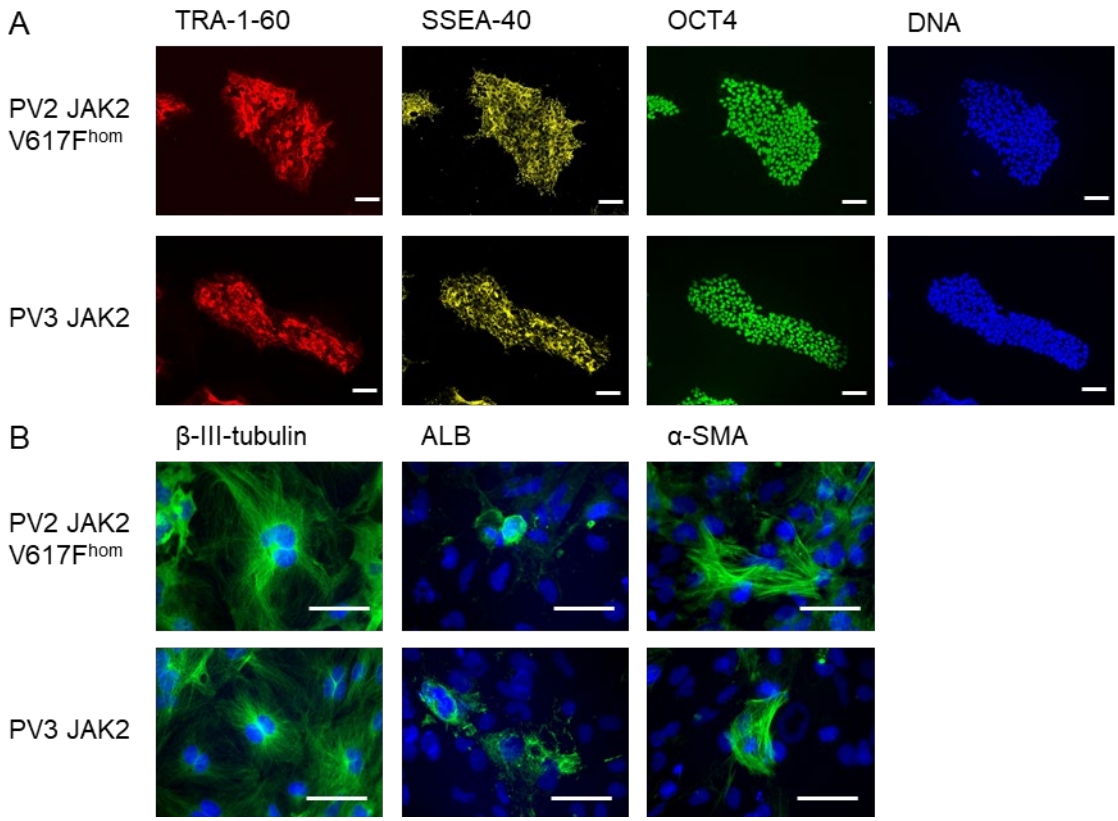

Figure 22: Pluripotency staining and 3 linage differentiations of PV2 JAK2 V617F^{hom} and PV3 JAK2. **(A)** Representative fluorescence images of PV2 JAK2 V617F^{hom} and PV3 JAK2. TRA-1-60 (red), SSEA4 (yellow), OCT4 (green) and nuclei (blue) were stained. Scale: 100 µm. **(B)** Representative fluorescence images of PV2 JAK2 V617F^{hom} and PV3 JAK2. β-III-tubulin (ectoderm), albumin (endoderm), and α-SMA (mesoderm, all green) were co-stained with the nuclei (blue). Further lineage marker staining in supplemental Figure 42. Scale: 50 µm.

3.2 CRISPR/Cas9 mediated genome editing

The CRISPR/Cas9 technology is a powerful tool to insert, eliminate or exchange gene fragments. In the present work, CRISPR was used to repair the JAK2 V617F mutation in PV2 JAK2 V617F^{hom} and create a knockout of the first exon of CXCL4 and CXCL4L1 in PV1 JAK2 and JAK2 V617F^{het}.

3.2.1 Missing JAK2 genotypes were generated by CRISPR/Cas9

In all three patient-derived iPS cells, one (PV2) or at maximum two out of three genotypes (PV1 and PV3) naturally occurred because of the high allele burden in PV2 (96%, only homozygous clones) and low allele burden in PV1 and PV3 (25% and 37%, only unmutated and heterozygous clones). To verify that phenotypes observed in later experiments are provoked by the JAK2 mutation and not by other patient-specific mutations, JAK2 unmutated and JAK2 V617F^{het} clones were generated from PV2 JAK2 V617F^{hom} using CRISPR/Cas9.

After electroporation of the PV2 JAK2 V617F^{hom} clone with JAK2 V617F targeting ribonucleoprotein (RNP) complex together with an ATTO-labeled guide, a clear shift of

the mean fluorescence intensity (MFI) was observed (Figure 23A). The 18.3% ATTO^{high} cells were seeded in single-cell suspension on a MEF feeder layer to generate clonal iPS colonies. The bulk screening showed a strong band of 229 bp for JAK2 after allele-specific PCR proving the successful application of CRISPR (Figure 23B). Comparing the JAK2 and JAK2 V617F band intensity (Bio-Rad CFX Maestro software), over 50% of the bulk cells were modified.

Single-cell derived colonies were picked 2 weeks later, analyzed by allele-specific PCR and colonies with the JAK2 band (unmutated) alone or with JAK2 and JAK2 V617F band (heterozygous) were analyzed by Sanger sequencing. Of 96 picked clones, 61 were stable and further analyzed. 23% of the colonies were unmutated, 51% heterozygous and 26% still non-edited JAK2 V617F^{hom} clones (Figure 23C). Three JAK2 unmuted clones (PV2 JAK2 052, PV2 JAK2 072, and PV2 JAK2 092) and one JAK2 heterozygous clone (JAK2 V617F^{het} 070) were generated.

For further experiments, PV2 JAK2 072 and JAK2 V617F^{het} 070 were selected and are further referred to as PV2 JAK2 and PV2 JAK2 V617F^{het} (Figure 23D, Table 23). To prove that CRISPR application did not affect the pluripotency status or the differentiation capacity into the three germ layers, immunostainings for pluripotency markers and lineage markers after differentiation were performed. PV2 JAK2 and PV2 JAK2 V617F^{het} undifferentiated cells express the surface marker TRA-1-60 and SSEA-40 as well as the transcription factor OCT4, proving the pluripotent status (Figure 23E). Differentiated cells express lineage-specific markers for ectoderm (β-III-tubulin, nestin), endoderm (albumin and AFP), and mesoderm (α-SMA and cTNT), which proved their differentiation capacity (Figure 23F, supplemental Figure 42).

In summary, the JAK2 V617F^{hom} was successfully repaired using CRISPR technology. PV2 JAK2 and JAK2 V617F^{het} clones were generated, are pluripotent, and can differentiate into all three germ layers.

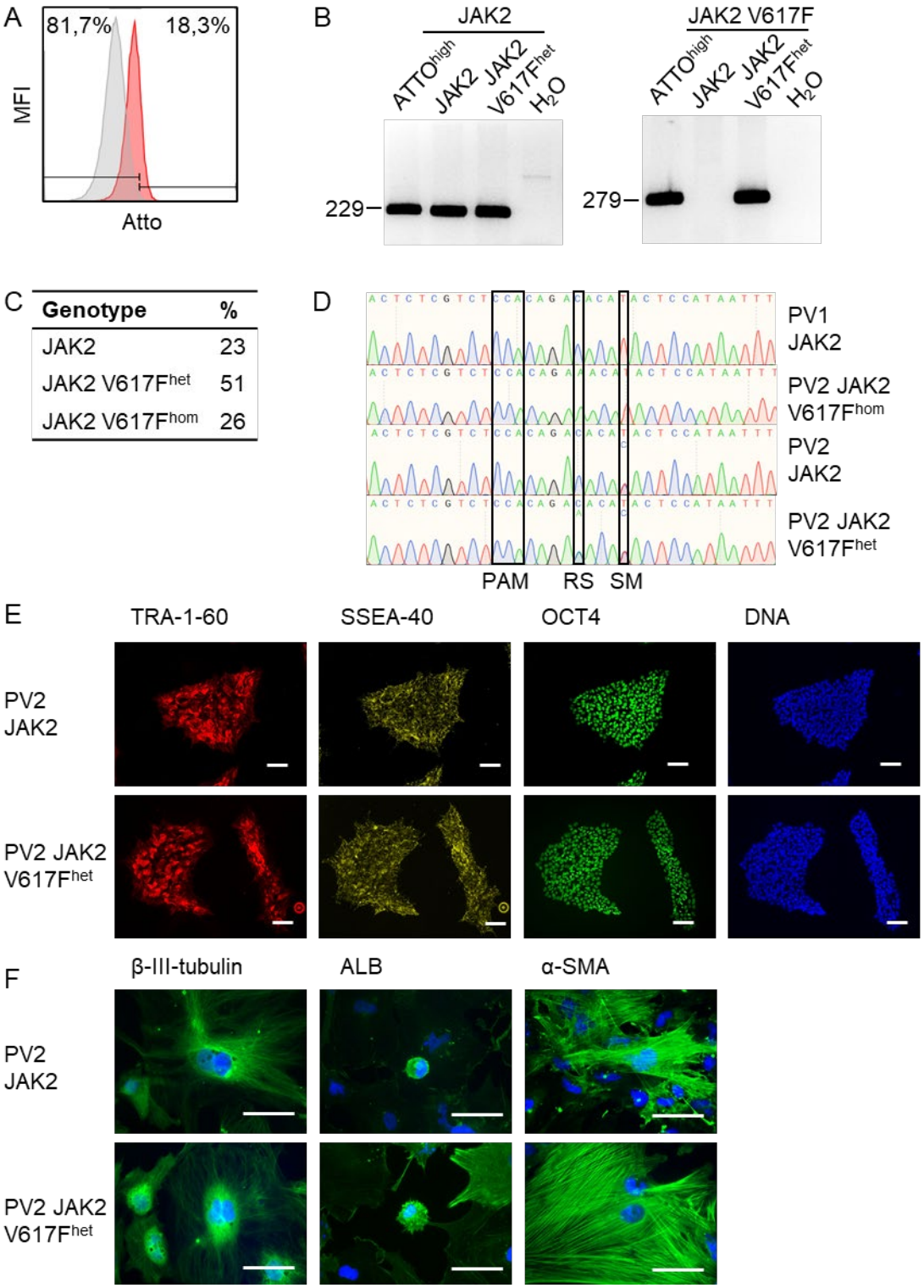

Figure 23: CRISPR/Cas9 mediated generation of JAK2 and JAK2 V617F^{het} iPS cell clones from JAK2 V617F^{hom} PV2.
(A) Sorting of ATTO^{high} cells 24 h after electroporation. 18.3 % of the cells were seeded for further screening. **(B)** Bulk screening with allele-specific PCR for JAK2 and JAK2 V617F of ATTO^{high} sorted cells. The JAK2 V617F^{hom} clones had a strong band or JAK2 and JAK2 V617F after CRISPR editing. **(C)** Distribution of genotype of picked colonies for JAK2 and JAK2 V617F. **(D)** DNA sequencing of selected iPS cell clones used in the thesis (PV1 JAK2 007, PV2 JAK2 V617F^{hom} 021, PV2 JAK2 072 and PV2 JAK2 V617F^{het} 070, Table 23). PAM sequence, JAK2 repaired side (RS) and introduced silent mutation (SM) are highlighted. **(E)** Representative fluorescence images of PV2 JAK2 and PV2 JAK2 V617F^{het} undifferentiated iPS cells. TRA-1-60 (red), SSEA4 (yellow), OCT4 (green) and DNA (blue) were stained. Scale: 100 µm. **(F)** Representative fluorescence images of PV2 JAK2 and PV2 JAK2 V617F^{het} after EB spontaneous differentiation assay.

β-III-tubulin (ectoderm), albumin (endoderm), and α-SMA (mesoderm, all green) were co-stained with the DNA (blue). Further lineage marker staining in supplemental Figure 42. Scale: 50 µm.

Table 23: CRISPR modified iPS cell clones used in this thesis.

Original clone	CRISPR modification
PV1 JAK2 007	PV1 JAK2:CXCL4^{KO}
PV1 JAK2 V617F^{het} 009	PV1 JAK2 V617F^{het}:CXCL4^{KO}
PV2 JAK2 V617F^{hom} 021	PV2 JAK2 072
	PV2 JAK2 V617F^{het} 070

3.2.2 Generation of CXCL4 and CXCL4/L1 deficient iPS cell clones

Gleitz et al. reported that CXCL4 is a central effector of bone marrow fibrosis in mice (H. Gleitz et al., 2020). To dissect the role of CXCL4 in a human system, a CRISPR/Cas9 mediated knockout of CXCL4 (CXCL4^{KO}) in iPS cells was performed (Boehnke et al., 2021). In contrast to the murine system, humans harbor CXCL4 and the variant CXCL4L1 (also PF4var1). This variant occurred most probably due to gene duplication with only three different amino acid residues in the mature protein compared to CXCL4. Because the CXCL4L1 protein could rescue the knockout of CXCL4, a CXCL4 and CXCL4L1 double knockout (CXCL4/L1^{dKO}) should be generated. Unlike the JAK2 V617F repair, no donor template was necessary to generate the CXCL4^{KO} and CXCL4/L1^{dKO}. The gRNA was designed to delete the first exon of CXCL4 and CXCL4L1 entirely.

After the nucleofection of PV1 JAK2 and PV1 JAK2 V617F^{het} with the RNP complex containing the Cas9 nickase of all four gRNAs, a strong band of around 250 bp was visible after bulk PCR screening for both clones (Figure 24A). The CRISPR/Cas9 nickase knockout had an efficiency of over 85% for both clones, comparing the bands' intensity.

Screening of 24 generated single-cell clones for each bulk, JAK2 and JAK2 V617F^{het}, resulted in 50% of the colonies with CXCL4^{KO} in both alleles (Figure 24B). Promising clones were further analyzed by DNA sequencing and one clone for JAK2 and JAK2 V617F^{het} was selected for deeper analysis, further referred in this thesis as JAK2:CXCL4^{KO} and JAK2 V617F^{het}:CXCL4^{KO}, respectively (Table 23, Boehnke et al., 2021). JAK2:CXCL4^{KO} had a biallelic deletion of 425 bp (Figure 24C). In contrast, both alleles had a different deletion length in JAK2 V617F^{het}:CXCL4^{KO}. To separate the signals, CRISPR-ID was used (Dehairs et al., 2016). This bioinformatic web application separates up to three alleles from a single Sanger sequencing file. CISPR-ID depicted a 399 bp deletion on one allele and a 402 bp deletion on the other allele (Figure 24D).

Furthermore, CXCL4^{KO} was verified on protein level by Western blot. JAK2:CXCL4^{KO} and JAK2 V617F^{het}:CXCL4^{KO} clones were differentiated into megakaryocytes until

day 14 of spin EB differentiation because iPS cells do not express CXCL4 in contrast to megakaryocytes. As a control, PV2 JAK2 V617F^{het} day 14 megakaryocytes and recombinant CXCL4 were used. For none of either knockout clone, a CXCL4 band was visible, verifying the successful CXCL4^{KO} (Figure 24E, entire Western blot in supplemental Figure 43, Boehnke et al., 2021). Both clones exhibit typical iPS-like characteristics, express the pluripotency marker TRA-1-60, SSEA-40, and OCT4 (Figure 24F), and showed differentiation capability into the three lineages ectoderm, endoderm, and mesoderm (Figure 24G, supplemental Figure 42, Boehnke et al., 2021).

A

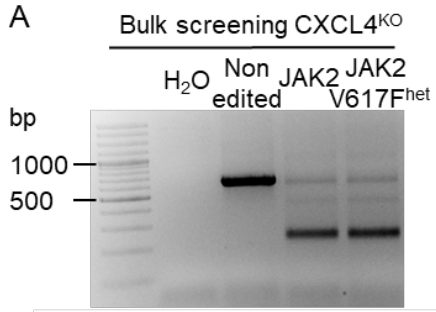

B

Genotype	CXCL4	CXCL4^{KO} het	CXCL4^{KO} hom
Bulk PV1 JAK2:CXCL4^{KO}	10%	40%	50%
Bulk PV1 JAK2 V617F^{het}:CXCL4^{KO}	8%	42%	50%

C

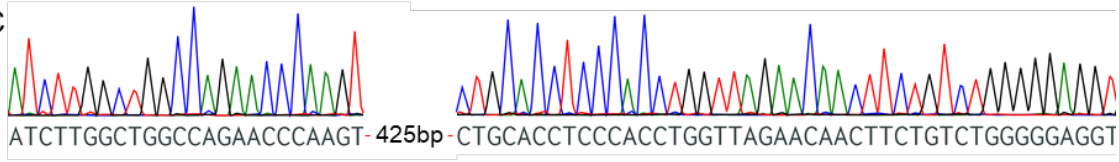

D

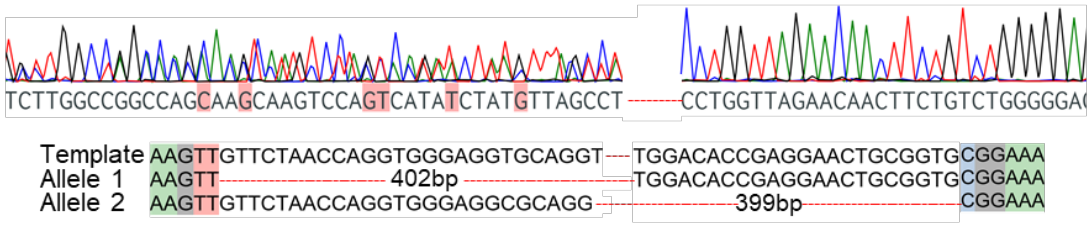

E

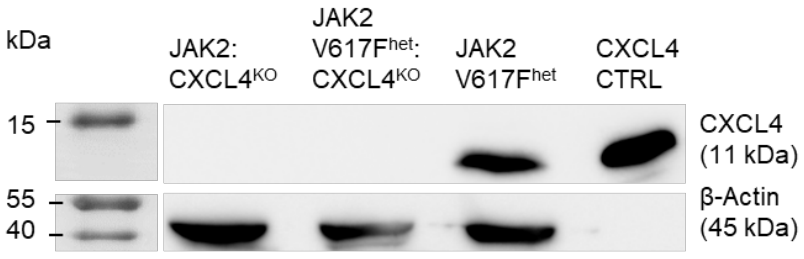

F

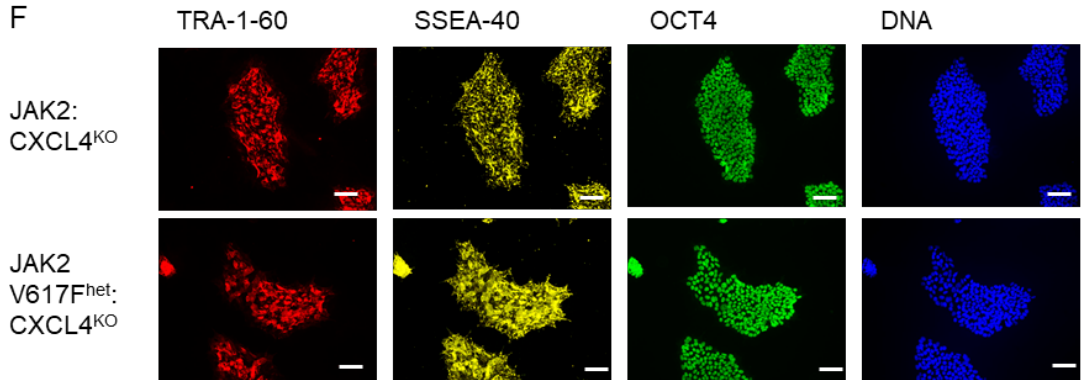

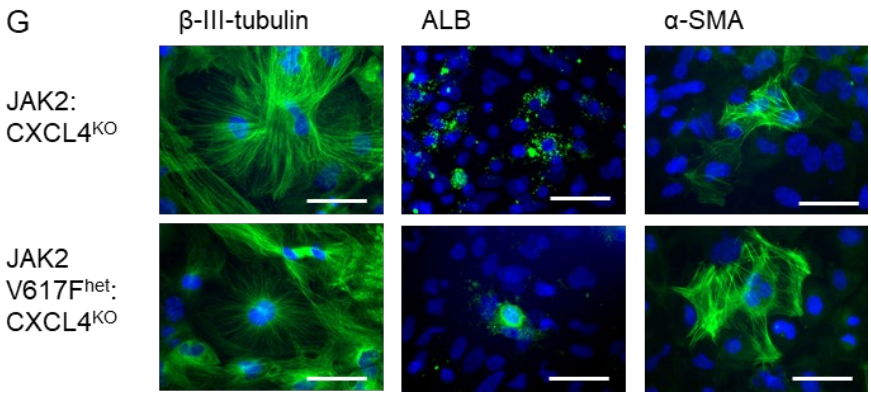

Figure 24: CRISPR/Cas9 nickase mediated CXCL4^{KO} in PV1 JAK2 and JAK2 V617F^{het}.
(A) Bulk PCR 1 day after application of CRISPR. A strong band at around 250 bp is visible for JAK2 and JAK2 V617F^{het,} with fainter bands at 641 bp and around 500 bp. **(B)** Frequencies of CXCL4, CXCL4^{KO} het, and CXCL4^{KO} hom clones after first PCR screening. Twenty-four clones of JAK2 and JAK2 V617F^{het} were picked. **(C)** Sanger sequencing of PV1 JAK2:CXCL4^{KO}. **(D)** Sanger sequencing of PV1 JAK2 V617F^{het}:CXCL4^{KO}. Deconvolution was performed using CRISPR-ID. **(E)** Western blot analysis of PV1 JAK2 V617F^{het}:CXCL4^{KO} and PV1 JAK2:CXCL4^{KO}. PV2 JAK2 V617F^{het} and recombinant CXCL4 protein were used as control. CXCL4 (11 kDa) and β-actin (45 kDa, loading control). **(F)** Representative fluorescence images of PV1 JAK2:CXCL4^{KO} and JAK2 V617F^{het}:CXCL4^{KO} undifferentiated iPS cells. TRA-1-60 (red), SSEA4 (yellow), OCT4 (green) and DNA (blue) were stained. Scale: 100 µm. **(G)** Representative fluorescence images of PV1 JAK2:CXCL4^{KO} and JAK2 V617F^{het}:CXCL4^{KO} after EB spontaneous differentiation assay. β-III-tubulin (ectoderm), albumin (endoderm), and α-SMA (mesoderm, all green) were co-stained with DNA (blue). Further lineage marker in supplemental Figure 42. Scale bar: 50 µm. Adapted from Boehnke et al., 2021.

As the usage of the Cas9 nickase system for the CXCL4/L1^{dKO} would require eight gRNAs (four for targeting CXCL4 and four for CXCL4L1), which was not possible because the genomic sequence of CXCL4 and CXCL4L1 share most of the nucleotide residues. The Cas9 nuclease system was used instead. Here, just one binding gRNA is needed for a double-strand break. gRNA 1 targeted CXCL4 and CXCL4L1, gRNA 2 targeted CXCL4, and gRNA 3 targeted CXCL4L1 (Figure 18).

The analysis of the CRISPR/Cas9 nuclease efficiency by bulk PCR showed strong bands with similar intensity at 400 bp and above 1000 bp and weak bands in between (Figure 25A). The calculated CRISPR efficiency of this reaction was 50%. As the used primer targeted both, CXCL4 and CXCL4L1, no statement can be made about the individual alleles. After single-cell seeding, 24 colonies for JAK2 and JAK2 V617F^{het} were picked and genotyped (Figure 25B). For CXCL4, 32% of all clones were targeted at least for one allele of the JAK2 and JAK2 V617F^{het} clone. For CXCL4L1, 40% were targeted for JAK2 and only 20% for JAK2 V617F^{het} on at least one allele. No clone with a biallelic knockout of CXCL4 and CXCL4L1 was generated.

In summary, CXCL4^{KO} clones were generated successfully for PV1 JAK2 and JAK2 V617F^{het}. The generated clones showed a normal phenotype, had no chromosomal aberrations, were pluripotent, and can differentiate into all three germ layers. The absence of CXCL4 was verified by Western blot. These clones will be a valuable tool to

investigate the role of CXCL4 in human myelofibrosis. The biallelic knockout of both CXCL4 and CXCL4L1 was not successful. The already generated CXCL4^{KO} clones could be used to knockout CXCL4L1 in these clones.

A

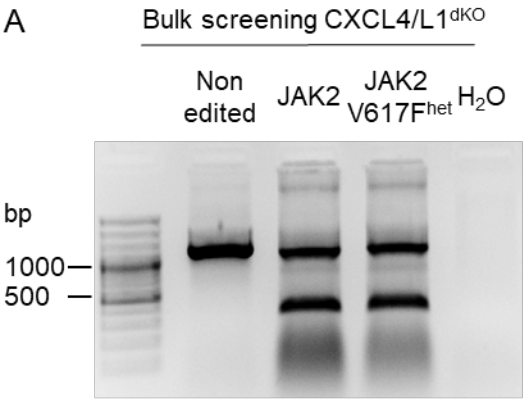

B

Genotype	CXCL4	CXCL4^{KO} het	CXCL4^{KO} hom	CXCL4L1	CXCL4L1^{KO} het	CXCL4L1^{KO} hom
PV1 JAK2: CXCL4/L1^{KO}	66,6%	16,6%	16,6%	58,3%	33,3%	8,3%
PV1 JAK2 V617F^{het}: CXCL4/L1^{KO}	68,8%	25%	6,3%	75%	12,5%	6,3%

Figure 25: CRISPR/Cas9 nuclease mediated CXCL4/CXCL4L1^{dko} in PV1 JAK2 and JAK2 V617F^{het}. **(A)** Bulk PCR 1 day after application of CRISPR. Two strong bands at around 400 bp and above 1000 bp were shown for the JAK2 and JAK2 V617F^{het} clone. **(B)** Distribution of CXCL4/L1, CXCL4/L1^{KO} het, and CXCL4/L1^{KO} hom clones after PCR screening. For JAK2 and JAK2 V617F^{het}, 24 colonies were picked. No CXCL4/L1^{dKO} clone was picked for JAK2 and JAK2 V617F^{het}.

3.3 Establishing a protocol for iPS cell differentiation into megakaryocytes

Three different protocols to generate megakaryocytes from iPS cells were evaluated: (1) a commercially available kit designed for megakaryocyte differentiation from PB derived CD34$^+$ HSC, (2) a previously published approach using 2D cell culture for iPS cell differentiation, and (3) a spin EB based approach also for iPS cells. All chosen protocols designated an easy-to-apply protocol with our laboratory equipment.

3.3.1 Megakaryocyte expansion supplement did not differentiate iPS cells

The StemSpan™ MES, containing SCF, IL-6, IL-9, and TPO, was developed to differentiate human CB or bone marrow-derived CD34$^+$ HSC into megakaryocytes.
When using StemSpan™ SFEM or StemPro™-34 SFM supplemented with MES, only a few, mainly apoptotic cells were observed after 14 days of culture. Thus, these media were not suitable for megakaryocyte production of iPS cell-derived HSC. On the other

hand, EB medium supplemented with MES resulted in the proliferation of $CD34^+$ cells. In contrast, EB medium with TPO led to the attachment of cells to the plastic surface of the cell culture dish (Figure 26A). Cells in the supernatant of both EB medium conditions were analyzed by flow cytometry to determine if generated cells were megakaryocytes. No $CD41^+$ or $CD42b^+$ cells were observed in either medium condition. Only 5% and 1% of all cells were $CD61^+$ in EB medium with MES or TPO, respectively (Figure 26B). As $CD61^+$ alone is not enough to characterize cells as megakaryocytes, the generation of megakaryocytes failed with all tested conditions.

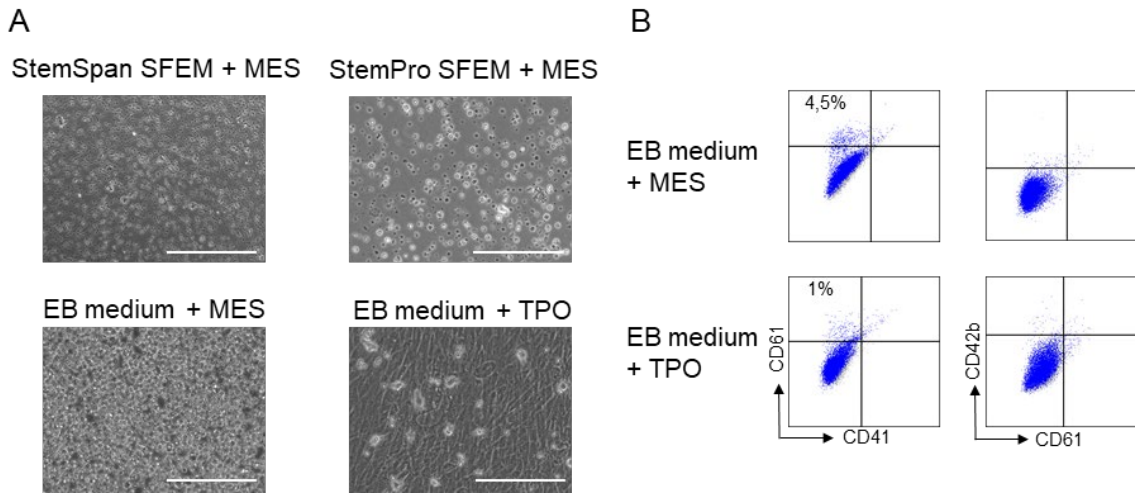

Figure 26: StemSpan™ Megakaryocyte Expansion Supplement is not suitable for megakaryocyte generation from iPS cell-derived HSC.
After 14 days of megakaryocyte differentiation using the StemSpan™ Megakaryocyte Expansion Supplement, **(A)** cell morphology was analyzed by phase-contrast microscopy and **(B)** megakaryocyte surface marker expression was measured by flow cytometry (CD41, CD42b, and CD61). Scale: 400 µm.

3.3.2 iPS cells did not produce megakaryocytes in 2D differentiation

In 2016 Börger et al. published a protocol to generate megakaryocytes from iPS cells in a 2D culture (Börger et al., 2016). In their approach, iPS cells were plated as single cells on laminin-coated plates and differentiated within 24 days into megakaryocytes. STEMdiff™ APEL™ 2 medium (further referred to as APEL2 medium) supplemented with VEGF, BMP4, TPO, SCF, and IL-3 (Figure 27A).

In our study, the clones PV1 JAK2 and JAK2V617F^{het} were differentiated according to the protocol, but after 24 days of differentiation, no suspension cells could be observed (Figure 27A). As megakaryocytes could still be attached to the cell layer, the layer was harvested with trypsin treatment and cells were analyzed by flow cytometry for the hematopoietic markers CD31, CD34, and CD45 as well as the megakaryocyte markers CD41, CD42b, and CD61.

Flow cytometry showed that 6% of cells were $CD31^+$ and 18% $CD34^+$. The surface markers CD31 and CD34 are expressed in hematopoietic cells but also markers for

endothelial cells and the hemogenic endothelium. All cells were CD45$^-$ and negative for the megakaryocyte markers CD41, CD42b, and CD61. As the cell layer did not produce suspension cells even 10 days after the endpoint of the protocol, the analyzed cells were most probably non-hematopoietic endothelial cells. Therefore, differentiation into cells of the hematopoietic system failed using this protocol.

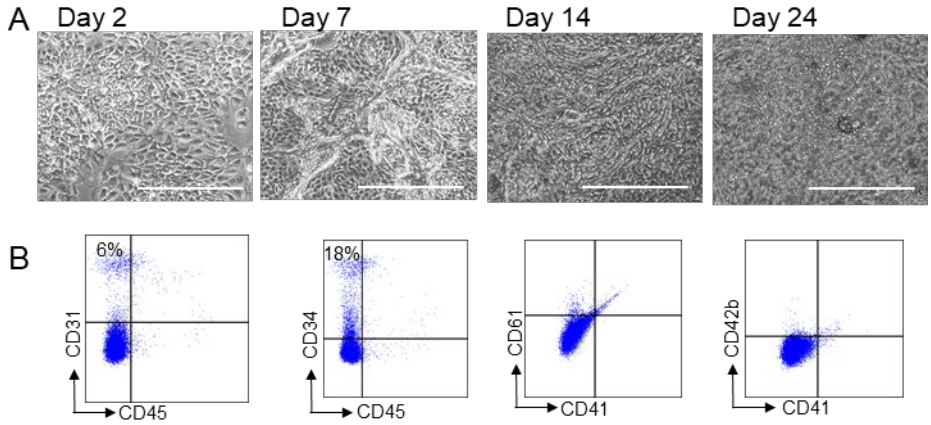

Figure 27: 2D megakaryocyte differentiation with APEL 2 medium.
(A) Phase-contrast pictures of 2D megakaryocyte differentiation with APEL 2 medium at day 2, 7, 14, and 24. Scale: 500 µm. **(B)** Cells were harvested on day 24 and analyzed for the expression of CD31, CD34, CD45, CD41, CD42b, and CD61 by flow cytometry. Only a few cells are CD31$^+$ and CD34$^+$ and all cells are CD41$^-$, CD42b$^-$, CD45$^-$, and CD61$^-$.

3.3.3 3D spin EB protocol generated a high number of megakaryocytes

Liu et al. published in 2015 a spin EB based method to differentiate feeder-free iPS cells into cells of the hematopoietic system and specifically into megakaryocytes (Liu et al., 2015). In our study, we used transferrin instead of insulin-transferrin-selenium and BSA at day 0 of differentiation as EB disintegrated using HSA at day 0 (data not shown). Liu et al. used BMP4 and VEGF until day 11 of differentiation. However, the BMP4 and VEGF receptor is expressed only in early stages of differentiation and reduced after mesodermal commitment (data not shown). No difference between the conditions supplementing VEGF and BMP4 until day 7 or day 14 was observed neither in the surface marker expression nor the cell quantity (Supplemental Figure 44). Therefore, VEGF and BMP4 were used only until day 7 of differentiation.

With the spin EB protocol, hematopoietic cells were successfully generated from iPS cells with all three different JAK2 genotypes. Three thousand single cells were forming an EB, which increased in diameter until day 14. First hematopoietic cells were in suspension starting from day 7 for JAK2 V617F^{hom} and at day 8 to 9 for JAK2 and JAK2 V617F^{het} iPS cells. For JAK2 V617F^{hom}, HSC were completely dense at day 14, recapitulated in the number of suspension cells counted at day 14 for each 96-well plate (Figure 28A). Clones with JAK2 revealed around 2.05 ±2.5 million, JAK2 V617F^{het} around 3.15 ±4.5 million cells, and JAK2 V617F^{hom} 8.85 ±4.4 million cells per plate. Those data

demonstrate that more suspension cells were released in cells with a homozygous JAK2 V617F background (28 B).

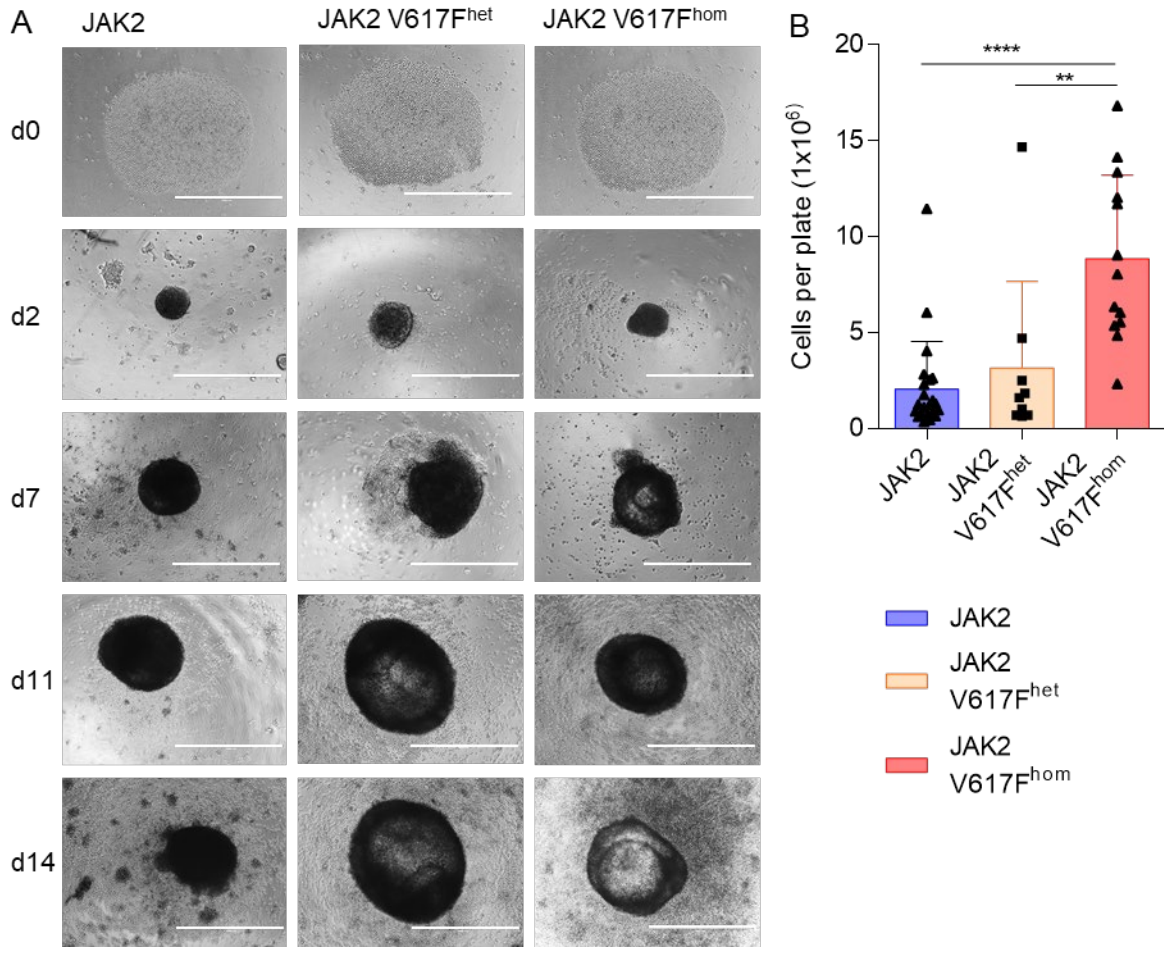

Figure 28: Spin EB megakaryocyte differentiation of JAK2, JAK2 V617F^{het}, and JAK2 V617F^{hom}. **(**A) Representative pictures of the EB development in spin EB differentiation from day 2 to day 14 for JAK2, JAK2 V617F^{het,} and JAK2 V617F^{hom}. Scale: 1000 µm. **(B)** Quantification of suspension cells per 96-well plate on day 14 of differentiation cumulated for JAK2 (n=22), JAK2 V617F^{het} (n=9), and JAK2 V617F^{hom} (n=13). Data is represented as means ± SD. Statistical significance was assessed by Student t-test (**p≤0.005, ****p≤0.0001).

3.3.4 Caspase inhibitor enhanced survival of purified megakaryocytes

Several techniques are available for isolating specific cells like fluorescence-activated (FACS) or magnetic-activated (MACS) cell sorting based on the surface protein expression. Cell survival after the purification is a crucial criterion. FACS can generate a stress response due to the shearing stress of the sheath fluid transporting the cells through the flow cell. Especially for larger cells like megakaryocytes, this can lead to enhanced apoptosis. Indeed, fluorescence sorted cells showed apoptosis rates of more than 75% 5 days after sorting CD41^{+}/CD61^{+} cells (data not shown).

MACS is around four to six times faster than FACS and can reduce cellular stress (Bowles et al., 2019) but has limitations regarding the selected surface markers.

Magnetic sorting of $CD61^+$ cells resulted in efficiencies of more than 95% of the sorted cells to be CD41/CD42b/CD61 expressing megakaryocytes. Still, the survival of the cells 5 days later remained on low levels. Alternative magnetic sorting of $CD42b^+$ cells and special MACS columns for larger cells did not enhance the viability.

Avanzi et al. reported in 2015 that the caspase inhibitor Q-VD-OPH increases the maturation and ploidy of megakaryocytes which produce more proplatelets (Avanzi et al., 2015). Therefore, we evaluated in our study the effect of Q-VD-OPH supplementation at 50 µM directly after magnetic sorting of $CD61^+$ megakaryocytes for 2 and 5 days (Figure 29). Two cell populations were observed in the FSC/SSC plot of flow cytometric data in the control conditions with DMSO for 5 days. The upper larger population was over 90% $CD41^+/CD61^+$, but most cells lost CD42b expression. The lower small population was also $CD41^+/CD61^+$ and over 60% of the double-positive cells were also $CD42b^+$.

In comparison, in both Q-VD-OPH treated conditions, the lower population in the FSC/SSC plot increased to more than 55% of detected cells. Similar to the untreated cells, the upper population was $CD41^+/CD61^+$ but $CD42b^-$. However, cells of the lower population were more than 75% $CD41^+/CD42b^+/CD61^+$. Supplementation with the caspase inhibitor for 5 days showed only a slight increase in triple-positive cells compared to 2 days of treatment.

In summary, Q-VD-OPH is suitable for enhancing the overall megakaryocyte survival after MACS and can be used for the maturation of sorted cells. As the difference between 2 days and 5 days of supplementation was only minor, 2 days of supplementation after sorting was used for further experiments.

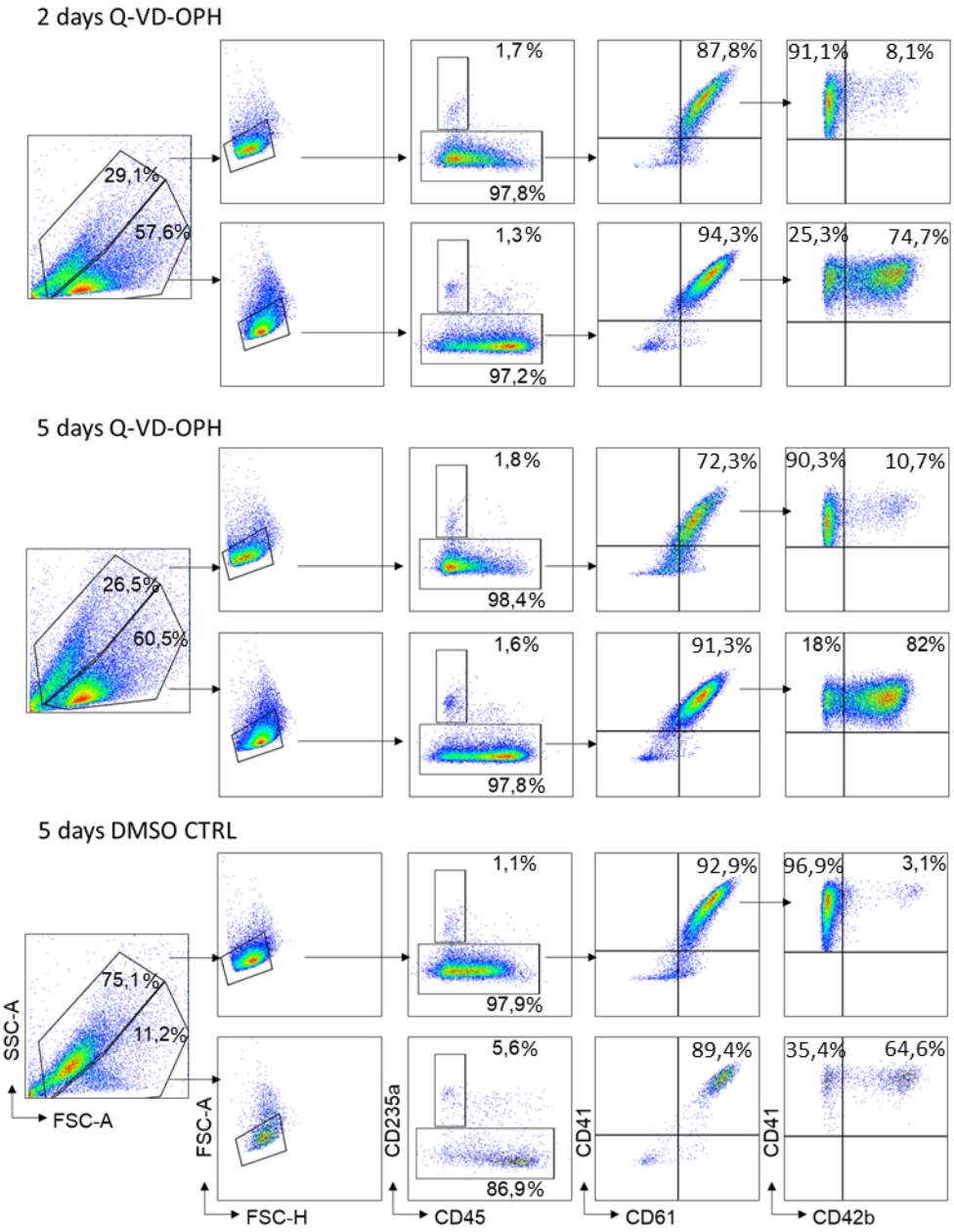

Figure 29: Effect of the caspase inhibitor Q-VD-OPH on cell survival after MACS purification.
Cells were MACS sorted on day 14 of spin EB differentiation for CD61⁺ cells and cultured for 2 or 5 days with 50 µM supplementation of Q-VD-OPH in the medium. As a control, DMSO was supplemented into the medium. Cells were analyzed by flow cytometry for indicated surface markers.

3.3.5 Megakaryocytes showed proplatelet production and have high ploidy

In addition to the expression of specific surface markers, there are further requirements to identify functional megakaryocytes. Premature megakaryocytes do not proliferate, but their nucleus is continuously dividing. This process called endomitosis leads to a multinucleated phenotype. Fully matured polyploid megakaryocytes start to build proplatelets budding from the outer cell membrane.

In Figure 30A, representative cytospins of day 14 megakaryocytes are shown for all three JAK2 genotypes. Megakaryocytes showed a high ploidy and no differences could be observed between the genotypes. Only around 10% of cells had a high ploidy visible in cytospins meaning that most megakaryocytes are non-mature but already $CD41^+/CD42b^+/CD61^+$. Maturation of megakaryocytes for longer times did not increase ploidy (data not shown). For a better comparison, flow cytometry analysis of the ploidy state should be performed in future.

The demarcation system producing the proplatelets was visible in cytospins and bright field microscopy (Figure 30A/B, indicated with black arrows). Long proplatelet structures emerged from the megakaryocyte's outer cell membrane. A platelet activation assay based on the stimulation with thrombin was performed to prove the functionality of these emerging platelets. Thrombin binds to the protease-activated receptors on the platelet surface and activates platelets (De Candia, 2012). As a control, freshly isolated platelets from CB were used. After stimulation, $CD41^+/CD61^+$ platelets were analyzed regarding their expression of p-selectin CD62b. Upon thrombin activation, CD62b, stored in non-activated platelets in α-granules, is translocated to the plasma membrane and therefore detectable by flow cytometry (J. Wang et al., 2005).

CB-derived platelets show a high population of over 87% $CD41^+/CD61^+$ cells, which express CD62p after thrombin treatment (Figure 30C/D). Although proplatelets and platelets were visible in both, phase contrast images and cytospins from iPS cells derived megakaryocytes, only a small proportion of the platelet population was $CD41^+/CD61^+$. No activated platelets were observed after the treatment with thrombin.

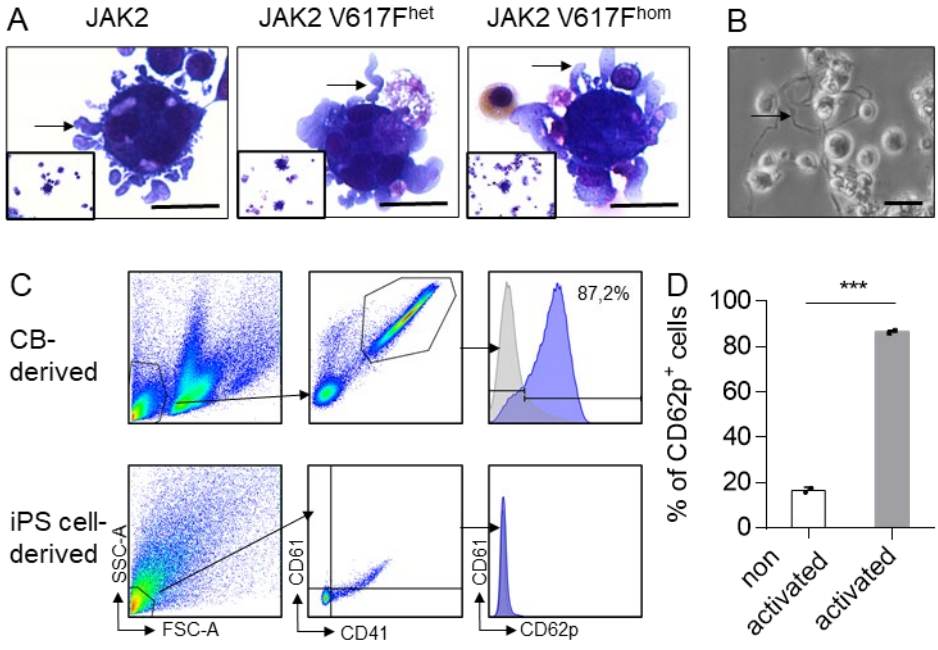

Figure 30: Morphologic characterization of iPS cell-derived megakaryocytes and platelets.

(A) Representative Diff-Quick stainings of PV2 JAK2, JAK2 V617F^{het,} and JAK2 V617F^{hom} iPS cell-derived megakaryocytes. Scale: 50 µm. **(B)** Representative phase-contrast picture of proplatelets forming from iPS cell-derived megakaryocytes. Scale: 50 µm. **(C)** Platelet activation assay of platelets derived from CB compared with iPS cell-derived platelets. **(D)** Platelet activation was quantified in CB-derived platelets in two independent experiments. Data is represented as means ± SD. Statistical significance was assessed by Student t-test (***≤0.001).

3.4 The JAK2 mutation is reflected in the megakaryocyte phenotype

With the establishment of the spin EB protocol for the generation of megakaryocytes, we had the opportunity to investigate the influence of the JAK2 mutation on megakaryocytic development. It is of great interest to what extent the mutation influences the cells' kinetics, maturation, and composition.

3.4.1 The JAK2 genotype had only minor effects on HSC

To determine if the different numbers of suspension cells produced by EB are caused by a general difference in kinetics based on the JAK2 genotype PV2 JAK2, JAK2 V617F^{het,} and JAK2 V617F^{hom} iPS cells were differentiated with the spin EB protocol. As the heterozygous and unmutated JAK2 clones were generated by repairing the mutation in the homozygous clone with CRISPR, the clones share all side mutations shown in Table 22. Therefore, observed differences are solely caused by the JAK2 mutation.

Cells were collected on day 11, 14, and 19 of differentiation. To further determine the effect of the JAK2 mutation, cells were differentiated with and without the supplementation of TPO. The JAK2 V617F mutation is expected to impact on the TPO effect directly. Cells were analyzed by flow cytometry using a hematopoietic panel with antibodies against CD31, CD34, CD43, CD45, and CD117.

CD34/CD45 are surface markers for hematopoietic stem cells with the potential to differentiate to most cells of the hematopoietic system, including megakaryocytes (Figure 31A). The percentage of double-positive cells remains on an elevated level over the analyzed 8 days of differentiation. The JAK2 V617F^{hom} clone has with around 40% fewer HSC than the other two genotypes with about 60% HSC.

CD34^{+}/CD43^{+} cells are described in the literature as early hematopoietic progenitors, which are also expressed in the early development of the MEP lineage. The number of CD34^{+}/CD43^{+} cells remained on a stably low level for JAK2 V617F^{hom} with around 20% (Figure 31B). In contrast, for JAK2 and JAK2 V617F^{het,} the number of double-positive cells was about 35%, decreasing over time to approximately 20%, similar to JAK2 V617F^{hom}.

CD117, also known as c-kit, is the SCF receptor and is expressed in early hematopoietic development. As expected, the level of c-kit^{+} cells declined for all three genotypes over

time and expression of c-kit on day 11 was higher for JAK2 V617F clones than the unmuted one (Figure 31C).

The platelet endothelial cell adhesion molecule PECAM-1, better known as CD31, is an adhesion protein expressed by endothelial cells and various hematopoietic stem cells like platelets, macrophages, granulocytes, lymphocytes, and megakaryocytes. The number of $CD31^+$ cells increased over time for JAK2 from under 60% to around 80%, is stable for JAK2 $V617F^{het}$ with approximately 80%, and decreases for JAK2 $V617F^{hom}$ starting with about 80% and reducing to 60% (Figure 31D).

Taken together, the analysis of the hematopoietic markers showed only minor effects in expression and conditions with and without TPO had no influence.

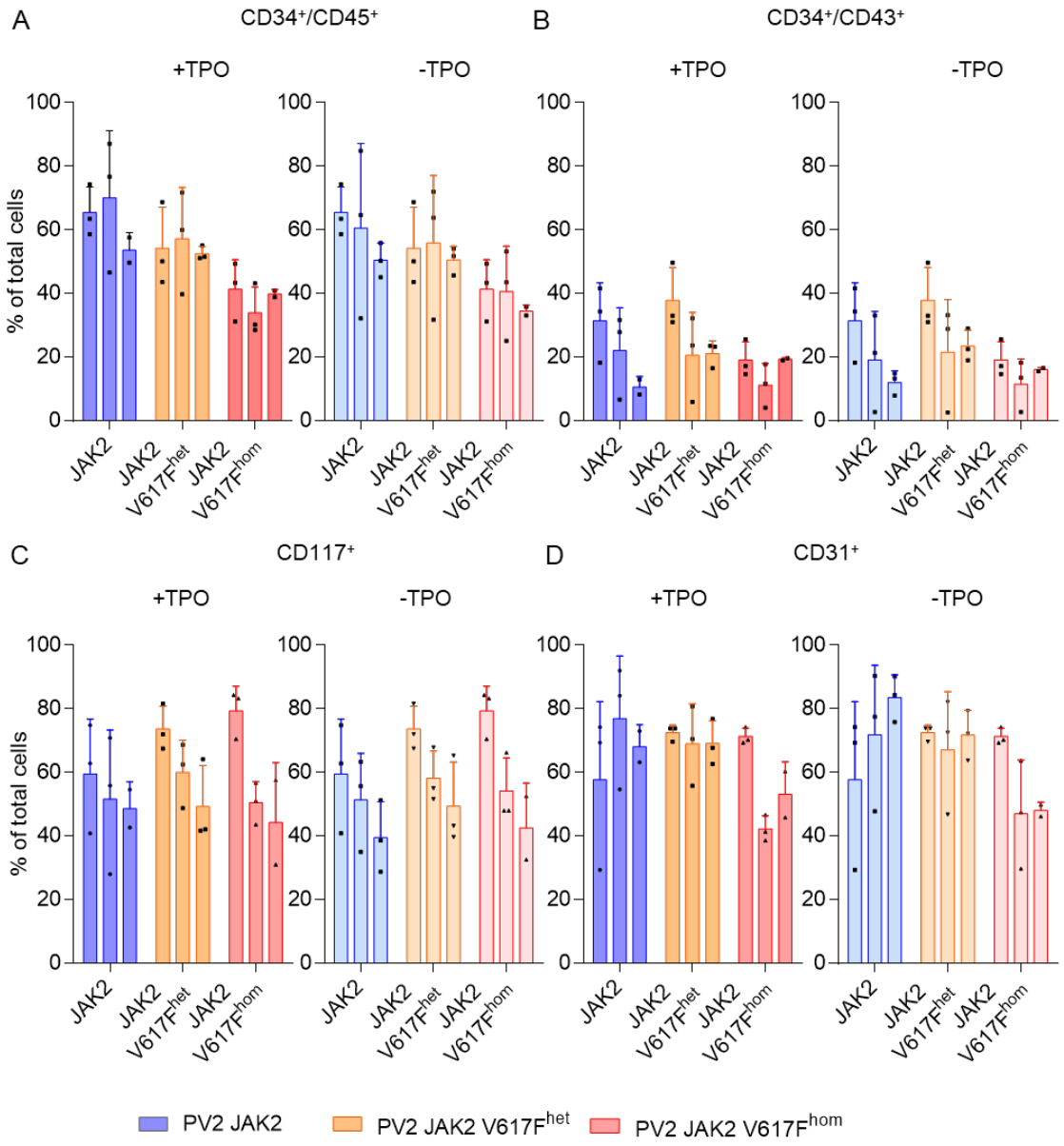

Figure 31: Differentiation kinetics of hematopoietic stem cell marker.
Suspension cells were analyzed by flow cytometry on day 11, 14, and 19 of differentiation. PV2 JAK2 (blue), JAK2 $V617F^{het}$ (yellow), and JAK2 $V617F^{hom}$ (red) were analyzed. TPO treated (dark color) and untreated

conditions (light color) were compared to analyze differences in TPO dependency on hematopoietic differentiation. **(A)** $CD34^+/CD45^+$, **(B)** $CD34^+/CD43^+$, **(C)** $CD117^+$ and **(D)** $CD31^+$ populations were analyzed. Three independet experiments were performed and data is represented as means ± SD.

3.4.2 JAK2 V617F had significant effects on megakaryocyte development

Even more interesting than the hematopoietic panel is the kinetics of megakaryocytic markers, as megakaryocytes are believed to be the main effector in myelofibrosis. Therefore, the same approach as in 3.4.1 was applied on the megakaryocytic markers CD41, CD42b, and CD61.

$CD41^+/CD61^+$ cells increased over time for the JAK2 unmuted clone from 15% at day 11 to 30% on day 19 (Figure 32A). The expression in JAK2 $V617F^{het}$ was stable around 30% at all time points, and markers decreased in the JAK2 $V617F^{hom}$ clone from 30% on day 11 to 20% on day 19. For JAK2 mutated clones, culture without TPO did not influence megakaryocyte counts. On the other hand, megakaryocyte numbers decreased over time to less than 10% in the JAK2 unmutated clone cultured without TPO.

$CD41^+/CD42b^+$ cells increased for JAK2 unmutated clones from around 15% on day 14 to more than 30% on day 19, while they were declining without TPO (Figure 32B). In contrast, higher $CD41^+/CD42b^+$ megakaryocytes levels were observed in JAK2 mutated clones with no difference between the heterozygous and homozygous condition nor the condition with and without TPO.

$CD41^+/CD42b^-$ megakaryocytes can be characterized, as described above, as more mature proplatelet forming cells. Other publications report that the CD42b expression remains stable over time, meaning that the loss of this marker can be identified as a hallmark of apoptotic cells. This is in line with the observations in 3.3.4, where $CD42b^+$ cells increased after the application of the caspase inhibitor. Numbers for JAK2 unmutated $CD41^+/CD42b^-$ megakaryocytes increased with the addition of TPO and remained on a low level (under 5%) for cells without TPO (Figure 32C). Also, for the JAK2 V617F muted clones, $CD41^+/CD42b^-$ cells increased over time, especially on day 19. No effects of conditions with and without TPO were observed.

Figure 32D shows the summarized marker expression of all analyzed clones on day 14 of spin EB. To not let the erythrocyte bias (more details in 3.4.3) of the homozygous clone cross-fade every other effect, cells were gated on $CD45^+$ cells and then analyzed for the megakaryocyte markers CD41, CD42b, and CD61. In JAK2 and JAK2 $V617F^{het}$ clones, more than 40% of the cells were $CD41^+/CD42b^+/CD61^+$ in the condition with TPO. In the JAK2 $V617F^{hom}$ clone, more than 70% were triple positive.

The JAK2 unmutated clones had with around 20% significantly fewer $CD41^+/CD42b^+/CD61^+$ cells in the condition without TPO. In JAK2 V617F clones, these

numbers remained stable without TPO. The observations made in Figure 32A/B/C are recapitulated in Figure 32D (and supplemental Figure 45 and Figure 46) and were significant due to the larger sample size and the missing erythrocytes. The patient-specific effects got less pronounced and the mutation-specific impact more prominent

In 2017, Sim et al. described that stem cell-derived megakaryocytes have different granularities based on their maturation state. Immature megakaryocytes have a low granularity which increases over time (Sim et al., 2017). SSC light enters the flow channel in flow cytometry from the light source, is refracted by cells in a direction outside the original light path and provides information about the internal complexity and granularity. Therefore, measurement of the SSC can be used to determine the maturation state of megakaryocytes. $CD41^{+}/CD42b^{+}/CD61^{+}$ cells were analyzed with regard to their FSC-A and SSC-A to determine the effect of the JAK2 mutation on maturation (Figure 32E). FSC-A, measuring the size of the cells, is at a similar level for JAK2, JAK2 $V617F^{het,}$ and JAK2 $V617F^{hom}$ cells. For SSC-A, measured values are higher, showing a higher granularity. Therefore, JAK2 $V617F^{het}$ and JAK2 $V617F^{hom}$ were more matured than the unmutated cells. Even though all JAK2 V617F clones have a larger SSC-A value than the unmutated, this effect is not significant due to the small sample size of n=3.

Altogether it can be concluded that the JAK2 genotype directly influences the kinetics of megakaryocyte development. For JAK2 unmuted clones, the number of megakaryocytes was lower than for mutated ones. Cells were developing slower and therefore also reached the peak of differentiation later. Furthermore, experiments show a direct influence of the JAK2 genotype on the TPO effect. For JAK2 unmuted clones, missing TPO causes a tremendous reduction of megakaryocytic differentiation. In contrast, only minor effects were observed for JAK2 $V617F^{het}$ and $V617F^{hom}$ clones without TPO. JAK2 $V617F^{hom}$ clones reached their peak of differentiation between day 11 and day 14. For JAK2, unmuted clones reached the highest megakaryocyte count on day 19. JAK2 $V617F^{het}$ clones were in between these extremes. The granularity confirmed this observation, as JAK2 mutant clones were less granular and therefore less mature.

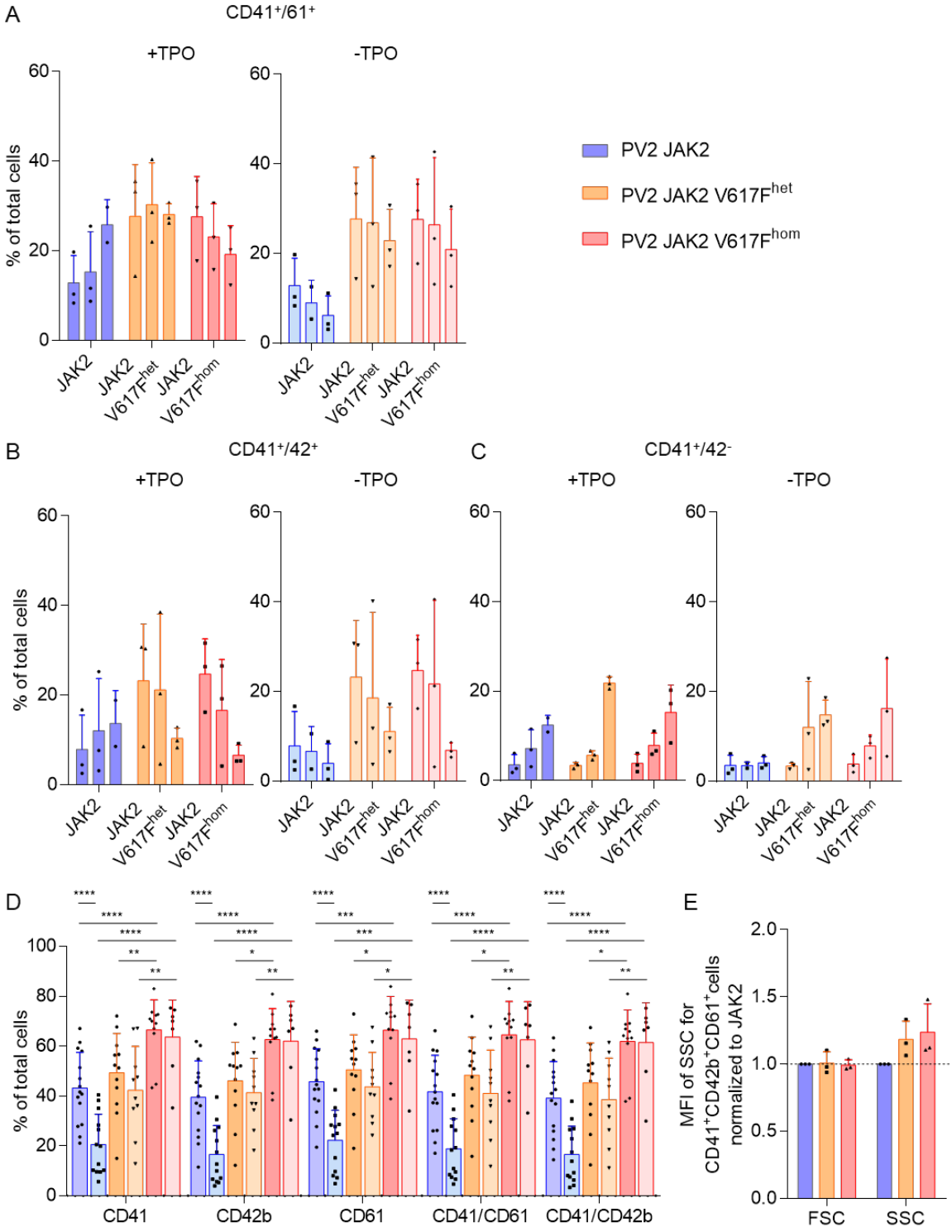

Figure 32: JAK2 genotype has significant effects on megakaryocytic markers expression and granularity.
Suspension cells of PV2 JAK2 (blue), JAK2 V617F^{het} (yellow), and JAK2 V617F^{hom} (red) were analyzed by flow cytometry on day 11, 14, and 19 of differentiation. TPO treated (dark color) and untreated conditions (light color) were compared to detect differences in TPO dependency on hematopoietic differentiation. **(A)** CD41^{+}/CD61^{+}, **(B)** CD41^{+}/CD42b^{+}, **(C)** CD41^{+}/CD42b^{-} cells were measured (all n=3). **(D)** Summary of differentiation from all three patients and genotypes (JAK2 + TPO n=15, JAK2 – TPO n=13, JAK2 V617F^{het} + TPO n=12, JAK2 V617F^{het} -TPO n=10, JAK2 V617F^{hom} + TPO n=11 and JAK2 V617F^{hom} -TPO n=7). **(E)** Analysis of changes in FSC and SSC populations (n=3). Data is represented as means ± SD. Statistical significance was assessed by Student t-test (*p≤0,05, **p≤0.005, ***p≤0.001, ****p≤0.0001).

3.4.3 JAK2 V617F caused erythrocyte bias in hematopoietic development

For further analysis of the effect of JAK2 V617F mutation on hematopoietic development, the number of erythrocytes was analyzed. In Figure 33A, representative flow cytometry plots for JAK2, JAK2 V617F^{het}, and JAK2 V617F^{hom} suspension cells on day 14 of differentiation are shown. 53% (±8.7) of differentiated cells were CD45^{-}/CD235a^{+} for the JAK2 V617F^{hom} clone. The JAK2 V617F^{het} clones had around 10.6% (±12.5) erythrocytes and the unmutated clones 1.6% (±1.6). Treatment with and without TPO had no effects on erythrocyte numbers. In contrast, conditions with and without TPO had a strong effect on the number of megakaryocytes.

In Figure 33B, erythrocyte numbers are depicted for day 11, 14, and 19 of the spin EB differentiation with and without TPO for all three genotypes of PV2. The number of erythrocytes was over 40% and remained stable over time for JAK2 V617F^{hom}. The JAK2 unmutated clone had less than 10% erythrocytes on day elven and the number declined until day 19. The JAK2 V617F^{het} clone had more than 20% erythrocytes on day 11, which reduced to about 10% on day 14 and day 19. The supplementation of TPO has no impact.

Figure 33C and supplemental Figure 45 shows the summarized CD235a expression of all analyzed clones on day 14 of spin EB with and without TPO. The observations of Figure 33B are recapitulated and JAK2 specific effects became more pronounced

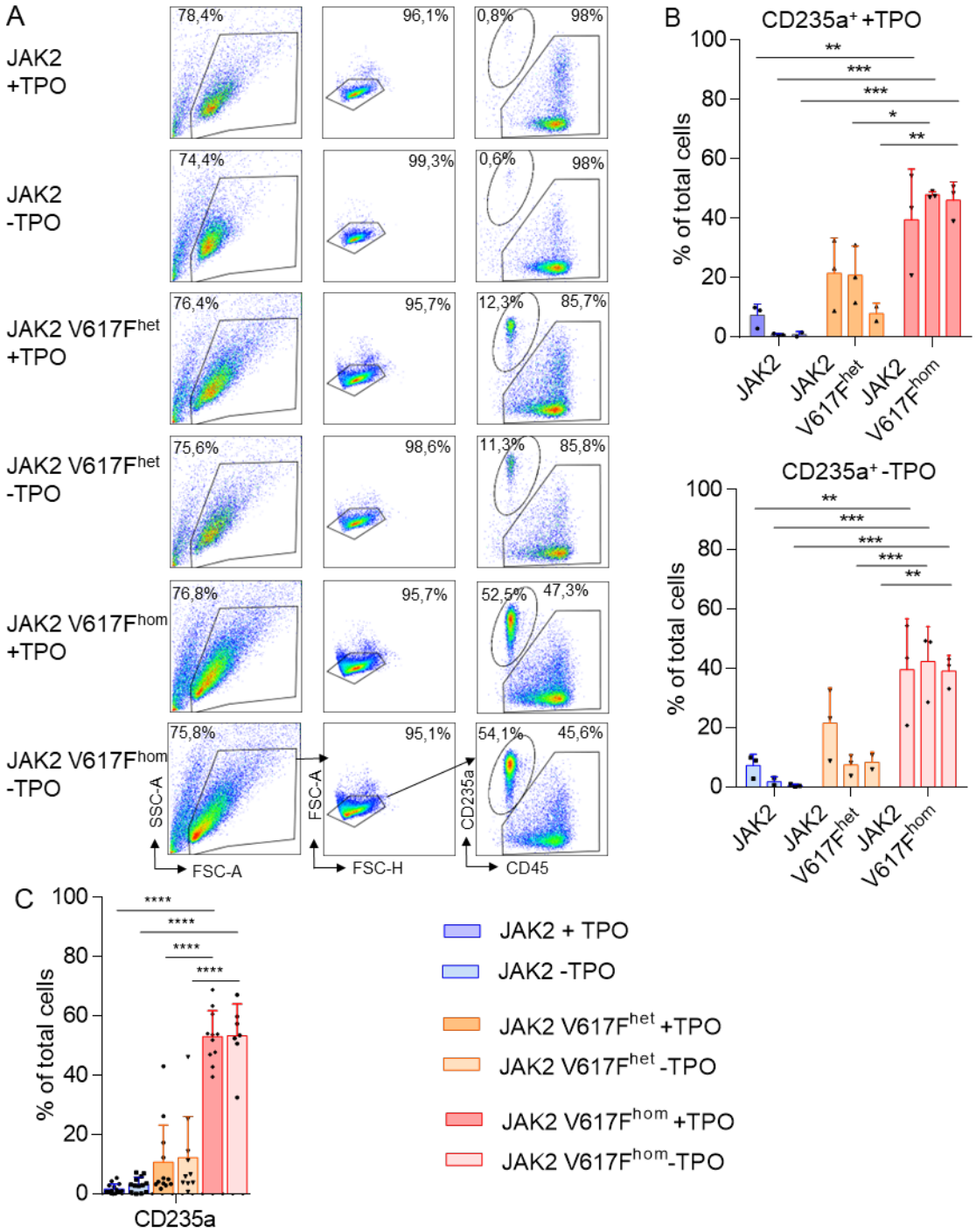

Figure 33: JAK2 V617F mutation causes bias towards erythrocytes.
(A) Representative flow cytometry plots of JAK2, JAK2 V617F^{het} and JAK2 V617F^{hom} iPS spin EB differentiation on day 14 with and without TPO treatment. **(B)** The CD235a expression was measured in suspension cells by flow cytometry on day 11, 14 and 19 of differentiation. PV2 JAK2 (blue), JAK2 V617F^{het} (yellow) and JAK2 V617F^{hom} (red) were analyzed. To analyze differences in TPO signaling, TPO treated (dark color) and untreated conditions (light color) were compared. (n=3) **(C)** Summary of CD235a expression from all three patients and genotypes (JAK2 + TPO n=15, JAK2 – TPO n=13, JAK2 V617F^{het} + TPO n=12, JAK2 V617F^{het} -TPO n=10, JAK2 V617F^{hom} + TPO n=11 and JAK2 V617F^{hom} -TPO n=7). Data is represented as means ± SD. Statistical significance was assessed by Student t-test (*p≤0,05, **p≤0.005, ***p≤0.001, ****p≤0.0001).

3.4.4 Erythrocyte bias is reflected in CFU assays with CD34$^+$ HSC

In CFU assays, colonies are counted after culture for 10 days in a semi-solid medium to determine the differentiation potential of CD34$^+$ HSC.

For the analysis of unbiased myeloid differentiation, CD34$^+$ cells were separated from day 14 spin EB suspension cells by MACS and cultured for 10 days in CFU medium. Colonies for erythrocytes (BFU-E and CFU-E), granulocytes (CFU-M), and macrophages (CFU-M), as well as mixed colonies (CFU-GM and CFU-GEMM), were quantified (Figure 34A). As bright field microscopy is a subjective quantification, colonies were further classified by staining picked colonies with Diff-Quick solution (Figure 34B).

Colonies were determined based on the following characteristics: Erythrocytes have the typical brownish color caused by hemoglobin's reaction with the benzidine peroxide solution. As they are not fully matured, they have a nucleus. Small spherical cells with a characteristic nucleus consisting of several segments are granulocytes. Macrophages are the biggest cells observed with a low nucleus to cytoplasm ratio and characteristic vacuoles. CFU-GM and CFU-GEMM are a heterogeneous mixture of the cells described above. Megakaryocytes are not visible in CFU as the medium composition does not favor megakaryocyte differentiation.

BFU-E, CFU-E, and CFU-GEMM occur in similar frequencies in all JAK2 genotypes (Figure 34C and supplemental Figure 47). In contrast, erythrocyte colonies were with 53.7% (±12.2) significantly more abundant in JAK2 V617F clones compared to JAK2 V617F^{het} with 29.9% (±14.2) erythrocytes and JAK2 unmutated clones with 24.2% (±16.3) erythrocytes. The number of granulocyte colonies was lower in JAK2 V617F^{hom} than JAK2 and JAK2 V617F^{het}, and macrophages colonies decreased significantly from JAK2 unmutated towards JAK2 V617F$^{het/hom}$.

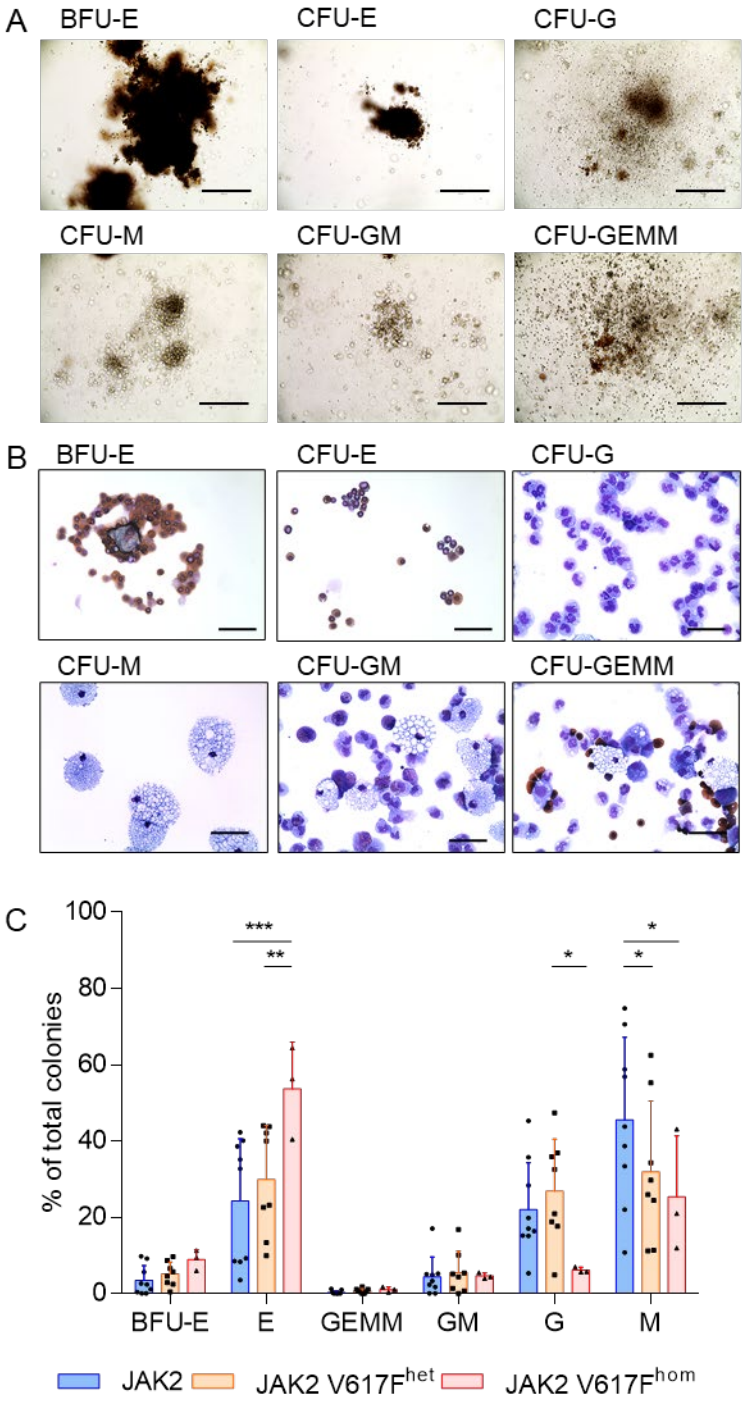

Figure 34: Quantification of colony-forming units from CD34⁺ cells cumulated from PV1-PV3. **(A)** CD34⁺ cells were seeded in a density of 10,000 cells per 12-well plate and cultured for 10 days. Bright-field images of the colonies after 10 days. BFU: burst forming unit, CFU: colony-forming unit, E: erythrocytes, G: granulocytes, M: macrophages. Scale: 400 µm **(B)** Cytospins of the colonies observed in A. Stained with Diff-Quick and benzidine peroxide solution. Scale: 50 µm **(C)** Quantification of the colonies after 10 days of culture. Genotypes are summarized over different clones to highlight the effect of the genotype (JAK2 n=9, JAK2 V617F^{het} n=8 and JAK2 V617F^{hom} n=3). Data is represented as means ± SD. Statistical significance was assessed by Student t-test (*p≤0,05, **p≤0.005, ***p≤0.001).

3.5 Gene expression analysis

By analyzing gene expression on mRNA level, it is possible to detect smallest changes caused by the JAK2 mutation. Therefore, RT-qPCR and RNA-Seq were performed.

3.5.1 RT-qPCR analysis revealed differential gene expression

mRNA gene expression analysis of $CD61^+$-purified megakaryocytes was performed using selected target genes on day 14 spin EB of all available clones. Studied genes can be divided into three subgroups: CXCL4, CXCL4L1, CXCL7 (also PPBP), and TGF-β as those genes associated with the development of myelofibrosis (Figure 35A), FLI1, GATA1, vWF, MPL, NF-E2, and EGF are essential genes during the differentiation of hematopoietic stem cells into megakaryocytes (Figure 35B) and IL-6 and TNF are genes that play an important role in inflammatory responses (Figure 35C). The results were summarized by JAK2 genotype from all patients. Results divided by patients are shown in supplemental Figure 48.

All tested myelofibrosis-related genes had the highest expression in JAK2 $V617F^{het}$ clones and were significantly upregulated compared to the JAK2 unmutated megakaryocytes. JAK2 unmutated and JAK2 $V617F^{hom}$ megakaryocytes were on the same level. Furthermore, the chemokines CXCL4 and CXCL7 were even higher expressed than the housekeeping gene GAPDH. The cytokine TGF-β, the driver of myofibroblast differentiation from MSC, was expressed in similar levels as GAPDH and CXCL4L1, which is only found in humans and unknown role in myelofibrosis, was less expressed than GAPDH.

Comparable to the expression of myelofibrosis-associated genes, higher expression of megakaryocyte developmental genes was also demonstrated in JAK2 $V617F^{het}$ clones. Overall expression was significantly lower compared with the myelofibrosis-associated genes, but this was expected because FLI1, GATA1, vWF, and NF-E2 are transcription factors that are generally expressed at low levels. GATA1 is an early transcription factor of megakaryocyte development, FLI1, VWF und EGF are intermediate factors, and NF-E2 is a late factor in the development. MPL as the TPO receptor was expected to be expressed stably over time. An important point to note is that all examined cells were $CD61^+$ with an additional high expression of the surfacer markers CD41 and CD42b, meaning that all analyzed cells were at least immature megakaryocytes. The higher expression of genes in JAK2 $V617F^{het}$ clones suggests that at day 14 of spin EB differentiation clones reached the peak of differentiation. JAK2 unmutated clones seemed to be rather immature, whereas the JAK2 $V617F^{hom}$ clone showed low expression of transcription factors which can be interpreted as more mature megakaryocytes.

Inflammation is an essential mechanism in myelofibrosis, leading to activation of MSC and deposition of fibers into the bone marrow. Analysis of the inflammatory-related genes IL-6 and TNF revealed no significant differences between different JAK2

genotypes. A slight trend showed an increased expression of these two genes in JAK2 V617F^{hom} clones, but as one out of the three measured samples had a low expression, this effect was not significant. This might indicate a more inflammatory phenotype in homozygous clones. To observe significant upregulation of inflammatory genes, day 14 of spin EB differentiation might be too early to detect significant upregulation of inflammatory genes.

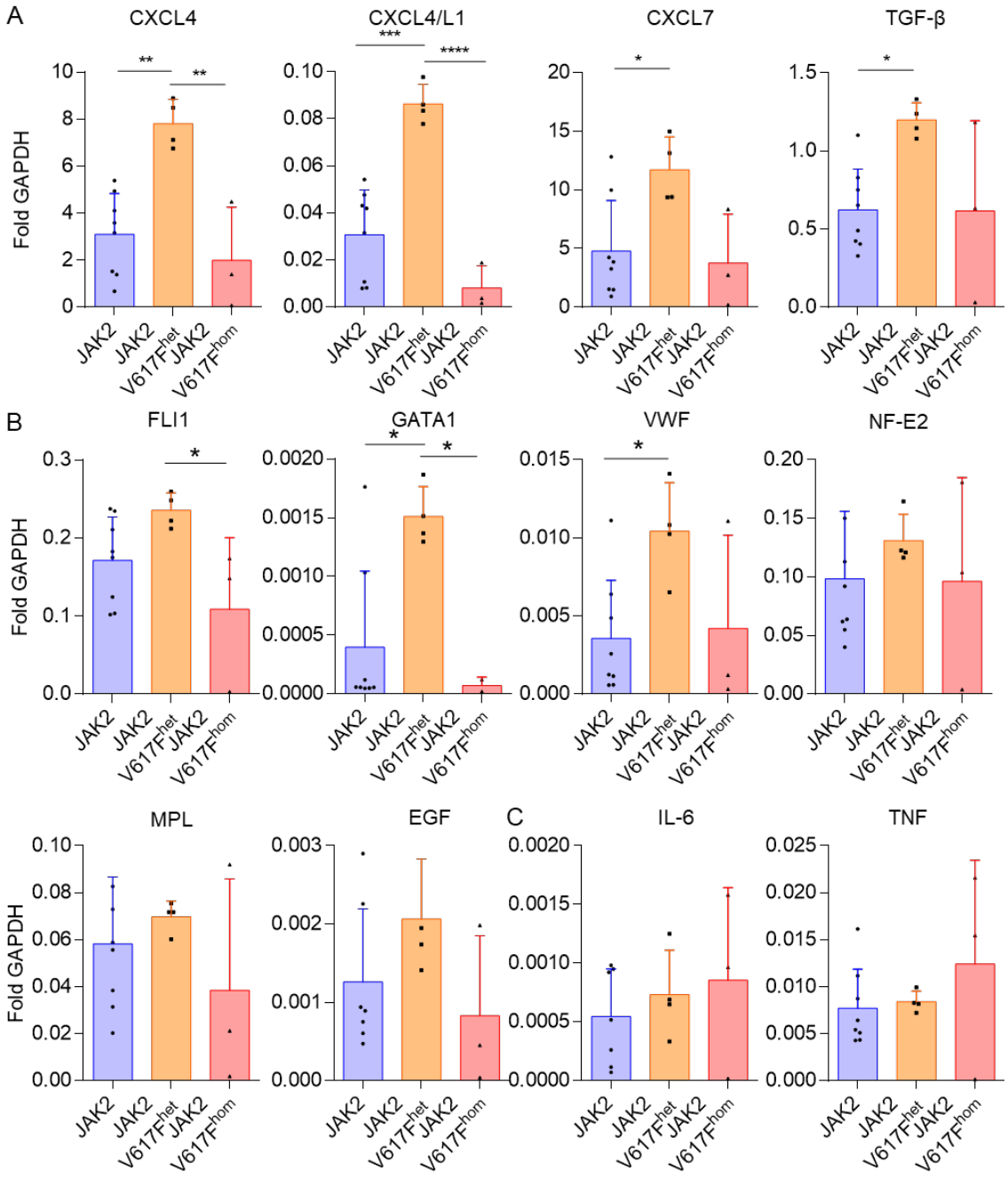

Figure 35: RT-qPCR analysis, genotypes summarized from all 3 patients.
mRNA expression analysis of day14 CD61^{+} megakaryocytes for PV1, PV2, and PV3. Genotypes are summarized for all patients and normalized to GAPDH. Blue: JAK2 (n=8), orange: JAK2 V617F^{het} (n=6) and red JAK2 V617F^{hom} (n=3). **(A)** Myelofibrosis associated genes, **(B)** megakaryocyte development genes **(C)** inflammatory genes were analyzed (JAK2 n=9, JAK2 V617F^{het} n=4 and JAK2 V617F^{hom} n=3). Data is represented as means ± SD. Statistical significance was assessed by Student t-test (*p≤0,05, **p≤0.005, ***p≤0.001, ****p≤0.0001).

3.5.2 Differential gene expression is reflected in transcriptome analysis

RNA-Seq analyses were performed on day 14 of PV2 JAK2 and JAK2 V617F^{hom} iPS cell-derived CD61^{+} megakaryocytes. The experiments were independently performed three times (in collaboration with K. Olschok, M.Sc. and M. A. S. de Toledo, Ph.D., Medical Clinic IV, RWTH Aachen University Hospital, Aachen, Germany). RNA-Seq data was analyzed was normalized by VOOM transformation (Law et al., 2014, in collaboration with M. Graßhoff, M.Sc. and I. Costa, Ph.D., Institute for Computational Genomics, Medical Faculty, RWTH Aachen University, Aachen, Germany). Thereby, the mean-variance relationship of the data is estimated and it is used to weight the data and translate logarithmic observations into linear models.

Unsupervised principal component analysis (PCA) was used to analyze the overall structure of our dataset (Jolliffe & Jackson, 1993). In Figure 36 A, the three JAK2 V617F^{hom} and the JAK2 unmutated megakaryocytes clustered together. Two JAK2 V617F^{hom} megakaryocytes also clustered close together and were more distant to the third RNA sample. The unsupervised clustering of differentially expressed genes (DEG) in Figure 36B showed the specific up- and down-regulation of different genes based on the genetic background and highlights the differences between those genotypes. Moreover, the sub clustering of the up- and downregulated DEG revealed specific patterns based on the genotype.

Gene ontology (GO) enrichment analysis can manage large data sets by classifying genes in specific predefined groups based on their biological function. GO analysis represents an easy but elegant way to compare gene expression patterns in differently treated samples or genotypes. In Figure 36C, we collected the top 20 up- and downregulated gene clusters. Only the three gene classes for organic, carboxylic, and sialic acid binding, were significantly upregulated in JAK2 V617F^{hom} compared to control. In total, 9 of these 20 upregulated genes were in the class of binding proteins. Other upregulated gene sets were mostly correlated to signaling and differentiation.

All gene clusters of the top 20 downregulated genes were significantly downregulated compared to the JAK2 unmutated sample (Figure 36C). Interestingly, 19 out of 20 gene clusters are related to ECM organization, ECM binding, and collagen organization. The only cluster not involved in ECM organization or interaction was the class of endoplasmic reticulum lumen genes.

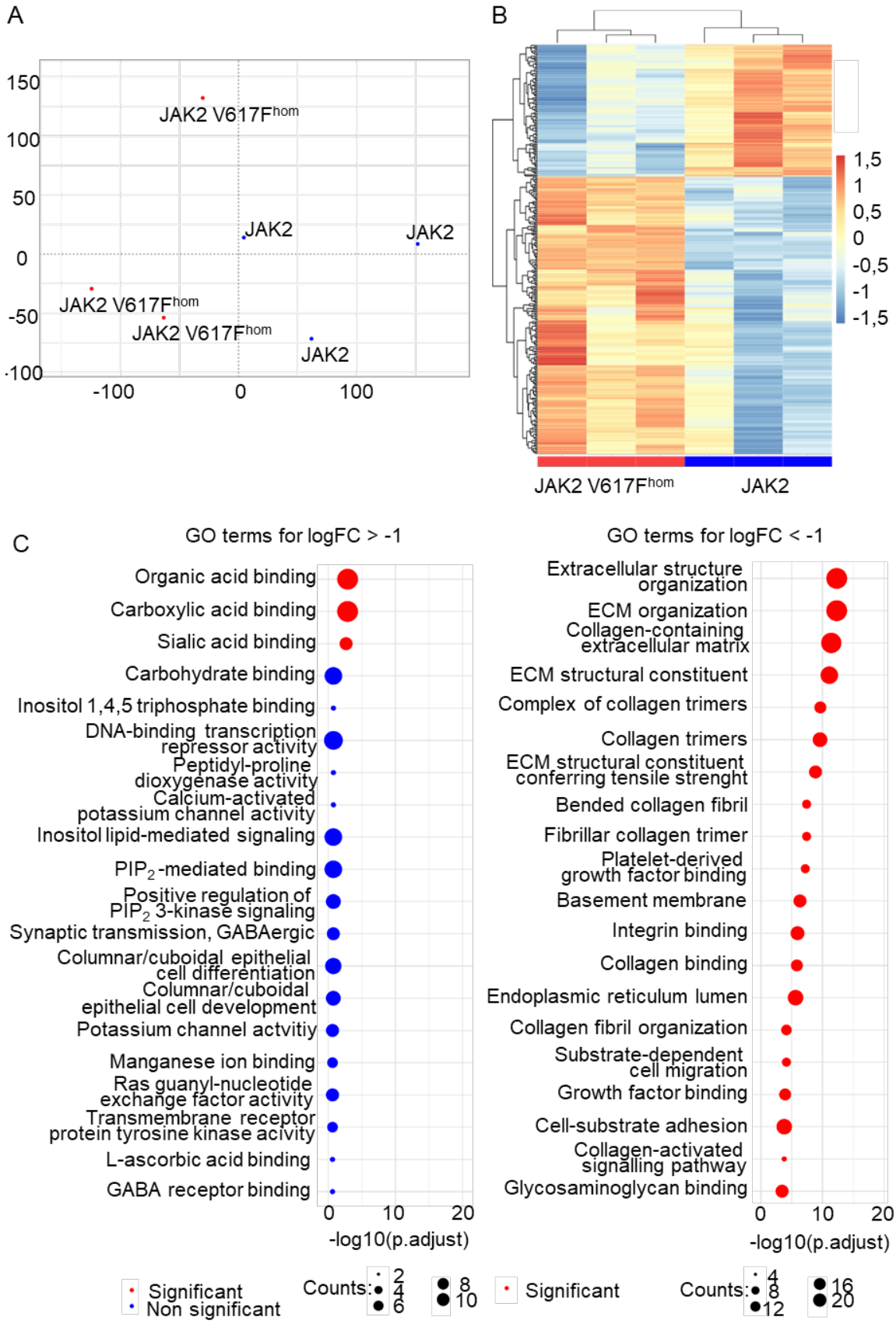

Figure 36: Analysis of megakaryocyte RNA-Seq data by PCA, VOOM transformed DEG analysis, and GO analysis.
(A) Principal component analysis (PCA) of JAK2 and JAK2 V617F^{hom} samples showed clustering by genotype **(B)** VOOM transformed differential expressed genes analysis (DEG) JAK2 and JAK2 V617F^{hom}

samples show distinct up- and downregulation of gene transcripts based on the underlying genotype. **(C)** Gene ontology (GO) of top up- and downregulated gene sets in JAK2 V617F^{hom} megakaryocytes compared to control. Data acquired in collaboration with K. Olschok, M.Sc. and M. A. S. de Toledo, Ph.D., (Medical Clinic IV, RWTH Aachen University Hospital, Aachen, Germany). Data analysis was performed in collaboration with M. Graßhoff, M.Sc. and I. Costa, Ph.D., (Institute for Computational Genomics, Medical Faculty, RWTH Aachen University, Aachen, Germany).

The more detailed analysis of the top 20 single up- and downregulated genes (Figure 37A) showed that 8 of the 20 upregulated genes are zinc finger proteins (highlighted in cyan), a heterogeneous group of proteins. They have 3D zinc finger structures with a zinc ion coordinating cysteine and histidine in common and play a role in DNA binding and transcriptional regulation, apoptosis, and protein folding. (Laity et al., 2001). Furthermore, 2 sialic acid-binding immunoglobulin-type lectins (Siglec) are upregulated. These proteins are mainly expressed by immune cells (Pillai et al., 2012). Seven of the top 20 downregulated genes are ECM proteins (six collagens and FN1). These findings are in line with the GO term analysis, where the ECM proteins were also downregulated. CXCL4L1 was also differentially expressed (*p=0.005) but not among the top 20 significantly up- and downregulated genes. Other genes from the RT-qPCR approach, including CXCL4 (*p=0.7), did not show a significantly changed expression. In total, more than 250 additional significant DEG were found comparing JAK2 V617F^{hom} megakaryocytes with the unmutated control (*p<0.05), including the downregulation of lysyl oxidase (LOX, p=*0.042), important as a regulator of ECM production 2020).

The analysis of pathway responsive genes (PROGENy) showed clustering of JAK2 and JAK2 V617F^{hom} megakaryocytes (Schubert et al., 2018; Figure 37B). No significant changes were observed in any of the analyzed pathways. However, a trend toward downregulation was observed for EGFR (*p=0.16), PI3K (*p=0.16), and TGF-β (*p=0.16) and a trend for upregulation for hypoxia-related genes (*p=0.17).

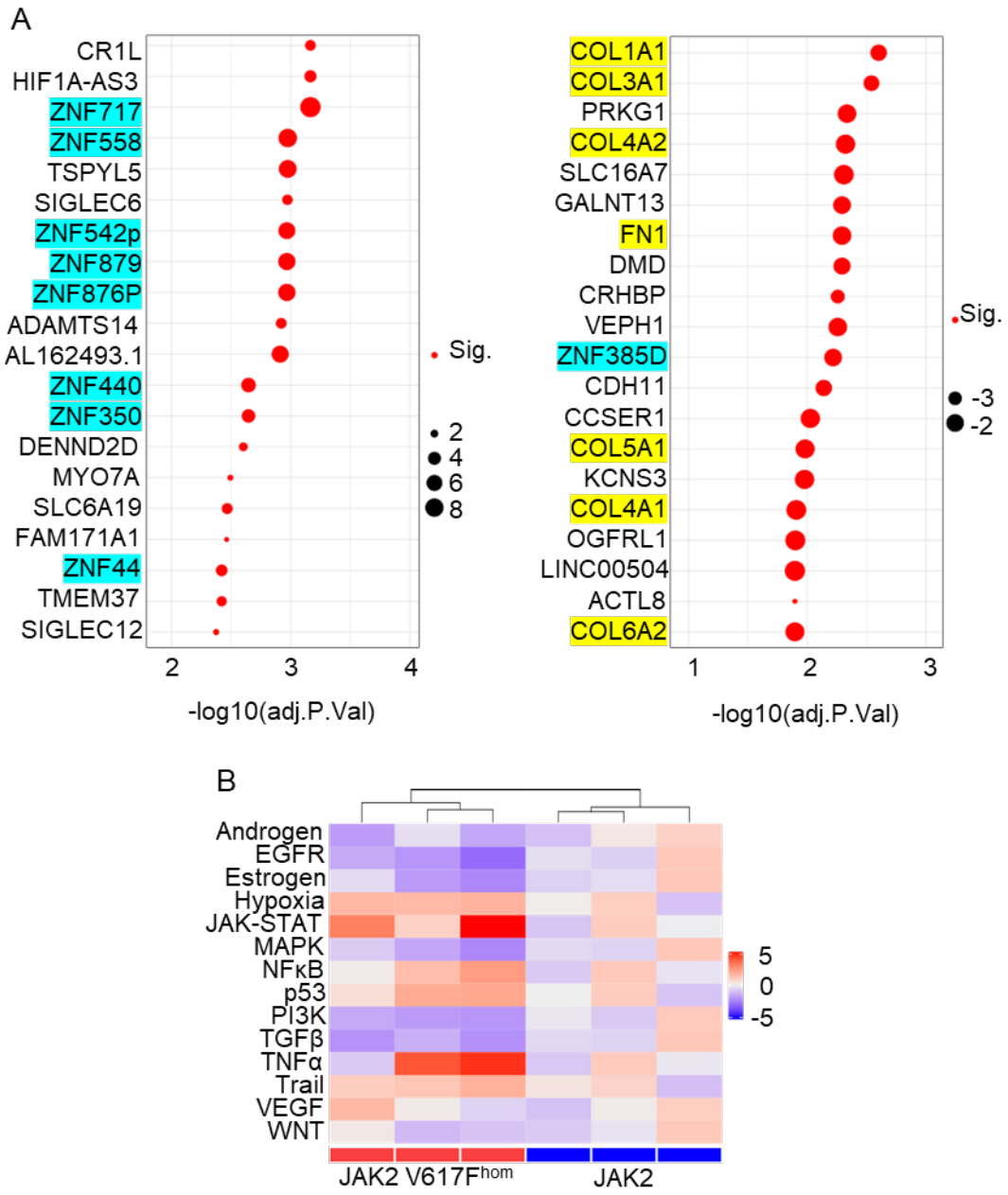

Figure 37: Top up- and downregulated genes in JAK2 V617F^{hom} compared to unmutated megakaryocytes and PROGENy analysis.
(A) Top 40 DEG divided in left, upregulated genes and right, downregulated genes. Zinc finger protein genes are highlighted in cyan, ECM proteins in yellow. **(B)** PROGENy analysis of JAK2 V617F^{hom} clones compared to the control. Data acquired in collaboration with K. Olschok, M.Sc. and M. A. S. de Toledo, Ph.D., (Medical Clinic IV, RWTH Aachen University Hospital, Aachen, Germany). Data analysis was performed in collaboration with M. Graßhoff, M.Sc. and I. Costa, Ph.D., (Institute for Computational Genomics, Medical Faculty, RWTH Aachen University, Aachen, Germany).

3.6 Generation of iPS-MSC and BM-MSC

One of the main points of this work was to establish an iPS cell-derived fibrosis model to dissect the interactions of megakaryocytes and MSC. The feasibility of BM- and iPS-MSC to undergo fibrosis is a major requirement of this system and is described in the following.

3.6.1 Isolation of BM-MSC from healthy donor hip bones

To answer whether cytokine stimulation can induce fibrosis on iPS-MSC, BM-MSC isolated of hip bone were used as a positive control. To circumvent donor-related variations, BM-MSC from 3 different donors were isolated and characterized for expression of typical MSC markers CD29, CD73, CD90, and CD105 and their capacity to undergo fibrosis.

The ideal time point was determined to perform the studies mentioned above in a preliminary experiment (data not shown). The strongest signal for α-SMA immunostainings was observed after 5 days of stimulation, which was then defined as the day of analysis for the following experiments. Isolated BM-MSC stimulated with CXCL4 or TGF-β/BMP4 expressed CD29, CD73, CD90, and CD105 (Figure 38A).

The degree of fibrosis was analyzed based on α-SMA expression, the amount of extracellular collagen, and the expression of distinct genes. After 5 days of TGF-β/BMP4 stimulation, BM-MSC had a 30% higher α-SMA expression than the untreated control. For CXCL4, only a slight upregulation was measurable. Quantification of all three patients showed a significant upregulation in the TGF-β/BMP4 condition (Figure 38B and C, supplemental Figure 50).

The immunostaining in Figure 38D and supplemental Figure 51 recapitulates the findings that the TGF-β/BMP4 stimulated condition expressed more α-SMA compared to the untreated control. Once again, the CXCL4 condition did not change the α-SMA expression. The immunostaining of GLI1 showed the same expression pattern in all three conditions.

Furthermore, staining of extracellular collagen fibers with Sirius Red solution after 5 days of stimulation showed increased fibrotic fibers in TGF-β/BMP4 stimulated BM-MSC compared to the unstimulated control. In the CXCL4 stimulated condition, only slightly more fibers were visible compared to unstimulated cells. BM-MSC treated with CXCL4 showed faint staining compared to unstimulated cells (Figure 38E).

To analyze gene expression after stimulation, RT-qPCR was performed. Again, validating experiments were performed to define the best time point for analysis on the gene level. Three different time points for stimulation were evaluated (1, 3, and 5 days), showing the strongest effects after 3 days of stimulation (data not shown). ECM genes like fibronectin (FN), the collagens COL1A1, COL1A2, and COL3A1 which are the base of reticulin fibers and the intracellular matrix gene α-SMA were analyzed. To elucidate the stimulation effect with TGF-β/BMP4 and CXCL4, their receptors TGF-βR, BMPR, and CXCR3, respectively, were analyzed. FAP, GLI1, CXCL4, and CXCL4L1 are genes described by other publications as possible effectors during fibrosis. MRTF and SRF are

serum response genes and regulate early genes in the cell cycle and cell differentiation pathways.

A significant upregulation of FN expression was observed after stimulation with TGF-β/BMP4. Furthermore, a slight but not significant increased expression was observed in COL1A1, CXCL4, GLI1, and α-SMA. All these genes are known effectors of fibrotic transformation. Overall, the treatment of CXCL4 showed no difference in gene expression compared to control. All other analyzed genes show no change in gene expression after stimulation (Figure 38F). For better visualization, tested genes and conditions are summarized in a heat map shown in Figure 38G. The upregulated genes COL1A1, CXCL4, GLI1, and α-SMA clustered together in the TGF-β/BMP4 condition. Of note, two of the three BM-MSC lines analyzed clustered after TGF-β/BMP4 stimulation separated from the other conditions, emphasizing donor-specific differences in primary material. No change in these genes could be observed after CXCL4 stimulation, the data suggest that the CXCL4 is not enough for fibrotic transformation in this human model.

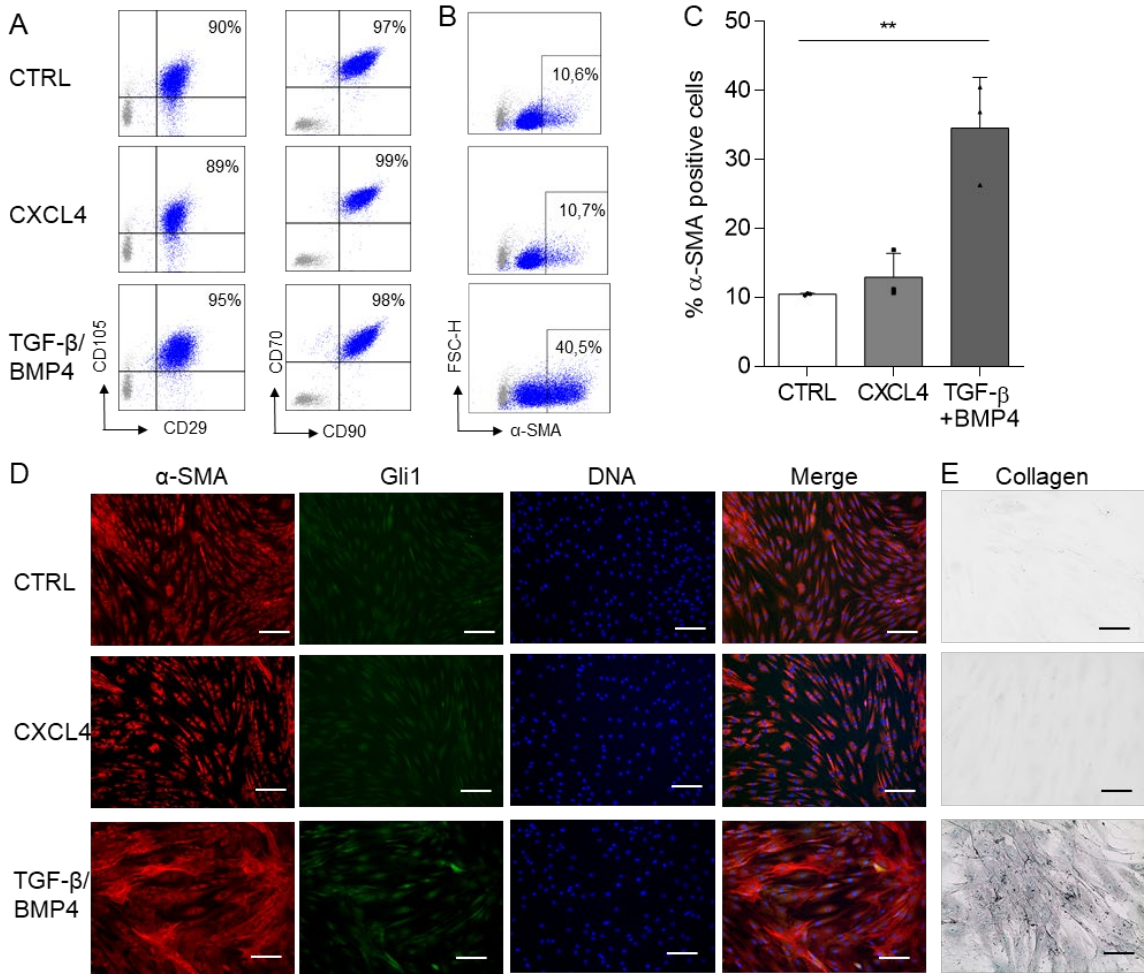

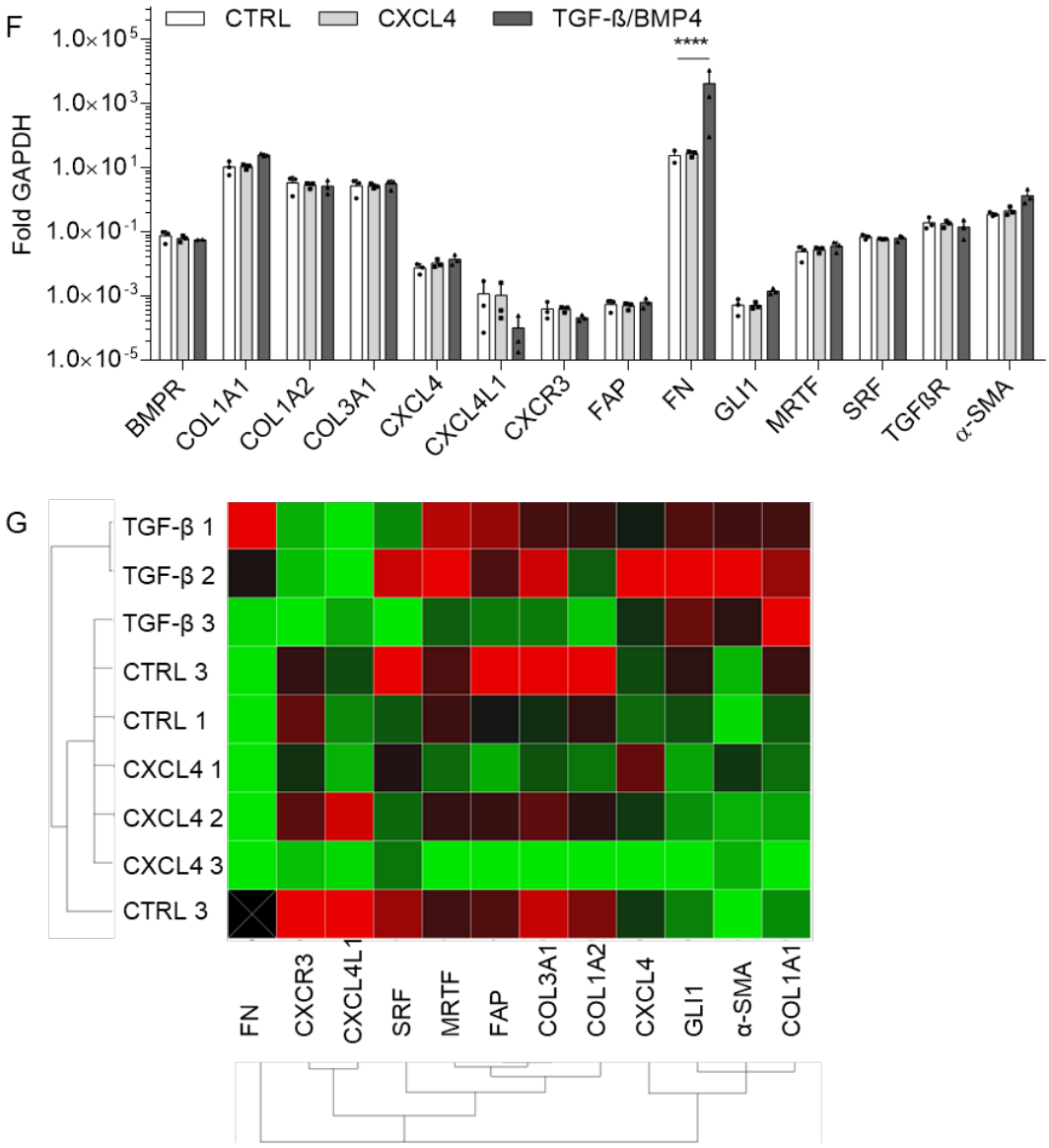

Figure 38: Characterization of BM-MSC from hip bones.
(A) BM-MSC expressed the MSC core marker CD29, CD73, CD90, and CD105 in flow cytometry analysis in control, CXCL4, and TGF-β/BMP4 conditions. Isotype control is displayed in grey. **(B)** Flow cytometry analysis of α-SMA expression is shown in control, CXCL4, and TGF-β/BMP4 conditions **(C)** α-SMA upregulation after stimulation of three different BM-MSC lines with CXCL4 or TGF-β/BMP4 was quantified (n=3). **(D)** Representative images of α-SMA (red), GLI1 (green), and DAPI (blue) immunostaining after stimulation of unstimulated BM-MSC, or stimulated BM-MSC with CXCL4 or TGF-β/BMP4 for 5 days. Scale: 100 µm **(E)** Syrius Red staining of collagen fibers for unstimulated BM-MSC or stimulated with CXCL4 or TGF-β/BMP4 for 5 days. Scale: 100 µm **(F)** RT-qPCR analysis of relevant genes of unstimulated MSC, or stimulated MSC with CXCL4 or TGF-β/BMP4 after 3 days (n=3). **(G)** Heatmap of gene expression from all three healthy donor BM-MSC in control, CXCL4, and TGF-β/BMP4 conditions. Data is represented as means ± SD. Statistical significance was assessed by Student t-test (**p≤0.005, ****p≤0.0001).

3.6.2 Directed differentiation of iPS-MSC

Donor-specific variation in MSC was observed when inducing fibrosis upon TGF-β/BMP4 stimulation. iPS cell-derived MSC were established to use them in a co-culture model with Megakaryocytes to overcome this limitation. Frobel et al. published in 2014 a protocol for efficient differentiation of iPS cells into MSC (Frobel et al., 2014). Since the

JAK2 V617F mutation has only been reported for the hematopoietic lineage and not for MSC, iPS-MSC generation was only performed with JAK2 unmutated clones.

On MEF layer cultured PV1 JAK2 iPS cells were transferred 5 days on ultra-low attachment plates to generate EB and further cultured on gelatin-coated plates. The cells had an MSC-like phenotype after 26 days (Figure 39A). Cells were characterized by flow cytometry with the MSC surface markers CD29, CD73, CD90, and CD105. The hematopoietic and endothelial markers CD31, CD34, and CD45 were analyzed as a control and were expected to be negative in MSC (Figure 39B). Over 95% of cells expressed the MSC markers but none of the endothelial and hematopoietic markers.

Furthermore, the differentiation capacity of the MSC towards the adipogenic and osteogenic lineage was evaluated. For adipogenic cells, lipid droplets were stained with BODYPI visible as green roundish droplets. Lipid droplets were observed in the stimulated condition. Alizarin Red S was used for the osteogenic lineage to stain calcium deposits which were only present in the differentiated condition (Figure 39C). Thus, iPS cells were successfully differentiated into functional MSC.

Next, we assessed whether the generated iPS-MSC differentiate into myofibroblasts after stimulation with TGF-β/BMP4. As described for BM-MSC, iPS-MSC were cultured for 5 days with TGF-β/BMP4 to test whether iPS-MSC generate fibrotic α-SMA fibers after stimulation. iPS-MSC were stimulated for 5 days and BM-MSC were used as a positive control. α-SMA is shown in representative pictures in Figure 39D. For stimulated BM-MSC, distinct α-SMA fibers were found, whereas only a background signal was observed for unstimulated cells.

In contrast, iPS-MSC showed less pronounced α-SMA fibers when stimulated. Compared to the unstimulated control, no difference in α-SMA expression was observed. To quantify the α-SMA expression, fibrotic clusters were randomly counted in 10 pictures and quantified for α-SMA positive clusters. For BM-MSC, α-SMA clusters were accumulated compared to control, while numbers of clusters were similar between iPS-MSC and controls. This means that although patient-specific iPS cells can be successfully differentiated into iPS-MSC, fibrosis induction was not confirmed. Therefore, iPS-MSC were not suitable to use in a 2D co-culture model with Megakaryocytes focusing on fibrosis induction. Therefore, BM-MSC were used for the establishment of a fibrosis model.

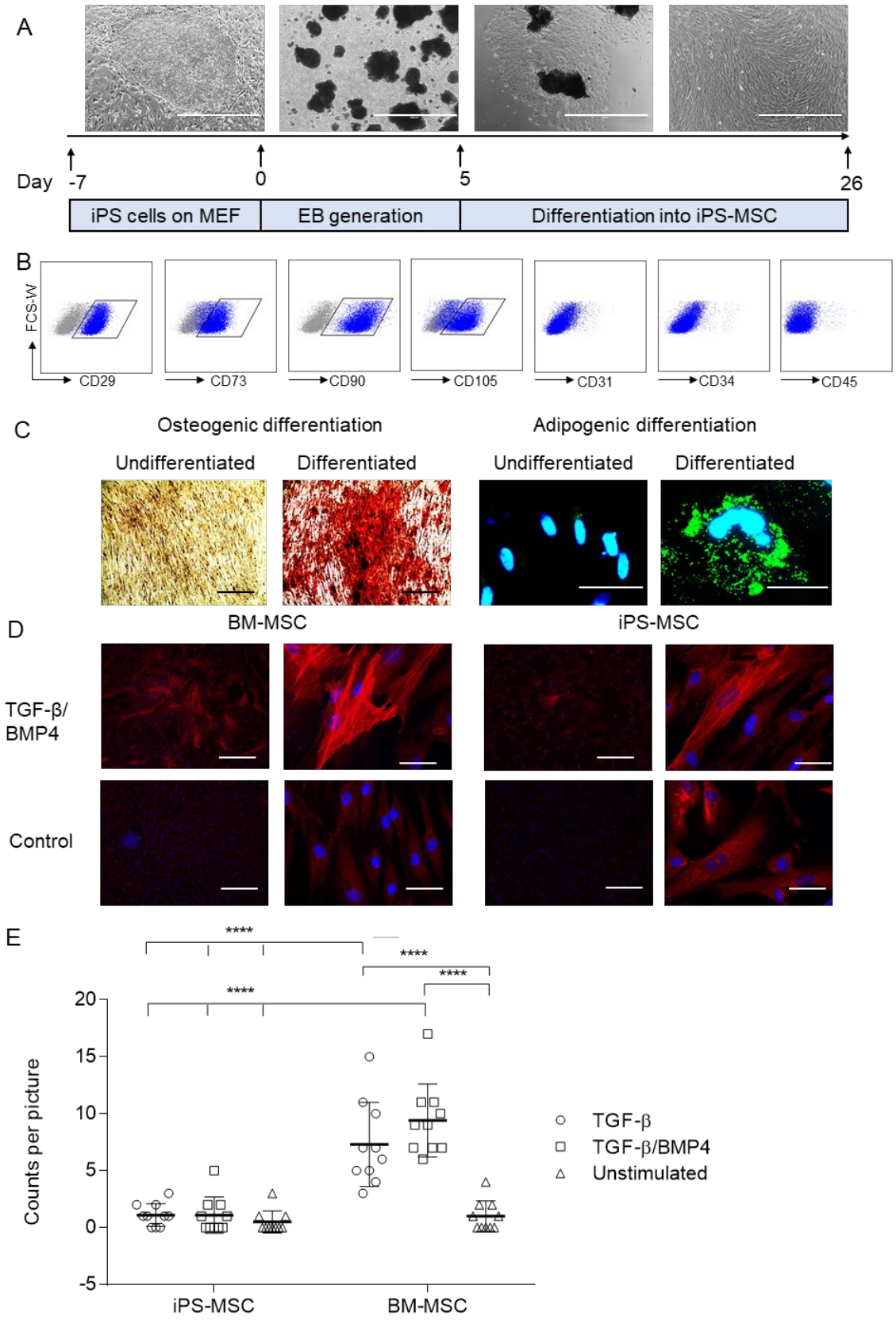

Figure 39: Generation and characterization of iPS-MSC.
(A) Scheme of differentiation of iPS cells into iPS-MSC with representative phase-contrast images of iPS cells on MEF, EB formation on ultra-low attachment plate, attachment of EB on gelatin-coated plates, and fully differentiated iPS-MSC. Scale: 1000 µm **(B)** iPS-MSC displayed expression for MSC core marker CD29, CD73, CD90, and CD105 and were negative for CD31, CD34, and CD45. Isotype control displayed in grey. **(C)** iPS-MSC differentiated towards the osteogenic and adipogenic lineage and were stained with alizarin

red and BODYPI/DAPI, respectively. iPS-MSC cultured with normal growth medium were used as control. Scale: 400 µm (osteogenic differentiation) and 50 µm (adipogenic differentiation). **(D)** Representative images of α-SMA (red) and DAPI (blue) immunostaining after stimulation of iPS-MSC and BM-MSC with TGF-β/BMP4 for 5 days. Scale: 400 µm and 50 µm **(E)** Quantification of α-SMA clusters in TGF-β/BMP4 stimulated cells versus control unstimulated cells in iPS-MSC and BM-MSC. Ten randomly picked images were analyzed. Data is represented as means ± SD. Statistical significance was assessed by Student t-test (****p≤0.0001).

3.7 Co-culture of iPS-MSC and iPS-MK

Due to mutations in the JAK-STAT pathways and its constitutive activation, cytokine expression is dysregulated (e.g., CXCL4), leading to the activation of $GLI1^+$ and $LepR^+$ MSC differentiating into myofibroblasts, producing the ECM, and therefore causing fibrosis in mice. (Decker et al., 2017; Schneider et al., 2017). A co-culture model from patient-derived iPS cells differentiated into megakaryocytes combined with isogenic or healthy donor MSC can help to elucidate this process.

To understand the mechanism of fibrosis in a 2D co-culture model, several factors must be considered: (i) which kind of MSC can be used (ii) which is the required density and the suitable medium for the culture of two different cell types, (iii) how to isolate and purify the iPS cell-derived megakaryocytes (iv) which timeframe is suitable for detecting the fibrosis.

As described in 3.6.2, BM-MSC were used in this model instead of iPS-MSC. The first experiments tested which medium is suitable for cultivating BM-MSC and iPS cell-derived megakaryocytes. Several publications describe the co-culture of MSC with mostly primary $CD34^+$ HSC or megakaryocytes. The goal in these protocols is to favor the megakaryocyte survival and enhance platelet production without activating them. The use of FCS to support the growth of MSC is common in all protocols (Mendelson et al., 2019; Schneider et al., 2017).

To minimize the number of FCS that could influence the megakaryocytes, culture tests were performed with 0%, 0.5%, 2%, and 10% FCS in SFM with TPO, IL-11, and SCF since this is the medium composition for iPS cell-derived megakaryocytes. 0.5% FCS still supported slow growth of BM-MSC, whereas 0% resulted in no proliferation. The cytokines had no influence on α-SMA expression in the TGF-β stimulation control (data not shown). The BM-MSC culture was started with 5,000 cells/cm² seeded 2 days before the start of the co-culture, which gave rise to a confluent layer at the end of the co-culture. Additionally, low-density MSC were used, not reaching confluency.

Before starting with the co-culture, tests were performed if the conditioned medium from JAK2 V617F megakaryocytes or the lysed cells were suitable to induce the transformation of BM-MSC into myofibroblasts. After 5 days, the staining of α-SMA showed fibrotic clusters in both JAK2 and JAK2 $V617F^{hom}$ cells and the lysate and conditioned medium. The α-SMA expression was higher with the conditioned medium

compared to the lysate condition, but no differences could be observed between JAK2 and JAK2 V617F^{hom} (Figure 40).

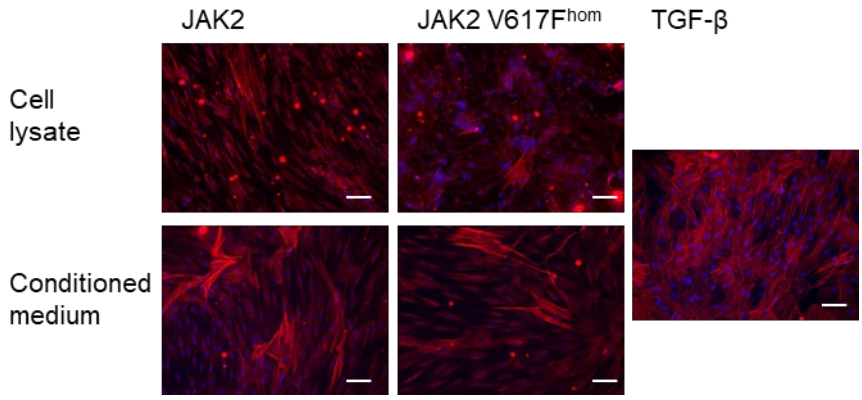

Figure 40: BM-MSC with conditioned medium and cell lysate.
BM-MSC were cultured 5 days with conditioned medium and lysate of JAK2 and JAK2 V617F^{hom} megakaryocytes. The medium was changed on day 3 and fresh lysate or conditioned medium was applied. Staining for α-SMA (red) and the nucleus (blue). Representative pictures. Scale: 100 µm.

Since the lysed cells and the conditioned medium showed no difference between JAK2 and JAK2 V617F^{hom}, the next step was to use a direct co-culture of BM-MSC and iPS cell-derived megakaryocytes. For further experiments of purified megakaryocytes, treatment with caspase inhibitor for 2 days was performed, followed by the co-culture. Furthermore, the day 11 unpurified HSC megakaryocytes population was harvested and co-cultured for 5 days.

Five days of BM-MSC co-culture with CD61^{+} JAK2 and JAK2 V617F^{hom} megakaryocytes increased the α-SMA in expression. The positive control with TGF-β and BMP4 showed a high upregulation with clearly visible α-SMA fibers (Figure 41A). Comparable results were observed for the co-culture of day 11 non purified HSC and megakaryocytes (data not shown).

The quantification of the α-SMA expression by flow cytometry did not show an upregulation compared to the unstimulated control. Day 11 non purified HSC and megakaryocytes were co-cultured for 5 days with BM-MSC in two different densities. For high-density BM-MSC, a slight shift in the population for JAK2 V617F^{hom} compared to unmutated and heterozygous mutated JAK2 was visible. However, all three conditions show less α-SMA expression than the unstained control and much less than the TGF-β and BMP4 stimulated positive control (Figure 41B).

Additionally, also the ECM protein collagen was stained to detect if fibrosis was induced. Only slightly more collagen fibers were observed in all three genotypes compared to the unstimulated control. Between the JAK2 genotypes, no differences were found. In contrast to the TGF-β/BMP4 stimulated positive control, where collagen fibers were visible (Figure 41C).

In summary, neither the MSC stimulation with megakaryocytic cell lysate nor conditioned medium nor the direct co-culture in different conditions drove the differentiation of MSC into myofibroblasts in a 2D model. Differences were found between the co-culture conditions and the control. The expected differences between JAK2 unmutated megakaryocytes compared with JAK2 V617F megakaryocytes was not observed.

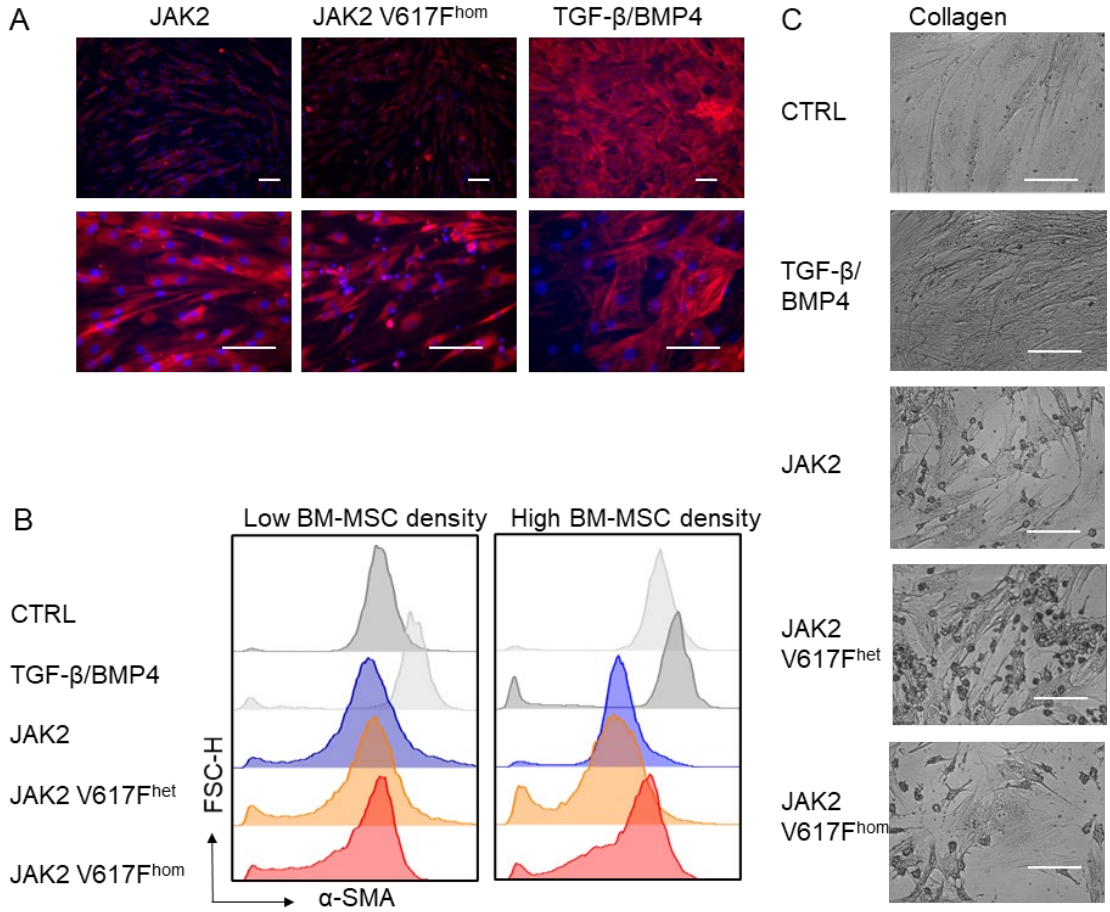

Figure 41: Analysis of α-SMA and collagen expression after co-culture of malignant iPS cell-derived megakaryocytes with BM-MSC.
(A) BM-MSC were co-cultured 5 days with CD61^{+} JAK2 and JAK2 V617F^{hom} megakaryocytes. Representative images of α-SMA staining and the nuclei are shown in red and blue, respectively. Scale: 100 µm (upper) and 50 µm (lower). **(B)** Flow cytometry analysis of α-SMA expression after co-culture of BM-MSC in 2 different densities with day 11 spin EB bulk population. **(C)** Collagen staining after co-culture of BM-MSC in 2 different densities with day 11 spin EB bulk population. Scale: 50 µm.

4 Discussion

4.1 Rationale and significance of this study

MPN are rare diseases with only 2 per 100,000 new diagnosed cases per year, mostly in adults over 60. Less than 1 of 100,000 patients develop myelofibrosis (Moulard et al., 2014). The underlying mechanisms and especially the corresponding mutations remained unidentified until the early 2000s.

With the discovery of the JAK2 mutation in 2005 (James et al., 2005), MPL mutation in 2006 (A. D. Pardanani, 2006), and CALR mutation in 2013 (Klampfl et al., 2013; Nangalia et al., 2013), the underlying driver mutations are known today. A study with more than 170 MPN patients described a low allele burden with a median of 25% in ET patients, a higher allele burden with a median of 40% in PV patients, and the highest allele burden in MF with 95% mutated JAK2 V617F (Alshemmari et al., 2014). The underlying mechanism in the different outcomes depending in the JAK2 V617F allele burden is still unknown.

Several murine models have been established recently to untangle the mechanistic, but translation into the human system needs to be improved. Also, JAK2 V617F MPN cell lines are commercially available (e.g., HEL and SET2) and are very well suited for basic mechanistic questions on individual protein functions or first drug screening studies (Fenerich et al., 2020). The drawback of these cell lines is their adaption to the artificial cell culture environment, which makes them behave like cancer cells and not reflect the phenotype of the patient (van Staveren et al., 2009). Due to their location in the bone marrow, patient material and particularly primary megakaryocytes are challenging to obtain.

With its potential to create patient-specific HSC, megakaryocytes and MSC in high amounts, the iPS cell technology allows us to create a human *in vitro* model to understand MPN and bone marrow fibrosis better. In combination with the CRISPR/Cas9 technology for precise gene editing and the NGS technologies for high throughput generation of gene expression data, this gives us the tools needed to unravel the disease mechanisms, identify new therapies, and a cure for myelofibrosis.

Ye et al. were the first group to reprogram JAK2 V617F heterozygous mutated MPN PBMNC into iPS cells and differentiating these cells into HSC (Ye et al., 2009). They could show that these cells are biased towards the erythrocytic lineage. In a later publication, they further tested JAK2 inhibitors in these iPS cell-derived cells (Ye et al., 2014). Subsequently, many other groups generated iPS cells from MPN patients and described EPO resistance of these cells (Saliba et al., 2013), involvement of endothelial

cells in thrombopoiesis (Guadall et al., 2018), and differentiation of MPN-derived JAK2 V617F iPS cells into megakaryocytes (W. Wang et al., 2018). A drawback in these studies is that no one analyzed the complete gene set of JAK2 unmutated, JAK2 V617F^{het,} and JAK2 V617F^{hom} cells, which is different from our study. Furthermore, the co-culture of MSC and patient-specific iPS cell-derived hematopoietic cells to dissect the mechanisms of myelofibrosis is a novel approach and was not published before. A co-culture model holds great potential to understand interactions of different cell types *in vitro* by representing the microenvironment.

4.2 Successful generation of patient derived iPS cell clones and CRISPR/Cas9 mediated genetic modification

In this study, we used reprogrammed iPS cells from three different PV patients. All clones exhibited an iPS cell-specific phenotype, expressed pluripotent markers, showed a three lineage differentiation potential, and had a normal karyotype. Previous studies have shown that MPN patients with JAK2 V617F mutation have precedent driver mutations correlated with poor survival (Papaemmanuil et al., 2013). The analysis of 31 genes associated with MPN by NGS (Kirschner et al., 2018; Toledo et al., 2021) revealed additional mutations and polymorphisms in TET2, CBL, ASXL1, EZH2, TP53, and SETB1 in our iPS cell clones.

Jeong et al. demonstrated in 2019 the cytokine-regulated activation of TET2 by JAK2 in hematopoiesis. Mutations in the TET2 gene are associated with increased self-renewal in the hematopoietic lineage cells and co-mutation with JAK2 V617F was reported to increase the oncogenic potential in patients (E. Chen et al., 2015). Mutations in CBL were found in high frequencies in patients with JAK2 V617F mutation and promoted an IL-3 hypersensitivity of these cells. (Jeong et al., 2019).

A higher mutation frequency in the genes ASXL1, EZH2 TP53, TET2, and SETB1 was described in MPN patients, but the observed polymorphisms have not been reported to influence MPN yet (Papaemmanuil et al., 2013).

The presence of different mutations in cells of the same patient reflects the clonal composition and genetic complexity in MPN. This highlights the value of the different generated iPS cell lines, reinforcing the importance of generating JAK2 unmutated and JAK2 V617F^{het} clones of the PV2 JAK2 V617F^{hom} clone, as these new clones share the whole genetic background with all side mutations.

.

4.2.1 Generation of the full complement of V617F JAK2 clones

A drawback of the previously mentioned studies was that they used just one or 2 iPS cell clones from one patient. However, to directly correlate the observed phenotypes with the genotype, all three JAK2 genotypes are required. Only then can it be safely assumed that observed differences are due to the JAK2 mutation and not caused by other patient-specific mutations.

We demonstrated that the allele burden of the patient directly correlates with the JAK2 genotype because patient samples with a JAK2 V617F allele burden lower than 37% resulted in JAK2 unmutated and JAK2 V617F^{het} clones after reprogramming. In contrast, patient samples with an allele burden of 96% resulted in homozygous clones.

To establish a complete set of genotypes for one patient, we successfully obtained the isogenic PV2 JAK2 unmutated and JAK2 V617F^{het} clones from the JAK2 V617F^{hom} clone using CRISPR/Cas9. The insertion or repair of the JAK2 V617F mutation to generate isogenic clones was performed so far only recently in an immortalized human erythroid progenitor cell line (Baik et al., 2021). The repair or insertion of the JAK2 V617F mutation in iPS cells has not been reported yet.

The application of the ALT-R CRISPR system demonstrated high efficiency in repairing the JAK2 V617F^{hom} mutation. Using the ATTO fluorescence label increased the efficiency of our approach as FACS of the cells with inserted CRISPR complex was possible.

The additional silence mutation was inserted into the donor template to prevent the JAK2 V617F gene sequence from being modified multiple times. Due to the two mismatches, the V617F mutation and the silent mutation, the gene sequence is not any more complementary to the gRNA, and the RNP complex cannot bind. Sanger sequencing of the successfully generated PV2 JAK2 V617F^{het} clones showed heterozygosity in the JAK2 V617F codon and the inserted silent mutation. Unexpectedly, also for the generated JAK2 unmutated clone, the inserted silent mutation was heterozygous modified. As both codons produce a valine, this fact has no further impact on the clone phenotype.

The off-target screening on the website of iDT DNA resulted in three possible protein-coding off-target in COA6 and CREBL2. These off-targets were different in at least three bases compared to the used sgRNA, of which at least two nucleotides were different in the seeding region. Sanger sequencing of these genes revealed no changes (data not shown, screening conducted by M. A. S. de Toledo, Institute for Biomedical Engineering, Department of Cell Biology, RWTH Aachen University, Medical School, Aachen, Germany).

4.2.2 Generation of CXCL4^{KO} iPS cells

Our study aimed to dissect the mechanisms of myelofibrosis in an *in vitro* system. In this context, CXCL4 has been shown to be an important chemokine in the murine system and the study of patient samples (H. Gleitz et al., 2020). Knockout of CXCL4 was performed using four gRNA where the combination of two gRNA caused a double-strand break in combination with the Cas9 nickase (Boehnke et al., 2021). This approach reduced the possibility of off-target modifications as two sgRNA that bind close to each other are required for a double-strand break. Therefore, the probability of off-targets is close to zero.

Nevertheless, off-targets were analyzed with the help of the iDT DNA website. All possible off-targets had at least two mismatches. In combination with the used nickase system, the off-target risk can be neglected. The resulting iPS cells showed normal growth, pluripotency marker expression, and differentiation potential. As CXCL4 is not expressed in the iPS cell state, this was expected (Boehnke et al., 2021). Additionally, no knockout effects on kinetics, morphology or differentiation efficiencies were detected during the differentiation of CXCL4^{KO} cells into megakaryocytes (data not shown).

Since the human system contains the chemokine CXCL4L1, which differs by only three amino acids in the protein-coding sequence, a double knockout of CXCL4/L1 was targeted. The function of CXCL4L1 is not fully known yet. It is possible that this protein rescues the CXCL4^{KO} and that no phenotype is visible in a single CXCL4 knockout. Analysis of the screened single-cell clones showed no clone with a biallelic knockout of both genes. The first screening by PCR showed that the CRISPR/Cas9 application had a relative efficiency of almost 50%. However, the calculated theoretic probability of finding a clone with a biallelic knockout in both genes has a probability of only 6% (0.5^4). In addition, gRNA 1 was designed to recognize both CXCL4 and CXCL4L1. It is possible that the RNP complex did not have the same binding efficiency for both genes.

In summary, there are 2 possible explanations: The number of single-cell clones analyzed was too low, and therefore, no CXCL4/L1^{dKO} clone was found. Alternatively, due to the possible unequal recognition of the genes, one gene was less affected. To avoid this problem for future experiments, it is helpful to perform a double knockout in two steps. First generating a biallelic CXCL4^{KO} and subsequently apply CRISPR/Cas9 again, specific for CXCL4L1. This approach is more time-consuming, but the probability of generating a CXCL4/L1^{dko} clone is higher. As the CXCL4^{KO} was already generated (Boehnke et al., 2021), the CXCL4L1^{KO} could be targeted as a next step.

4.3 iPS cell differentiation into megakaryocytes

After establishing all required iPS cell clones, a megakaryocyte differentiation protocol was required to generate patient-specific megakaryocytes. The protocol should be easy to apply to generate a high number of megakaryocytes in a reasonable time. The megakaryocytes should resemble adult human primary megakaryocytes, ideally in morphology, gene expression profiles, and other properties.

Many different protocols are available for megakaryocyte differentiation. Most protocols aim to generate megakaryocytes from healthy donor iPS cells as an *in vitro* source for platelets (Börger et al., 2016; Sugimoto & Eto, 2017). In this study, we aimed to find a protocol without the need for complex technologies such as culture in bioreactors (Eicke et al., 2018) or the integration of foreign DNA into our cells, e.g., in forward reprogramming techniques (Moreau et al., 2016).

Since the first generation of iPS cells in 2007, more than 130 studies were published using iPS cells to generate megakaryocytes (pubmed.ncbi.nlm.nih.gov, searching for “iPS cells” and “megakaryocytes”, 31.05.2021). The number of publications for the generation of other hematopoietic lineages from iPS cells is 10 times higher.

The number of published studies reflects the difficulties and the need to generate HSC and megakaryocytes from iPS cells. Generation of autologous HSC and specified hematopoietic cells like megakaryocytes or platelets is a long-standing goal in regenerative medicine. This would overcome graft-versus-host-disease and the bottleneck of missing transplant material. In addition, no clinical application of iPS cell-derived megakaryocytes or platelets is on the market yet (Deinsberger et al., 2020). So far, our knowledge on hematopoiesis and especially malignant changes in the hematopoietic niche are limited (Ackermann et al., 2015).

In our study, two different protocols for the differentiation of iPS cells into megakaryocytes were tested before the successful application of the spin EB protocol. The first protocol was the commercially available MES supplement, designed to differentiate $CD34^+$ cells from PB into megakaryocytes. The differentiation of $CD34^+$ HSC into megakaryocytes with this method failed. Possible reasons for the failure might be differences between primary and iPS cell-derived HSC. Several studies showed that *in vitro* generated HSC have an altered differentiation potential and resembled embryonic hematopoiesis (Demirci & Tisdale, 2018; Demirci et al., 2020). In addition, the genetic background of iPS cells may also influence differentiation, as the MES kit was developed for the differentiation of healthy donor HSC. The genetic background might also be the reason for the failure of the tested 2D differentiation protocol as the published protocol used healthy donor iPS cells (Börger et al., 2016).

The differentiation protocol used in this thesis was initially published in 2015 by Liu et al. With slight modifications, we could reduce the costs and maintain the number of generated megakaryocytes. Generated megakaryocytes expressed the markers CD41, CD42b, and CD61 and proplatelet production was observed.

After MACS purification of $CD61^+$ megakaryocytes, we observed a high percentage of apoptotic cells and downregulation of CD42b after 5 days. Sim et al. described in a publication from 2017 that CD42b is downregulated in apoptotic megakaryocytes and is associated with lower proplatelet production (Sim et al., 2017). In normal megakaryopoiesis, CD42b is expressed during the whole megakaryopoiesis and thrombopoiesis (Liu et al., 2015; N. Zhang & Newman, 2019). By using the caspase inhibitor Q-VD-OPH, described by Avanzi et al. in 2015 and Sim et al. 2017, we developed an approach to purify megakaryocytes based on the expression of the marker CD61 and showed that the viability of cells increased significantly after using the caspase inhibitor(Avanzi et al., 2015; Sim et al., 2017).

Nevertheless, the analysis of megakaryocytes has shown that only 10% of cells had a high ploidy and the platelet activation assay failed. Liu et al. reported that only 16% of their analyzed megakaryocytes had a ploidy over 4N. They also observed that only 16% of platelets were $CD41^+/CD42b^+$ and that ADP could activate only 6% of these proplatelets. Sugimoto and Eto described in a review from 2021 that the low ploidy and low (pro)platelet production in iPS cell-derived protocols is a general problem of differentiation from iPS cells due to the embryonic state of megakaryocytes (Sugimoto & Eto, 2021). The yield of platelets can be enhanced by using stirred bioreactors, causing shear forces and enhancing platelet production (Eicke et al., 2018). However, the overall embryonic state reflects that there are still some unknown components missing to develop mature megakaryocytes.

In our study, several reasons for the low platelet production are possible: (i) platelets were cultured for too long and could therefore not be activated anymore, (ii) our iPS cell-derived megakaryocytes do not produce functional platelets, (iii) observed platelets were largely debris, and therefore activation was not possible. More investigations and improvements for the generation of (pro)platelets are needed to solve this problem. As our study aims to generate patient-specific megakaryocytes from iPS cells for analysis and later co-culture models, the megakaryocytes obtained are nevertheless suitable for this approach.

4.4 iPS cell derived megakaryocytes reflected patient phenotypes

The most prominent symptom in PV is an elevated erythrocyte count. This can lead to thrombosis, strokes, and myocardial infarctions (Levine et al., 2007; Putter &

Seghatchian, 2021). Additionally, some PV cases can develop into myelofibrosis, but the underlying mechanism is still poorly understood.

The most evident observation in this work was the significantly higher number of HSC for the JAK2 V617F^{hom} clone in the spin EB protocol. Cell counts of suspension cells derived from EB were significantly higher in JAK2 V617F^{hom} clones, followed by JAK2 V617F^{het} clones and JAK2 unmutated clones. The JAK2 V617F mutation causes constitutive activation of JAK-STAT pathways without an external stimulus like cytokine binding, causing enhanced proliferation of HSC. Further experiments to determine which cell type is the effector of the increased HSC counts would give further insights into the mechanism. On the one hand, it could be that the hematopoietic layer in the EB produces more HSC or on the other hand that the CD34^{+} HSC have a higher proliferation capacity (Fasouli & Katsantoni, 2021).

Furthermore, JAK2 V617F^{hom} clones had significantly higher erythrocyte counts compared to JAK2 V617F^{het}. JAK2 had almost no erythrocyte production. These findings were verified in the CFU assay as the spin EB protocol favors the MEP lineage, including erythrocytes. Instead, the CFU assay is a tool to analyze the unbiased differentiation potential of CD34^{+} HSC towards myeloid hematopoietic lineages. Again, erythrocyte differentiation was significantly lower in JAK2 unmutated cells compared to control. These observations are in line with previous publications and reflect the situation in patients (Barbui et al., 2018; Senquan et al., 2016)

In addition, our investigations on differentiation kinetics showed that the JAK2 mutation directly influenced the number of generated megakaryocytes. JAK2 V617F^{hom} had the highest percentage of megakaryocytes on day 11, and the percentage decreased on further days. In contrast, JAK2 unmutated clones had the highest percentage of megakaryocytes on day 19. Also, the overall megakaryocyte differentiation was higher in JAK2 V617F clones, especially when considering CD45^{+} cells. These findings show an accelerated megakaryocyte development caused by the JAK2 V617F mutation. Megakaryocytic hyperplasia belongs to the diagnosis criteria of PV according to the WHO (Barbui et al., 2018).

Our findings are also in line with a study by McKerrell et al. from 2017, where the enhanced engraftment of JAK2 V617F HSC clones was shown in MPN patients (McKerrell et al., 2017). The enhanced engraftment and proliferation can be one of the reasons for the observed megakaryocytic hyperplasia.

In addition, the response of the hematopoietic cells to TPO was altered. JAK2 unmutated cells developed significantly fewer megakaryocytes without TPO compared to supplementation with TPO. JAK2 V617F^{het} and JAK2 V617F^{hom} clones showed similar

megakaryocyte numbers with and without the TPO supplementation. The JAK2 V617F mutation causes activation of the JAK-STAT pathway even without binding of TPO. These findings align with the observation by Takei et al. (2018), who reported the TPO-independent megakaryocyte development of JAK2 V617F iPS cells. Moreover, studies showed that the TPO level in the blood of PV patients is increased (Cerutti et al., 1997; Takei et al., 2018). In healthy conditions, the level of TPO is inversely related to the number of megakaryocytes and platelets. It might be that TPO is no longer degraded because of the TPO-independent signaling, which would explain the higher TPO blood levels. Studies of TPO level in the medium for JAK2 unmutated and mutated clones could answer this missing information.

In summary, the analysis demonstrated that our model of *in vitro* generated megakaryocytes reflects the situation in patients to a large extent. Other groups have already published comparable results, but the strength of our approach is that we used clones from 3 independent patients. Moreover, we generated all three JAK2 genotypes from one patient with CRISPR/Cas9, giving us the unique opportunity to compare isogenic clones only differing in the JAK2 mutation. For PV2 clones we showed that repair of the JAK2 V617F mutation rescued most of the malignant phenotype. The differentiation kinetics and erythrocyte bias were reduced, and the megakaryocytic hyperplasia reversed. The missing genotypes are currently generated for patient PV1 and PV3, making our model even more valuable.

4.5 Gene expression analysis showed differences based on the JAK2 genotype

Next, changes on mRNA level were analyzed for all generated clones by RT-qPCR and in more depth for PV2 JAK2 unmutated and JAK2 V617F^{hom} by RNA-Seq. The RT-qPCR revealed significant upregulation of megakaryocyte developmental genes in the JAK2 V617F^{het} clone compared to JAK2 unmutated and JAK2 V617F^{hom}. Analysis of the differentiation kinetics showed that JAK2 V617F^{hom} reached the maximum percentage of megakaryocytes already at day 11 of the spin EB protocol, JAK2 V617F^{het} clones at day 14, and JAK2 unmutated clones at day 19. Therefore, it can be assumed that the increased expression of megakaryocyte developmental genes is due to different kinetics. These findings would need to be verified with further RT-qPCR assays on day 11 and day 19.

Furthermore, the expression of genes suspected to play a role in myelofibrosis was analyzed. Especially CXCL4, CXCL7, and TGF-β were described to be upregulated on RNA level in murine MPN models and HSC of MPN patients and influencing myelofibrosis development (H. Gleitz et al., 2020; Meier-Abt et al., 2021; Schneider et

al., 2017). Additionally, CXCL4L1 was examined due to the high similarity to CXCL4. The analysis of these genes unveiled an upregulation in the JAK2 V617F^{het} clones compared to the unmutated and homozygous mutated JAK2 clone. CXCL4 and CXCL7 are stored in the α-granules of platelets (Flad & Brandt, 2010). Therefore, it can be assumed that the altered expression depends rather on the different kinetics of the clones. The same holds true for TGF-β, which plays an essential role in the maturation of megakaryocytes (Abbonante et al., 2016). More mechanistic studies are needed to reveal the function of CXCL4L1.

As inflammation is an essential mechanism in PV and especially later in myelofibrosis, the inflammatory genes TNFα and IL-6 were analyzed. (Y. Wang & Zuo, 2019). IL-6 also plays a general role in thrombocytosis (Kaser et al., 2001; Noetzli et al., 2019). These genes were not higher expressed in JAK2 V617F megakaryocytes compared to the unmutated counterpart. The analyzed time point at day 14 of the spin EB protocol might be too early for inflammatory processes.

RNA-Seq analysis revealed more than 300 DEG between JAK2 and JAK2 V617F^{hom}. Two different studies from 2020 performed single-cell transcriptome analysis of CD34^{+} PB cells of PV and ET patients harboring the JAK2 V617F mutation (Hsu et al., 2020; Psaila et al., 2020). They showed heterogeneity in different patients and differentiation bias of mutated cells towards the MEP lineage. Our transcriptome analysis investigated the expression differences between iPS cell-derived megakaryocytes with JAK2 and JAK2 V617F megakaryocytes, allowing us to analyze the primary effector cells.

The RNA-Seq data revealed a significant upregulation, especially in ECM protein related genes and related factors. The establishment of the demarcation system in megakaryocytes for proplatelet production is a well-described process in which the ECM plays an essential role (Leiva et al., 2018; Noetzli et al., 2019). The detected significant downregulation of lysyl oxidase (LOX) must also be considered in this context. This enzyme was described as a regulator of ECM production in MPN and was upregulated in megakaryocytes of MPN patients (Piasecki et al., 2020). Moreover, Abbonante et al. described in 2016 the regulation of ECM components by autocrine TGF-β signaling (Abbonante et al., 2016). ECM proteins and TGF-β signaling were shown to be upregulated in CD34^{+} JAK2 V617F cells of MPN proteins. In contrast, our PROGENy analysis revealed downregulation of TGF-β signaling. The fact that we analyzed the expression in megakaryocytes might explain these differences.

Importantly, another recent study showed the downregulation of TGF-β signaling in combination with low expression of CXCL4 as a possible mechanism of myelofibrosis (Meier-Abt et al., 2021). Our results are in line with these observations and might be a

hint to an early pre-fibrotic phenotype of our megakaryocytes. Further investigations need to be performed to clarify this hypothesis, also addressing the conflicting results of the TGF-β expression showed in RT-qPCR.

Surprisingly, only CXC4L1 was upregulated in JAK2 V617F^{hom} megakaryocytes, whereas CXCL4 was lower expressed in 2 out of 3 samples. This is in contrast with studies reporting an increase of CXCL4 in pre-fibrotic patients (H. Gleitz et al., 2020). Also, other known upregulated genes in the development of myelofibrosis like CXCL7, CXCL12, or S100A were not differentially expressed in our RNA-Seq data.

Other differently regulated genes were not restricted to any particular function but belonged to a wide variety of pathways. PROGENy analysis revealed a slight upregulating trend in hypoxia, EGFR, and PI3K pathways. These changes were not significant. Increased sample size, including the other two patients, would help clarify the role of these pathways.

Our collected data showed that significant differences exist between JAK2 V617F^{hom} and JAK2 unmutated iPS cell-derived megakaryocytes. The lower expression of ECM proteins in combination with low TGF-β signaling and the unchanged expression of myelofibrosis-typical genes indicate that our megakaryocytes differ from other analyses. Most published studies used patient material with auxilliary side mutations and mostly unspecified JAK2 V617F allele burden.

In our experiments, however, we use a clonal patient-derived system in which the observed changes are solely due to the JAK2 V617F mutation. The analysis of further iPS cell-derived megakaryocytes from other patients will shed light on whether the observations are a patient-specific effect or a previously undescribed mechanism in myelofibrosis. The lower maturation of the cells, also supported by the low proplatelet production and low ploidy of our cells at day 14 of the spin EB differentiation, could affect our observations.

In summary, our generated megakaryocytes represent an essential tool for understanding the processes in MPN and myelofibrosis. Our clonal system has the strength to determine the effect of the JAK2 V617F mutation on myelofibrosis unbiased by other mutations or variable allele burden. All intermediate stages can be modeled with our generated cells from healthy bone marrow to fully developed myelofibrosis.

4.6 iPS cell-derived megakaryocytes for the establishment of an *in vitro* co-culture model

MSC are a heterogeneous group of cells and are found in most tissues of the human body, including the bone marrow. Here, they are the main effectors of myelofibrosis which get activated by malignant megakaryocytes. To generate a co-culture model with

JAK2 unmutated iPS-MSC and JAK2 V617F iPS cell-derived megakaryocytes, iPS cells were differentiated into iPS-MSC using various protocols and media. The generated iPS-MSC could be classified as MSC but were lacking the property of differentiating into myofibroblasts. Frobel et al. (2014) described differences of iPS-MSC in marker expression intensity, differentiation potential, and epigenetics compared to BM-MSC (Frobel et al., 2014). Moreover, other studies reported similar results describing that iPS-MSC show differences in their characteristics compared to primary material (Deyle et al., 2012; Diederichs & Tuan, 2014).

Several different MSC populations are found in human bone marrow with different expression profiles and characteristics and have different myelofibrosis effects (Crane et al., 2017; H. Gleitz et al., 2020). Therefore, the major challenge is not solely to generate iPS-MSC but to generate the right MSC reflecting the characteristics of BM-MSC suitable for modeling myelofibrosis. More investigations are necessary to find suitable differentiation processes of iPS-MSC concerning material stiffness, 2D and 3D culture, and possibly other, still unknown factors (Frobel et al., 2014; Goetzke et al., 2019).

For these reasons, the use of iPS-MSC was not further pursued, and healthy donor MSC from 3 different patients showing the potential to differentiate into myofibroblasts were used for further investigations. Several publications described the 2D MSC megakaryocytes co-culture to enhance platelet production and maturation of the megakaryocytes *in vitro* (Cheng et al., 2000; Robinson et al., 2006). Furthermore, murine Gli^{+}-MSC were co-cultured with TPO overexpressing murine megakaryocytes for fibrosis studies (H. Gleitz et al., 2020; Schneider et al., 2017).

The co-culture in this thesis was successfully established and iPS cell-derived megakaryocytes were cultured together with BM-MSC for up to two weeks. Direct interaction of the cells was visible by the attachment of some megakaryocytes to the MSC layer. Nevertheless, no upregulation of intracellular α-SMA or extracellular collagen was observed in any tested conditions. Furthermore, stimulation of BM-MSC with CXCL4 did not show an upregulation of any fibrosis-related genes.

There might be three major reasons why fibrosis was not visible in our co-culture: (i) other components are missing during myelofibrosis, such as immune cells, (ii) generated megakaryocytes are unsuitable for the fibrosis model due to their rather embryonic phenotype, (iii) 2D co-culture is to artificial, as the bone marrow is a 3D environment. 3D cell-cell contacts may be missing to activate the mechanisms of fibrosis.

Recent studies showed that CXCL4 suppresses the tolerogenic dendritic cells (DC) (Silva-Cardoso et al., 2020) and that CXCL4 stimulation of DC can induce fibroblast activation and sclerosis. It might be that immune cells such as DC are important for the

development of myelofibrosis and are the missing link in our co-culture model. To exclude the possibility that our used iPS cell-derived megakaryocytes are not suitable for the *in vitro* modeling of bone marrow fibrosis, comparison with primary $CD34^+$ derived megakaryocytes from MPN patients would be suitable for positive control and should be included in further studies. For a 3D co-culture model of iPS cell-derived megakaryocytes and MSC, collagen or calcium scaffolds might be suitable for mimicking the bone marrow (Noreikaitė et al., 2017). Furthermore, we only had one JAK2 $V617F^{hom}$ clone. There might be further unknown mutations that lead in combination with the JAK2 V617F mutation to the development of PV into myelofibrosis.

In summary, the 2D co-culture of BM-MSC and iPS cell-derived megakaryocytes was successfully established. However, our experiments have shown that 2D co-culture might not be suitable for a myelofibrosis model. Nevertheless, the performed experiments provide information on possible missing components that can be targeted in further experiments.

4.7 Conclusion and future perspective

In this work, PV patient-derived iPS cells from three different donors were fully characterized, and missing JAK2 genotypes were generated to extend the set of iPS cells to study MPN, including myelofibrosis. For this purpose, additionally, $CXCL4^{KO}$ clones were generated from two different iPS cell clones (Boehnke et al., 2021), as CXCL4 is believed to be one of the main effectors in early myelofibrosis. This provides the basis for mechanistic research on MPN with a broad set of clones. Furthermore, these clones will be a valuable tool to generate an *in vitro* model for bone marrow fibrosis. In this context, further efforts are needed to establish more missing clones.

Subsequently, a protocol for differentiation of iPS cells into megakaryocytes was established in our laboratory using the generated clones and improved by optimizing media composition. The combination of magnetic beads based purification and a caspase inhibitor for the maturation of megakaryocytes made them suitable for longer culture and integration into a co-culture model. The generated iPS cell-derived megakaryocytes were examined by various functional, phenotypic, and genotypic methods. They were proven to be multinucleated and able to form proplatelets.

JAK2 V617F megakaryocytes were found to exhibit accelerated differentiation kinetics. First hints showed tendencies of higher granularity and, therefore, higher maturation in JAK2 V617F clones compared to control. Moreover, the erythrocyte bias known from PV patients was also present in JAK2 $V617F^{hom}$ megakaryocytes and was not present in JAK2 unmutated megakaryocytes. Furthermore, JAK2 V617F clones showed a TPO-independent megakaryocyte production. Transcriptome analysis of JAK2 unmutated

megakaryocytes compared to JAK2 V617F^{hom} megakaryocytes showed a different expression pattern. In JAK2 V617F^{hom} megakaryocytes, ECM production, TGF-β signaling, EGF3, and PI3K pathways were slightly downregulated.

In addition, iPS cell derived JAK2 unmutated MSC were generated. They reflected BM-MSC characteristics such as the expression of CD29, CD70, CD90, and CD105 and the differentiation capacity into the adipogenic and osteogenic lineage. However, they missed the differentiation capacity into myofibroblasts upon stimulation with TGF-β and were not suitable for co-culture experiments. Therefore, primary BM-MSC were used from 3 different donors. Here, CXCL4 stimulation alone was not enough to drive the fibrotic differentiation. Different strategies of BM-MSC with iPS cell-derived megakaryocytes were tested, but no induction of fibrosis in BM-MSC cultured with JAK2 V617F^{hom} megakaryocytes were observed compared to control.

In future work, the generation of the missing JAK2 V617F^{hom} clones in PV1 and PV3 is needed. Furthermore, integration of iPS cells derived from PMF patients would give further insights into the mechanistic of myelofibrosis. Preliminary 3D co-culture experiments with calcium scaffolds were already performed and showed promising results. Here, megakaryocytes derived from primary CD34^{+} cells of MPN patients would be a valuable control. After establishing a functional myelofibrosis model, the integration of CXCL4^{KO} clones could elucidate the effect of CXCL4 in myelofibrosis. Further steps would be mechanistic assays and the use of the model for drug screenings of promising molecules and targets in myelofibrosis. Here, the observed DEG in the class of ECM protein genes and the hypoxia, EGFR, and PI3K pathway can be used to find new targets.

5 Bibliography

Abbonante, V., Di Buduo, C. A., Gruppi, C., Malara, A., Gianelli, U., Celesti, G., Anselmo, A., Laghi, L., Vercellino, M., Visai, L., Iurlo, A., Moratti, R., Barosi, G., Rosti, V., & Balduini, A. (2016). Thrombopoietin/TGF-β1 loop regulates megakaryocyte extracellular matrix component synthesis. *Stem Cells*, *34*(4), 1123–1133. https://doi.org/https://doi.org/10.1002/stem.2285

Ackermann, M., Liebhaber, S., Klusmann, J.-H., & Lachmann, N. (2015). Lost in translation: pluripotent stem cell-derived hematopoiesis. *EMBO Molecular Medicine*, *7*(11), 1388–1402. https://doi.org/10.15252/emmm.201505301

Alshemmari, S. H., Rajaan, R., Ameen, R., Al-Drees, M. A., & Almosailleakh, M. R. (2014). JAK2V617F allele burden in patients with myeloproliferative neoplasms. *Annals of Hematology*, *93*(5), 791–796. https://doi.org/10.1007/s00277-013-1988-6

Arber, D. A., Orazi, A., Hasserjian, R., Thiele, J., Borowitz, M. J., Le Beau, M. M., Bloomfield, C. D., Cazzola, M., & Vardiman, J. W. (2016). The 2016 revision to the World Health Organization classification of myeloid neoplasms and acute leukemia. *Blood*, *127*(20), 2391–2405. https://doi.org/10.1182/blood-2016-03-643544

Arinobu, Y., Mizuno, S., Chong, Y., Shigematsu, H., Iino, T., Iwasaki, H., Graf, T., Mayfield, R., Chan, S., Kastner, P., & Akashi, K. (2007). Reciprocal activation of GATA-1 and PU.1 marks initial specification of hematopoietic stem cells into myeloerythroid and myelolymphoid lineages. *Cell Stem Cell*, *1*(4), 416–427. https://doi.org/10.1016/j.stem.2007.07.004

Arranz, L., Sánchez-Aguilera, A., Martín-Pérez, D., Isern, J., Langa, X., Tzankov, A., Lundberg, P., Muntión, S., Tzeng, Y. S., Lai, D. M., Schwaller, J., Skoda, R. C., & Méndez-Ferrer, S. (2014). Neuropathy of haematopoietic stem cell niche is essential for myeloproliferative neoplasms. *Nature*, *512*, 78–81. https://doi.org/10.1038/nature13383

Asprer, J. S. T., & Lakshmipathy, U. (2015). Current methods and challenges in the comprehensive characterization of human pluripotent stem cells. *Stem Cell Reviews and Reports*, *11*(2), 357–372. https://doi.org/10.1007/s12015-014-9580-6

Avanzi, M. P., Izak, M., Oluwadara, O. E., & Mitchell, W. B. (2015). Actin inhibition increases megakaryocyte proplatelet formation through an apoptosis-dependent mechanism. *PloS One*, *10*(4), e0125057–e0125057. https://doi.org/10.1371/journal.pone.0125057

Baik, R., Wyman, S. K., Kabir, S., & Corn, J. E. (2021). Genome editing to model and reverse a prevalent mutation associated with myeloproliferative neoplasms. *PloS*

One, *16*(3), e0247858–e0247858. https://doi.org/10.1371/journal.pone.0247858

Barbui, T., Thiele, J., Gisslinger, H., Kvasnicka, H. M., Vannucchi, A. M., Guglielmelli, P., Orazi, A., & Tefferi, A. (2018). The 2016 WHO classification and diagnostic criteria for myeloproliferative neoplasms: document summary and in-depth discussion. *Blood Cancer Journal*, *8*(2), 15. https://doi.org/10.1038/s41408-018-0054-y

Barrangou, R., Fremaux, C., Deveau, H., Richards, M., Boyaval, P., Moineau, S., Romero, D. A., & Horvath, P. (2007). CRISPR provides acquired resistance against viruses in prokaryotes. *Science*, *315*(5819), 1709 LP – 1712. https://doi.org/10.1126/science.1138140

Behrens, K., & Alexander, W. S. (2018). Cytokine control of megakaryopoiesis. *Growth Factors*, *36*(3–4), 89–103. https://doi.org/10.1080/08977194.2018.1498487

Bellin, M., Marchetto, M. C., Gage, F. H., & Mummery, C. L. (2012). Induced pluripotent stem cells: the new patient? *Nature Reviews Molecular Cell Biology*, *13*(11), 713–726. https://doi.org/10.1038/nrm3448

Bilz, N. C., Willscher, E., Binder, H., Böhnke, J., Stanifer, M. L., Hübner, D., Boulant, S., Liebert, U. G., & Claus, C. (2019). Teratogenic rubella virus alters the endodermal differentiation capacity of human induced pluripotent stem cells. *Cells*, *8*(8), 870. https://doi.org/10.3390/cells8080870

Boehnke, J., Atakhanov, S., Toledo, M. A. S., Schüler, H. M., Sontag, S., Chatain, N., Koschmieder, S., Brümmendorf, T. H., Kramann, R., & Zenke, M. (2021). CRISPR/Cas9 mediated CXCL4 knockout in human iPS cells of polycythemia vera patient with JAK2 V617F mutation. *Stem Cell Research*, *55*, 102490. https://doi.org/https://doi.org/10.1016/j.scr.2021.102490

Börger, A.-K., Eicke, D., Wolf, C., Gras, C., Aufderbeck, S., Schulze, K., Engels, L., Eiz-Vesper, B., Schambach, A., Guzman, C. A., Lachmann, N., Moritz, T., Martin, U., Blasczyk, R., & Figueiredo, C. (2016). Generation of HLA-universal iPSC-derived megakaryocytes and platelets for survival under refractoriness conditions. *Molecular Medicine*, *22*, 274–285. https://doi.org/10.2119/molmed.2015.00235

Bowles, K. R., Tcw, J., Qian, L., Jadow, B. M., & Goate, A. M. (2019). Reduced variability of neural progenitor cells and improved purity of neuronal cultures using magnetic activated cell sorting. *PloS One*, *14*(3), e0213374–e0213374. https://doi.org/10.1371/journal.pone.0213374

Brand, M., & Morrissey, E. (2020). Single-cell fate decisions of bipotential hematopoietic progenitors. *Current Opinion in Hematology*, *27*(4). https://journals.lww.com/co-hematology/Fulltext/2020/07000/Single_cell_fate_decisions_of_bipotential.4.aspx

Brigida, A. L., & Siniscalco, D. (2016). Induced pluripotent stem cells as a cellular model for studying Down Syndrome. *Journal of Stem Cells & Regenerative Medicine*, *12*(2), 54–60. https://doi.org/10.46582/jsrm.1202009

Buikema, J. W., & Wu, S. M. (2017). Untangling the biology of genetic cardiomyopathies with pluripotent stem cell disease models. *Current Cardiology Reports*, *19*(4), 30. https://doi.org/10.1007/s11886-017-0842-1

Carlson, J., Baxter, S. A., Dréau, D., & Nesmelova, I. V. (2013). The heterodimerization of platelet-derived chemokines. *Biochimica et Biophysica Acta*, *1834*(1), 158–168. https://doi.org/10.1016/j.bbapap.2012.09.010

Cerutti, A., Custodi, P., Duranti, M., Noris, P., & Balduini, C. L. (1997). Thrombopoietin levels in patients with primary and reactive thrombocytosis. *British Journal of Haematology*, *99*(2), 281–284. https://doi.org/https://doi.org/10.1046/j.1365-2141.1997.3823196.x

Chen, E., & Mullally, A. (2014). How does JAK2V617F contribute to the pathogenesis of myeloproliferative neoplasms? *Hematology*, *2014*(1), 268–276. https://doi.org/10.1182/asheducation-2014.1.268

Chen, E., Schneider, R. K., Breyfogle, L. J., Rosen, E. A., Poveromo, L., Elf, S., Ko, A., Brumme, K., Levine, R., Ebert, B. L., & Mullally, A. (2015). Distinct effects of concomitant Jak2V617F expression and Tet2 loss in mice promote disease progression in myeloproliferative neoplasms. *Blood*, *125*(2), 327–335. https://doi.org/10.1182/blood-2014-04-567024

Chen, S.-Z., Ning, L.-F., Xu, X., Jiang, W.-Y., Xing, C., Jia, W.-P., Chen, X.-L., Tang, Q.-Q., & Huang, H.-Y. (2016). The miR-181d-regulated metalloproteinase Adamts1 enzymatically impairs adipogenesis via ECM remodeling. *Cell Death and Differentiation*, *23*(11), 1778–1791. https://doi.org/10.1038/cdd.2016.66

Cheng, L., Qasba, P., Vanguri, P., & Thiede, M. A. (2000). Human mesenchymal stem cells support megakaryocyte and pro-platelet formation from CD34+ hematopoietic progenitor cells. *Journal of Cellular Physiology*, *184*(1), 58–69. https://doi.org/https://doi.org/10.1002/(SICI)1097-4652(200007)184:1<58::AID-JCP6>3.0.CO;2-B

Chotinantakul, K., & Leeanansaksiri, W. (2012). Hematopoietic stem cell development, niches, and signaling pathways. *Bone Marrow Research*, *2012*, 270425. https://doi.org/10.1155/2012/270425

Corsa, C. A. S., Brenot, A., Grither, W. R., Van Hove, S., Loza, A. J., Zhang, K., Ponik, S. M., Liu, Y., DeNardo, D. G., Eliceiri, K. W., Keely, P. J., & Longmore, G. D. (2016). The action of discoidin domain receptor 2 in basal tumor cells and stromal cancer-

associated fibroblasts is critical for breast cancer metastasis. *Cell Reports*, *15*(11), 2510–2523. https://doi.org/10.1016/j.celrep.2016.05.033

Crane, G. M., Jeffery, E., & Morrison, S. J. (2017). Adult haematopoietic stem cell niches. *Nature Reviews Immunology*, *17*(9), 573–590. https://doi.org/10.1038/nri.2017.53

De Alarcon, P. A., & Graeve, J. L. A. (1996). Analysis of megakaryocyte ploidy in fetal bone marrow biopsies using a new adaptation of the feulgen technique to measure DNA content and estimate megakaryocyte ploidy from biopsy specimens. *Pediatric Research*, *39*(1), 166–170. https://doi.org/10.1203/00006450-199601000-00026

De Candia, E. (2012). Mechanisms of platelet activation by thrombin: A short history. *Thrombosis Research*, *129*(3), 250–256. https://doi.org/10.1016/j.thromres.2011.11.001

Decker, M., Leslie, J., Liu, Q., & Ding, L. (2018). Hepatic thrombopoietin is required for bone marrow hematopoietic stem cell maintenance. *Science*, *360*(6384), 106–110. https://doi.org/10.1126/science.aap8861

Decker, M., Martinez-Morentin, L., Wang, G., Lee, Y., Liu, Q., Leslie, J., & Ding, L. (2017). Leptin-receptor-expressing bone marrow stromal cells are myofibroblasts in primary myelofibrosis. *Nature Cell Biology*, *19*, 677–688. https://doi.org/10.1038/ncb3530

Dehairs, J., Talebi, A., Cherifi, Y., & Swinnen, J. V. (2016). CRISP-ID: decoding CRISPR mediated indels by Sanger sequencing. *Scientific Reports*, *6*(1), 28973. https://doi.org/10.1038/srep28973

Deinsberger, J., Reisinger, D., & Weber, B. (2020). Global trends in clinical trials involving pluripotent stem cells: a systematic multi-database analysis. *Npj Regenerative Medicine*, *5*(1), 15. https://doi.org/10.1038/s41536-020-00100-4

Demirci, S., Leonard, A., & Tisdale, J. F. (2020). Hematopoietic stem cells from pluripotent stem cells: Clinical potential, challenges, and future perspectives. *Stem Cells Translational Medicine*, *9*(12), 1549–1557. https://doi.org/10.1002/sctm.20-0247

Demirci, S., & Tisdale, J. F. (2018). Definitive erythropoiesis from pluripotent stem cells: recent advances and perspectives. *Cell Biology and Translational Medicine*, *3*(1107), 1–13. https://doi.org/10.1007/5584_2018_228

Deyle, D. R., Khan, I. F., Ren, G., Wang, P.-R., Kho, J., Schwarze, U., & Russell, D. W. (2012). Normal collagen and bone production by gene-targeted human osteogenesis imperfecta iPSCs. *Molecular Therapy : The Journal of the American Society of Gene Therapy*, *20*(1), 204–213. https://doi.org/10.1038/mt.2011.209

Diederichs, S., & Tuan, R. S. (2014). Functional comparison of human-induced

pluripotent stem cell-derived mesenchymal cells and bone marrow-derived mesenchymal stromal cells from the same donor. *Stem Cells and Development*, *23*(14), 1594–1610. https://doi.org/10.1089/scd.2013.0477

Ditadi, A., Sturgeon, C. M., & Keller, G. (2016). A view of human haematopoietic development from the Petri dish. *Nature Reviews Molecular Cell Biology*, *18*(1), 56–67. https://doi.org/10.1038/nrm.2016.127

Dominici, M., Le Blanc, K., Mueller, I., Slaper-Cortenbach, I., Marini, F. C., Krause, D. S., Deans, R. J., Keating, A., Prockop, D. J., & Horwitz, E. M. (2006). Minimal criteria for defining multipotent mesenchymal stromal cells. The International Society for Cellular Therapy position statement. *Cytotherapy*, *8*(4), 315–317. https://doi.org/10.1080/14653240600855905

Dorrance, A. (2021). "Mast"ering drug discovery with iPSCs. *Blood*, *137*(15), 1993–1994. https://doi.org/10.1182/blood.2020010456

Eicke, D., Baigger, A., Schulze, K., Latham, S. L., Halloin, C., Zweigerdt, R., Guzman, C. A., Blasczyk, R., & Figueiredo, C. (2018). Large-scale production of megakaryocytes in microcarrier-supported stirred suspension bioreactors. *Scientific Reports*, *8*(1), 10146. https://doi.org/10.1038/s41598-018-28459-x

El Agha, E., Kramann, R., Schneider, R. K., Li, X., Seeger, W., Humphreys, B. D., & Bellusci, S. (2017). Mesenchymal stem cells in fibrotic disease. *Cell Stem Cell*, *21*(2), 166–177. https://doi.org/https://doi.org/10.1016/j.stem.2017.07.011

Elzi, D. J., Song, M., Houghton, P. J., Chen, Y., & Shiio, Y. (2015). The role of FLI-1-EWS, a fusion gene reciprocal to EWS-FLI-1, in Ewing sarcoma. *Genes & Cancer*, *6*(11–12), 452–461. https://doi.org/10.18632/genesandcancer.86

Fasouli, E. S., & Katsantoni, E. (2021). JAK-STAT in Early Hematopoiesis and Leukemia. *Frontiers in Cell and Developmental Biology*, *9*, 669363. https://doi.org/10.3389/fcell.2021.669363

Fenerich, B. A., Fernandes, J. C., Rodrigues Alves, A. P. N., Coelho-Silva, J. L., Scopim-Ribeiro, R., Scheucher, P. S., Eide, C. A., Tognon, C. E., Druker, B. J., Rego, E. M., Machado-Neto, J. A., & Traina, F. (2020). NT157 has antineoplastic effects and inhibits IRS1/2 and STAT3/5 in JAK2V617F-positive myeloproliferative neoplasm cells. *Signal Transduction and Targeted Therapy*, *5*(1), 5. https://doi.org/10.1038/s41392-019-0102-5

Fischer, M., Goldschmitt, J., Peschel, C., Brakenhoff, J. P. G., Kallen, K.-J., Wollmer, A., Grötzinger, J., & Rose-John, S. (1997). A bioactive designer cytokine for human hematopoietic progenitor cell expansion. *Nature Biotechnology*, *15*(2), 142–145. https://doi.org/10.1038/nbt0297-142

Flad, H.-D., & Brandt, E. (2010). Platelet-derived chemokines: pathophysiology and therapeutic aspects. *Cellular and Molecular Life Sciences*, *67*(14), 2363–2386. https://doi.org/10.1007/s00018-010-0306-x

Fleischer, J., Grage-Griebenow, E., Kasper, B., Heine, H., Ernst, M., Brandt, E., Flad, H.-D., & Petersen, F. (2002). Platelet factor 4 inhibits proliferation and cytokine release of activated human T cells. *The Journal of Immunology*, *169*(2), 770 LP – 777. https://doi.org/10.4049/jimmunol.169.2.770

Frobel, J., Hemeda, H., Lenz, M., Abagnale, G., Joussen, S., Denecke, B., Šarić, T., Zenke, M., & Wagner, W. (2014). Epigenetic rejuvenation of mesenchymal stromal cells derived from induced pluripotent stem cells. *Stem Cell Reports*, *3*(3), 414–422. https://doi.org/https://doi.org/10.1016/j.stemcr.2014.07.003

Fuchs, D. A., McGinn, S. G., Cantu, C. L., Klein, R. R., Sola-Visner, M. C., & Rimsza, L. M. (2012). Developmental differences in megakaryocyte size in infants and children. *American Journal of Clinical Pathology*, *138*(1), 140–145. https://doi.org/10.1309/ajcp4emtjya0vgye

Fukuda, T. (1974). Fetal hemopoiesis. *Virchows Archiv B*, *16*(1), 249. https://doi.org/10.1007/BF02894080

Furitsu, T., Tsujimura, T., Tono, T., Ikeda, H., Kitayama, H., Koshimizu, U., Sugahara, H., Butterfield, J. H., Ashman, L. K., Kanayama, Y., & al., et. (1993). Identification of mutations in the coding sequence of the proto-oncogene c-kit in a human mast cell leukemia cell line causing ligand-independent activation of c-kit product. *The Journal of Clinical Investigation*, *92*(4), 1736–1744. https://doi.org/10.1172/JCI116761

Galet, B., Cheval, H., & Ravassard, P. (2020). Patient-derived midbrain organoids to explore the molecular basis of parkinson's disease. *Frontiers in Neurology*, *11*, 1005. https://doi.org/10.3389/fneur.2020.01005

Gao, L., Hu, Y., Tian, Y., Fan, Z., Wang, K., Li, H., Zhou, Q., Zeng, G., Hu, X., Yu, L., Zhou, S., Tong, X., Huang, H., Chen, H., Liu, Q., Liu, W., Zhang, G., Zeng, M., Zhou, G., Qingyu, H., Ji, H., Chen, L. (2019). Lung cancer deficient in the tumor suppressor GATA4 is sensitive to TGFBR1 inhibition. *Nature Communications*, *10*(1), 1665. https://doi.org/10.1038/s41467-019-09295-7

Gleitz, H., Dugourd, A. J. F., Leimkühler, N. B., Snoeren, I. A. ., Fuchs, S. N. R., Menzel, S., Ziegler, S., Kroeger, N., Triviai, I., Büsche, G., Kreipe, H., Banjanin, B., Pritchard, J., Hoogenboezem, R., Bindels, E., Schumacher, N., Rose-John, S., Elf, S., Saez-Rodriguez, J., Kramann, R., & Schneider, R. K. (2020). Increased CXCL4 expression in hematopoietic cells links inflammation and progression of bone

marrow fibrosis in MPN. *Blood*, *18*(136), 2051–2064. https://doi.org/10.1182/blood.2019004095

Gleitz, H. F. E., Kramann, R., & Schneider, R. K. (2018). Understanding deregulated cellular and molecular dynamics in the haematopoietic stem cell niche to develop novel therapeutics for bone marrow fibrosis. *The Journal of Pathology*, *245*(2), 138–146. https://doi.org/10.1002/path.5078

Gnanasambandan, K., & Sayeski, P. P. (2011). A structure-function perspective of JAK2 mutations and implications for alternate drug design strategies: the road not taken. *Current Medicinal Chemistry*, *18*(30), 4659–4673. https://doi.org/10.2174/092986711797379267

Godfrey, A. L., Chen, E., Pagano, F., Ortmann, C. A., Silber, Y., Bellosillo, B., Guglielmelli, P., Harrison, C. N., Reilly, J. T., Stegelmann, F., Bijou, F., Lippert, E., McMullin, M. F., Boiron, J.-M., Döhner, K., Vannucchi, A. M., Besses, C., Campbell, P. J., & Green, A. R. (2012). JAK2V617F homozygosity arises commonly and recurrently in PV and ET, but PV is characterized by expansion of a dominant homozygous subclone. *Blood*, *120*(13), 2704–2707. https://doi.org/10.1182/blood-2012-05-431791

Goetzke, R., Keijdener, H., Franzen, J., Ostrowska, A., Nüchtern, S., Mela, P., & Wagner, W. (2019). Differentiation of induced pluripotent stem cells towards mesenchymal stromal cells is hampered by culture in 3D hydrogels. *Scientific Reports*, *9*(1), 15578. https://doi.org/10.1038/s41598-019-51911-5

Green, C. J., Charles, R. S., Edwards, B. F., & Johnson, P. H. (1989). Identification and characterization of PF4varl, a human gene variant of platelet factor 4. *Molecular and Cellular Biology*, *9*(4), 1445 LP – 1451. https://doi.org/10.1128/MCB.9.4.1445

Guadall, A., Lesteven, E., Letort, G., Awan Toor, S., Delord, M., Pognant, D., Brusson, M., Verger, E., Maslah, N., Giraudier, S., Larghero, J., Vanneaux, V., Chomienne, C., El Nemer, W., Cassinat, B., & Kiladjian, J. J. (2018). Endothelial cells harbouring the JAK2 V617F mutation display pro-adherent and pro-thrombotic features. *Thrombosis and Haemostasis*, *118*(9), 1586–1599. https://doi.org/10.1055/s-0038-1667015

Guglielmelli, P., Barosi, G., Rambaldi, A., Marchioli, R., Masciulli, A., Tozzi, L., Biamonte, F., Bartalucci, N., Gattoni, E., Lupo, M. L., Finazzi, G., Pancrazzi, A., Antonioli, E., Susini, M. C., Pieri, L., Malevolti, E., Usala, E., Occhini, U., Grossi, A., Caglio, S., Paratore, S., Bosi, A., Babui, T., Vannucchi, A., investigators on behalf of the A.-G. I. M. M. (AGIMM). (2011). Safety and efficacy of everolimus, a mTOR inhibitor, as single agent in a phase 1/2 study in patients with myelofibrosis. *Blood*, *118*(8),

2069–2076. https://doi.org/10.1182/blood-2011-01-330563

Gump, J. M., & Dowdy, S. F. (2007). TAT transduction: the molecular mechanism and therapeutic prospects. *Trends in Molecular Medicine*, *13*(10), 443–448. https://doi.org/https://doi.org/10.1016/j.molmed.2007.08.002

Haas, S., Trumpp, A., & Milsom, M. D. (2018). Causes and consequences of hematopoietic stem cell heterogeneity. *Cell Stem Cell*, *22*(5), 627–638. https://doi.org/10.1016/j.stem.2018.04.003

Haeckel, E. (1868). *Haeckel, E. Natürliche Schöpfungsgeschichte (Georg Reimer, 1868)*.

Horvath, P., & Barrangou, R. (2010). CRISPR/Cas, the immune system of bacteria and archaea. *Science*, *327*(5962), 167 LP – 170. https://doi.org/10.1126/science.1179555

Hsu, C.-C., Chen, Y.-J., Huang, C.-E., Wu, Y.-Y., Wang, M.-C., Pei, S.-N., Liao, C.-K., Lu, C.-H., Chen, P.-T., Tsou, H.-Y., Li, C.-P., Chuang, W.-H., Chuang, C.-K., Yang, C.-Y., Lai, Y.-H., Lin, Y.-H., & Chen, C.-C. (2020). Molecular heterogeneity unravelled by single-cell transcriptomics in patients with essential thrombocythaemia. *British Journal of Haematology*, *188*(5), 707–722. https://doi.org/https://doi.org/10.1111/bjh.16225

Huber, T. L., Kouskoff, V., Fehling, H. J., Palis, J., & Keller, G. (2004). Haemangioblast commitment is initiated in the primitive streak of the mouse embryo. *Nature*, *432*, 625–630. https://doi.org/10.1038/nature03122

Ianotto, J. C., Chauveau, A., Boyer-Perrard, F., Gyan, E., Laribi, K., Cony-Makhoul, P., Demory, J. L., de Renzis, B., Dosquet, C., Rey, J., Roy, L., Dupriez, B., Knoops, L., Legros, L., Malou, M., Hutin, P., Ranta, D., Benbrahim, O., Ugo, V., Lippert, E., & Kiladjian, J. J. (2018). Benefits and pitfalls of pegylated interferon-α2a therapy in patients with myeloproliferative neoplasm-associated myelofibrosis: A french intergroup of myeloproliferative neoplasms (FIM) study. *Haematologica*, *103*(3), 438–446. https://doi.org/10.3324/haematol.2017.181297

Ikonomi, P., Noguchi, C. T., Miller, W., Kassahun, H., Hardison, R., & Schechter, A. N. (2000). Levels of GATA-1/GATA-2 transcription factors modulate expression of embryonic and fetal hemoglobins. *Gene*, *261*(2), 277–287. https://doi.org/https://doi.org/10.1016/S0378-1119(00)00510-2

Ishino, Y., Shinagawa, H., Makino, K., Amemura, M., & Nakata, A. (1987). Nucleotide sequence of the iap gene, responsible for alkaline phosphatase isozyme conversion in Escherichia coli, and identification of the gene product. *Journal of Bacteriology*, *169*(12), 5429–5433. https://doi.org/10.1128/jb.169.12.5429-5433.1987

James, C., Ugo, V., Le Couédic, J.-P., Staerk, J., Delhommeau, F., Lacout, C., Garçon, L., Raslova, H., Berger, R., Bennaceur-Griscelli, A., Villeval, J. L., Constantinescu, S. N., Casadevall, N., & Vainchenker, W. (2005). A unique clonal JAK2 mutation leading to constitutive signalling causes polycythaemia vera. *Nature*, *434*(7037), 1144–1148. https://doi.org/10.1038/nature03546

Jeong, J. J., Gu, X., Nie, J., Sundaravel, S., Liu, H., Kuo, W.-L., Bhagat, T. D., Pradhan, K., Cao, J., Nischal, S., McGraw, K. L., Bhattacharyya, S., Bishop, M. R., Artz, A., Thirman, M. J., Moliterno, A., Ji, P., Levine, R., Godley, L., Steidl, U., Bieker, J., List, A., Sauntharajah, Y., He, C., Verma, A., & Wickrema, A. (2019). Cytokine-regulated phosphorylation and activation of TET2 by JAK2 in hematopoiesis. *Cancer Discovery*, *9*(6), 778 LP – 795. https://doi.org/10.1158/2159-8290.CD-18-1138

Jinek, M., Chylinski, K., Fonfara, I., Hauer, M., Doudna, J. A., & Charpentier, E. (2012). A Programmable Dual-RNA – Guided. *Science (New York, N.Y.)*, *337*(6096), 816–821. https://doi.org/10.1126/science.1225829

Jolliffe, I. T., & Jackson, J. (1993). A user's guide to principal components. *The Statistician*, *42*, 76–77. https://doi.org/10.1002/0471725331

Jones, D. L., & Wagers, A. J. (2008). No place like home: anatomy and function of the stem cell niche. *Nature Reviews Molecular Cell Biology*, *9*(1), 11–21. https://doi.org/10.1038/nrm2319

Jones, A. V, Kreil, S., Zoi, K., Waghorn, K., Curtis, C., Zhang, L., Score, J., Seear, R., Chase, A. J., Grand, F. H., White, H., Zoi, C., Loukopoulos, D., Terpos, E., Vervessou, E., Schultheis, B., Emig, M., Ernst, T., Reiter, A., Langenfelder, E., Hehlmann, R., Hochhaus, A., Oscier, D., Silver, R., Reiter, A., Cross, N. C. P. (2005). Widespread occurrence of the JAK2 V617F mutation in chronic myeloproliferative disorders. *Blood*, *106*(6), 2162–2168. https://doi.org/10.1182/blood-2005-03-1320

Jordan, H. E. (1916). Evidence of hemogenic capacity of endothelium. *The Anatomical Record*. https://doi.org/10.1002/ar.1090100508

Junt, T., Schulze, H., Chen, Z., Massberg, S., Goerge, T., Krueger, A., Wagner, D. D., Graf, T., Italiano, J. E., Shivdasani, R. A., & von Andrian, U. H. (2007). Dynamic Visualization of Thrombopoiesis Within Bone Marrow. *Science*, *317*(5845), 1767 LP – 1770. https://doi.org/10.1126/science.1146304

Kaser, A., Brandacher, G., Steurer, W., Kaser, S., Offner, F. A., Zoller, H., Theurl, I., Widder, W., Molnar, C., Ludwiczek, O., Atkins, M. B., Mier, J. W., & Tilg, H. (2001). Interleukin-6 stimulates thrombopoiesis through thrombopoietin: role in

inflammatory thrombocytosis. *Blood*, *98*(9), 2720–2725. https://doi.org/10.1182/blood.V98.9.2720

Kelly, S. J. (1977). Studies of the developmental potential of 4- and 8-cell stage mouse blastomeres. *Journal of Experimental Zoology*, *200*(3), 365–376. https://doi.org/https://doi.org/10.1002/jez.1402000307

Kennedy, M., D'Souza, S. L., Lynch-Kattman, M., Schwantz, S., & Keller, G. (2007). Development of the hemangioblast defines the onset of hematopoiesis in human ES cell differentiation cultures. *Blood*. https://doi.org/10.1182/blood-2006-09-047704

Kfoury, Y., & Scadden, D. T. (2015). Mesenchymal cell contributions to the stem cell niche. *Cell Stem Cell*, *16*(3), 239–253. https://doi.org/10.1016/j.stem.2015.02.019

Kiel, M. J. (2005). SLAM family receptors distinguish hematopoietic stem and progenitor cells and reveal endothelial niches for stem cells. *Cell*, *121*. https://doi.org/10.1016/j.cell.2005.05.026

Kiladjian, J.-J., Massé, A., Cassinat, B., Mokrani, H., Teyssandier, I., le Couédic, J.-P., Cambier, N., Almire, C., Pronier, E., Casadevall, N., Vainchenker, W., Chomienne, C., Delhommeau, F., & (FIM), for the F. I. of M. N. (2010). Clonal analysis of erythroid progenitors suggests that pegylated interferon α-2a treatment targets JAK2V617F clones without affecting TET2 mutant cells. *Leukemia*, *24*(8), 1519–1523. https://doi.org/10.1038/leu.2010.120

Kinouchi, T., Uemura, M., Wang, C., Ishizuya, Y., Yamamoto, Y., Hayashi, T., Matsuzaki, K., Nakata, W., Yoshida, T., Jingushi, K., Kawashima, A., Ujike, T., Nagahara, A., Fujita, K., Imamura, R., Ueda, Y., Kitae, K., Tsujikawa, K., & Nonomura, N. (2017). Expression level of CXCL7 in peripheral blood cells is a potential biomarker for the diagnosis of renal cell carcinoma. *Cancer Science*, *108*(12), 2495–2502. https://doi.org/10.1111/cas.13414

Kirschner, M., Maurer, A., Wlodarski, M. W., Ventura Ferreira, M. S., Bouillon, A.-S., Halfmeyer, I., Blau, W., Kreuter, M., Rosewich, M., Corbacioglu, S., Beck, J., Schwarz, M., Bittenbring, J., Radsak, M. P., Wilk, C. M., Koschmieder, S., Begemann, M., Kurth, I., Schemionek, M., Brümmendorf, T., Beier, F. (2018). Recurrent somatic mutations are rare in patients with cryptic dyskeratosis congenita. *Leukemia*, *32*(8), 1762–1767. https://doi.org/10.1038/s41375-018-0125-x

Kisseleva, T., Bhattacharya, S., Braunstein, J., & Schindler, C. W. (2002). Signaling through the JAK/STAT pathway, recent advances and future challenges. *Gene*, *285*(1), 1–24. https://doi.org/https://doi.org/10.1016/S0378-1119(02)00398-0

Klampfl, T., Gisslinger, H., Harutyunyan, A. S., Nivarthi, H., Rumi, E., Milosevic, J. D., Them, N. C. C., Berg, T., Gisslinger, B., Pietra, D., Chen, D., Vladimer, G. I., Bagienski, K., Milanesi, C., Casetti, I. C., Sant'Antonio, E., Ferretti, V., Elena, C., Schischlik, F., Cleary, C., Six, M., Schalling, M., Schönegger, A., Bock, C., Pascutto, C., Superti-Furga, G., Cazzola, M., & Kralovics, R. (2013). Somatic mutations of calreticulin in myeloproliferative neoplasms. *New England Journal of Medicine*, *369*(25), 2379–2390. https://doi.org/10.1056/NEJMoa1311347

Kramann, R., & Schneider, R. K. (2018). The identification of fibrosis-driving myofibroblast precursors reveals new therapeutic avenues in myelofibrosis. *Blood*, *131*(19), 2111 LP – 2119. https://doi.org/10.1182/blood-2018-02-834820

Kuo, J.-H., Chen, Y.-P., Liu, J.-S., Dubrac, A., Quemener, C., Prats, H., Bikfalvi, A., Wu, W., & Sue, S.-C. (2013). Alternative C-terminal helix orientation alters chemokine function: strucutre of the anti-angiogenic chemokine, CXCL4L1. *Journal of Biological Chemistry*, *288*(19), 13522–13533. https://doi.org/https://doi.org/10.1074/jbc.M113.455329

Küstermann, C. (2019). Modeling MPN pathogenesis and the IFNα signaling pathway in murine bone marrow cells and patient derived iPS cells. https://doi.org/doi:10.18154/rwth-2019-10844

Kuvardina, O. N., Herglotz, J., Kolodziej, S., Kohrs, N., Herkt, S., Wojcik, B., Oellerich, T., Corso, J., Behrens, K., Kumar, A., Hussong, H., Urlaub, H., Koch, J., Serve, H., Bonig, H., Stocking, C., Rieger, M. A., & Lausen, J. (2015). RUNX1 represses the erythroid gene expression program during megakaryocytic differentiation. *Blood*, *125*(23), 3570–3579. https://doi.org/10.1182/blood-2014-11-610519

Lacaud, G., & Kouskoff, V. (2017). Hemangioblast, hemogenic endothelium, and primitive versus definitive hematopoiesis. *Experimental Hematology*, *49*, 19–24. https://doi.org/10.1016/j.exphem.2016.12.009

Laity, J. H., Lee, B. M., & Wright, P. E. (2001). Zinc finger proteins: new insights into structural and functional diversity. *Current Opinion in Structural Biology*, *11*(1), 39–46. https://doi.org/https://doi.org/10.1016/S0959-440X(00)00167-6

Lange, L., Morgan, M., & Schambach, A. (2021). The hemogenic endothelium: a critical source for the generation of PSC-derived hematopoietic stem and progenitor cells. *Cellular and Molecular Life Sciences*. https://doi.org/10.1007/s00018-021-03777-y

Lasagni, L., Grepin, R., Mazzinghi, B., Lazzeri, E., Meini, C., Sagrinati, C., Liotta, F., Frosali, F., Ronconi, E., Alain-Courtois, N., Ballerini, L., Netti, G. S., Maggi, E., Annunziato, F., Serio, M., Romagnani, S., Bikfalvi, A., Romagnani, P., Ballerini, L., Liotta, F. (2007). PF-4/CXCL4 and CXCL4L1 exhibit distinct subcellular localization

and a differentially regulated mechanism of secretion. *Blood*, *109*(10), 4127–4134. https://doi.org/10.1182/blood-2006-10-052035

Laurenti, E., & Göttgens, B. (2018). From haematopoietic stem cells to complex differentiation landscapes. *Nature*, *553*(7689), 418–426. https://doi.org/10.1038/nature25022

Law, C. W., Chen, Y., Shi, W., & Smyth, G. K. (2014). voom: Precision weights unlock linear model analysis tools for RNA-seq read counts. *Genome Biology*, *15*(2), R29–R29. https://doi.org/10.1186/gb-2014-15-2-r29

Leiva, O., Leon, C., Kah Ng, S., Mangin, P., Gachet, C., & Ravid, K. (2018). The role of extracellular matrix stiffness in megakaryocyte and platelet development and function. *American Journal of Hematology*, *93*(3), 430–441. https://doi.org/10.1002/ajh.25008

Levine, R. L., Pardanani, A., Tefferi, A., & Gilliland, D. G. (2007). Role of JAK2 in the pathogenesis and therapy of myeloproliferative disorders. *Nature Reviews Cancer*, *7*(9), 673–683. https://doi.org/10.1038/nrc2210

Liu, Y., Wang, Y., Gao, Y., Forbes, J. A., Qayyum, R., Becker, L., Cheng, L., & Wang, Z. Z. (2015). Efficient generation of megakaryocytes from human induced pluripotent stem cells using food and drug administration-approved pharmacological reagents. *Stem Cells Translational Medicine*, *4*(4), 309–319. https://doi.org/10.5966/sctm.2014-0183

Lo, B. K. K., Yu, M., Zloty, D., Cowan, B., Shapiro, J., & McElwee, K. J. (2010). CXCR3/ligands are significantly involved in the tumorigenesis of basal cell carcinomas. *The American Journal of Pathology*, *176*(5), 2435–2446. https://doi.org/10.2353/ajpath.2010.081059

Ma, D. C., Sun, Y. H., Chang, K. Z., & Zuo, W. (1996). Developmental change of megakaryocyte maturation and DNA ploidy in human fetus. *European Journal of Haematology*, *57*(2), 121–127. https://doi.org/https://doi.org/10.1111/j.1600-0609.1996.tb01349.x

Maherali, N., & Hochedlinger, K. (2008). Guidelines and techniques for the generation of induced pluripotent stem cells. *Cell Stem Cell*, *3*(6), 595–605. https://doi.org/https://doi.org/10.1016/j.stem.2008.11.008

Mahla, R. S. (2016). Stem cells applications in regenerative medicine and disease therapeutics. *International Journal of Cell Biology*, *2016*, 6940283. https://doi.org/10.1155/2016/6940283

McCormack, M. P., Hall, M. A., Schoenwaelder, S. M., Zhao, Q., Ellis, S., Prentice, J. A., Clarke, A. J., Slater, N. J., Salmon, J. M., Jackson, S. P., Jane, S. M., & Curtis, D.

J. (2006). A critical role for the transcription factor Scl in platelet production during stress thrombopoiesis. *Blood*, *108*(7), 2248–2256. https://doi.org/10.1182/blood-2006-02-002188

McKerrell, T., Park, N., Chi, J., Collord, G., Moreno, T., Ponstingl, H., Dias, J., Gerasimou, P., Melanthiou, K., Prokopiou, C., Antoniades, M., Varela, I., Costeas, P. A., & Vassiliou, G. S. (2017). JAK2 V617F hematopoietic clones are present several years prior to MPN diagnosis and follow different expansion kinetics. *Blood Advances*, *1*(14), 968–971. https://doi.org/10.1182/bloodadvances.2017007047

Meier-Abt, F., Wolski, W. E., Tan, G., Kummer, S., Amon, S., Manz, M. G., Aebersold, R., & Theocharides, A. P. A. (2021). Reduced CXCL4/PF4 expression as a driver of increased human hematopoietic stem and progenitor cell proliferation in polycythemia vera. *Blood Cancer Journal*, *11*(2), 31. https://doi.org/10.1038/s41408-021-00423-5

Melo, J. V., & Barnes, D. J. (2007). Chronic myeloid leukaemia as a model of disease evolution in human cancer. *Nature Reviews Cancer*, *7*, 441–453. https://doi.org/10.1038/nrc2147

Mendelson, A., Strat, A. N., Bao, W., Rosston, P., Fallon, G., Ohrn, S., Zhong, H., Lobo, C., An, X., & Yazdanbakhsh, K. (2019). Mesenchymal stromal cells lower platelet activation and assist in platelet formation in vitro. *JCI Insight*, *4*(16). https://doi.org/10.1172/jci.insight.126982

Merker, J. D., Jones, C. D., Oh, S. T., Schrijver, I., Gotlib, J., & Zehnder, J. L. (2010). Design and evaluation of a real-time PCR assay for quantification of JAK2 V617F and wild-type JAK2 transcript levels in the clinical laboratory. *The Journal of Molecular Diagnostics : JMD*, *12*(1), 58–64. https://doi.org/10.2353/jmoldx.2010.090068

Mesa, R. A., Vannucchi, A. M., Mead, A., Egyed, M., Szoke, A., Suvorov, A., Jakucs, J., Perkins, A., Prasad, R., Mayer, J., Demeter, J., Ganly, P., Singer, J. W., Zhou, H., Dean, J. P., te Boekhorst, P. A., Nangalia, J., Kiladjian, J. J., & Harrison, C. N. (2017). Pacritinib versus best available therapy for the treatment of myelofibrosis irrespective of baseline cytopenias (PERSIST-1): an international, randomised, phase 3 trial. *The Lancet Haematology*. https://doi.org/10.1016/S2352-3026(17)30027-3

Moreau, T., Evans, A. L., & Ghevaert, C. J. G. (2018). Differentiation of Human Pluripotent Stem Cells to Megakaryocytes by Transcription Factor-Driven Forward Programming. In J. M. Gibbins & M. Mahaut-Smith (Eds.), *Platelets and Megakaryocytes : Volume 4, Advanced Protocols and Perspectives* (pp. 155–176).

Springer New York. https://doi.org/10.1007/978-1-4939-8585-2_10

Moreau, T., Evans, A. L., Vasquez, L., Tijssen, M. R., Yan, Y., Trotter, M. W., Howard, D., Colzani, M., Arumugam, M., Wu, W. H., Dalby, A., Lampela, R., Bouet, G., Hobbs, C. M., Pask, D. C., Payne, H., Ponomaryov, T., Brill, A., Soranzo, N., Ouwehand, W., Pedersen, R. A., & Ghevaert, C. (2016). Large-scale production of megakaryocytes from human pluripotent stem cells by chemically defined forward programming. *Nature Communications*, *7*, 11208. http://dx.doi.org/10.1038/ncomms11208

Moulard, O., Mehta, J., Fryzek, J., Olivares, R., Iqbal, U., & Mesa, R. A. (2014). Epidemiology of myelofibrosis, essential thrombocythemia, and polycythemia vera in the European Union. *European Journal of Haematology*, *92*(4), 289–297. https://doi.org/https://doi.org/10.1111/ejh.12256

Murray, P. D. F. (1932). The development in vitro of the blood of the early chick embryo. *Proceedings of the Royal Society of London. Series B, Containing Papers of a Biological Character*. https://doi.org/10.1098/rspb.1932.0070

Nangalia, J., Massie, C. E., Baxter, E. J., Nice, F. L., Gundem, G., Wedge, D. C., Avezov, E., Li, J., Kollmann, K., Kent, D. G., Aziz, A., Godfrey, A. L., Hinton, J., Martincorena, I., Van Loo, P., Jones, A. V., Guglielmelli, P., Tarpey, P., Harding, H., Fitzpatrick, J., Goudie, C., Ortmann, C., Loughran, S., Reine, K., Jones, D., Butler, A., Teague, J., O´Meara, S., McLaren, S., Bianchi, M., Silber, Y., Dimitropoulou, D., Bloxham, A., Mudie, L., Maddison, M., Robinson, B., Keohane, C., Maclean, C., Hill, K., Orchard, K., Tauro, S., Du, M-Q., Greaves, M., Bowen, D., Huntly, B., Harrison, C., Cross, N., Ron, D., Vannucchi, A. M., Papaermmanuil, E., Campbell, P. J., & Green, A. R. (2013). Somatic CALR mutations in myeloproliferative neoplasms with nonmutated JAK2. *New England Journal of Medicine*, *369*(25), 2391–2405. https://doi.org/10.1056/NEJMoa1312542

Nimmo, R. A., May, G. E., & Enver, T. (2015). Primed and ready: Understanding lineage commitment through single cell analysis. *Trends in Cell Biology*, *25*(8), 459–467. https://doi.org/10.1016/j.tcb.2015.04.004

Noetzli, L. J., French, S. L., & Machlus, K. R. (2019). New insights into the differentiation of megakaryocytes from hematopoietic progenitors. *Arteriosclerosis, Thrombosis, and Vascular Biology*, *39*(7), 1288–1300. https://doi.org/10.1161/ATVBAHA.119.312129

Noreikaitė, A., Antanavičiūtė, I., Mikalayeva, V., Darinskas, A., Tamulevičius, T., Adomavičiūtė, E., Šimatonis, L., Akramienė, D., & Stankevičius, E. (2017). Scaffold design for artificial tissue with bone marrow stem cells. *Medicina*, *53*(3), 203–210.

https://doi.org/https://doi.org/10.1016/j.medici.2017.07.001

Notta, F. (2016). Distinct routes of lineage development reshape the human blood hierarchy across ontogeny. *Science*, *351*(6269), aab2116. https://doi.org/doi: 10.1126/science.aab2116

Nowell, P. C. (1962). The minute chromosome (Phl) in chronic granulocytic leukemia. *Blut*, *8*, 65—66. https://doi.org/10.1007/bf01630378

Olschok, K., Han, L., de Toledo, M. A. S., Böhnke, J., Graßhoff, M., Costa, I. G., Theocharides, A., Maurer, A., Schüler, H. M., Buhl, E. M., Pannen, K., Baumeister, J., Kalmer, M., Gupta, S., Boor, P., Gezer, D., Brümmendorf, T. H., Zenke, M., Chatain, N., & Koschmieder, S. (2021). CALR frameshift mutations in MPN patient-derived iPSCs accelerate maturation of megakaryocytes. *Stem Cell Reports*. https://doi.org/10.1016/j.stemcr.2021.09.019

Papaemmanuil, E., Gerstung, M., Malcovati, L., Tauro, S., Gundem, G., Van Loo, P., Yoon, C. J., Ellis, P., Wedge, D. C., Pellagatti, A., Shlien, A., Groves, M. J., Forbes, S. A., Raine, K., Hinton, J., Mudie, L. J., McLaren, S., Hardy, C., Latimer, C., Della Porta, M., O`Meara, S., Ambaglio, I., Galli, A., Butler, A., Walldin, G., Teague, J., Quek, L., Sternberg, A., Gambacorti-Passerini, C., Cross, N., Green, A., Boultwood, J., Vjas, P., Hellstrom-Lindberg, E., Bowen, D., Cazzola, M., Stratton, M., Consortium, C. M. D. W. G. of the I. C. G. (2013). Clinical and biological implications of driver mutations in myelodysplastic syndromes. *Blood*, *122*(22), 3616–3699. https://doi.org/10.1182/blood-2013-08-518886

Pardanani, A. D. (2006). MPL515 mutations in myeloproliferative and other myeloid disorders: a study of 1182 patients. *Blood*, *108*(10), 3472–3476. https://doi.org/10.1182/blood-2006-04-018879

Pardanani, A., Harrison, C., Cortes, J. E., Cervantes, F., Mesa, R. A., Milligan, D., Masszi, T., Mishchenko, E., Jourdan, E., Vannucchi, A. M., Drummond, M. W., Jurgutis, M., Kuliczkowski, K., Gheorghita, E., Passamonti, F., Neumann, F., Patki, A., Gao, G., & Tefferi, A. (2015). Safety and efficacy of fedratinib in patients with primary or secondary myelofibrosis: A randomized clinical trial. *JAMA Oncology*, *1*(5), 643–651. https://doi.org/10.1001/jamaoncol.2015.1590

Piasecki, A., Leiva, O., & Ravid, K. (2020). Lysyl oxidase inhibition in primary myelofibrosis: A renewed strategy. *Archives of Stem Cell and Therapy*, *1*(1), 23–27. https://doi.org/10.46439/stemcell.1.005

Pillai, S., Netravali, I. A., Cariappa, A., & Mattoo, H. (2012). Siglecs and Immune Regulation. *Annual Review of Immunology*, *30*(1), 357–392. https://doi.org/10.1146/annurev-immunol-020711-075018

Psaila, B., Wang, G., Rodriguez-Meira, A., Li, R., Heuston, E. F., Murphy, L., Yee, D., Hitchcock, I. S., Sousos, N., O'Sullivan, J., Anderson, S., Senis, Y. A., Weinberg, O. K., Calicchio, M. L., Iskander, D., Royston, D., Milojkovic, D., Roberts, I., Bodine, D., Thongjuea, S., & Mead, A. J. (2020). Single-cell analyses reveal megakaryocyte-biased hematopoiesis in myelofibrosis and identify mutant clone-specific targets. *Molecular Cell*, *78*(3), 477-492.e8. https://doi.org/https://doi.org/10.1016/j.molcel.2020.04.008

Purushothaman, K.-R., Purushothaman, M., Turnbull, I. C., Adams, D. H., Anyanwu, A., Krishnan, P., Kini, A., Sharma, S. K., O'Connor, W. N., & Moreno, P. R. (2017). Association of altered collagen content and lysyl oxidase expression in degenerative mitral valve disease. *Cardiovascular Pathology : The Official Journal of the Society for Cardiovascular Pathology*, *29*, 11–18. https://doi.org/10.1016/j.carpath.2017.04.001

Putter, J. S., & Seghatchian, J. (2021). Polycythaemia vera: molecular genetics, diagnostics and therapeutics. *Vox Sanguinis*, *116*, 617–627. https://doi.org/https://doi.org/10.1111/vox.13069

Ran, F. A., Hsu, P. D., Lin, C. Y., Gootenberg, J. S., Konermann, S., Trevino, A. E., Scott, D. A., Inoue, A., Matoba, S., Zhang, Y., & Zhang, F. (2013). Double nicking by RNA-guided CRISPR cas9 for enhanced genome editing specificity. *Cell*, *154*(6), 1380–1389. https://doi.org/10.1016/j.cell.2013.08.021

Rao, Y., Hao, R., Wang, B., & Yao, T.-P. (2014). A mec17-myosin II effector axis coordinates microtubule acetylation and actin dynamics to control primary cilium biogenesis. *PloS One*, *9*(12), e114087–e114087. https://doi.org/10.1371/journal.pone.0114087

Ren, Y., Qiu, L., Lü, F., Ru, X., Li, S., Xiang, Y., Yu, S., & Zhang, Y. (2016). TALENs-directed knockout of the full-length transcription factor Nrf1α that represses malignant behaviour of human hepatocellular carcinoma (HepG2) cells. *Scientific Reports*, *6*, 23775. https://doi.org/10.1038/srep23775

Robinson, S. N., Ng, J., Niu, T., Yang, H., McMannis, J. D., Karandish, S., Kaur, I., Fu, P., Del Angel, M., Messinger, R., Flagge, F., de Lima, M., Decker, W., Xing, D., Champlin, R., & Shpall, E. J. (2006). Superior ex vivo cord blood expansion following co-culture with bone marrow-derived mesenchymal stem cells. *Bone Marrow Transplantation*, *37*(4), 359–366. https://doi.org/10.1038/sj.bmt.1705258

Royer, Y., Staerk, J., Costuleanu, M., Courtoy, P. J., & Constantinescu, S. N. (2005). Janus kinases affect thrombopoietin receptor cell surface localization and stability. *Journal of Biological Chemistry*, *280*(29), 27251–27261.

https://doi.org/10.1074/jbc.M501376200

Ruytinx, P., Proost, P., & Struyf, S. (2018). CXCL4 and CXCL4L1 in cancer. *Cytokine*, *109*, 65–71. https://doi.org/https://doi.org/10.1016/j.cyto.2018.02.022

Saliba, J., Hamidi, S., Lenglet, G., Langlois, T., Yin, J., Cabagnols, X., Secardin, L., Legrand, C., Galy, A., Opolon, P., Benyahia, B., Solary, E., Bernard, O. A., Chen, L., Debili, N., Raslova, H., Norol, F., Vainchenker, W., Plo, I., & Di Stefano, A. (2013). Heterozygous and homozygous JAK2(V617F) states modeled by induced pluripotent stem cells from myeloproliferative neoplasm patients. *PloS One*, *8*(9), e74257–e74257. https://doi.org/10.1371/journal.pone.0074257

Sanjuan-Pla, A. (2013). Platelet-biased stem cells reside at the apex of the haematopoietic stem-cell hierarchy. *Nature*, *502*, 232–236. https://doi.org/10.1038/nature12495

Schaffner, A., Rhyn, P., Schoedon, G., & Schaer, D. J. (2005). Regulated expression of platelet factor 4 in human monocytes—role of PARs as a quantitatively important monocyte activation pathway. *Journal of Leukocyte Biology*, *78*(1), 202–209.
https://doi.org/https://doi.org/10.1189/jlb.0105024

Scheuerer, B., Ernst, M., Dürrbaum-Landmann, I., Fleischer, J., Grage-Griebenow, E., Brandt, E., Flad, H.-D., & Petersen, F. (2000). The CXC-chemokine platelet factor 4 promotes monocyte survival and induces monocyte differentiation into macrophages. *Blood*, *95*(4), 1158–1166.
https://doi.org/https://doi.org/10.1182/blood.V95.4.1158.004k31_1158_1166

Schlenk, R. F., Stegelmann, F., Reiter, A., Jost, E., Gattermann, N., Hebart, H., Waller, C., Hochhaus, A., Platzbecker, U., Schafhausen, P., Blau, I. W., Verbeek, W., Heidel, F. H., Werner, M., Kreipe, H., Teleanu, V., Benner, A., Döhner, H., Grießhammer, M., & Döhner, K. (2017). Pomalidomide in myeloproliferative neoplasm-associated myelofibrosis. *Leukemia*, *31*(4), 889–895. https://doi.org/10.1038/leu.2016.299

Schneider, R. K., Mullally, A., Dugourd, A., Peisker, F., Hoogenboezem, R., Van Strien, P. M. H., Bindels, E. M., Heckl, D., Büsche, G., Fleck, D., Müller-Newen, G., Wongboonsin, J., Ventura Ferreira, M., Puelles, V. G., Saez-Rodriguez, J., Ebert, B. L., Humphreys, B. D., & Kramann, R. (2017). Gli1+ mesenchymal stromal cells are a key driver of bone marrow fibrosis and an important cellular therapeutic target. *Cell Stem Cell*, *20*(6), 785-800.e8. https://doi.org/10.1016/j.stem.2017.03.008

Schofield, R. (1978). The relationship between the spleen colony-forming cell and the haemopoietic stem cell. *Blood Cells Molecules and Diseases*, *4*(1–2), 7–25. https://app.dimensions.ai/details/publication/pub.1082377481

Schubert, M., Klinger, B., Klünemann, M., Sieber, A., Uhlitz, F., Sauer, S., Garnett, M. J., Blüthgen, N., & Saez-Rodriguez, J. (2018). Perturbation-response genes reveal signaling footprints in cancer gene expression. *Nature Communications*, *9*(1), 20. https://doi.org/10.1038/s41467-017-02391-6

Schutgens, F., & Clevers, H. (2020). Human Organoids: Tools for Understanding Biology and Treating Diseases. *Annual Review of Pathology: Mechanisms of Disease*, *15*(1), 211–234. https://doi.org/10.1146/annurev-pathmechdis-012419-032611

Senquan, L., Williams, D. M., Moliterno, A. R., Spivak, J. L., Huang, H., Gao, Y., Ye, Z., & Cheng, L. (2016). Generation, characterization and genetic modification of human iPSCs vontaining Calr, MPL and JAK2 mutations found in MPN patients. *Blood*, *128*(22), 3139. https://doi.org/10.1182/blood.V128.22.3139.3139

Shallis, R. M., & Podoltsev, N. A. (2021). Emerging agents and regimens for polycythemia vera and essential thrombocythemia. *Biomarker Research*, *9*(1), 40. https://doi.org/10.1186/s40364-021-00298-5

Shimoda, K., Feng, J., Murakami, H., Nagata, S., Watling, D., Rogers, N. C., Stark, G. R., Kerr, I. M., & Ihle, J. N. (1997). Jak1 plays an essential role for receptor phosphorylation and Stat activation in response to granulocyte colony-stimulating factor. *Blood*, *90*(2), 597–604. https://doi.org/https://doi.org/10.1182/blood.V90.2.597

Silva-Cardoso, S. C., Tao, W., Fernández, B. M., Boes, M., Radstake, T. R. D. J., & Pandit, A. (2020). CXCL4 suppresses tolerogenic immune signature of monocyte-derived dendritic cells. *European Journal of Immunology*, *50*(10), 1598–1601. https://doi.org/10.1002/eji.201948341

Sim, X., Jarocha, D., Hayes, V., Hanby, H. A., Marks, M. S., Camire, R. M., French, D. L., Poncz, M., & Gadue, P. (2017). Identifying and enriching platelet-producing human stem cell-derived megakaryocytes using factor V uptake. *Blood*, *130*(2), 192–204. https://doi.org/10.1182/blood-2017-01-761049

Singh, P., Jenkins, L. M., Horst, B., Alers, V., Pradhan, S., Kaur, P., Srivastava, T., Hempel, N., Győrffy, B., Broude, E. V, Lee, N. Y., & Mythreye, K. (2018). Inhibin Is a Novel Paracrine Factor for Tumor Angiogenesis and Metastasis. *Cancer Research*, *78*(11), 2978–2989. https://doi.org/10.1158/0008-5472.CAN-17-2316

Slukvin, I. I. (2016). Review Article Hematopoietic specification from human pluripotent stem cells : current advances and challenges toward de novo generation of hematopoietic stem cells. *Blood*, *122*(25), 4035–4046. https://doi.org/10.1182/blood-2013-07-474825.patients

Sontag, S. (2017). Modeling IRF8 deficient human hematopoiesis and dendritic cell

development with engineered iPS cells. https://doi.org/doi:10.18154/rwth-2017-07926

Sontag, S., Förster, M., Qin, J., Wanek, P., Mitzka, S., Schüler, H. M., Koschmieder, S., Rose-John, S., Seré, K., & Zenke, M. (2017). Modelling IRF8 deficient human hematopoiesis and dendritic cell development with engineered iPS cells. *Stem Cells*, *35*(4), 898–908. https://doi.org/10.1002/stem.2565

Sugimoto, N., & Eto, K. (2017). Platelet production from induced pluripotent stem cells. *Journal of Thrombosis and Haemostasis*, *15*(9), 1717–1727. https://doi.org/10.1111/jth.13736

Sugimoto, N., & Eto, K. (2021). Generation and manipulation of human iPSC-derived platelets. *Cellular and Molecular Life Sciences*, *78*(7), 3385–3401. https://doi.org/10.1007/s00018-020-03749-8

Surani, A., & Tischler, J. (2012). A sporadic super state. *Nature*, *487*(7405), 43–44. https://doi.org/10.1038/487043a

Szabo, E., Rampalli, S., Risueño, R. M., Schnerch, A., Mitchell, R., Fiebig-Comyn, A., Levadoux-Martin, M., & Bhatia, M. (2010). Direct conversion of human fibroblasts to multilineage blood progenitors. *Nature*, *468*(7323), 521–526. https://doi.org/10.1038/nature09591

Szalai, G., LaRue, A. C., & Watson, D. K. (2006). Molecular mechanisms of megakaryopoiesis. *Cellular and Molecular Life Sciences CMLS*, *63*(21), 2460–2476. https://doi.org/10.1007/s00018-006-6190-8

Takahashi, K., Tanabe, K., Ohnuki, M., Narita, M., Ichisaka, T., Tomoda, K., & Yamanaka, S. (2007). Induction of Pluripotent Stem Cells from Adult Human Fibroblasts by Defined Factors. *Cell*, *131*(5), 861–872. https://doi.org/10.1016/j.cell.2007.11.019

Takei, H., Edahiro, Y., Mano, S., Masubuchi, N., Mizukami, Y., Imai, M., Morishita, S., Misawa, K., Ochiai, T., Tsuneda, S., Endo, H., Nakamura, S., Eto, K., Ohsaka, A., Araki, M., & Komatsu, N. (2018). Skewed megakaryopoiesis in human induced pluripotent stem cell-derived haematopoietic progenitor cells harbouring calreticulin mutations. *British Journal of Haematology*, *181*(6), 791–802. https://doi.org/10.1111/bjh.15266

Tefferi, A. (2021). Primary myelofibrosis: 2021 update on diagnosis, risk-stratification and management. *American Journal of Hematology*, *96*(1), 145–162. https://doi.org/https://doi.org/10.1002/ajh.26050

Thon, J. N., Mazutis, L., Wu, S., Sylman, J. L., Ehrlicher, A., Machlus, K. R., Feng, Q., Lu, S., Lanza, R., Neeves, K. B., Weitz, D. A., & Jr, J. E. I. (2014). Platelet

bioreactor-on-a-chip. *Blood*, *124*(12), 1857–1868. https://doi.org/10.1182/blood-2014-05-574913.The

Toledo, M. A. S., Gatz, M., Sontag, S., Gleixner, K. V, Eisenwort, G., Feldberg, K., Hamouda, A. E. I., Kluge, F., Guareschi, R., Rossetti, G., Sechi, A. S., Dufva, O. M. J., Mustjoki, S. M., Maurer, A., Schüler, H. M., Goetzke, R., Braunschweig, T., Valent, P., Kaiser, A., Panse, J., Jawhar, M., Reiter, A., Hilberg, F., Ettmayer, P., Wagner, W., Koschmieder, S., Brümmendorf, T.H., Chatain, N., & Zenke, M. (2021). Nintedanib targets KIT D816V neoplastic cells derived from induced pluripotent stem cells of systemic mastocytosis. *Blood*, *137*(15), 2070–2084. https://doi.org/10.1182/blood.2019004509

Tursky, M. L., Loi, T. H., Artuz, C. M., Alateeq, S., Wolvetang, E. J., Tao, H., Ma, D. D., & Molloy, T. J. (2020). Direct comparison of four hematopoietic differentiation methods from human induced pluripotent stem cells. *Stem Cell Reports*, *15*(3), 735–748. https://doi.org/https://doi.org/10.1016/j.stemcr.2020.07.009

Vainchenker, W., & Kralovics, R. (2017). Genetic basis and molecular pathophysiology of classical myeloproliferative neoplasms. *Blood*, *129*(6), 667–679. https://doi.org/10.1182/blood-2016-10-695940

Vakulskas, C. A., Dever, D. P., Rettig, G. R., Turk, R., Jacobi, A. M., Collingwood, M. A., Bode, N. M., McNeill, M. S., Yan, S., Camarena, J., Lee, C. M., Park, S. H., Wiebking, V., Bak, R. O., Gomez-Ospina, N., Pavel-Dinu, M., Sun, W., Bao, G., Porteus, M. H., & Behlke, M. A. (2018). A high-fidelity Cas9 mutant delivered as a ribonucleoprotein complex enables efficient gene editing in human hematopoietic stem and progenitor cells. *Nature Medicine*, *24*(8), 1216–1224. https://doi.org/10.1038/s41591-018-0137-0

Van, R. K., Proost, P., Van, D. J., & Struyf, S. (2014). PF4 (platelet factor 4). *Atlas of Genetics and Cytogenetics in Oncology and Haematology*, *4*(8).
https://doi.org/10.4267/2042/54016

van Staveren, W. C. G., Solís, D. Y. W., Hébrant, A., Detours, V., Dumont, J. E., & Maenhaut, C. (2009). Human cancer cell lines: Experimental models for cancer cells in situ? For cancer stem cells? *Biochimica et Biophysica Acta (BBA) - Reviews on Cancer*, *1795*(2), 92–103. https://doi.org/https://doi.org/10.1016/j.bbcan.2008.12.004

Velten, L. (2017). Human haematopoietic stem cell lineage commitment is a continuous process. *Nat. Cell Biol.*, *19*. 271-281 (2017) https://doi.org/10.1038/ncb3493

Vrij, Rijken, Wersch, V., & Stockbrügger. (2000). Platelet factor 4 and β-thromboglobulin in inflammatory bowel disease and giant cell arteritis. *European Journal of Clinical*

Investigation, *30*(3), 188–194. https://doi.org/https://doi.org/10.1046/j.1365-2362.2000.00616.x

Wang, J., Li, J., & Liu, Q. (2005). Association between platelet activation and fibrinolysis in acute stroke patients. *Neuroscience Letters*, *384*(3), 305–309. https://doi.org/https://doi.org/10.1016/j.neulet.2005.04.090

Wang, W., Wang, T., Kotini, A. G., Iancu-Rubin, C., Hoffman, R., & Papapetrou, E. P. (2018). Modeling calreticulin-mutant myeloproliferative neoplasms with isogenic induced pluripotent stem cells. *Blood*, *132*(Supplement 1), 4319. https://doi.org/10.1182/blood-2018-99-111512

Wang, Y., & Zuo, X. (2019). Cytokines frequently implicated in myeloproliferative neoplasms. *Cytokine: X*, *1*(1), 100005. https://doi.org/https://doi.org/10.1016/j.cytox.2019.100005

Williams, N., Lee, J., Moore, L., Baxter, J. E., Hewinson, J., Dawson, K. J., Menzies, A., Godfrey, A. L., Green, A. R., Campbell, P. J., & Nangalia, J. (2020). Driver mutation acquisition in utero and childhood followed by lifelong clonal evolution underlie myeloproliferative neoplasms. *Blood*, *136*(Supplement_2), LBA-1-LBA-1. https://doi.org/10.1182/blood-2020-143813

Yamashita, Y. M., Yuan, H., Cheng, J., & Hunt, A. J. (2010). Polarity in stem cell division: asymmetric stem cell division in tissue homeostasis. *Cold Spring Harbor Perspectives in Biology*, *2*(1), a001313–a001313. https://doi.org/10.1101/cshperspect.a001313

Ye, Z., Liu, C. F., Lanikova, L., Dowey, S. N., He, C., Huang, X., Brodsky, R. A., Spivak, J. L., Prchal, J. T., & Cheng, L. (2014). Differential sensitivity to JAK inhibitory drugs by isogenic human erythroblasts and hematopoietic progenitors generated from patient-specific induced pluripotent stem cells. *Stem Cells (Dayton, Ohio)*, *32*(1), 269–278. https://doi.org/10.1002/stem.1545

Ye, Z., Zhan, H., Dowey, S., Williams, D. M., Jang, Y., Dang, C. V, Spivak, J. L., Moliterno, A. R., Cheng, L., & Mali, P. (2009). Human-induced pluripotent stem cells from blood cells of healthy donors and patients with acquired blood disorders. *Blood Cells*, *114*(27), 5473–5480. https://doi.org/10.1182/blood-2009-04-217406.

Yoder, M. C. (2014). Inducing definitive hematopoiesis in a dish. *Nature Biotechnology*, *32*(6), 539–541. https://doi.org/10.1038/nbt.2929

Yu, J., Vodyanik, M. A., Smuga-Otto, K., Antosiewicz-Bourget, J., Frane, J. L., Tian, S., Nie, J., Jonsdottir, G. A., Ruotti, V., Stewart, R., Slukvin, I. I., & Thomson, J. A. (2007). Induced pluripotent stem cell lines derived from human somatic cells. *Science*, *318*(5858), 1917 LP – 1920. https://doi.org/10.1126/science.1151526

Yu, L., Wei, Y., Duan, J., Schmitz, D. A., Sakurai, M., Wang, L., Wang, K., Zhao, S., Hon, G. C., & Wu, J. (2021). Blastocyst-like structures generated from human pluripotent stem cells. *Nature*, *591*, 620–626. https://doi.org/10.1038/s41586-021-03356-y

Zeevaert, K., Elsafi Mabrouk, M. H., Wagner, W., & Goetzke, R. (2020). Cell mechanics in embryoid bodies. *Cells*, *9*(10), 2270. https://doi.org/10.3390/cells9102270

Zhang, C. C., & Sadek, H. A. (2014). Hypoxia and metabolic properties of hematopoietic stem cells. *Antioxidants & Redox Signaling*, *20*(12), 1891–1901.
https://doi.org/10.1089/ars.2012.5019

Zhang, M., Guan, J., Huo, Y.-L., Song, Y.-S., & Chen, L.-Z. (2019). Downregulation of serum CXCL4L1 predicts progression and poor prognosis in prostate cancer patients treated by radical prostatectomy. *Asian Journal of Andrology*, *21*(4), 387–392. https://doi.org/10.4103/aja.aja_117_18

Zhang, N., & Newman, P. J. (2019). Packaging functionally important plasma proteins into the α-granules of human-induced pluripotent stem cell-derived megakaryocytes. *Journal of Tissue Engineering and Regenerative Medicine*, *13*(2), 244–252. https://doi.org/10.1002/term.2785

Zovein, A. C., Hofmann, J. J., Lynch, M., French, W. J., Turlo, K. A., Yang, Y., Becker, M. S., Zanetta, L., Dejana, E., Gasson, J. C., Tallquist, M. D., & Iruela-Arispe, M. L. (2008). Fate tracing reveals the endothelial origin of hematopoietic stem cells. *Cell Stem Cell*, *3*(6), 625–636. https://doi.org/10.1016/j.stem.2008.09.018

6 Appendix

6.1 Supplementary figures and tables

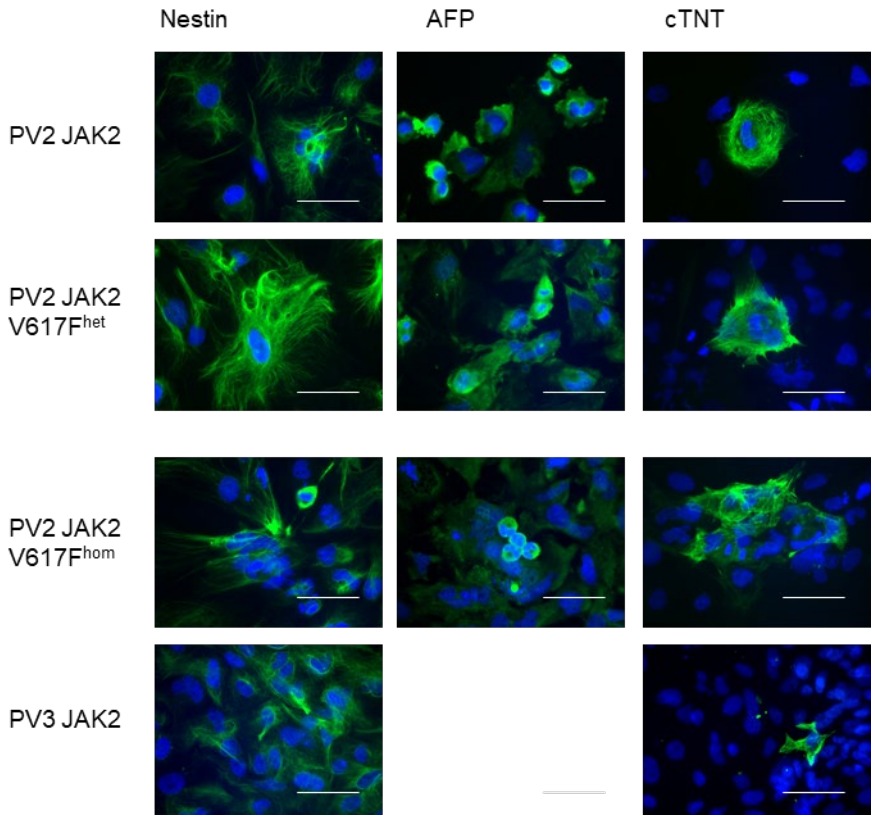

Figure 42: Staining of the 3-lineage marker nestin, AFP and cTNT.
Representative fluorescence images of PV2 JAK2, PV2 JAK2 V617F^{het}, PV2 JAK2 V617F^{hom} and PV3 JAK2 iPS cells differentiated by an EB assay. β-III-tubulin (ectoderm), albumin (endoderm) and α-SMA (mesoderm, all green) were co-stained with the nuclei (blue). Scale: 50 µm.

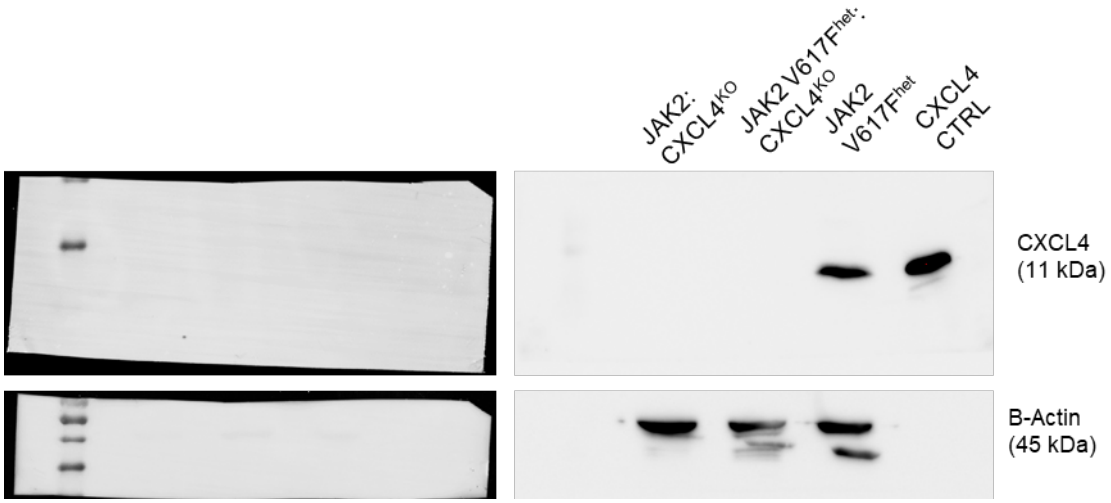

Figure 43: Complete Western blot of CXCL4^{KO} clones.
Western blot analysis of PV1 JAK2 V617F^{het}:CXCL4^{KO} and PV1 JAK2:CXCL4^{KO}. PV2 JAK2 V617F^{het} and recombinant CXCL4 protein was used as control. Recombinant CXCL4 with (11 kDa) and β-actin (45 kDa) as loading control was used.

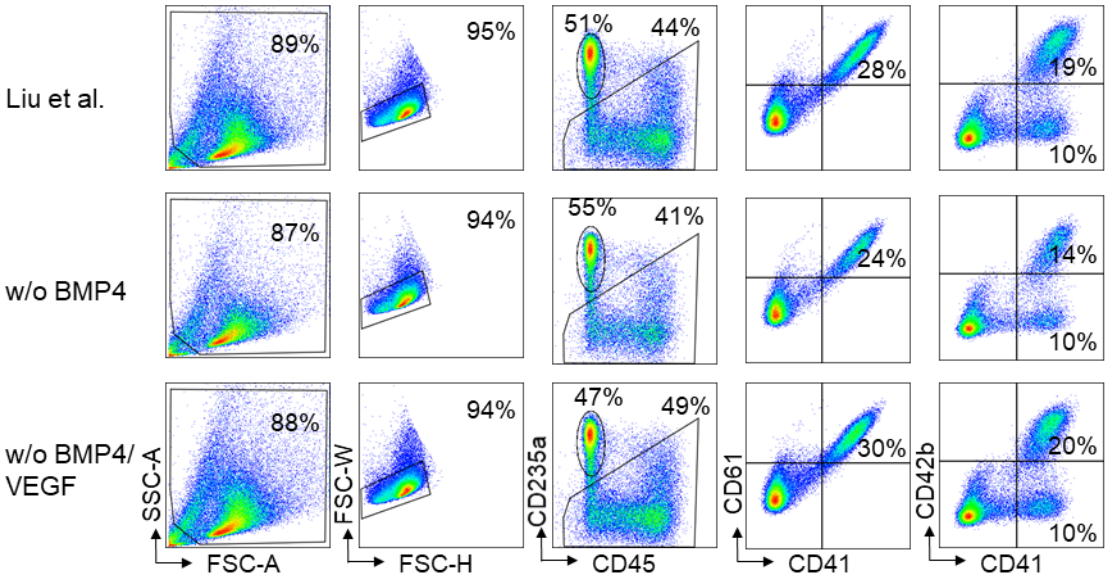

Figure 44 :Test of spin EB medium with and without BMP4 and VEGF supplementation.
Spin EB differentiation of PV2 JAK2 V617^{hom} was tested with BMP4 and VEGF for 14 days (top panel), compared to conditions with BMP4 and VEGF supplemented until day 7 (w/o BMP4 and w/o BMP4/VEGF, lower panels). Flow cytometry analysis were performed at day 14 with the indicated surface markers.

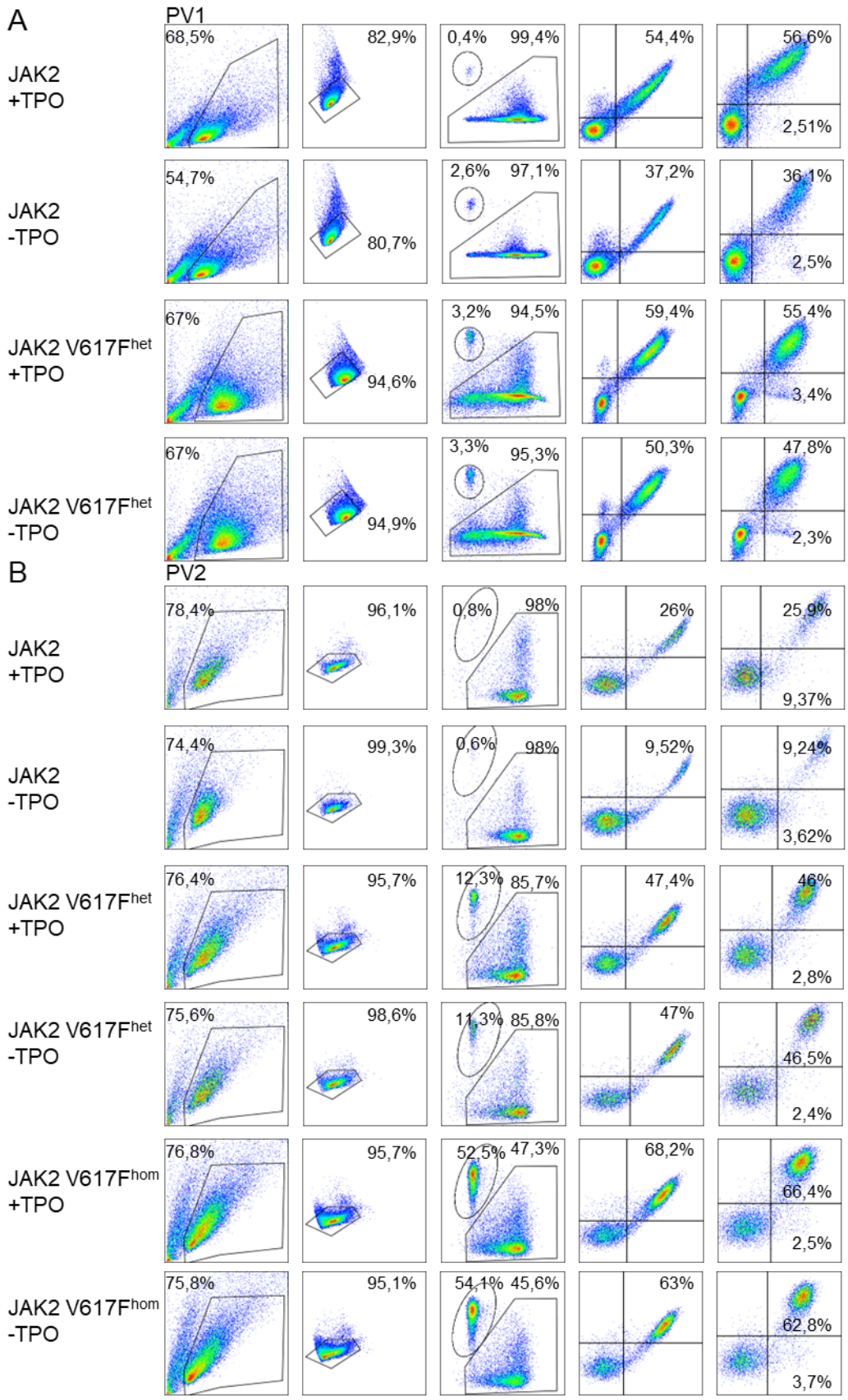
A
PV1
JAK2 +TPO
68,5%
82,9%
0,4%
99,4%
54,4%
56,6%
2,51%
JAK2 -TPO
54,7%
80,7%
2,6%
97,1%
37,2%
36,1%
2,5%
JAK2 V617Fhet +TPO
67%
94,6%
3,2%
94,5%
59,4%
55,4%
3,4%
JAK2 V617Fhet -TPO
67%
94,9%
3,3%
95,3%
50,3%
47,8%
2,3%
B
PV2
JAK2 +TPO
78,4%
96,1%
0,8%
98%
26%
25,9%
9,37%
JAK2 -TPO
74,4%
99,3%
0,6%
98%
9,52%
9,24%
3,62%
JAK2 V617Fhet +TPO
76,4%
95,7%
12,3%
85,7%
47,4%
46%
2,8%
JAK2 V617Fhet -TPO
75,6%
98,6%
11,3%
85,8%
47%
46,5%
2,4%
JAK2 V617Fhom +TPO
76,8%
95,7%
52,5%
47,3%
68,2%
66,4%
2,5%
JAK2 V617Fhom -TPO
75,8%
95,1%
54,1%
45,6%
63%
62,8%
3,7%

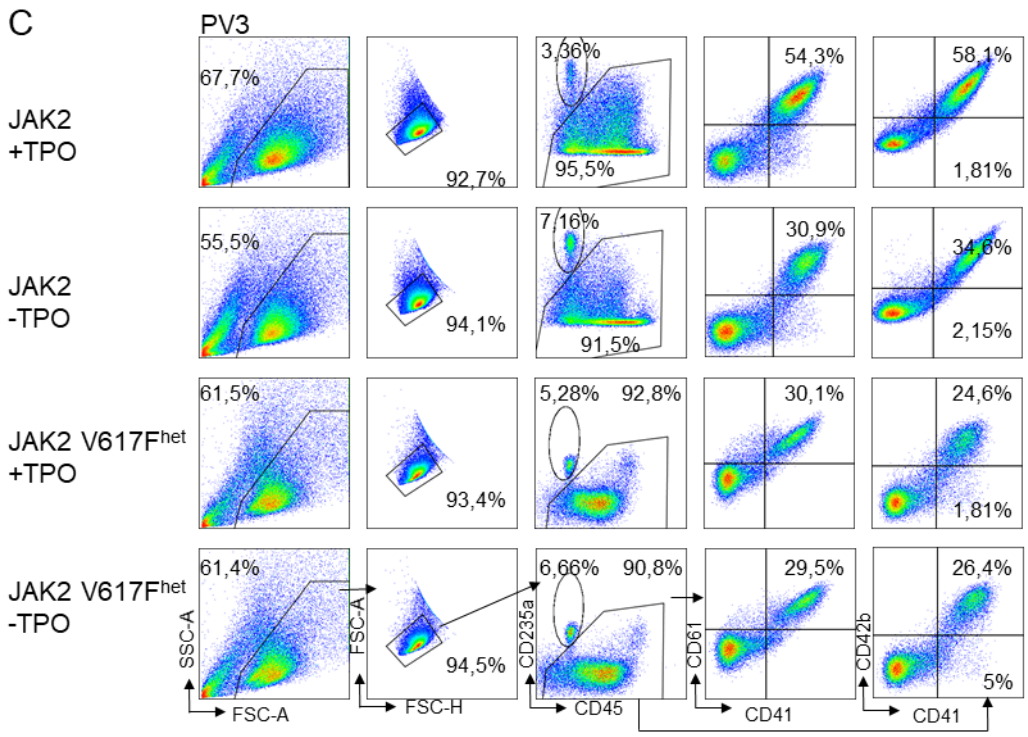

Figure 45: Representative flow cytometry plots on day 14 spin EB for PV1, PV2, and PV3. Representative plots of flow cytometry analysis of day 14 spin EB differentiation with and without TPO of **(A)** PV1 JAK2 and JAK2 V617F^{het}, **(B)** PV2 JAK2, JAK2 V617F^{het} and JAK2 V617F^{hom} and **(C)** PV3 JAK and JAK2 V617F^{het}.

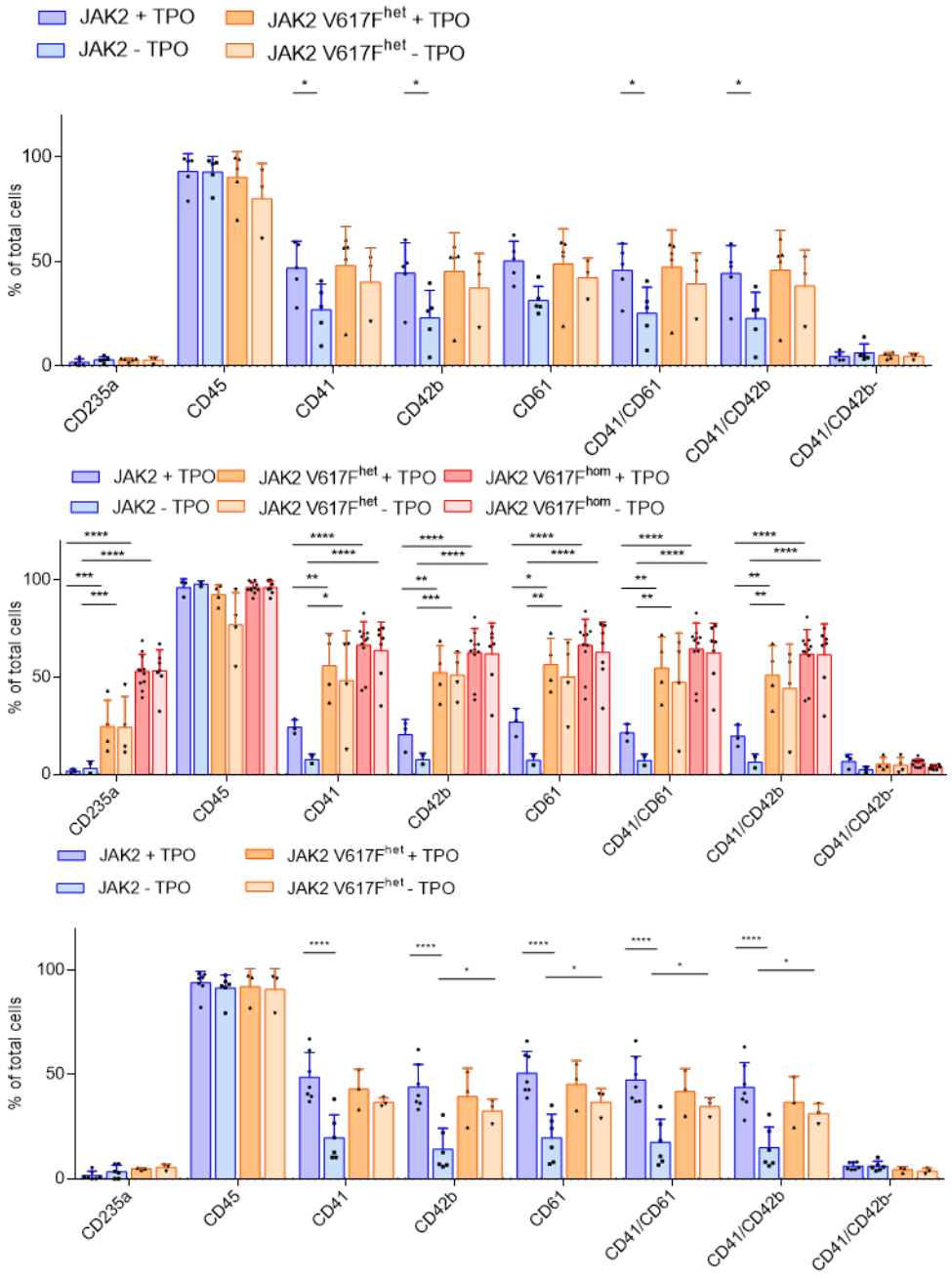

Figure 46: Quantification of surface markers after spin EB differentiation.
Surface marker expression was observed after 14 days of spin EB differentiation with and without TPO. Upper plot with PV1 JAK2 and JAK2 V617F^{het} (both n=5), middle plot with PV2 JAK2 (n=3) JAK2 V617F^{het} (n=4) and JAK2 V617F^{hom} (n=7) and lower plot with PV3 JAK2 (n=6) and JAK2 V617F^{het} (n=3). Data is represented as means ± SD. Statistical significance was assessed by Student t-test (*p≤0,05, **p≤0.005, ***p≤0.001, ****p≤0.0001).

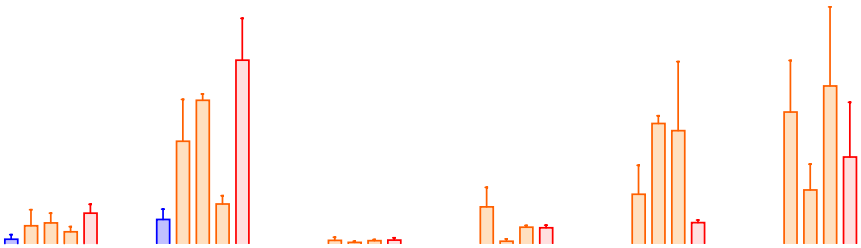

Figure 47: Quantification of colonies in CFU assays, separated by patients.
Day 10 CFU assays of CD34$^+$ HSC were counted and are displayed separated by patients and genotype. N=3. Data is represented as means ± SD. Statistical significance was assessed by Student t-test (*p≤0,05, **p≤0.005, ***p≤0.001, ****p≤0.0001).

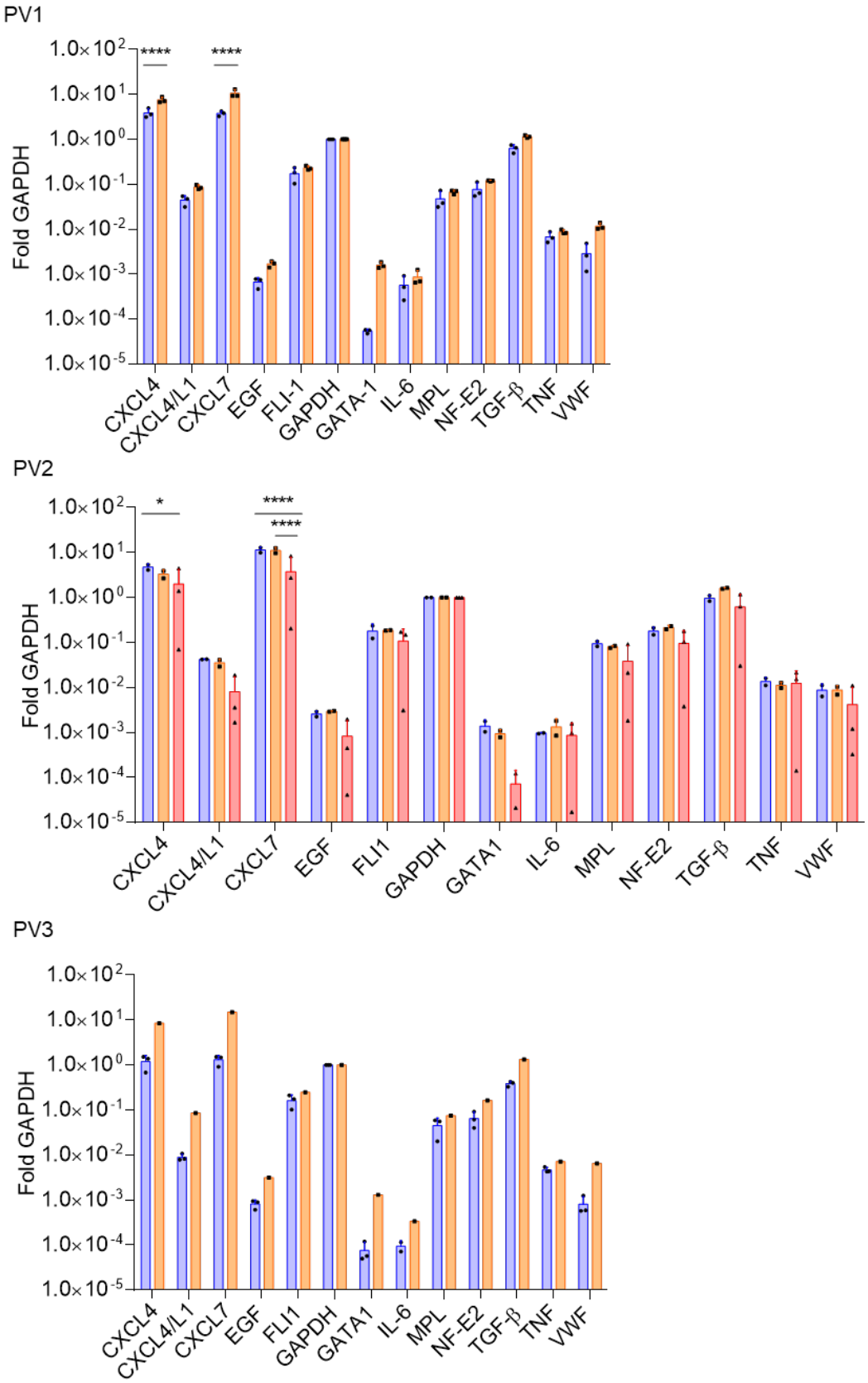

Figure 48: RT-qPCR analysis of PV1, PV2 and PV3 separately.
mRNA gene expression analysis of day 14 CD61^{+} megakaryocytes for PV1, PV2 and PV3. Normalized to GAPDH. Blue: JAK2, orange: JAK2 V617F^{het} and red JAK2 V617F^{hom}. Top left: PV1 JAK2 (n=3) and JAK2 V617F^{het} (n=3). Top right: JAK2 and JAK2 V617F^{het} (n=2), JAK2 V617F^{hom} (n=3). Lower plot: PV3 JAK2 (n=3) and JAK2 V617F^{het} (n=1). Data is represented as means ± SD. Statistical significance was assessed by Student t-test (*p≤0,05, ****p≤0.0001).

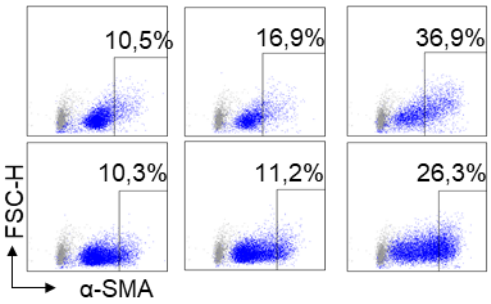

Figure 49: Quantification of α-SMA by flow cytometry for 3 healthy donor BM-MSC.
BM-MSC were isolated from three healthy donors and α-SMA expression was analyzed by flow cytometry after 5 days of stimulation with TGF-β and BMP4. Grey: unstained control, blue: stimulated BM-MSC.

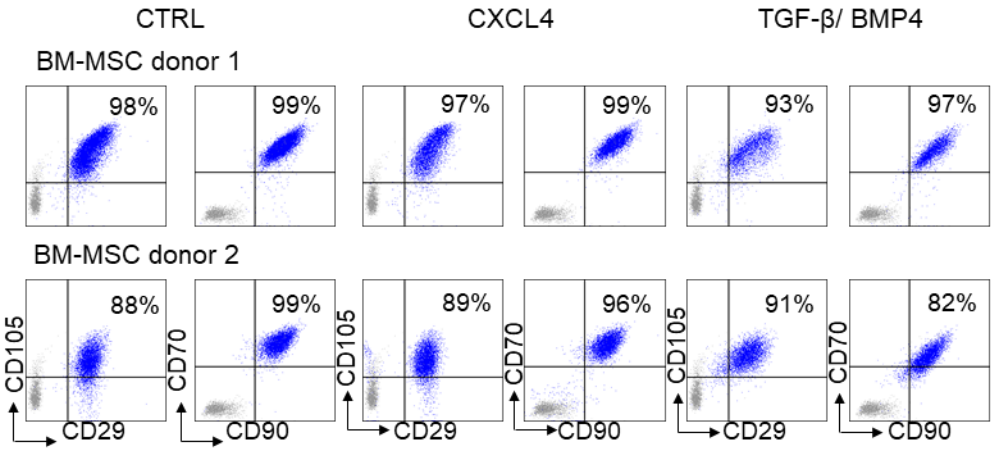

Figure 50: Analysis of BM-MSC surface marker expression after stimulation with TGF-β/BMP4 and CXCL4.
BM-MSC from three healthy donors were stimulated 5 days with CXCL4 and TGF-β/BMP4. MSC surface marker expression was measured by flow cytometry. Grey: unstained control, blue: stimulated BM-MSC.

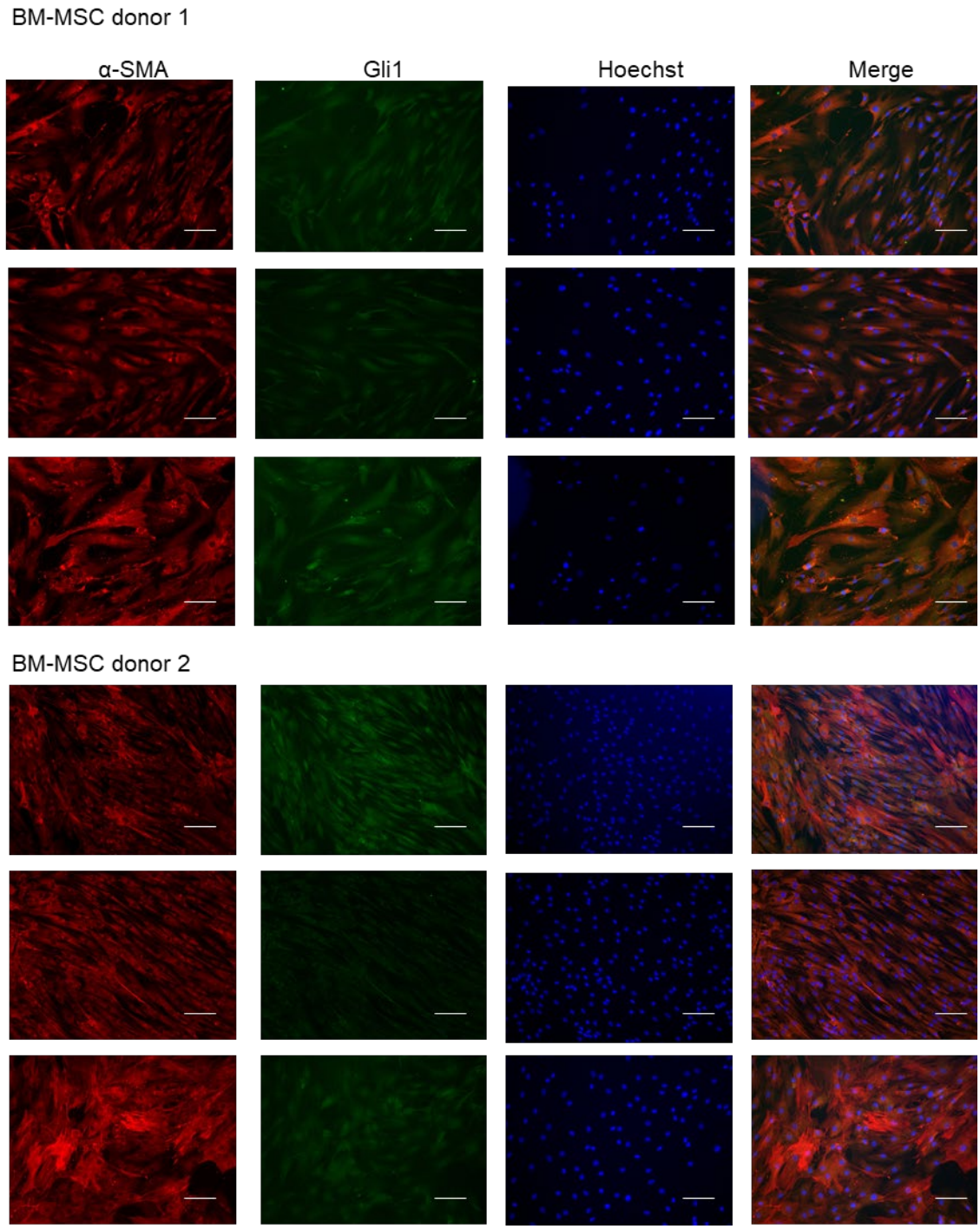

Figure 51: Immunostaining of healthy donor BM-MSC GLI1 and α-SMA.
Representative images of α-SMA (red), GLI1 (green) and nuclei (blue) immunostaining of BM-MSC donor 1 and 2 unstimulated or stimulated with CXCL4 or TGF-β/BMP4 for 5 days. Scale: 100 µm

Table 24: RT-qPCR primer.

Gene	Primer sequence		Reference
BMPR	Fwd.	TGAAATCAGACTCCGACCAGA	Singh et al.,
	Rev.	TGGCAAAGCAATGTCCATTAGTT	2018
COL1A1	Fwd.	ATCAACCGGAGGAATTTCCGT	Chen et al.,
	Rev.	CACCAGGACGACCAGGTTTTC	2016
COL1A2	Fwd.	GGCCCTCAAGGTTTCCAAGG	Corsa et al.,
	Rev.	CACCCTGTGGTCCAACAACTC	2016
COL3A1	Fwd.	TGGTCTGCAAGGAATGCCTGGA	Purushothama
	Rev.	TCTTTCCCTGGGACACCATCAG	n et al., 2017
CXCL4	Fwd.	GGGTTGCTGCTCCTGCCAC	J. Boehnke,
	Rev.	ACAGCGGGGCTTGCAGGTCC	unpublished
CXCL4L1	Fwd.	AGGAGATGCTGTTCTTGGCGTTGC	J. Boehnke,
	Rev.	TGTACAGCAGGGCTTGCAGATCCAA	unpublished
CXCL7	Fwd.	CTGGCTTCCTCCACCAAAGG	Kinouchi et al.,
	Rev.	GACTTGGTTGCAATGGGTTCC	2017
CXCR3	Fwd.	AAGTACGGCCCTGGAAGACT	Lo et al., 2010
	Rev.	GGCGTCATTTAGCACTTGGT	
EGF	Fwd.	CCTGCAAATGTAGCAGTTGATCC	M.A.S. de
	Rev.	GCCGCTTATCAAGCACATCC	Toledo, Ph.D.
FAP	Fwd.	CCAAACTGGATTTCAGGACAAGA	N. Flosdorf,
	Rev.	AGTATCTCCAAAGCATGGTTCTA	M.Sc.
FLI1	Fwd.	GTGCTGTTGTCACACCTCAG	Elzi et al.,
	Rev.	TACTGATCGTTTGTGCCCCT	2015
FN	Fwd.	CGGTGGCTGTCAGTCAAAG	Ren et al.,
	Rev.	AAACCTCGGCTTCCTCCATAA	2016
GAPDH	Fwd.	GAAGGTGAAGGTCGGAGTC	Furitsu et al.,
	Rev.	GAAGATGGTGATGGGATTTC	1993
GATA1	Fwd.	GGGATCACACTGAGCTTGC	Szabo et al.,
	Rev.	ACCCCTGATTCTGGTGTGG	2010
GLI1	Fwd.	GGGTGCCGGAAGTCATACTC	Rao et al.,
	Rev.	GCTAGGATCTGTATAGCGTTTGG	2014
IL-6	Fwd.	TCCAAAGATGTAGCCGCCC	Sontag, 2017
	Rev.	CAGTGCCTCTTTGCTGCTTTC	
JAK2	Fwd.	GATAAAGCACACAGAAACTATTCAGAGTC	Merker et al.,
	Rev.	AGAATATTCTCGTCTCCACAAAC	2010

JAK2 V617F	Fwd.	GATAAAGCACACAGAAACTATTCAGAGTC	Merker et al., 2010
	Rev.	AGAATATTCTCGTCTCCACAAAA	
MPL	Fwd.	CTGCCACTTCAAGTCACGAA	Olschok et al., 2021
	Rev.	CTGCCACTCCAATTCCAGAT	
MRTF	Fwd.	AACAGCACCTCACTGACTGG	M.A.S. de Toledo, Ph.D.
	Rev.	TCTTGATAGGCTCGAAGGCG	
NF-E2	Fwd.	TGAGCAGGGGCAGTAAGTTG	Olschok et al., 2021
	Rev.	CTGTGACTCCACCACAGGTTT	
SRF	Fwd.	CGTTCAGACCCCACAACAGA	M.A.S. de Toledo, Ph.D.
	Rev.	GATGGTGGAGGTTGTACCCG	
TGF-β	Fwd.	GAGCCTGAGGCCGACTACTA	Design by Zenke Lab
	Rev.	CTTCTCGGAGCTCTGATGTGTT	
TGF-βR	Fwd.	CACAGAGTGGGAACAAAAAGGT	Gao et al., 2019
	Rev.	CCAATGGAACATCGTCGAGCA	
TNF	Fwd.	ACTTTGGAGTGATCGGCCC	Sontag, 2017
	Rev.	CATTGGCCAGGAGGGCATT	
vWF	Fwd.	CAACACCTGCATTTGCCGAA	Olschok et al., 2021
	Rev.	TGACCTGTGACAAGGCACTC	
α-SMA	Fwd.	TCCTTCATCGGGATGGAGTCT	J. Boehnke, unpublished
	Rev.	TACATAGTGGTGCCCCCTGA	

6.1 Abbreviations

AFP	alpha-fetoprotein
AGM	aorta-gonad-mesonephros
ALB	albumin
ANGPT1	angiopoietin 1
bFGF	basic fibroblast growth factor
BFU-E	burst forming unit - erythrocyte
BLAST	Basic Local Alignment Search Tool
BM	bone marrow
BMP4	bone morphogenic protein 4
B	bases
Bp	base pairs
BSA	bovine serum albumin
CALR	calreticulin
CAR	CXCL12 abundant reticular
Cas	CRISPR associated gene
CB	cord blood
CD	cluster of differentiation
cDNA	complementary DNA
CFU	colony forming unit
CFU-E	erythroid colony forming units
CFU-G	granulocyte colony forming units
CFU-GM	granulocyte macrophage colony forming units
CFU-M	macrophage colony forming units
CFU-GEMM	granulocyte erythrocyte macrophage
	megakaryocyte colony forming unit
CML	chronic myeloid leukemia
CMP	common myeloid progenitor
Col	collagen
CTRL	control
CRISPR	clustered regularly interspaced short palindromic repeats
crRNA	CRISPR RNA
Ct	threshold cycle
CXCL	C-X-C motif ligand
cTNT	cardiac troponin
d	day
DC	dendritic cells
DMEM	Dulbecco’s modified Eagle medium
DMSO	dimethyl sulfoxide
DNA	deoxyribonucleic acid
dNTP	deoxynucleotide triphosphates
e.g.	for example
EB	embryoid bodies
ECM	extracellular matrix
EDTA	ethylene diamine tetra acetic acid
EPO	erythropoietin
hES cells	human embryonic stem cells
ET	essential thrombocythemia
etc.	et cetera
FACS	fluorescence-activated cell sorting

FCS	fetal calf serum
FLT3L	fms-like tyrosine kinase 3 ligand
FN	fibronectin
FSC	forward scatter
g	gravitational acceleration
GAPDH	glyceraldehyde 3-phosphate dehydrogenase
G-CSF-R	granulocyte colony stimulating factor receptor
gDNA	genomic deoxyribonucleic acid
GFP	green fluorescent protein
gRNA	guide RNA
Gy	gray
h	hour
Het	heterozygous
Hom	homozygous
HSC	hematopoietic stem cells
ICM	inner cell mass
IFN	interferon
IgG	immunoglobulin G
IgM	immunoglobulin M
IL	interleukin
MEF	mouse embryonic fibroblasts
iPS	induced pluripotent
JAK	janus kinase
kb	kilo base pairs
kDa	kilo dalton
KO-DMEM	KnockOut™-Dulbecco's Modified Eagle Medium
LepR	leptin receptor
LT	long term
MEP	megakaryocyte erythroid progenitors
MF	myelofibrosis
min	minute
mM	millimolar
MPN	myeloproliferative neoplasm
MPL	thrombopoietin receptor
mRNA	messenger ribonucleic acid
MSC	mesenchymal stem/stromal cells
NCBI	National Center for Biotechnology Information
Nes	nestin
NGS	next-generation sequencing
NK	natural killer cells
OCT4	octamer binding transcription factor 4
P	p-value
PI3K	phosphatidylinositol-3-kinase
PB	peripheral blood
PBMNC	peripheral blood mononuclear cells
PBS	phosphate-buffered saline
PCR	polymerase chain reaction
PFA	paraformaldehyde
PI	propidium iodide
PMF	primary myelofibrosis
PV	polycythemia vera
PVDF	polyvinylidene difluoride

RT-qPCR	reverse transcription quantitative polymerase chain reaction
RNA	ribonucleic acid
Rpm	rounds per minute
RT	room temperature
s	seconds
SCF	stem cell factor
SDS	sodium dodecyl sulfate
SDS-PAGE	sodium dodecyl sulfate-polyacrylamide gel electrophoresis
SFM	serum-free medium
sgRNA	single guide RNA
SH2	src-homology 2
SNP	single nucleotide polymorphisms
SMA	smooth muscle actin
SOX2	sex determining region Y (SRY)- box 2
SSC	sideward scatter
SSEA	stage specific embryonic antigen
St	short term
STAT	signal transducer and activator of transcription
TALEN	transcription activator-like effector nucleases
TBS	tris-buffered saline
TGF	transforming growth factor
TNF	tumor necrosis factor
TPO	thrombopoietin
TRA	tumor related antigen
tracrRNA	trans-activating CRISPR RNA
t-TBS	tween-tris-buffered saline
U	units
VEGF	vascular endothelial growth factor
W	week
WHO	world health organization
ZFN	zinc finger nucleases

6.2 List of figures

6.3 List of tables

7 Publications

Part of this work is published in the following publication:

Boehnke, J., Atakhanov, S., Toledo, M. A. S., Schüler, H. M., Sontag, S., Chatain, N., Koschmieder, S., Brümmendorf, T. H., Kramann, R., & Zenke, M. (2021). CRISPR/Cas9 mediated CXCL4 knockout in human iPS cells of polycythemia vera patient with JAK2 V617F mutation. *Stem Cell Research*, *55*, 102490.

Further Publications:

Olschok, K., Han, L., de Toledo, M. A. S., **Boehnke, J.**, Graßhoff, M., Costa, I. G., Theocharides, A., Maurer, A., Schüler, H. M., Buhl, E. M., Pannen, K., Baumeister, J., Kalmer, M., Gupta, S., Boor, P., Gezer, D., Brümmendorf, T. H., Zenke, M., Chatain, N., & Koschmieder, S. (2021). CALR frameshift mutations in MPN patient-derived iPS cells accelerate maturation of megakaryocytes. *Stem Cell Reports*. https://doi.org/10.1016/j.stemcr.2021.09.019

Satoh, T., Toledo, M. A. S., **Boehnke, J.**, Olschok, K., Flosdorf, N., Götz, K., Küstermann, C., Sontag, S., Seré, K., Koschmieder, S., Brümmendorf, T. H., Chatain, N., Tagawa, Y.-I., & Zenke, M. (2021). Human DC3 Antigen Presenting Dendritic Cells From Induced Pluripotent Stem Cells. *Frontiers in Cell and Developmental Biology*, *9*, 667304. https://doi.org/10.3389/fcell.2021.667304

Conference

Boehnke, J., Flosdorf, N. Studying myelofibrosis with iPS cell derived JAK2 V617F megakaryocytes. 10th International Meeting of the Stem Cell Network NRW, virtual, 2021.

8 Acknowledgements

To honor the fact that research is rarely an entirely solitary process, I decided to use the first-person pronoun “we” in the text. Many people helped me along the way of this thesis, and without them, I could not have finalized this work.

My most enormous thanks go to Prof. Dr. Martin Zenke, who entrusted me with this fascinating topic. In the three years, he has been of immense support. Thank you for your guidance during these three years.

Furthermore, I would like to thank Prof. Dr. Dr. Wolfgang Wagner. He supported me as the second examiner on the way to this thesis. Through the cooperation with him and his entire working group, this thesis has gained in value.

I would also like to thank Prof. Dr. Pradel, who took the time to evaluate my work as the third examiner.

In addition, I would like to thank our collaborators in the MPN Network Aachen. Here, especially Prof. Dr. Rebekka Schneider-Kramann and Prof. Dr. Rafael Kramann, who have influenced my project with their research to Prof. Dr. Steffen Koschmieder and Dr. Nicolas Chatain, who supported me in the field of hematology and oncology and the group of Prof. Dr. Ivan Costa and in particular Martin Graßhoff, who made a significant contribution through the bioinformatic evaluation of the results.

Next, I want to thank all members of the Zenke Lab. Not naming you in person does not mean that you were less important in the last three years. In particular, I would like to mention Dr. Marcelo de Toledo, who was always there for me as a supervisor in the first year, but also beyond that, with advice and support. In addition, I want to thank Salim Atakhanov for his support on our manuscript and Niclas Flosdorf for overtaking the project and bringing it forward.

My thanks also go to Kathrin Olschok. Thank you for your essential part in this work, not only in many experiments, and during the weekend shifts but also by carefully reading this thesis. The same applies to Olivia Cypris, who was a great help since the start of my thesis.

Zuletzt danke ich meiner Mutter, welche immer an mich geglaubt hat und mich auf meinem Weg immer bedingungslos unterstützt hat und Fabio, welcher mich durch alle Höhen und Tiefen begleitet und unterstützt hat.

Acknowledgements

9 Declaration of authorship

Eidesstattlicher Erklärung

I, Janik Böhnke
declare that this thesis and the work presented in it are my own and has been generated by me as the result of my own original research.

Hiermit erkläre ich an Eides statt/ I do solemnly swear that:

1. This work was done wholly or mainly while in candidature for the doctoral degree at this faculty and university;
2. Where any part of this thesis has previously been submitted for a degree or any other qualification at this university or any other institution, this has been clearly stated;
3. Where I have consulted the published work of others or myself, this is always clearly attributed;
4. Where I have quoted from the work of others or myself, the source is always given. This thesis is entirely my own work, with the exception of such quotations;
5. I have acknowledged all major sources of assistance;
6. Where the thesis is based on work done by myself jointly with others, I have made clear exactly what was done by others and what I have contributed myself;
7. Parts of this work have been published before as:

Boehnke, J., Atakhanov, S., Toledo, M. A. S., Schüler, H. M., Sontag, S., Chatain, N., Koschmieder, S., Brümmendorf, T. H., Kramann, R., & Zenke, M. (2021). CRISPR/Cas9 mediated CXCL4 knockout in human iPS cells of polycythemia vera patient with JAK2 V617F mutation. *Stem Cell Research*, *55*, 102490.

14.06.2022
Janik Böhnke